

Università della Calabria

Facoltà di Ingegneria

Scuola di Dottorato "Pitagora" in Scienze Ingegneristiche

I Ciclo (2007-2010)

---

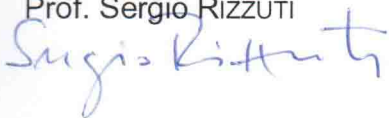
SETTORE SCIENTIFICO DISCIPLINARE: ICAR/01 – Idraulica

Dissertazione per il conseguimento del titolo di Dottore di Ricerca in Scienze Ingegneristiche

FLOW-ALTERING COUNTERMEASURES AGAINST LOCAL  
SCOUR AT BRIDGE PIERS

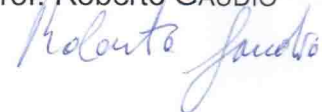
Director of the School

Prof. Sergio RIZZUTI



Supervisor

Prof. Roberto GAUDIO



Candidate

Ali Tafarajnoruz



November 2010



*To my parents*



## Table of Contents

<b>Table of Contents .....</b>	<b>V</b>
<b>Abstract .....</b>	<b>IX</b>
<b>Acknowledgements .....</b>	<b>XI</b>
<b>List of tables .....</b>	<b>XIII</b>
<b>List of figures .....</b>	<b>XV</b>
<b>Symbols .....</b>	<b>XXV</b>
<b>Introduction .....</b>	<b>1</b>
<b>Chapter 1: Local scouring at bridge piers: general description .....</b>	<b>5</b>
1.1. Introduction .....	5
1.2. Flow pattern around a circular bridge pier .....	5
1.3. Scouring process .....	10
1.4. Modelling of turbulent flow and scour process at the pier .....	12
1.5. Prediction of scour depth using empirical formulae .....	15
1.5.1. Selected formulae .....	15
1.5.2. Comparison between formulae based on randomly generated data .....	17
1.5.2.1. Data generation .....	17
1.5.2.2. Result analysis .....	18
1.5.3. Comparison of the formulae based on field data .....	19
<b>Chapter 2: Effective factors and dimensional analysis of bridge pier scouring .....</b>	<b>23</b>
2.1. Introductions .....	23

## Table of contents

---

2.2. Dimensionless parameters.....	24
2.3. Flow intensity and sediment grading.....	25
2.4. Side walls.....	26
2.5. Sediment size.....	27
2.6. Flow depth.....	28
2.7. Time.....	29
2.8. Pier size.....	30
2.9. Required conditions to achieve the maximum scour depth at a pier.....	32
<b>Chapter 3: Review of flow-altering countermeasures against local scour at bridge piers ....</b>	<b>35</b>
3.1. Introduction.....	35
3.2. Openings through the piers.....	36
3.2.1. Internal connecting tubes.....	36
3.2.2. Pier group.....	37
3.2.3. Pier slot.....	38
3.3. Pier-attachments.....	41
3.3.1. Threading.....	41
3.3.2. Collars and horizontal plates.....	42
3.3.3. Plates.....	46
3.4. Bed-attachments.....	47
3.4.1. Sacrificial piles.....	47
3.4.2. Vanes and sills.....	49
3.4.3. Surface guide panels.....	53
3.4.4. Sleeve and collared sleeve.....	54
3.5. Other methods.....	55
3.5.1. Suction applied to the pier.....	55
3.5.2. Modifying pier shape and texture.....	55
3.5.3. Footing and caisson.....	56
3.6. Combination of countermeasures.....	57
3.6.1. Slot and collar.....	57
3.6.2. Collar and pier group.....	57
3.6.3. Permeable sheet piles and riprap.....	57
3.6.4. Suction and riprap.....	57
3.6.5. Collar and riprap.....	57
3.6.6. Slot and bed-sill.....	58
3.6.7. Submerged vanes and bed-sill.....	58
3.6.8. Other combinations.....	58
3.7. Evaluation of the experiments.....	59
3.7.1. Side-wall effect.....	59
3.7.2. Sediment size effect.....	59
3.7.3. Flow shallowness effect.....	59
3.7.4. Time effect.....	60
3.8. Limitations and difficulties in practical applications.....	60
3.8.1. Debris flow.....	60
3.8.2. Flow obliqueness.....	60
3.8.3. High flow intensity.....	61
3.8.4. Other problems.....	61

3.9. Conclusions .....	61
<b>Chapter 4: Experimental facilities and procedure .....</b>	<b>63</b>
4.1. Introduction .....	63
4.2. Flume and related facilities .....	63
4.2.1. Bed longitudinal slope .....	65
4.3. Design of the tests .....	66
4.4. Experimental procedure .....	70
4.5. Locations and time-schedule to measure scour depth .....	76
4.5.1. Steady flow tests .....	76
4.5.2. Unsteady flow tests .....	76
4.6. Equilibrium criterion .....	76
4.7. Calculation of efficiency .....	83
<b>Chapter 5: Result analysis and discussion .....</b>	<b>85</b>
5.1. Introduction .....	85
5.2. Steady flow tests .....	85
5.2.1. Unprotected pier: test S0 .....	85
5.2.2. Transverse sacrificial piles .....	90
5.2.3. Collar .....	96
5.2.4. Threading .....	103
5.2.5. Pier slot .....	106
5.2.6. Combination of a collar with pier slot .....	117
5.2.7. Combination of a pier slot with sacrificial piles .....	120
5.2.8. Combination of a collar with sacrificial piles .....	122
5.2.9. Combination of collar with bed-sill as scour countermeasure .....	124
5.2.9.1. Location of bed-sill respect to pier .....	124
5.2.9.2. Dimensions of bed-sill .....	135
5.2.9.3. Recommended configuration for design .....	143
5.3. Unsteady flow tests .....	150
5.3.1. Test U00 .....	151
5.3.2. Test U0 .....	153
5.3.3. Test U1 .....	157
5.3.4. Test U2 .....	159
5.3.5. Test U3 .....	162
5.3.6. Test U4 .....	165
5.3.7. Test U5 .....	168
5.3.8. Test U6 .....	170
5.3.9. Test U7 .....	172
5.3.10. Test U8 .....	174
5.4. Possible problems in application .....	177
5.4.1. Required space .....	177
5.4.2. Application in live-bed conditions .....	177
<b>Chapter 6: Conclusions and recommendations .....</b>	<b>179</b>

**Table of contents**

---

**References..... 181**

**Appendix A: Discharge measurement ..... A1**

**Appendix B: Bed-surface acquisition..... B1**



## Abstract

The ability to protect bridge piers and abutments against scour is critical to bridge safety. Excessive pier scour can cause high maintenance costs or even bridge collapse resulting in the interruption of traffic and possibly death.

Up to now, various types of countermeasures have been recommended to reduce scouring around pier foundations. The countermeasures against pier scour can be broadly classified into two categories: (1) flow-altering and (2) bed-armouring countermeasures.

This thesis focuses on the first category of countermeasures. Based on a comprehensive review of the up-to-date studies on various types of flow-altering countermeasures, these can be classified into four main groups based on their shapes and performances: (1) openings through piers, (2) pier attachments, (3) bed attachments and (4) other devices. After evaluation and considering all the countermeasures, a few countermeasures were recommended for further investigations. Among them, five countermeasures were selected for analysis in the present thesis. They are transverse sacrificial piles, collar, threading, pier slot and bed-sill.

The first part of the experiments, were performed in clear-water scour condition, near threshold condition of sediment movement. In this part, countermeasures were tested individually. Afterwards, countermeasures that showed appropriate efficiency in scour depth reduction were combined one by one. Results of this part showed that a collar, pier slot and sacrificial piles may show efficiency of about 30% in scour depth reduction; however, threading cannot be assumed as a reliable pier scour countermeasure. Results show that the blockage ratio of sacrificial piles is an important parameter, since by increasing the number of piles from three to five, the efficiency reduces. In this part also optimum size and location of a pier slot were criticised and best configuration based on previous and present studies was proposed. In fact, the best configuration can be suggested as a pier slot half as long as the flow depth plus maximum scour depth. In this case, the pier slot near the water surface may not significantly increase the efficiency. A combination of sacrificial piles with a collar and sacrificial piles with a slot showed that they cannot reduce the scour depth significantly with respect to each individual countermeasure. In particular, a combination of a collar and sacrificial piles increases the rate of

scouring with respect to a single collar. At the end of this part, a combination of a bed-sill and cut-collar was selected as the best configuration. Two forms of this countermeasure were proposed for further studies. In the first proposed countermeasure, the use of a sill as wide as the channel width was recommended. This form, although reliable to prevent scouring at the upstream part of the bed-sill, may not be applicable for some practical purposes. Therefore, in another attempt, a shorter bed-sill was also proposed, protected with two side-walls, in order to reduce the risk of scour intrusion in front of the bed-sill. These two proposed countermeasures showed efficiencies of 68.5% and 64.5% in scour depth reduction, however owing to the use of a border around the collar rim, the scour did not reach the pier body.

In next part, the later form of proposed countermeasure that consists of a shorter bed-sill and seems to be more practical, was evaluated in unsteady flow tests with the peak flow intensity slightly greater than the threshold for the inception of sediment movement. In this section of the thesis, circular and round nose and tail rectangular piers were tested in both configurations of single and two in-line piers. The results of unsteady flow tests also show that the proposed combined countermeasure can protect pier foundation during a flood event. Specifically, it seems that the proposed countermeasure is more effective when it is applied to round nose and tail rectangular piers than circular ones.

## Acknowledgements

This work is result of three years of my life spent to improve my knowledge about pier scouring phenomenon. I hope to be also useful for other researchers who are interested in this topic.

An interesting aspect of my study was to live abroad. This opportunity helped me to know, meet or contact new people from several countries who guided, helped and encouraged me for a better progress during my PhD course.

First and foremost, I would like to thank Prof. Francesco Calomino *Dipartimento di Difesa del Suolo “V. Marone”*, *Università della Calabria*, for his advice and ideas along the way. His recommendations in laboratory and during the experiments were priceless.

In the course of the study, I received much advice and assistance from several people. In particular, I wish to thank following people:

Prof. Subhasish Dey of the Indian Institute of Technology, Kharagpur, West Bengal, India, and Prof. António H. Cardoso of the *Instituto Superior Técnico, Universidade Técnica de Lisboa*, Lisboa, Portugal, for their advice about experiment conditions;

Prof. Robert Ettema, Dean of the College of Engineering and Applied Science, Univ. of Wyoming at Laramie, USA, Prof. Amir R. Zarrati of the Dept. of Civil and Environmental Engineering, Amirkabir University of Technology, Iran, Prof. Emeritus Subhash C. Jain of the College of Engineering, The Univ. of Iowa at Iowa City, USA, Prof. Yee-Meng Chiew, Head of the Division of Environmental and Water Resources Engineering, Nanyang Technological Univ., Singapore, and Prof. Umesh C. Kothiyari of the Department of Civil Engineering, Indian Institute of Technology, Roorkee, India, for their extra-explanations about their research articles;

Prof. Gary Parker of the Dept. of Civil and Environmental Engineering and Dept. of Geology, Univ. of Illinois at Urbana-Champaign, USA, and Prof. Peder Hjorth of the Department

## Acknowledgements

---

of Water Resources Engineering, Lund University, Lund, Sweden, for sending their valuable report and bulletin;

Dr. Luigi De Napoli of *Dipartimento di Meccanica, Università della Calabria*, for having lent the 3D Laser scanner instrument and related scientific supports;

Mr. Carlo Lauria of *Laboratorio di Geotecnica, Dipartimento di Difesa del Suolo “V. Marone”, Università della Calabria*, for sediment grading analysis;

Dr. Carmelo Grimaldi of the Hydraulic Structures Division, Lombardi SA Engineering Limited, Switzerland, and Eng. Francesco Greco, who graduated in our Department, for giving their outstanding thesis. Specially Carmelo’ thesis was a comprehensive guideline for me to design and conduct my experiments.

I also would like to thank all my friends, office-mates, colleagues and anyone who has helped me in any manner.

Last, but not least, I wish to thanks my family, in particular my parents. They encouraged me during my study to overcome all the problems. Without their encouragements this study would never have been finished.

The financial support received from *Università della Calabria, Scuola di Dottorato “Pitagora” in Scienze Ingegneristiche* is acknowledged.

## LIST OF TABLES

Tab. 1. Percentage of points falling below, inside and over the $\pm 10\%$ bands in clear-water condition.....	18
Tab. 2. Percentage of points falling below, inside and over the $\pm 10\%$ bands in live-bed condition .....	18
Tab. 3. Percentage of points falling inside the asymmetric bands.....	21
Tab. 4. Effective parameters for scouring at bridge piers .....	24
Tab. 5. Required conditions to achieve the maximum scour depth at a circular pier .....	33
Tab. 6. Grain-size distribution of the sand before and after sieving .....	67
Tab. 7. Grain-size distribution of the sand before and after sieving .....	67
Tab. 8. Observations of the tests to estimate critical velocity of sediment movement .....	69
Tab. 9. Experimental conditions of tests S0 to S23 and at the peak flow of test U00 .....	70
Tab. 10. Experimental conditions at the peak flow of tests U0 to U8 .....	70
Tab. 11. Comparison of experimental conditions and results of test S0 with some other tests.....	89
Tab. 12. Geometric parameters of configurations in tests S1 and S2 .....	90
Tab. 13. Results of tests S1 and S2.....	91
Tab. 14. Experimental conditions and best efficiency of transverse sacrificial piles by Haque <i>et al.</i> (2007) .....	96
Tab. 15. Geometric parameters of countermeasure of test S3 .....	97
Tab. 16. Results of test S3.....	102

## List of tables

---

Tab. 17. Experimental conditions and results in application of a $3b$ -wide collar at the bed level.....	102
Tab. 18. Configuration and results of test S4 .....	105
Tab. 19. Experimental conditions and results of optimum configuration of threading by Dey <i>et al.</i> (2006) .....	105
Tab. 20. Results of experiments with slot (tests S5 to S8).....	107
Tab. 21. Experimental conditions and results of tests with slot ( $l_s=h$ ) by Grimaldi <i>et al.</i> (2009b).....	113
Tab. 22. Geometric parameters of countermeasures of tests S9 and S10.....	118
Tab. 23. Results of tests S9 and S10 .....	119
Tab. 24. Geometric parameters of countermeasures in test S11.....	120
Tab. 25. Results of test S11.....	121
Tab. 26. Geometric parameters of countermeasures in test S12.....	123
Tab. 27. Results of test S12.....	123
Tab. 28. Configurations and efficiencies in the combinations of a bed-sill and a collar .....	128
Tab. 29. Definitions and recommended values for the best configuration.....	144
Tab. 30. Configurations of unsteady flow tests .....	150
Tab. 31. Efficiency of the proposed combined countermeasures in unsteady flow tests .....	176

## LIST OF FIGURES

Fig. 1. Examples of scour at bridge pier foundation or bridge collapse due to pier scour .....	2
Fig. 2. (a) Components of total scour; (b) effective agents in local scouring process .....	3
Fig. 3. Direction and magnitude of normalised mean velocity ahead of the pier at equilibrium (Melville and Raudkivi, 1977).....	6
Fig. 4. Topological structure of flow upstream to cylinder (modified from Dargahi, 1990) .....	7
Fig. 5. (a, b) Non-dimensional velocity field and (c, d) vorticity field ( $s^{-1}$ ) in the plane of symmetry (modified from Graf and Istiarto, 2002) .....	8
Fig. 6. Streamline plots of the flow in the channel symmetry axis (Modified from Unger and Hager, 2007) .....	9
Fig. 7. Scour profiles along the plane of symmetry: A=upper slope; B=lower slope; C=concave slope (modified from Dargahi, 1990) .....	10
Fig. 8. General scour patterns upstream to cylinder along plane of symmetry (modified from Dargahi, 1990).....	11
Fig. 9. locations of initial scours around the pier (modified from Gao <i>et al.</i> , 1993) .....	12
Fig. 10. Results of some previous studies in simulation of flow and scour at pier using numerical models .....	14
Fig. 11. Comparison of scour depths predicted by formulae taken two by two (formula A on the abscissa) .....	20
Fig. 12. Comparison of predicted and observed values of the scour depths in clear-water condition.....	21
Fig. 13. Comparison of predicted and observed values of the scour depths in live-bed condition.....	22

## List of figures

---

Fig. 14. Local scour depth variation with flow intensity (modified from Melville and Coleman, 2000) ...	26
Fig. 15. Distribution of approaching flow velocity for: (a) $B/h \leq 3$ ; (b) $B/h > 5$ (modified from Graf and Altinakar, 1998).....	26
Fig. 16. Variation of the sediment size corrective factor with the sediment coarseness in different studies .....	27
Fig. 17. Influence of sediment size on scour depth: (a) Raudkivi and Ettema (1983); (b) Chiew and Melville (1987).....	28
Fig. 18. Variation of the flow depth corrective factor with the flow shallowness.....	29
Fig. 19. Stagnation pressure head ( $H$ ) for two pier sizes in the same flow (Ettema <i>et al.</i> , 1998a).....	31
Fig. 20. Variation of $d_{se0}/b$ with $b$ and $Fr_p$ for constant approaching flow velocity (Ettema <i>et al.</i> , 2006)..	32
Fig. 21. Main types of riprap failure (Chiew, 1995; Lauchlan and Melville, 2001).....	36
Fig. 22. Classification of flow-altering countermeasures against pier scouring.....	37
Fig. 23. Configuration of internal connecting tubes: (a) side view; (b) typical cross-sections (modified from Abd El-Razek <i>et al.</i> , 2003) .....	38
Fig. 24. Partial pier group ( $\theta=60^\circ$ ); (a) side view; (b) plan view (Vittal <i>et al.</i> , 1994).....	39
Fig. 25. (a) Configuration of a slot through a pier; b) scour depth reduction versus angle of attack (modified from Kumar <i>et al.</i> , 1999).....	39
Fig. 26. Equilibrium scour reduction versus angle of attack for an in-line pier group of three circular piers with slots; (a) $s/b=2$ ; (b) $s/b=4$ (modified from Heidarpour <i>et al.</i> , 2003) .....	41
Fig. 27. Application of (a) single, (b) double and (c) triple threading as pier scour countermeasure (Dey <i>et al.</i> , 2006).....	42
Fig. 28. Configurations of collars or plates attached to a circular pier: (a) circular collar; (b) horizontal plate (Kim <i>et al.</i> , 2005); (c) Joukowski collar (Dargahi, 1987); (d) quadrangular collar (Sani Khani <i>et al.</i> , 2008).....	42
Fig. 29. Time evolution of the scour depth for an unprotected pier and a pier with collar (modified from Mashahir <i>et al.</i> , 2004) .....	44
Fig. 30. (a) side view of attachment of several collars to a pier (Richardson and York, 1999); (b) plan view of attachment of a collar to a rectangular pier with circular nose and tail (Zarrati <i>et al.</i> , 2004); (c) plan view of independent collars for a transverse group of two circular piers; (d) plan view of a continuous collar for an in-line group of two circular piers (Zarrati <i>et al.</i> , 2006).....	45
Fig. 31. Different types of pier-attached plates and vanes .....	46



Fig. 32. (a) General arrangement of a triangular array of sacrificial piles upstream to a circular pier (Melville and Hadfield, 1999); (b) configuration of transverse sacrificial piles upstream to a rectangular pier (Haque *et al.*, 2007) ..... 48

Fig. 33. Submerged vanes (Iowa vanes): (a) general configuration; (b) curve vanes (Odgaard and Wang, 1987); (c) flat plates (Lauchlan, 1999)..... 49

Fig. 34. Configuration of (a) single and (b) double submerged vanes (Ghorbani and Kells, 2008)..... 50

Fig. 35. Application of a sacrificial sill upstream to a square pier (Chiew and Lim, 2003)..... 51

Fig. 36. Permeable sheet piles; (a) uncovered; (b) partially covered with plates; (c) completely covered with plates (Parker *et al.*, 1998)..... 52

Fig. 37. Configuration of a downstream bed-sill (Grimaldi *et al.*, 2009a)..... 53

Fig. 38. Configuration of surface guide panels (Huang *et al.*, 2005)..... 53

Fig. 39. Configuration of a collared sleeve (Singh *et al.*, 2001)..... 54

Fig. 40. Suction applied to a circular pier (modified from Parker *et al.*, 1998) ..... 55

Fig. 41. Some of the most effective pier shapes for local scour depth reduction ..... 56

Fig. 42. Configuration of a circular pier with a foundation..... 56

Fig. 43. (a) Combination of riprap and collar (Zarrati *et al.*, 2006); (b) combination of pier plates and collar (Odgaard and Wang, 1987)..... 58

Fig. 44. General view of the flume ..... 64

Fig. 45. Plan-view of the flume and other facilities (units: cm) ..... 64

Fig. 46. Side-view of the flume (units: cm) ..... 65

Fig. 47. (a) Recess box; (b) and adjustable tailgate ..... 65

Fig. 48. (a) Jacks; (b) caulking the borders of the tailgate ..... 66

Fig. 49. Size distribution curve of bed sediment ..... 68

Fig. 50. (a) Aluminium bar and (b) trowels used to level the sediment bed ..... 70

Fig. 51. (a) Hose to fill the flume from downstream; (b) point gauge; (c) dental mirror to control the level of point gauge tip in collar tests..... 71

Fig. 52. Application of two-part pier (a): before and (b): after starting the test ..... 72

Fig. 53. (a) Sand coverage on the false floor before and (b ,c) after a test with peak flow in live-bed conditions..... 72

## List of figures

---

Fig. 54. (a) Motorised valve; (b) electrical current regulator .....	73
Fig. 55. Imposed hydrograph with the peak in clear-water condition (test U00) .....	74
Fig. 56. Imposed hydrograph with the peak in live-bed condition (test U0).....	74
Fig. 57. Relation between flow discharge and approach flow depth .....	74
Fig. 58. Relation between flow discharge and approach flow velocity .....	75
Fig. 59. Variation of approach flow depth during hydrograph test.....	75
Fig. 60. Variation of flow intensity during hydrograph test .....	75
Fig. 61. Configuration and scour hole at the end of test S14 .....	77
Fig. 62. (a) Temporal evolution of the maximum scour depth at two locations in test S14; (b) close up of the maximum scour depth temporal evolution for values of $Ut/b > 10^6$ .....	77
Fig. 63. Identification of phases in scouring process.....	78
Fig. 64. Definition of time to equilibrium according to Cardoso and Bettess (1999) for a single pier test (modified from Lança <i>et al.</i> , 2010).....	78
Fig. 65. Temporal evolution of scour depth in front of pier in tests S0 and Grimaldi (2005).....	80
Fig. 66. Temporal evolution of scour depth at the pier in tests S0 and Lança <i>et al.</i> (2010).....	80
Fig. 67. Comparison of unprotected pier test (S0, present study) with test #5 by Lança <i>et al.</i> (2010).....	81
Fig. 68. End scour depth based on data of test S0 and (E.14) .....	82
Fig. 69. Dimensionless ratio $d_s/d_{se0}$ vs. $t/t_e$ ; (a) test S0; (b) from Melville and Chiew (1999) .....	82
Fig. 70. (a) Schema to illustrate the scour in front of a bed-sill and (b) around a bordered-collar.....	83
Fig. 71. Scour hole at the end of test S0.....	86
Fig. 72. 3D pattern of scour in test S0 at equilibrium (units: mm) .....	86
Fig. 73. Contour lines of equilibrium scour hole in test S0 (units: mm) .....	86
Fig. 74. Coefficient $K_\sigma$ as a function of $\sigma_g$ ( Breusers and Raudkivi, 1991) .....	87
Fig. 75. Bed-forms downstream of the pier scour; (a) test S0; (b) Melville and Raudkivi (1977) .....	88
Fig. 76. Contour lines of equilibrium scour hole at unprotected pier (Mansueto, 2009) (units: mm) .....	88
Fig. 77. Contour lines of equilibrium scour hole in test A0 by Grimaldi (2005) (units: m) .....	89
Fig. 78. Configuration of transverse sacrificial piles; (a) test S1; (b) test S2.....	90

Fig. 79. Temporal evolution of scour depth in front of the pier in tests S0, S1 and S2 ..... 91

Fig. 80. Scour around the pier in test S1; (a) filling the pier scour by sediments eroded around the piles; (b) scour hole at the end of test..... 91

Fig. 81. 3D pattern of equilibrium scour hole in test S1 (units: mm) ..... 92

Fig. 82. Contour lines of equilibrium scour hole in test S1 (units: mm) ..... 92

Fig. 83. (a) Scour after 2 min; (b) scour hole at the end of test S2 ..... 93

Fig. 84. 3D pattern of equilibrium scour hole in test S2 (units: mm) ..... 93

Fig. 85. Contour lines of equilibrium scour hole in test S2 (units: mm) ..... 94

Fig. 86. Plan view of separation vortices for rectangular piers (modified from Ettema *et al.*, 1998b)..... 94

Fig. 87. Dimensionless ratio  $d_{sc0}/b$  versus  $L/b$  for rectangular piers (modified from Ettema *et al.*, 1998b) 95

Fig. 88. Comparison of temporal evolution of scour depth at piers protected with  $2b$  and  $3b$  collars flush with the initial bed level (modified from Mashahir *et al.* 2004)..... 97

Fig. 89. Schematic pattern of scour development around a collar ( $w_c=3b$ )..... 97

Fig. 90. Scour evolution around pier protected with collar (test S3) ..... 98

Fig. 91. Temporal evolution of scour depth in front of the pier in tests S0 and S3 ..... 99

Fig. 92. 3D pattern of equilibrium scour hole in test S3 (units: mm) ..... 99

Fig. 93. Contour lines of equilibrium scour hole in test S3 (units: mm) ..... 100

Fig. 94. Sketch of horseshoe vortex on a rigid flat bed (modified from Muzzammil and Gangadhariah, 2003)..... 101

Fig. 95. Vortex size on a rigid bed (modified from Muzzammil and Gangadhariah, 2003) ..... 101

Fig. 96. (a) A pier protected with threading; (b) scour hole at the end of test S4..... 103

Fig. 97. Temporal evolution of scour depth in front of the pier in tests S0 and S4 ..... 104

Fig. 98. 3D pattern of equilibrium scour hole in test S4 (units: mm) ..... 104

Fig. 99. Contour lines of equilibrium scour hole in test S4 (units: mm) ..... 105

Fig. 100. Flow depth adjustment factor (modified from Raudkivi and Ettema, 1983)..... 106

Fig. 101. Temporal evolution of scour depth in front of the pier in tests S0 and S5 to S8 ..... 107

Fig. 102. Comparison of scour depth evolution in present study with Grimaldi's (2005) data in pier slot tests ..... 108

## List of figures

---

Fig. 103. Scour hole at the end of tests (a) S5; (b) S6; (c) S7; (d) S8.....	109
Fig. 104. 3D pattern of equilibrium scour hole in test S5 (units: mm) .....	109
Fig. 105. Contour lines of equilibrium scour hole in test S5 (units: mm).....	110
Fig. 106. 3D pattern of equilibrium scour hole in test S6 (units: mm) .....	110
Fig. 107. Contour lines of equilibrium scour hole in test S6 (units: mm).....	111
Fig. 108. 3D scour pattern around the pier in test S7 (units: mm).....	111
Fig. 109. Contour lines of equilibrium scour hole in test S7 (units: mm).....	112
Fig. 110. 3D scour pattern in test S8 (units: mm).....	112
Fig. 111. Contour lines of equilibrium scour hole test S8 (units: mm).....	113
Fig. 112. Configuration of tests S5 to S8 (units: mm) .....	114
Fig. 113. Configuration of test series A by Grimaldi <i>et al.</i> (2009b) (units: mm) .....	114
Fig. 114. Configuration of test series B by Grimaldi <i>et al.</i> (2009b) (units: mm) .....	114
Fig. 115. Configuration of test series C by Grimaldi <i>et al.</i> (2009b) (units: mm) .....	115
Fig. 116. Relationship of $r_{de}$ versus $(d_{se}-z_s)/b$ .....	116
Fig. 117. Effect of a slot positioned near the water surface on scour depth (Chiew, 1992).....	117
Fig. 118. Temporal evolution of scour depth downstream of collar in tests S9 and S10.....	118
Fig. 119. Scour hole at the end of tests (a) S9 and (b) S10 .....	119
Fig. 120. Longitudinal profile of the scoured bed in test S9 .....	119
Fig. 121. Schema of passage flow through the pier slot .....	119
Fig. 122. (a): Configuration of test S11 before starting the test and (b): scour hole at the end of test S11.	120
Fig. 123. Temporal evolution of scour depth in front of the pier in tests S0, S1, S5 and S11 .....	121
Fig. 124. 3D pattern of equilibrium scour hole in test S11 (units: mm) .....	121
Fig. 125. Contour lines of equilibrium scour hole in test S11 (units: mm).....	122
Fig. 126. (a) Scour intrusion from upstream of the collar; (b) scour hole at the end of test S12.....	123
Fig. 127. Temporal evolution of scour depth in front of the pier in tests S0, S1, S3 and S12 .....	123
Fig. 128. 3D pattern of equilibrium scour hole in test S12 (units: mm) .....	124

Fig. 129. Contour lines of equilibrium scour hole in test S12 (units: mm) ..... 124

Fig. 130. Configuration of test S13..... 125

Fig. 131. Temporal evolution of the maximum scour depth in tests S0 and S13 ..... 126

Fig. 132. Scour hole at different time instants in test S13..... 127

Fig. 133. Contour lines of equilibrium scour hole in test S13 (units: mm) ..... 128

Fig. 134. Contour lines of equilibrium scour hole in test S14 (units: mm) ..... 129

Fig. 135. Scour hole at different time instants in test S14..... 130

Fig. 136. Temporal evolution of the maximum scour depth in tests S0 and S14 ..... 131

Fig. 137. Scour around the pier in test S15 ..... 132

Fig. 138. Contour lines of equilibrium scour hole in test S15 (units: mm) ..... 132

Fig. 139. Temporal evolution of the maximum scour depth in the movable bed in tests S0 and S15 ..... 133

Fig. 140. (a) Initial configuration of test S16; (b) scour hole at the end of the test ..... 133

Fig. 141. Contour lines of equilibrium scour hole in test S16 (units: mm) ..... 134

Fig. 142. Temporal evolution of the maximum scour depth in tests S0 and S16 ..... 134

Fig. 143. Configuration and dimensions of the bordered-collar used in tests S17 to S22 ..... 135

Fig. 144. Configuration of test S17..... 136

Fig. 145. Scour progress in test S17 ..... 136

Fig. 146. Temporal evolution of the maximum scour depth in tests S0 and S17 ..... 137

Fig. 147. Scour hole at the end of test S17..... 137

Fig. 148. Configuration and contour lines of equilibrium scour hole in test S17 (units: mm) ..... 137

Fig. 149. Scour hole at the end of test S18..... 138

Fig. 150. Temporal evolution of scour depth in front of the bed-sill in tests S18, S19 and S20 ..... 139

Fig. 151. (a) Initial configuration of test S19; (b) scour hole at the end of the test ..... 139

Fig. 152. (a) Scour hole after 1 day for test S20; (b) scour hole at the end of the test..... 140

Fig. 153. (a) Location of possible passage of scour towards upstream of the bed-sill; (b) improved configuration in test S21 ..... 141

Fig. 154. (a) Grooves at  $t=8$  min in test S21; (b) scour hole at the end of the test ..... 141

## List of figures

---

Fig. 155. Temporal evolution of the maximum scour depth in tests S0 and S21 .....	141
Fig. 156. Movable bed in test S22: (a) initial configuration; (b, c) at the end of the test.....	142
Fig. 157. Contour lines of equilibrium scour hole in test S22 (units: mm) .....	143
Fig. 158. Temporal evolution of the maximum scour depth in the movable bed in tests S0 and S22 .....	143
Fig. 159. (a) A cut-collar; (b) border; (c) a bordered cut-collar ( $t_{cb}=b$ ) .....	144
Fig. 160. Proposed configuration for pier protection with higher priority .....	145
Fig. 161. Sketch showing possible optimum shape of the bed-sill.....	146
Fig. 162. Temporal evolution of the maximum scour depth in the movable bed in test S23 .....	146
Fig. 163. Contour lines of equilibrium scour hole in test S23.....	147
Fig. 164. (a) Movable bed at the end of test S23; (b) exposure of the border .....	147
Fig. 165. Preliminary estimation of maximum scour intrusion to upstream of the bed-sill (units: mm) ...	148
Fig. 166. Configuration of the proposed combined countermeasure with lower priority .....	149
Fig. 167. Proposed combined countermeasure for unsteady flow tests .....	150
Fig. 168. Hydrograph and temporal evolution of scour depth in front of the pier in test U00 .....	152
Fig. 169. Scour pattern at the end of test U00 .....	152
Fig. 170. Hydrograph and temporal evolution of scour depth in front of the pier in test U0.....	153
Fig. 171. Longitudinal profile of the scour hole in the plane of symmetry at the end of test U0 .....	154
Fig. 172. Scour pattern at the end of test U0 .....	154
Fig. 173. (a) Variation of local scour depth with flow intensity (modified from Melville and Coleman, 2000); (b) temporal evolution of scour depth in clear-water and live-bed conditions.....	155
Fig. 174. Temporal evolution of the scour depth in front of the pier in tests S0, U0 and U00.....	156
Fig. 175. Configuration and location of maximum scour depth at the end of test U1 (units: cm).....	157
Fig. 176. Hydrograph and temporal evolution of the maximum scour depth in the movable bed in test U1 .....	157
Fig. 177. (a) General scour pattern of scour at the end of test U1; (b) close up of the scour hole near the border of the cut-collar at the end of the test.....	158
Fig. 178. Scour hole at different time instants in test U2.....	160
Fig. 179. Hydrograph and temporal evolution of scour depth in front of the pier in test U2.....	161

Fig. 180. Longitudinal profile of the scour hole in the plane of symmetry at the end of test U2 ..... 161

Fig. 181. Bordered cut-collar adapted to a round nose and tail rectangular pier ( $t_{cb}=b$ )..... 162

Fig. 182. Configuration and location of the maximum scour depths at the end of test U3 (units: cm) ..... 163

Fig. 183. Hydrograph and temporal evolution of the maximum scour depth in zones A and B in test U3 163

Fig. 184. (a) Scour pattern at the end of test U3; (b) close up of scour hole downstream of the bordered cut-collar ..... 164

Fig. 185. Configuration of test U4 and location of the maximum scour depths at the end of the test (units: cm)..... 165

Fig. 186. Scour development in test U4..... 166

Fig. 187. Hydrograph and temporal evolution of scour depth in front of the piers in test U4 ..... 167

Fig. 188. Longitudinal profile of the scour hole in the plane of symmetry at the end of test U4 ..... 167

Fig. 189. Configuration and location of the maximum scour depths at the end of test U5 (units: cm) ..... 168

Fig. 190. Hydrograph and temporal evolution of the maximum scour depth in zones A and B in test U5 169

Fig. 191. Scour pattern at different times in test U5 ..... 169

Fig. 192. Configuration and location of the maximum scour depths at the end of test U6 (units: cm) ..... 170

Fig. 193. Hydrograph and temporal evolution of scour depth in front of each pier in test U6..... 170

Fig. 194. Longitudinal profile of the scour holes in the plane of symmetry at the end of test U6..... 171

Fig. 195. Scour pattern at the end of test U6 ..... 171

Fig. 196. Configuration and location of the maximum scour depths at the end of test U7 (units: cm) ..... 172

Fig. 197. Hydrograph and temporal evolution of the maximum scour depth in zones A to D in test U7 .. 173

Fig. 198. Scour pattern at the end of test U7 ..... 173

Fig. 199. Configuration and location of the maximum scour depths at the end of test U8 (units: cm) ..... 174

Fig. 200. Hydrograph and temporal evolution of the maximum scour depths in zones A to C in test U8. 175

Fig. 201. Scour pattern at the end of test U8 ..... 175

Fig. 202. Scour downstream of a collar in a test with a combined countermeasure of collar and bed-sill 177

Fig. 203. Temporal evolution of the maximum scour depth downstream of bed-sill (modified from Gaudio and Marion, 2003) ..... 178

## List of figures

---

Fig. A1. Geometrical properties of the Thomson weir used to measure flow; (a) front view of the weir; (b) detail of the weir edge (units: cm) .....	A2
Fig. A2. Longitudinal section of the caisson holding the weir (units: cm) .....	A2
Fig. A3. Schema of point gauge fitted with a decimal vernier; (a) placed in the piezometer; (b) installed above the caisson .....	A2
Fig. A4. Identification of measurement sections, inside the caisson to determine $zero_T$ .....	A4
Fig. A5. (a) Verification of the pressure transducer <i>Druck</i> ; (b) LED display panel of <i>DPI 280 Series</i> ; (c) channel board; (d) pressure transducer connected to the piezometer.....	A6
Fig. A6. Relations of average voltage in 30 seconds and water level inside the piezometer .....	A6
Fig. B1. (a) 3D laser scanner (model Vivid 300/VI-300 produced by Minolta); (b) sketch (units: mm) ...	B2
Fig. B2. Main elements of the 3D laser scanner .....	B2
Fig. B3. Schema of a sensor that operates on the basis of the principle of similar triangles.....	B3
Fig. B4. Operation of the Galvano mirror for emission of laser on predetermined area.....	B3
Fig. B5. Distance between 3D laser scanner and object surface ( $H_L$ ).....	B4
Fig. B6. Two separate images (a) before and (b) after merging .....	B5
Fig. B7. Details of the installation used to acquire the eroded surface .....	B6
Fig. B8. Flowchart of preparing 3D pattern and contour lines of bed surface using 3D laser scanner.....	B7



## SYMBOLS

$A_e$ [L <sup>3</sup> ]	= planimetric area of scour hole at a pier protected with a countermeasure
$A_{e0}$ [L <sup>3</sup> ]	= planimetric area of scour hole at an unprotected pier
$B$ [L]	= top width of the channel cross section
$b$ [L]	= pier width
$b_e$ [L]	= pier width projected orthogonally to the approach flow
$b_f$ [L]	= diameter of cylindrical foundation
$b_g$ [L]	= diameter of individual piers in a pier group countermeasure
$b_p$ [L]	= pier width projected on the transversal axis of the pile group
$b_r$	= blockage ratio
$b_s$ [L]	= pier width smaller than $b$ ( $b_s < b$ )
$D_p$ [L]	= pile diameter
$D_s$ [L]	= sleeve diameter
$D_v$ [L]	= diameter of primary vortex or mean vortex size
$d$ [L]	= opening diameter of internal connecting tubes
$d_{16, 84, 95}$ [L]	= sediment size for which 16%, 84%, 95% by weight of sediment is finer, respectively
$d_{50}$ [L]	= median grain size of sediments
$d_c$ [L]	= threading cable diameter
$d_s$ [L]	= scour depth
$d_{s0}$ [L]	= maximum scour depth in proximity to unprotected pier during the test
$d_{scb}$ [L]	= maximum scour depth under the collar or adjacent to the collar border during the test
$d_{se}$ [L]	= equilibrium maximum scour depth in proximity to protected pier
$d_{se0}$ [L]	= equilibrium maximum scour depth for unprotected pier
$d_{sec}$ [L]	= maximum scour depth under the collar or adjacent to the collar border at equilibrium

## Symbols

---

$d_{sem}$ [L]	= equilibrium maximum scour depth in the whole movable bed
$d_{sm}$ [L]	= maximum scour depth in the whole movable bed during the test
$d_{sp}$ [L]	= maximum scour depth in proximity to protected pier during the test
$e$ [L]	= pier roughness
$e_v$ [L]	= longitudinal spacing of submerged vanes
$Fr=U/(gh)^{0.5}$	= Froude number
$Fr_c=U_c/(gh)^{0.5}$	= critical Froude number
$G$	= parameter describing the effect of the lateral distribution of flow in approach channel
$g$ [LT <sup>-2</sup> ]	= gravity acceleration
$H$ [L]	= stagnation head
$h$ [L]	= undisturbed approach flow depth
$h_{bs}$ [L]	= bed-sill elevation above the bed
$h_c$ [L]	= distance of collar from the water surface
$h_i$ [L]	= distance between openings in internal connecting tubes
$H_L$ [L]	= distance between 3D laser scanner and object surface
$h_T$ [L]	= water head respect to the lowest point of Thomson weir
$h_v$ [L]	= height of submerged vanes measured from average bed level
$h'_{50}$ [L]	= level of water surface 50 cm at caisson upstream to weir vertex
$h'_{p,fin}$ [L]	= final level of piezometer connected to caisson
$h'_{p,in}$ [L]	= initial level of piezometer connected to caisson
$h'_v$ [L]	= level of lowest point on weir vertex
$K_1$	= correction factor for pier nose shape
$K_2$	= correction factor for angle of attack
$K_3$	= correction factor for bed condition
$K_4$	= correction factor for bed armouring
$K_d$	= sediment size (adjustment) factor
$K_G$	= channel geometry factor
$K_h$	= flow depth (adjustment) factor
$K_{hb}$ [L]	= depth scale factor
$K_I$	= flow intensity factor
$K_s$	= pier shape factor
$K_w$	= correction factor for wide piers in shallow water
$K_\theta$	= pier alignment factor
$K_\sigma$	= sediment grading (adjustment) factor
$L$ [L]	= length of non circular pier
$l_{bs}$ [L]	= centre to centre distance of pier and bed-sill
$l_p$ [L]	= distance between panel and pier in surface guide panels
$l_v$ [L]	= submerged vane length
$l_s$ [L]	= slot length
$l_{sw}$ [L]	= side-wall length
$m$	= number of selected formulae

$n [L^{-1/3}T]$	= Manning's roughness coefficient
$N_p$	= number of piles
$o_w [L]$	= leading opening of surface guide panels
$p_1, p_3, p_5 [L]$	= parameters which are obtained by regression analysis
$p_2, p_4, p_6 [L^{-1}T^{-1}]$	= parameters which are obtained by regression analysis
$P_d [L]$	= submerged depth of panel in surface guide panels
$p_w [L]$	= weir height
$Q [L^3T^{-1}]$	= discharge
$R^2$	= coefficient of determination
$R_h [L]$	= hydraulic radius
$Re_p = Ub/v$	= pier Reynolds number
$r$	= radius of circular pier
$r_1$	= arc radius, distance between the location of the maximum scour depth downstream of the bed-sill and the upstream uneroded bed
$r_2 = 1.2r_1$	= arc radius, maximum scour intrusion upstream of the bed sill, with respect to the location of the maximum scour depth downstream of the bed-sill
$r_A$	= a factor related to liquid area reduction in the caisson of weir
$r_{Ae}$	= planimetric scour area reduction at the equilibrium condition
$r_{de}$	= scour depth reduction at the equilibrium condition
$r_{ds}$	= scour depth reduction at the end of test (equilibrium probably not achieved)
$r_{Ve}$	= scour volume reduction at the equilibrium condition
$S$	= channel-bed (riverbed) slop
$S_f$	= friction slope
$s [L]$	= pier spacing in pier group
$t [T]$	= time
$t^* [T]$	= time at which the bed-sill downstream of the pier starts to be effective
$t_{bs} [L]$	= bed-sill thickness
$t_c [L]$	= collar thickness
$t_{cb} [L]$	= bordered-collar thickness
$t_d [T]$	= test duration
$t_e [L]$	= time to equilibrium
$t_w [L]$	= thickness of weir
$U [LT^{-1}]$	= approach flow velocity
$U_a [LT^{-1}]$	= mean approaching flow velocity at the armour peak
$U_c [LT^{-1}]$	= critical flow velocity for the beginning of sediment motion
$U_{cp} [LT^{-1}]$	= critical velocity for the motion of sediment particles at the pier nose
$u [LT^{-1}]$	= velocity component in the streamwise $x$ direction
$u^* [LT^{-1}]$	= shear velocity
$u^*_c [LT^{-1}]$	= shear velocity at initiation of sediment motion
$V_e [L^3]$	= volume of scour hole at a pier protected with a countermeasure
$V_{e0} [L^3]$	= volume of scour hole at an unprotected pier

## Symbols

---

$w$ [ $LT^{-1}$ ]	= velocity component in vertical $z$ direction
$w_{bs}$ [L]	= bed-sill width
$w_c$ [L]	= collar width
$w_s$ [L]	= slot width
$x$ [L]	= Cartesian coordinate in the longitudinal direction
$X_0$ [L]	= distance of side openings with respect to the upstream opening in internal connecting tubes
$x_0$ [L]	= horizontal dimension of the vortex
$X_p$ [L]	= distance from the transversal axis of the pile group to the upstream pier face
$X_v$ [L]	= displacement of vanes from upstream pier face
$y$ [L]	= Cartesian coordinate in the transverse direction
$y_f$ [L]	= depth of top of foundation below initial bed level
$y_L$ [L]	= height of the partial pier group above the bed
$z$ [L]	= Cartesian coordinate in the vertical direction
$z_s$ [L]	= sinking depth of the slot
$z_v$ [L]	= lateral spacing between vanes
$\alpha$	= inclination angle of internal connecting tubes with respect to the approach flow direction
$\alpha_d$	= angle of attack in delta-wing vane
$\alpha_o$	= opening ratio [ $=(B-b)/B$ ]
$\alpha_T$ [L]	= constant in the discharge coefficient of the Thomson weir formula
$\alpha_t$	= thread angle
$\alpha_v$	= vane angle to the approach flow
$\beta$	= angle of attack of undisturbed approach flow or skew angle between approach flow and pier axis
$\gamma_f$	= fluid specific weight
$\gamma_s$	= sediment specific weight
$\Delta$	= submerged sediment specific gravity
$\theta$	= orientation of pier group
$\theta_S$	= Shields mobility parameter
$\theta_s$	= sector angle of double vanes adjacent to the pier
$\theta_v$	= vertical inclination of bed-sill
$\theta_p$	= interior angle of surface guide panels
$\mu$	= discharge coefficient
$\mu_0$	= constant in the discharge coefficient of the Thomson weir formula
$\nu$ [ $L^2T^{-1}$ ]	= kinematic viscosity of the fluid
$\rho$ [ $ML^{-3}$ ]	= mass density of water
$\rho_f$ [ $ML^{-3}$ ]	= mass density of fluid
$\rho_s$ [ $ML^{-3}$ ]	= mass density of sediments
$\rho_s'$ [ $ML^{-3}$ ]	= buoyant sediment density ( $=\rho_s-\rho$ )
$\sigma$ [ $ML^{-1}T^{-2}$ ]	= surface tension

$\sigma_g$	= geometric standard deviation of the grain size distribution
$\tau$ [ML <sup>-1</sup> T <sup>-2</sup> ]	= bed shear stress
$\tau_c$ [ML <sup>-1</sup> T <sup>-2</sup> ]	= critical bed shear stress
$\phi$	= coefficient based on the shape of the pier nose



## Introduction

Flowing water erodes, transports and deposits sediments in the river and continuously changes its bed. Any changes in river bed may be due to natural causes or human activities leading to altered river geometry or river bed. Scour around a bridge pier foundation is an example of human interference in the rivers. Most people, including many civil engineers, who are not familiar with the fluvial hydraulics, imagine that constructing a bridge across a river is entirely a problem of structural engineering. However, results of several investigations regarding bridge failures clarifies that scour around pier foundation is one of the most important causes of bridge damage. According to Murillo (1987), summation of bridge failures due to earthquake, wind, structural problems, corrosion, accidental causes and construction is not greater than the number of failures caused by scouring. Following examples of historical bridge failures also emphasise the importance of scour at bridge piers and abutments:

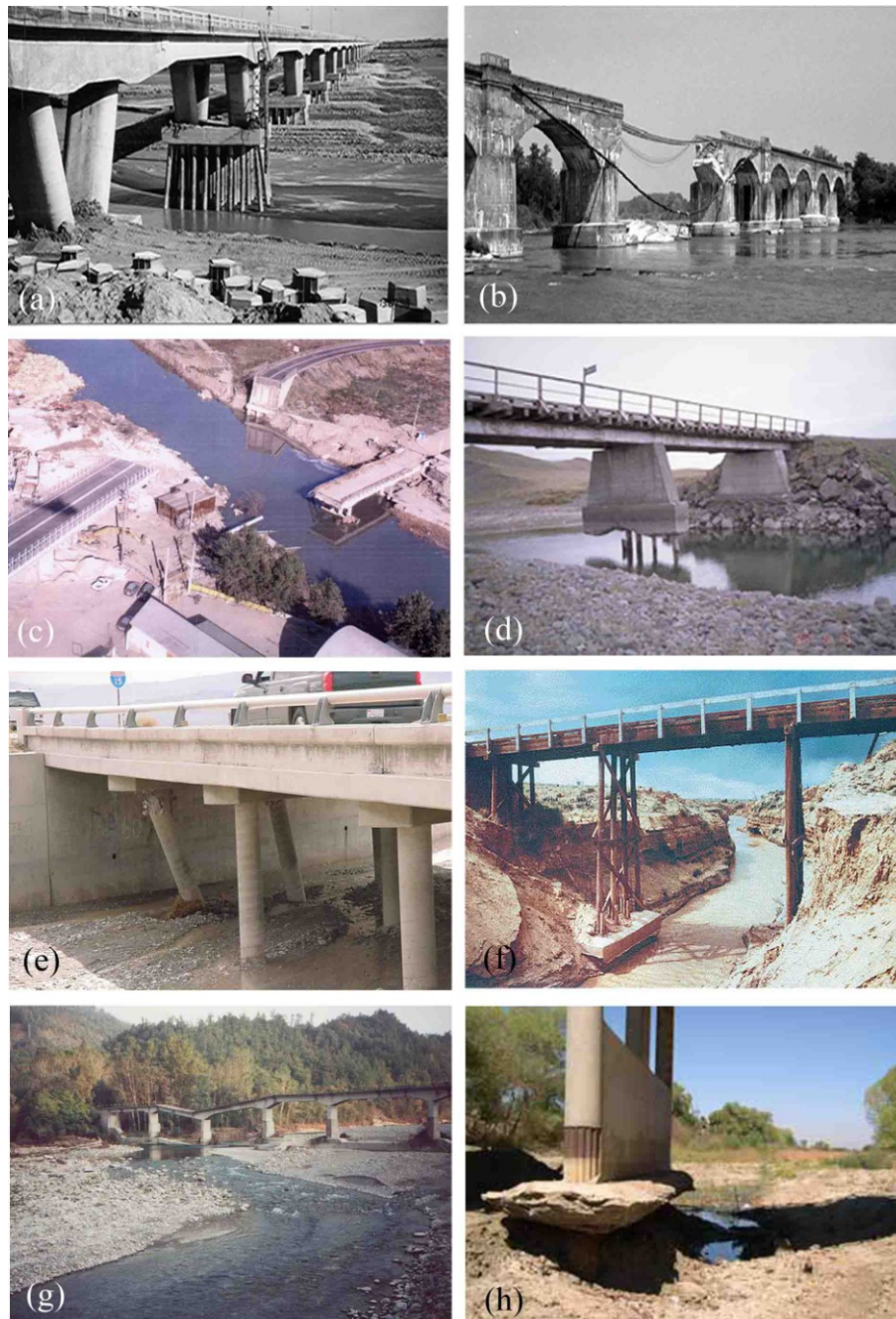
- in 1985, 73 bridges were destroyed by floods in Pennsylvania, Virginia and West Virginia (Richardson and Davis, 2001);
- during the spring floods of 1987, 17 bridges in New York and New England were damaged or destroyed by scour (Richardson and Davis, 2001);
- a report about the most serious bridge damage occurrence between 1960 and 1984 in New Zealand showed that, 29 cases out of 108 were related to abutment scouring (Melville, 1992);
- piers of Turag-Bhakartha Bridge near Dhaka city in Bangladesh were settled during two floods, the former in 1995 and the latter in 1998, owing to scouring (Haque *et al.*, 2007);
- the failure of Kaoping Bridge in Southern Taiwan in August 2000 occurred because of scouring around the piers (Chiew and Lim, 2003).

Figure 1 illustrates some examples of scour at bridge pier foundation or bridge collapse due to pier scour. Figure 1a shows local scour and degradation aggravated by sand extraction at a bridge in Taiwan, Republic of China (Melville and Coleman, 2000). Figure 1b depicts rail bridge failure on the Po River (Turin, Italy) occurred in November 1994 and caused by local scouring at the central pier (Franzetti and Ballio, 1998). Figure 1c shows collapse of two bridges during the

## Introduction

---

flood of the Esaro River (Crotona, Calabria, Italy) in 1996. Other figures are related to other pier scour events occurred all over the world.



**Fig. 1. Examples of scour at bridge pier foundation or bridge collapse due to pier scour**

Three scour types may occur at a bridge site when a pier in a mobile bed interferes with the flow (Raudkivi and Ettema, 1983):

1. general scouring, which would occur regardless of whether the bridge was present or not (Fig. 2a);



2. constriction scouring, which may occur because of the constriction of the waterway;
3. local scouring, which is caused by the local flow field around the pier.

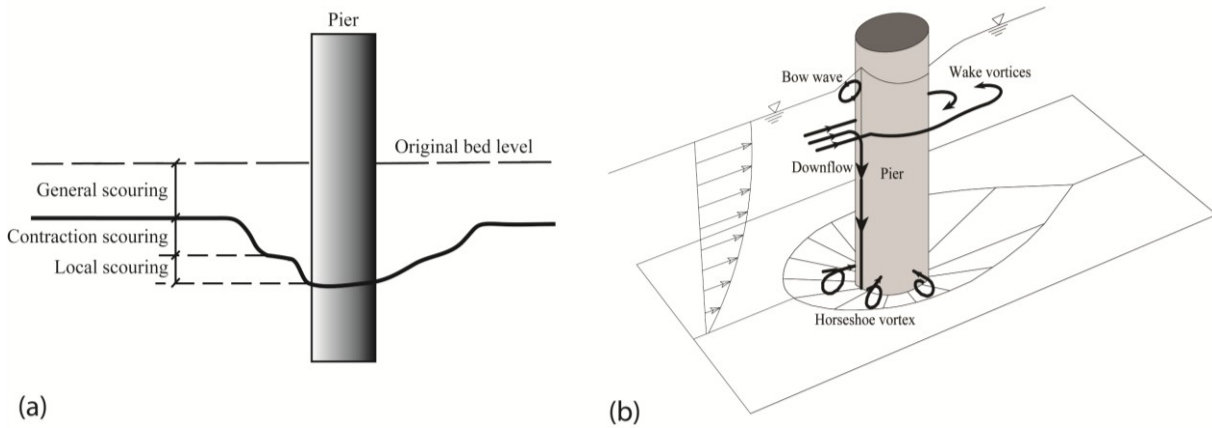


Fig. 2. (a) Components of total scour; (b) effective agents in local scouring process

Detailed explanations about general scouring and constriction scouring (types 1 and 2) can be found in some engineering books and manuals (e.g., Melville and Coleman, 2000; Richardson and Davis, 2001). This study focuses on local scour (type 3) and a specific type of countermeasures called *flow-altering* and used for the scour depth reduction.

The turbulent flow field at a bridge pier embedded vertically in an erodible bed becomes more complex as the scour hole develops. The flow field at a pier was investigated by Hjorth (1975), Dargahi (1990), Dey *et al.* (1995), Graf and Istiarto (2002) and Dey and Raikar (2007). Briefly, approach velocity stagnates at the front face of the pier and causes the formation of a downflow parallel to the pier face and a “bow wave” at the free surface adjacent to the pier (Fig. 2b). Downflow impinges the streambed and interacts with the approaching flow; consequently, a complex vortex system is formed which is called “horseshoe vortex”. It pushes the downflow inside the scour hole closer to the pier. Separation of flow at the two sides of the pier creates other vortices, which are called “wake vortices”. The scour hole develops downstream of the pier owing to the wake vortices. Several parameters may affect the turbulent flow field around the pier and, therefore, the scouring agents. These effective parameters, which are generally dimensionless groups, should respect specific conditions in order to achieve the maximum local scour depth for a certain pier.

Due to the fact that pier scour is an important cause of bridge failures, finding solutions to prevent or at least reduce the scour depth at pier foundation is an important research topic and in this field a large number of studies has been conducted by several researchers during the last decades. All types of countermeasures against local scour at bridge pier are classified in two main groups; namely *bed-armouring* and *flow-altering countermeasures*.

In the first group, the scour protection is provided by physical barriers which are typically large and heavy units that cannot be moved by the flow. In this category, perhaps riprap stones is the most common and economical method to protect bridge piers against local scouring. It is

necessary to indicate that in some cases ripraps encounter different kinds of failure. In this case, Chiew (1995), Chiew and Lim (2000) and Unger and Hager (2006) conducted extensive investigations on four major kinds of riprap failures, e.g. shear failure, winnowing failure, edge failure and embedment failure.

The second method of scour reduction (flow-altering countermeasures) decreases the strength of the eroding agents, i.e. downflow and horseshoe vortex, which are primarily responsible for scouring at the pier foundations. For example, by drilling a slot through a pier, a part of downflow diverts into it and, consequently, vortices may develop with lesser strength at the pier foundation. Up to now, although several investigations have been performed to propose design criteria for the first group of countermeasures, the behaviour of flow-altering countermeasures is almost unclear and further research is needed to define reliable design criteria. Anyway, proper design criteria and implementation guidelines for both groups are necessary to increase the performance of countermeasures and reduce the risk of bridge failure. For instance, the Schoharie Creek Bridge, in New York State, collapsed in April 1987. This disaster focused public attention on the devastating effect that bridge pier scour can have. Ten people were killed in that event. During subsequent investigations it was found that recommended rehabilitation of the riprap protection had not been adopted (Robison, 1995). Probably if clear guidelines had existed for the implementation of riprap this disaster would have been avoided (Lauchlan, 1999).

The aim of this study is to review and consider all types of flow-altering countermeasures in order to identify the efficient and practical ones. New test series have been properly designed and performed for selected countermeasures to ensure about their efficiencies. Countermeasures showing appropriate efficiency have been then combined two by two in order to find the highest efficiency in scour depth reduction. Particular cases typical of Calabrian rivers have been finally considered also in unsteady flow conditions.

The present thesis comprises 6 chapters, as follows.

In the first chapter a general description of pier scouring based on studies available in the literature is presented. Chapter 1 deals specifically with basic knowledge about scouring process, turbulent flow around the pier, numerical modelling of flow around the pier, empirical equations to estimate scour depth.

In the following chapter effective factors and Dimensional Analysis applied to pier scouring is discussed. Therefore, Chapter 2 constitutes a basis to design original experiments.

In Chapter 3 a comprehensive review of flow-altering countermeasures is presented. Countermeasures recommended in the literature are criticised with respect to their efficiency and applicability in the field. In addition, the experiments carried out by other researchers are evaluated according to the proper design of them.

Chapter 4 describes the experimental facilities and procedures. This chapter is an introduction to Chapter 5 which presents the results of the experiments.

Finally, in Chapter 6 conclusions are drawn and recommendations are summarised.

# Chapter 1

## LOCAL SCOURING AT BRIDGE PIERS: GENERAL DESCRIPTION

### 1.1. Introduction

Numerous investigations have been carried out since late 1950s to understand the flow and erosion mechanism around bridge piers and estimate the scour depth. However, a lack of understanding of the flow structure and scour process makes it difficult to predict the scour by empirical formulae or mathematical models. In general, a unidirectional flow in a mobile channel that approaches a protruding vertical obstacle becomes three-dimensional and such flow pattern around a cylinder is complex and difficult to assess hydro-dynamically (Graf and Istiarto, 2002). In this case, more study is necessary to obtain more accuracy in flow simulation and prediction of scour pattern at bridge pier. In this chapter, based on available studies, a description about flow pattern around the pier, a short introduction to the studies about application of numerical models in pier scour analysis and a brief analysis of empirical formulae are presented.

### 1.2. Flow pattern around a circular bridge pier

One of the early, but comprehensive works about turbulent flow fields and measuring velocity magnitude at a pier with a DISA hot-film anemometer and hydrogen-bubble method was carried out by Melville and Raudkivi (1977). They measured the flow field at the upstream axis of symmetry and near-bed turbulence intensity for the cases of flat bed, intermediate (after 30 min) and equilibrium scour holes. Before starting measurements, the loose sediment bed was coated with plaster. The main results addressed the flow patterns in vertical and horizontal planes, the turbulence intensity and the bed shear stress distribution. Figure 3 shows direction and magnitude of mean velocity past a 50.8 mm diameter pier in the vertical plane of symmetry ahead of the

cylinder at equilibrium scour hole. The velocity magnitudes have been normalised by dividing by the mean approach velocity.

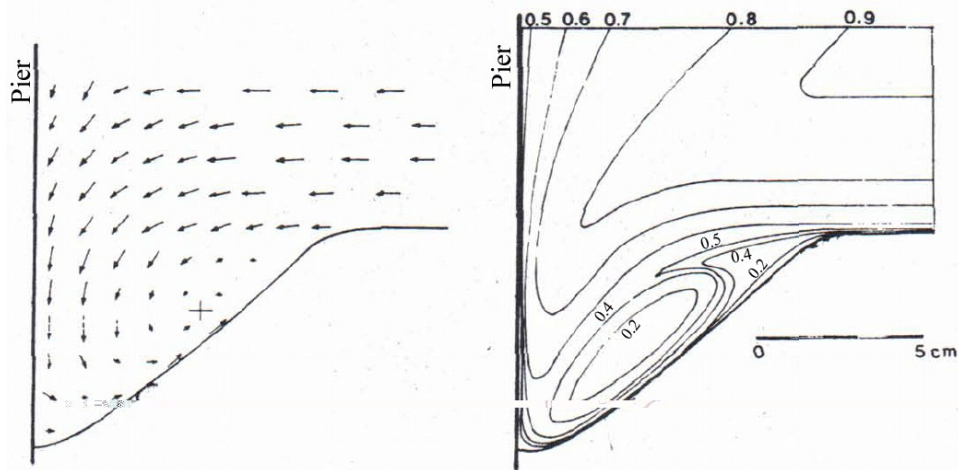


**Fig. 3. Direction and magnitude of normalised mean velocity ahead of the pier at equilibrium (Melville and Raudkivi, 1977)**

Baker (1979, 1980 and 1985) investigated the detailed characteristics of the horseshoe vortex at a circular cylinder embedded in a horizontal fixed bed. His 1979 and 1980 works refer to the laminar and turbulent boundary layer separations, respectively. The pressure distribution beneath the horseshoe vortex system was measured and the horseshoe vortex position was determined experimentally. Baker (1985) described the geometric position of points of zero shear stress – along the separation line – and of the maximum shear stress beneath the main horseshoe vortex. For all flow conditions, he observed a horseshoe vortex system consisting of at least two vortices. In contrast, Eckerle and Langston (1987) found under well-defined flow conditions the existence of a single main horseshoe vortex and one saddle point in the streamwise plane of symmetry. Their results were based on a detailed investigation of the pressure and the velocity distributions around a circular cylinder using a five-hole Pitot tube.

Qadar (1981) explored the interactions between the horseshoe vortex and the temporal increase of scour depth. He concluded that the maximum scour depth is a function of the strength of the vortex ahead of the pier. He also found that the depth of the approach flow alone has little measurable effect on the maximum scour depth. However, a minimum flow depth, greater than the vortex size, is essential for the vortex action to fully develop. On the other hand, he concluded that sediment size seems to be important at the initial stage of the scouring process.

Dargahi (1987, 1989 and 1990) conducted a detailed study of the flow field around a circular cylinder. The results of his study showed that the vortices are generated within the main separated region of the flow as a consequence of several local separations. In other words, the boundary layer upstream to the cylinder must overcome a strong pressure gradient set up by the cylinder. This leads to separation of the flow. In the separated region, a vortex system is developed that is stretched around the cylinder like a horseshoe. Dargahi (1987) used a fixed flat

bed flume to consider system of horseshoe vortices acting in scouring phenomena. He could find five major vortices as shown in Fig. 4.

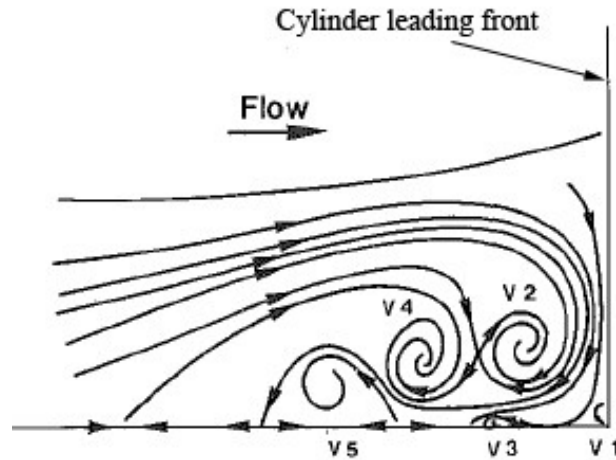


Fig. 4. Topological structure of flow upstream to cylinder (modified from Dargahi, 1990)

Ahmed and Rajaratnam (1998) and Sarker (1998) investigated the downflow characteristics for a mobile sediment bed with a Preston tube and the Acoustic Doppler Velocimetry (ADV), respectively. Ahmed and Rajaratnam (1998) investigated influence of bed roughness on flow around bridge piers. Their experiments were performed in three bed conditions, i.e. smooth, rough and mobile bed. Their results show that bed roughness increases the magnitude of bed shear stress as well as the area over which the shear amplification was felt and the extension of the separation zone.

Graf and Yulistiyanto (1998) and later Graf and Istiarto (2002) determined experimentally the velocity, the turbulence intensity, the turbulent kinetic energy and the bed shear stress distributions around a sediment embedded circular bridge pier. According to Graf and Istiarto (2002) the major characteristics of the flow field downstream of and upstream to a vertical cylinder are:

- directly upstream to the cylinder, a rather strong clockwise vortex (caused by the adverse pressure gradient) is found – the horseshoe vortex –, positioned at the foot of the cylinder (Fig. 5a);
- downstream of the cylinder, there exists a flow reversal towards the water surface. In this region, the streamwise velocity  $u$ -components are small and show clearly flow reversal towards the water surface. This is rather pronounced immediately after the cylinder, but gradually returns to a logarithmic profile further downstream. In fact, moving outwards from the scour hole the  $u$ -components increase and flow reversal diminishes (Fig. 5b). The vorticity in this region is rather weak;
- a trailing wake-vortex system is also formed in the rear of the cylinder over the entire flow depth. In this region, the turbulence intensity increases and consequently erosion and transport of sediments is enhanced;

## Chapter 1: Local scour at bridge piers: general description

- due to a change in the bottom inclination, a positive vorticity is strong at the brink and downstream part of the scour hole. Positive vorticity in the vicinity of the scoured bed is probably due to the boundary-layer flow (Fig. 5c);
- very weak negative vorticity is evident in the upper layers, resulting in the weak counter-clockwise vortex, which disappears when the flow moves out of the scour hole (Fig. 5d);
- the shear stress is considerably reduced in the scour hole in comparison with its value in the approach flow.

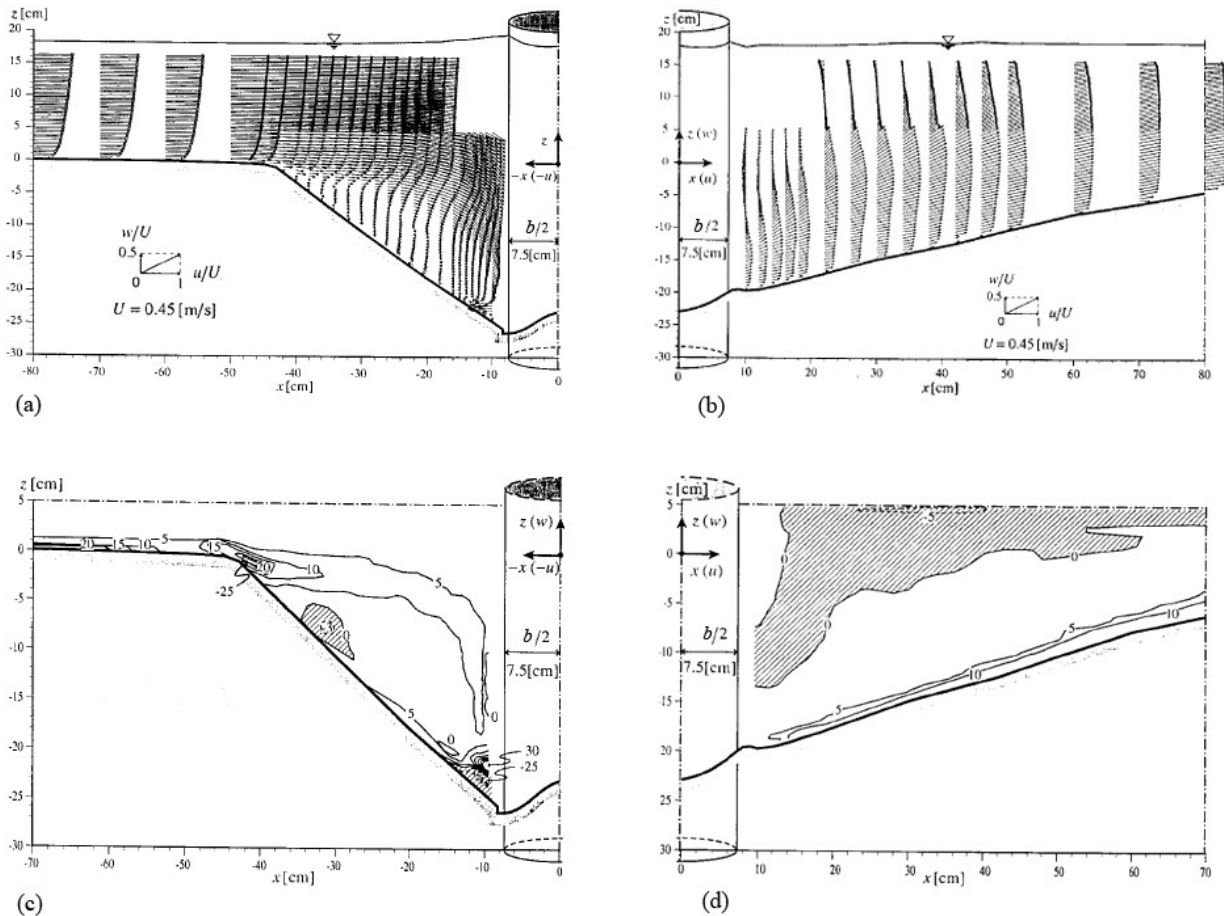


**Fig. 5. (a, b) Non-dimensional velocity field and (c, d) vorticity field ( $s^{-1}$ ) in the plane of symmetry (modified from Graf and Istiarto, 2002)**

In an interesting study by Muzzammil and Gangadharaiah (2003), the vortex size, vortex velocity and vortex strength were determined in terms of the relevant hydraulic and geometric parameters and the temporal scour hole evolution. The Authors described a linear increase of the temporal vortex size and proposed a complex power function for the temporal evolution of the vortex velocity and vortex strength.

Dey and Raikar (2007) carried out an extensive study about the flow and turbulence characteristics of the horseshoe vortex change with the development of the scour hole at a circular pier, providing a detailed data set and proposing some important scaling issues related to

the flow and turbulence. The contour lines of the time-averaged velocities, turbulence intensities and Reynolds stresses at different azimuthal planes ( $0^\circ$ ,  $45^\circ$  and  $90^\circ$ ) were prepared in different stages of scour evolution having intermediate scour depths of 0.25, 0.50 and 0.75 times the equilibrium scour depth. Vector plots of the flow field at azimuthal planes reveal the evolution of the characteristics of the horseshoe vortex flow associated with a downflow from intermediate stages to equilibrium condition of scour holes.

In few other studies, the flow field around bridge piers was measured with the Particle Image Velocimetry (PIV), a non-intrusive and instantaneous velocity measuring method (Pogozelski *et al.*, 1997; Johnson and Ting, 2003; Unger and Hager, 2007). Among them, an interesting study was carried out by Unger and Hager (2007) with a large-scale PIV setup. In that study, flow features of horseshoe vortex and the downflow proceed in four principal phases, from scour entrainment laterally from the pier generating the initial vortex at the pier front to the advanced scour process characterised by the fully developed horseshoe vortex system. Figure 6 shows an example of flow field at a circular pier (having width  $b=26$  cm) at different time instants; the approach flow depth was  $h=16.6$  cm (Unger and Hager, 2007). At time  $t=60$  s no scour was observed, since scour started always from lateral sides of the pier.

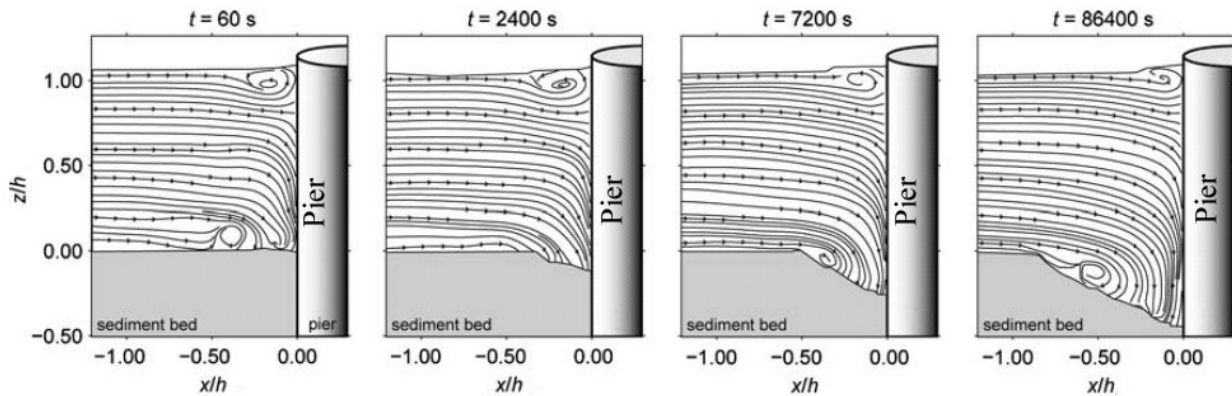


Fig. 6. Streamline plots of the flow in the channel symmetry axis (Modified from Unger and Hager, 2007)

The flow upstream to the pier at  $x/h \leq -0.75$  was unaffected by the presence of the pier. Closer to the leading pier front, at  $-0.75 < x/h < -0.25$ , the flow decelerated, but the velocity profile preserved its logarithmic shape. Toward the pier, the flow was strongly deflected in the vertical direction, resulting in two vertical jets directly at the pier front starting from the stagnation point. The upper jet, the so-called upflow, is directed to the water surface whereas the lower jet, the downflow, towards the sediment surface. At  $t=2,400$  s, the scour zone had expanded from the pier sides to the channel axis; all flow features were conserved, except for the initial vortex. In this flow phase, the downflow was completely deflected in the transverse direction after having reached the sediment surface. The scour progressed and the horseshoe vortex was developed. In its initial stage at  $t=7,200$  s, it consisted of a single vortex located above the rim inside the scour hole. At  $t=86,400$  s, both the vortex diameter and the maximum vorticity had continuously increased. Again, the approach flow, the downflow and the upflow, the stagnation point as well

as the surface recirculation conserved their structure, independent from the temporal scour evolution.

### 1.3. Scouring process

For a certain flow velocity in the channel, the sediment particles close to the cylinder begin to move and the scour is initiated. The eroded particles will follow the flow pattern and are carried away from the front of the cylinder towards the downstream. Upon an increase in the flow velocity, more and more particles are dislodged, forming a scour hole increasing in size and depth (Graf and Istiarto, 2002). The scouring process is coupled to the horseshoe and wake vortices. Dargahi (1990) distinguished three different phases in scouring process: 1) initiation; 2) primary scouring; 3) gradual reduction. During phase 1, the change of the boundary condition from fixed bed to mobile bed causes no appreciable change in the structure of the flow around the cylinder. The profiles are formed during the primary phase and characterised by the existence of three main slopes that are directly caused by the horseshoe vortices (Fig. 7).

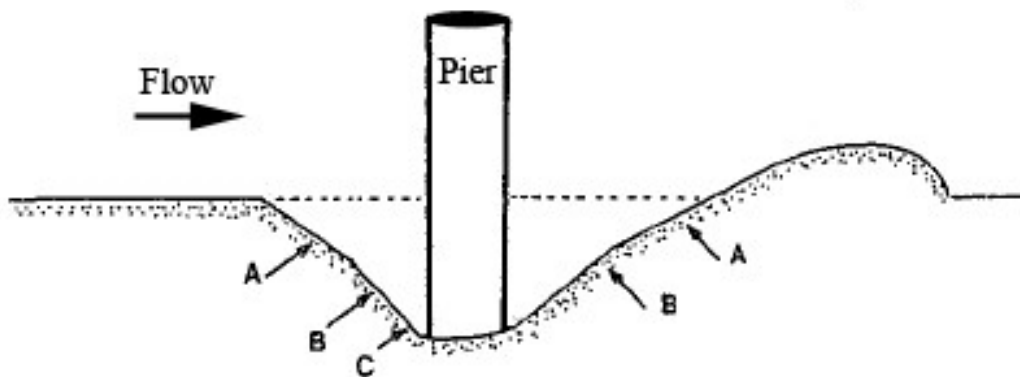


**Fig. 7. Scour profiles along the plane of symmetry: A=upper slope; B=lower slope; C=concave slope (modified from Dargahi, 1990)**

Both the upper and the lower slope angles increase during a short period of initial scouring. In this time interval, the upper slope is steeper than the lower slope. Also in clear-water scour condition, the transport phenomenon is quasi-periodical. The length, the angle and the position of the slopes fluctuate periodically.

Figure 8 shows the general scour patterns upstream to the cylinder along plane of symmetry. In fact, Fig. 8 illustrates the performance of the vortices in scouring process. The scouring commences under vortex 1 (Fig. 6a) and at either side of the cylinder at about  $\pm 45^\circ$ , and then scouring also starts simultaneously under vortices 2, 3, 4 and 5 and two small depressions are formed in the bed (Fig. 6b).



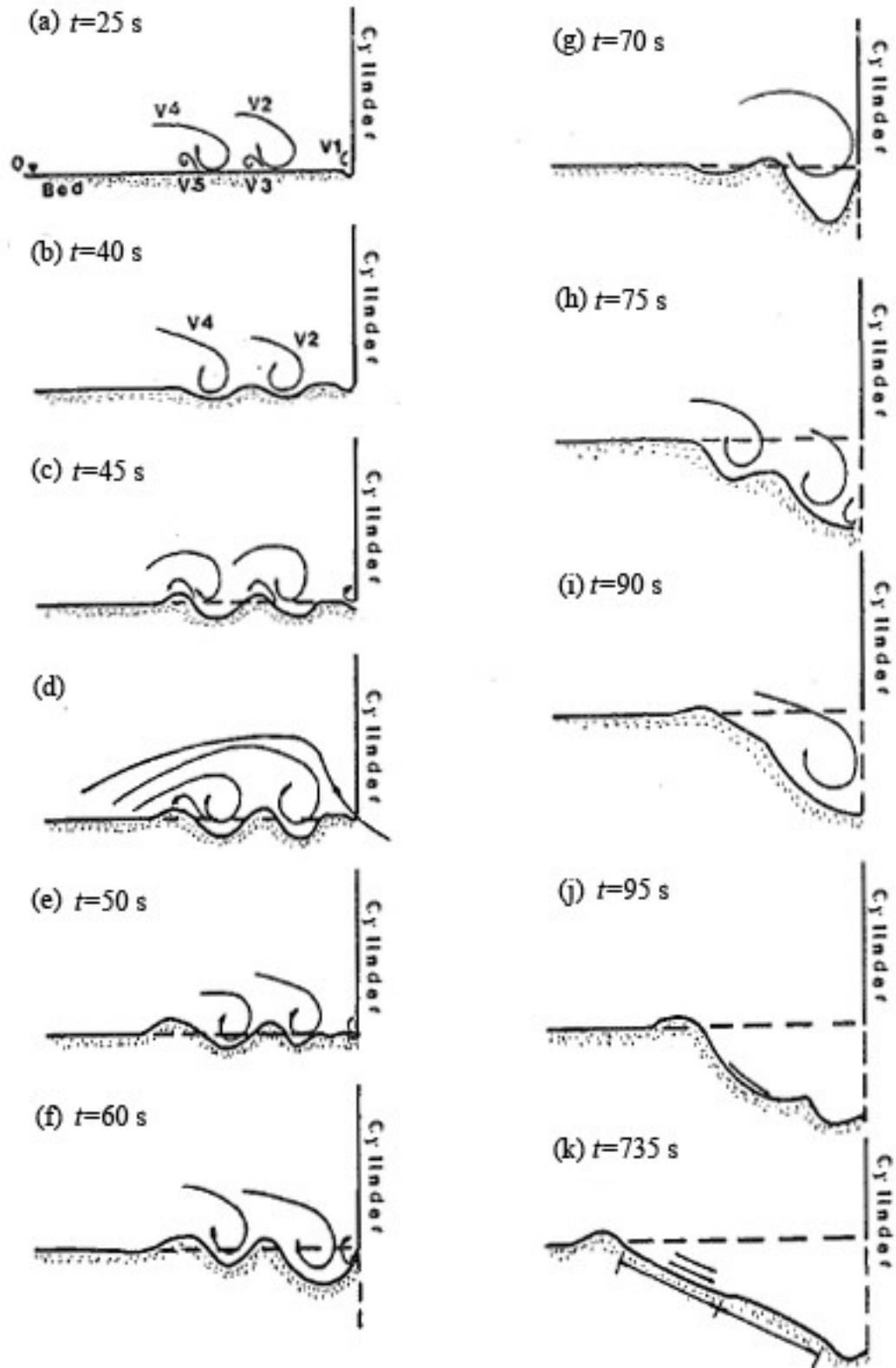


Fig. 8. General scour patterns upstream to cylinder along plane of symmetry (modified from Dargahi, 1990)

Note that about the angle of two initial scours, higher values of  $70^\circ$  (Breusers *et al.*, 1977) and  $75^\circ$  (Oliveto and Hager, 2002) from channel axis were also reported (Fig. 9).

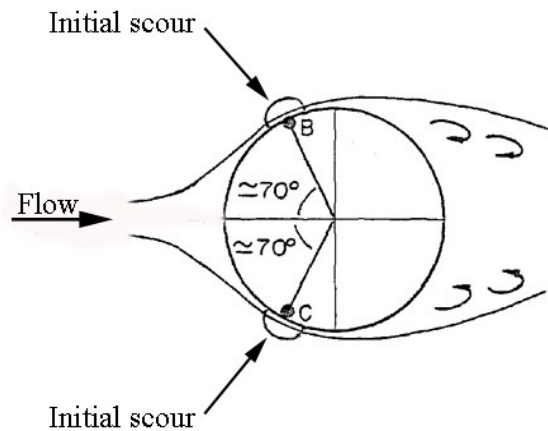


Fig. 9. locations of initial scours around the pier (modified from Gao *et al.*, 1993)

Two depressions (Fig. 8b) extend rapidly towards the upstream face of the cylinder. The sediments picked up by vortices 2 and 4 are fed into vortices 3 and 5. The trapped sediment is then deposited in the form of two sediment humps (Fig. 8c). Vortex 1 continues to lift up sediment, part of which is transported downstream and the rest piled up (accumulated) ahead of the cylinder. Scouring takes place under the arms of the vortices. In the next stage, the depression between vortices one and two becomes flattened by the action of vortex two and it takes the shape of a concave curve (Fig. 8f). The depressions under vortices two and four develop into two small slopes (Fig. 8h). As vortices two and three move toward the cylinder, they transport more sediment, which is partly eroded from the bed and partly supplied by continuous sliding of sediment on the upper slope. After a relative long time, the lower and upper slopes become roughly the same length (Fig. 8k).

It is necessary to indicate that the above process is related to clear-water scouring and uniform-graded fine sand. So, in other conditions (live-bed or non-uniform sediments) the scouring process may be different from the above one. There is also a balance between the scouring rate upstream to the cylinder and the deposition rate downstream of the cylinder, and in the wake of cylinder the deposition depth is greater than the scour depth, as additional sediment scoured from the sides of the cylinder is deposited on the sediment mound (Dargahi, 1990).

### 1.4. Modelling of turbulent flow and scour process at the pier

During the last 20 years, owing to the progress in speed of processors and capacity of computer memories, application of mathematical and numerical models in all sectors of engineering science extensively increased. In the field of pier scouring, these models were employed for both simulation of turbulent flow and scour process. Olsen and Melaaen (1993) used a steady-state Navier-Stokes solver coupled with a sediment transport model to simulate the development of a

scour hole at the base of a circular pier. Figure 10a shows the measured and calculated contour lines of scour hole which indicates a good agreement between measured and calculated scour hole. Later, Richardson and Panchang (1998) performed simulation of flow around the pier and inside the scour hole in three stages of flatbed, intermediate and equilibrium hole. They applied the *FLOW-3D*<sup>®</sup> code to simulate data measured by Melville and Raudkivi (1977). In their study only the turbulent flow field around the pier was simulated in static condition for each scour stage; however, their study did not include the scour evolution.

Olsen and Kjellesvig (1998) applied 3D numerical model to estimate maximum local scour depth at a circular cylinder. The shear stress on the bed was calculated by turbulence model. The concentration of the bed as a function of the shear stress was calculated by Van Rijn (1987) formula and the model could calculate the three dimensional scour hole around the cylinder. The improvement of this study respect to previous one, i.e. Olsen and Melaaen (1993), is that in this study the models include transient terms in order to calculate maximum scour depth. They also compared results of the maximum scour depth in front of a 1.5 m pier using their model with some empirical formulae. Their results show that the maximum predicted scour depth by model is in the range of those predictions by empirical formulae. Figure 10b shows the time evolution of scour in front of the pier as predicted by the numerical model of Olsen and Kjellesvig (1998).

Salaheldin *et al.* (2004) used the *FLUENT*<sup>®</sup> code to compare different turbulence models. They found that the  $k-\varepsilon$  models show some discrepancy with the measured bed shear stress; however, the Reynolds stress model (RSM) performed quite well in simulating velocity distribution on flat bed and scour hole as well as shear stress distribution on flat bed at circular piers. Figure 10c shows comparison of scour initiation area ( $\tau/\tau_c > 1$ , where  $\tau$  and  $\tau_c$  are the actual and the critical bed shear stress, respectively) simulated using RSM and experimental data by Salaheldin *et al.* (2004).

Another interesting simulation of scour process was performed by Roulund *et al.* (2005). The Authors coupled the steady-state flow model with a morphologic model to calculate scour around a vertical cylinder in steady flow conditions and for non-cohesive sediments. The morphologic model included a two-dimensional bed load sediment transport description, and a description of surface-layer sand slides for bed slopes exceeding the angle of repose.

They found that the numerical simulation captures all the main features of the scour process. The equilibrium scour depth obtained from the simulation agrees well with the experiments for the upstream scour hole. Figure 10d shows simulated scour at a pile after 2 h.

Recently, Kirkil *et al.* (2008) applied the Large-Eddy Simulation (LES) method to investigate the coherent structure of flow field around a pier inside the scour hole. Afterwards, Kirkil *et al.* (2009) performed flow field simulation by Detached Eddy Simulation for a higher value of Reynolds number, which was outside the possible range for Large Eddy Simulation (LES).

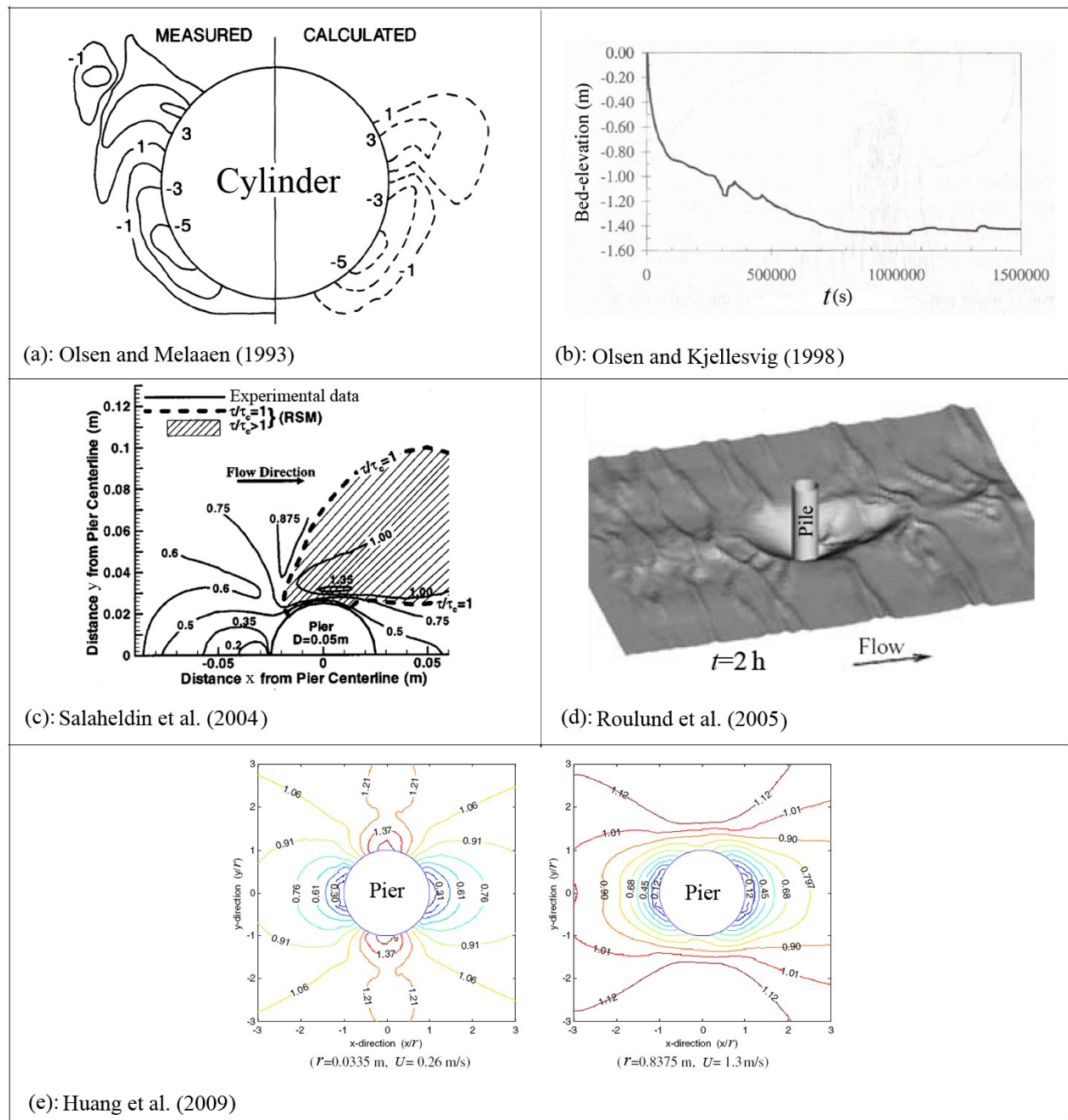


Fig. 10. Results of some previous studies in simulation of flow and scour at pier using numerical models

Another application of numerical models in the analysis of scale effect in turbulent flows around a pier was conducted by Huang *et al.* (2009), who compared the flow around a small scale cylinder with that around a larger one. They found that simulation based only on the Froude similarity law (i.e., ignoring Reynolds similarity) in physical modelling may result in significant errors in simulating scour at large bridge piers. Figure 10e shows a comparison between flow around a small pier (left) and around a larger pier (right) based on the Froude similarity law,  $r$  being the radius of the circular pier; the velocity contour lines are normalised with the approach

flow velocity,  $U$ . Figure 10e shows that the velocity field in small and larger piers are significantly different and similarity based only on the Froude law is not satisfying.

Application of numerical models in pier scour analysis is an ongoing topic and probably in future these models will be reliable methods in prediction of turbulent flow field and scouring process.

## **1.5. Prediction of scour depth using empirical formulae**

Due to the fact that application of numerical models is complex and also these models are already under research and development, empirical formulae as quick solution in estimation of scour depth are widely used. Up to now numerous formulae have been proposed to predict the scour depth and most of them were derived before year 2000. Based on a brief consideration of the literature, Johnson (1995) used field data to consider the accuracy and limitations of seven pier-scour formulae in various field conditions. An extensive analysis and comparison of field data with predictions of five selected formulae by Landers and Mueller (1996) showed that none of the selected formulae accurately estimates the depth of scour in all the measured conditions. Their results also clarified that some of the equations performed well as conservative design formula; however they overestimated many observed scour depths by large amounts. The results of a more recent study by Mohamed *et al.* (2006) showed that the CSU formula, which was later, improved and published as FHWA (HEC-18) formula (Richardson and Davis, 2001), is more accurate in comparison to other three selected pier-scour formulae.

All proposed equations can be classified in two groups: 1) formulae developed through a correlation among effective parameters and scour depth; 2) formulae based on envelope curves, in order to estimate the maximum scour depth for safe design purposes. In this study, six well-known pier scour formulae were selected for comparison. All of the selected formulae were recommended in literature for design procedure. Owing to the general lack of field datasets, a comparison between formulae (two by two) can be carried out using large synthetic datasets, which can be generated in various hydraulic and sediment conditions. The main purpose of the following sections is to compare the performance of selected bridge pier scour equations using both randomly generated and field data (Gaudio *et al.*, 2010).

### **1.5.1. Selected formulae**

The selected formulae are presented below.

a) Breusers *et al.* (1977) formula (hereinafter BR) for clear-water and live-bed scour conditions:

$$\frac{d_{se0}}{b} = 2 \left( 2 \frac{U}{U_c} - 1 \right) \tanh \left( \frac{h}{b} \right) \cdot K_s \cdot K_\theta \quad (\text{E.1})$$

where  $d_{se0}$  is the maximum scour depth at equilibrium for an unprotected pier,  $U$  the approach flow velocity,  $U_c$  the critical velocity for sediment motion – computed with the Neill (1973) equation in SI units ( $U_c = 31.08\theta_s^{1/2}h^{1/6}d_{50}^{1/3}$ ), where the Shields mobility parameter,  $\theta_s$ , can be computed based on sediment size (see Mueller and Wagner, 2005, p. 20) –  $K_s$  the pier shape factor and  $K_\theta$  the pier alignment factor (see details in Breusers *et al.*, 1977). The ratio of  $U/U_c$  as it will be discussed in next chapter is called ‘flow intensity’ parameter.

b) Jain and Fischer (1979) formula (hereinafter JF) for clear-water and live-bed scour conditions:

$$d_{se0} = 1.84b \left(\frac{h}{b}\right)^{0.3} Fr_c^{0.25}, \text{ valid for maximum scour depth in clear-water conditions;} \quad (\text{E.2a})$$

$$d_{se0} = 2.0b \left(\frac{h}{b}\right)^{0.5} (Fr - Fr_c)^{0.25}, \text{ valid for } Fr - Fr_c \geq 0.2 \text{ in live-bed conditions} \quad (\text{E.2b})$$

where  $Fr = U/(gh)^{0.5}$  and  $Fr_c = U_c/(gh)^{0.5}$  are the Froude number and the critical Froude number, respectively.

For  $0 < Fr - Fr_c < 0.2$  the largest value which is obtained from (E.2a,b) is to be taken.

c) Froehlich (1988) formula (hereinafter FL) for live-bed scour condition:

$$d_{se0} = 0.32b\phi Fr^{0.2} \left(\frac{b_e}{b}\right)^{0.62} \left(\frac{h}{b}\right)^{0.46} \left(\frac{b}{d_{50}}\right)^{0.08} \quad (\text{E.3})$$

where  $b_e$  is the width of the bridge pier projected orthogonally to the approach flow,  $\phi$  a coefficient based on the shape of the pier nose and  $d_{50}$  the median grain size.

d) Kothyari *et al.* (1992) formula (hereinafter KR) for clear-water scour condition:

$$\frac{d_{se0}}{b} = 1.0 \left(\frac{b}{d_{50}}\right)^{-0.25} \left(\frac{h}{d_{50}}\right)^{0.16} \left[ \frac{U^2 - U_{cp}^2}{\frac{\Delta\gamma_s}{\rho_f} d_{50}} \right]^{0.4} \alpha_o^{-0.3}, \quad U_{cp}^2 = 1.2 \left(\frac{\Delta\gamma_s}{\rho_f} d_{50}\right) \left(\frac{b}{d_{50}}\right)^{-0.11} \left(\frac{h}{d_{50}}\right)^{0.16}, \quad \Delta\gamma_s = \gamma_s - \gamma_f \quad (\text{E.4})$$

where  $U_{cp}$  is the critical velocity for the motion of sediment particles at the pier nose,  $\gamma_s$  the sediment specific weight,  $\gamma_f$  the fluid specific weight,  $\rho_f$  the fluid mass density and  $\alpha_o = (B-b)/B$  the opening ratio,  $B$  being the flume width or centre-to-centre spacing between two transverse piers with the flow. In this study,  $B$  was assumed to be much greater than  $b$  and, therefore, its effect was neglected.

e) Melville (1997) formula (hereinafter ML) for clear-water and live-bed scour conditions:

$$d_{se0} = K_{hb}K_IK_dK_SK_\theta K_G \quad (E.5)$$

where  $K_{hb}$ ,  $K_I$ ,  $K_d$ ,  $K_S$ ,  $K_\theta$  and  $K_G$  are coefficients taking into account the depth scale, the flow intensity, the sediment size, pier shape, pier alignment and channel geometry effects on scour depth, respectively;  $K_{hb}$ ,  $K_I$  and  $K_d$ , can be calculated as follows:

$$K_{hb} = \begin{cases} 2.4b & \text{for } b/h < 0.7 \\ 2\sqrt{hb} & \text{for } 0.7 < b/h < 5.0 \\ 4.5h & \text{for } b/h > 5.0 \end{cases} \quad K_I = \begin{cases} \frac{U}{U_c} & \text{for } \frac{U}{U_c} < 1 \\ 1 & \text{for } \frac{U}{U_c} \geq 1 \end{cases} \quad K_d = \begin{cases} 0.57 \log\left(2.24 \frac{b}{d_{50}}\right) & \text{for } \frac{b}{d_{50}} \leq 25 \\ 1 & \text{for } \frac{b}{d_{50}} > 25 \end{cases} \quad (E.6)$$

Factors  $K_S$  and  $K_\theta$  can be also calculated by using the Tables proposed in Melville (1997). In addition,  $K_G = 1$  for piers.

f) FHWA (HEC-18) formula (Richardson and Davis, 2001) (hereinafter HC) for clear-water and live-bed scour conditions:

$$\frac{d_{se0}}{b} = 2K_1K_2K_3K_4K_w \left(\frac{b}{h}\right)^{0.35} Fr^{0.43} \quad (E.7)$$

where  $K_1$ ,  $K_2$ ,  $K_3$ ,  $K_4$  and  $K_w$  are correction factors accounting for pier nose shape, flow angle of attack, presence of bed forms, bed armouring and wide piers in shallow flows, respectively (see Richardson and Davis, 2001, for details).

## 1.5.2. Comparison between formulae based on randomly generated data

### 1.5.2.1. Data generation

The following conditions were assumed in the data generation procedure:

- 1) the pier shape is circular;
- 2) the bed materials are incoherent uniform sediments with geometric standard deviation of particle size distribution  $\sigma_g < 1.5$  and relative submerged sediment density  $\Delta = 1.65$ ;
- 3) flow regime is assumed to be uniform (the riverbed slope is equal to the friction slope:  $S = S_f$ ) in clear-water ( $0.5 \leq U/U_c < 1$ ) and at the inception of sediment motion or in live-bed ( $U/U_c \geq 1$ ) scour conditions, in a wide channel ( $R_h \approx h$ ),  $R_h$  being the hydraulic radius;
- 4) the well-known Manning and Strickler equations (respectively  $U = R_h^{2/3} S^{0.5} / n$  and  $n = 0.041 d_{50}^{1/6}$ ,  $n$  being the Manning roughness coefficient) were used to calculate the approaching

flow velocity;  $U_c$  was estimated through the Neill (1973) equation.

In this part of study, 10,000 triplet input data ( $h, b, d_{50}$ ) were synthetically generated for clear-water conditions and 10,000 data for live-bed conditions in the following ranges of values, which are typical of many natural watercourses:  $0.5 \leq h \leq 10$  m,  $0.5 \leq b \leq 5$  m and  $0.062 \leq d_{50} \leq 64$  mm, discarding unrealistic combinations of the variables. Hence, the Manning roughness coefficient,  $n$ , was computed with the Strickler formula and  $U_c$  with the Neill (1973) equation. Afterwards, 10,000 values of  $U$  were randomly generated in order to verify the condition  $0.5 \leq U/U_c < 1$  for clear-water, scour and other 10,000 values in order to have  $U/U_c \geq 1$  for the inception of sediment motion or live-bed scour conditions. Finally, the corresponding values of bed slope,  $S$ , were computed through the Manning formula, verifying that they were compatible with realistic cases (from  $4.04 \cdot 10^{-5}\%$  to  $0.68\%$  in clear-water condition; from  $0.0034\%$  to  $1\%$  in live-bed condition). In addition,  $\sigma_g$  was generated in the range 1 to 1.5 for uniform bed sediments. The characteristic sediment size which is required in (E.7) was calculated as  $d_{95} = d_{50} \sigma_g^{1.645}$  (see Mueller and Wagner, 2005, p. 16). The bed form factor in HEC-18 formula was assumed to be  $K_3=1.1$  (as recommended for dune height less than 3 m in live-bed scour condition). For each pair of formulae, 10,000 values of  $d_{se0}$  were calculated and compared. The number of comparisons between  $m$  formulae taken two by two is equal to  $m(m-1)/2$ . Among the 6 considered formulae, 4 were developed for both clear-water and live-bed scour conditions (BR, JF, ML and HC), 1 for clear-water scour condition (KR) and 1 for live-bed scour condition (FL). Therefore, 10 comparisons in clear-water scour condition and 10 comparisons in live-bed scour condition were carried out, for a total of 20 comparisons.

**1.5.2.2. Result analysis**

Fig. 11 shows some examples of the matching between the output of formulae taken two by two, with the perfect agreement lines and the  $\pm 10\%$  bands. The percentage of simulated points located below, inside and over the band is presented in Tabs. 1 and 2 for clear-water and live-bed conditions, respectively.

**Tab. 1. Percentage of points falling below, inside and over the  $\pm 10\%$  bands in clear-water condition**

		B			
		HC	ML	KR	JF
A	BR	11, 24, 65	0, 3, 97	2,37,61	4, 21, 75
	JF	44, 55, 1	41, 26, 33	50,30,20	-
	KR	26,31,43	15,30,55	-	-
	ML	43, 28, 29	-	-	-

**Tab. 2. Percentage of points falling below, inside and over the  $\pm 10\%$  bands in live-bed condition**

		B			
		HC	ML	FL	JF
A	BR	0, 2, 98	0, 4, 96	34, 42, 24	1, 8, 91
	JF	5, 32, 63	53, 26, 21	82, 10, 8	-
	FL	2, 3, 95	6, 13, 81	-	-
	ML	5, 12, 83	-	-	-

For example, Tab. 1 shows that HC formula in 44%, 55% and 1% of simulated conditions furnishes respectively values smaller than, almost equal to, and higher than those given by the JF formula in the same condition. In other words, in few conditions HC formula may give higher prediction with respect to JF formula (see also Fig. 11a). The agreement between formulae A and



B can be considered as “strong”, “moderate” or “weak” if 75 to 100%, 50 to 75% and 0 to 50% of simulated points fall inside the  $\pm 10\%$  band, respectively.

In clear-water condition, Tab. 1 shows that a strong agreement between two formulae is never found. Only the JF formula is in moderate agreement with the HC formula, with only 55% of simulated data falling inside the  $\pm 10\%$  band (Fig. 11a). The other formulae show weak agreements with all the other ones (see, e.g., Fig. 11b). The JF formula produced overestimations with respect to the other formulae in many simulated conditions (see, e.g., Fig. 11c,d), due to the fact that it estimates the maximum clear-water scour depth for  $U \approx U_c$ .

In live-bed scour condition, no strong nor moderate agreements were found. The best (but weak) agreement was obtained between FL and BR formulae (42% of points falls inside the  $\pm 10\%$  band; see Tab. 2). However, as shown in Fig. 11e, the FL formula may predict scour depths significantly higher than BR formula in some conditions. Lower agreements may be expected between the JF and HC or ML formulae. Even if sometimes the output scatter was not very high, as in the case of the comparison between the ML and BR formulae (Fig. 11f), the agreements were very weak.

### **1.5.3. Comparison of the formulae based on field data**

The predictions of the selected formulae were also compared with available field data for 29 bridge piers in uniform bed sediments ( $\sigma_g < 1.5$ ). Data was selected from the whole dataset by Mueller and Wagner (2005), which was collected at 79 river sites in the USA. In fact, two aspects of each formula should be evaluated: 1) owing to safety problems, the predicted values of each formula need to be around or higher than the observed field values; 2) owing to economical problems, the formulae should not overestimate excessively. Based on these two considerations, an asymmetric band was defined to evaluate the performance of the selected formulae. The upper and lower limits of the band were assumed to be +50% and -10%. In other words, a maximum safety factor equal to 1.5 was accepted for economical reasons, whereas a minimum underestimation factor equal to 0.9 was accepted for safety reasons. Table 3 shows the percentage of points falling inside the asymmetric bands. Although all the formulae do not perform satisfactorily, in clear-water scour condition the HC formula predicts the scour depth better than the other ones (see Fig. 12a). Both overestimated and underestimated values were obtained by applying the BR formula (see Fig. 12b). The ML, JF and KR formulae predicted the scour depths significantly higher than the observed values (see, e.g., Figs. 12c,d). Similar result was reported by Grimaldi *et al.* (2006) comparing predictions of the ML formula with laboratory data.

In live-bed scour conditions, more overestimations were obtained by using the selected equations. Among them, the HC and FL formulae predicted the scour depth better than the other ones; however, in many conditions they significantly overestimated the scour depths (see Figs. 13a,b). With the other selected formulae, the scour depths in live-bed scour conditions are even more overestimated (see, e.g., Figs. 13c,d).

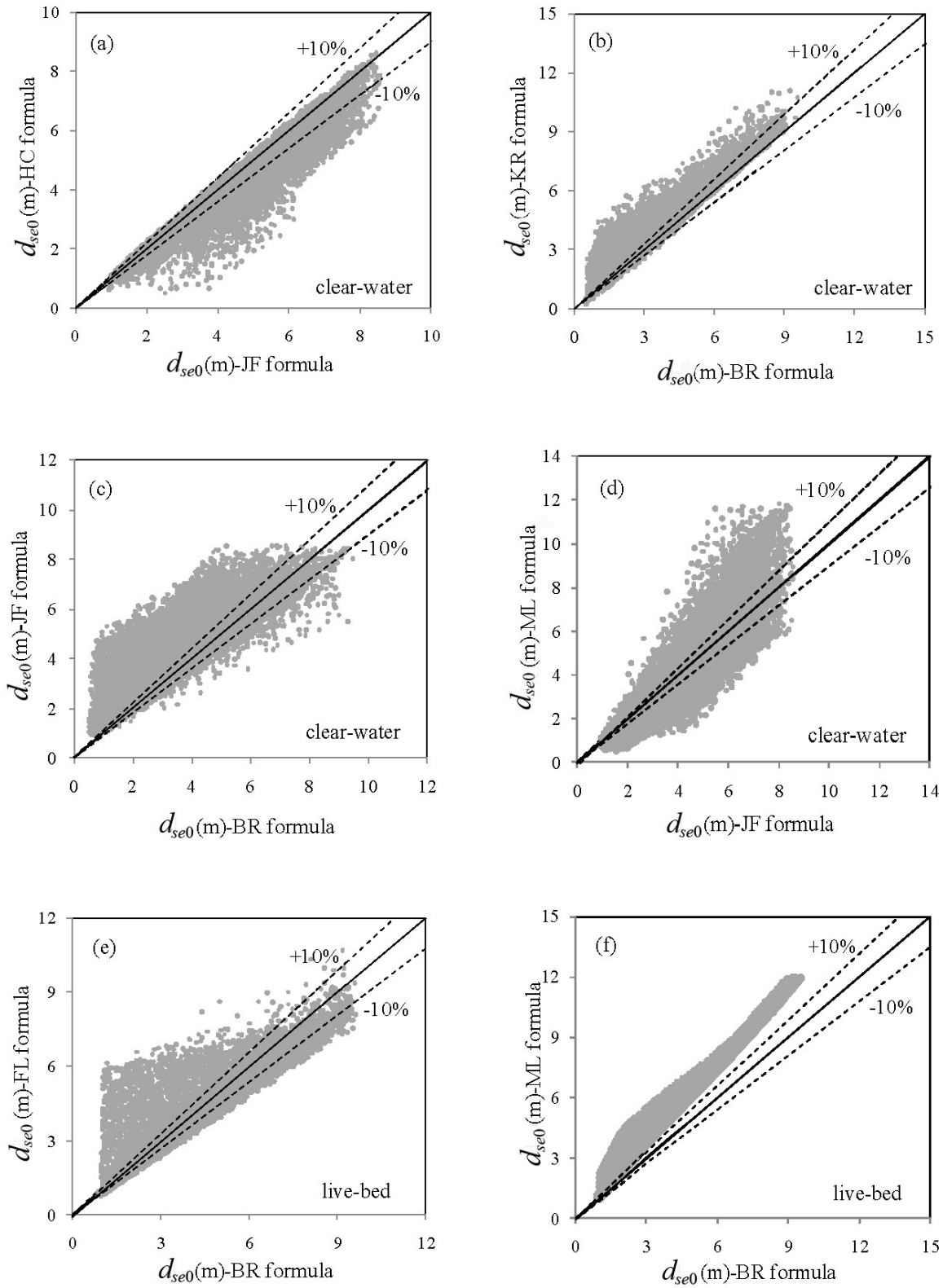


Fig. 11. Comparison of scour depths predicted by formulae taken two by two (formula A on the abscissa)

Tab. 3. Percentage of points falling inside the asymmetric bands

Scour condition	BR	JF	FL	KR	ML	HC
Clear-water	14	0	-	14	0	43
Live-bed	18	14	23	-	9	23

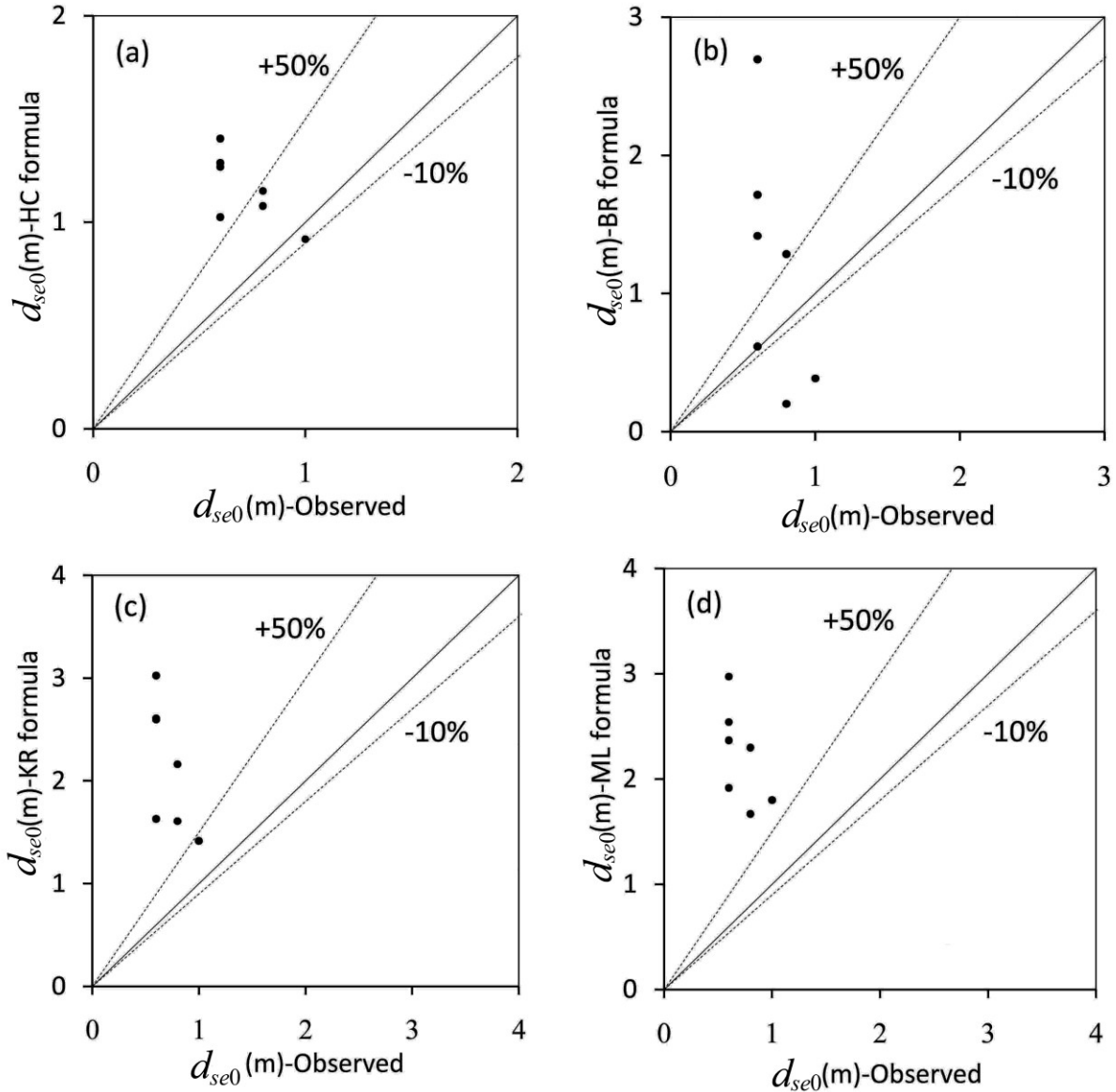


Fig. 12. Comparison of predicted and observed values of the scour depths in clear-water condition

In summary, in this section, six well-known design formulae for predicting the maximum equilibrium scour depths at bridge piers in clear-water or live-bed conditions were compared two by two, by using synthetic randomly generated data. The results show that in most conditions the agreement between formulae is weak, being good at best in 55% of the analysed cases.

The formulae were also tested on a field dataset available in the literature for uniform sediments, producing unsatisfactory results. The HC formula in both clear-water and live-bed

scour and the FL formula in live-bed condition predicted the measured scour depths better than the other selected formula.

This study evidences that none of the selected formulae accurately predicts the maximum equilibrium scour depths in the field and that high result variations are often obtained by using different pier scour formulae. Further research is needed to give a more comprehensive evaluation of pier scour formulae.

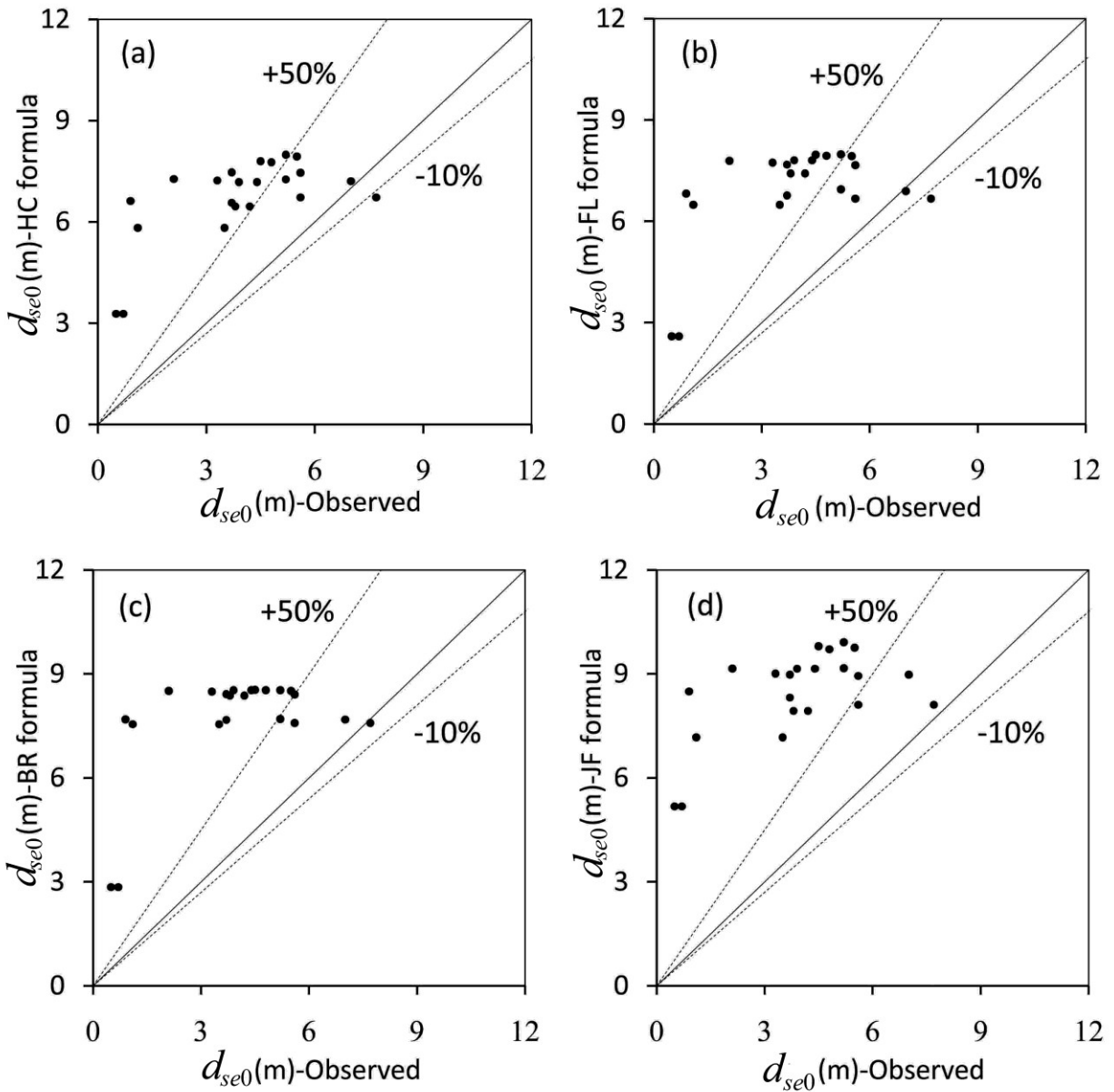


Fig. 13. Comparison of predicted and observed values of the scour depths in live-bed condition

## Chapter 2

### EFFECTIVE FACTORS AND DIMENSIONAL ANALYSIS OF BRIDGE PIER SCOURING

#### 2.1. Introductions

A proper selection of effective parameters is the first stage in the design of experiments and in physical modelling. Depending on the physical variables governing a phenomenon, specific parameters have to be selected. In pier scouring, various parameters have been already considered as influencing the phenomenon by various researchers. In general, a countermeasure should be able to protect the pier for the extreme condition in which the scour hole at the pier reaches the maximum depth. It should be noted that such condition represents the minimum requirement for performing proper tests in clear-water scour condition in application of a certain countermeasure (Tafarojnoruz *et al.*, 2010b). As it will be indicated in present and next chapters, the maximum scour depth for an unprotected pier is expected when the flow intensity is near the critical condition of sediment movement. On the other hand, previous studies showed that for some flow-altering countermeasures it is possible that the scour increases as the flow intensity increases, with values greater than 1. In this study, tests have been considered in both steady flow and unsteady flow in clear-water conditions or with a peak flow slightly greater than threshold condition of sediment movement. Therefore, in the present chapter, after an introduction to the parameters influencing the pier scour phenomenon, the required conditions to obtain the maximum scour depth will be presented. These conditions will be considered in Chapter 4 as a guideline for an effective design of the experiments.

## 2.2. Dimensionless parameters

The factors influencing scour at bridge piers can be divided into four major categories, i.e. the geomorphic, flood-flow transport, bed sediment and bridge geometric factors. Among them, except the first one, the other three factors influence local scour at bridge piers (Melville and Coleman, 2000).

Transport factors relate to water transport, sediment transport and debris transport. They are important for determining both general and local scours. For scour purposes, the water flow is characterised using a flood flow hydrograph and spatial and temporal distributions of flow velocity and flow depth.

Sediment transport factors determine whether conditions are of live-bed or clear-water scour. Under live-bed conditions, the sediment transport rate and bed-form characteristics are important factors.

Bed sediment factors at bridge sites comprise particle size distribution and, for non-cohesive sediments, the spatial distribution of sediments size, areally and vertically. The scour susceptibility of fine grained soils cannot be evaluated on the basis of grain-size characteristics because of the complex physio-chemical interactions between colloidal particles.

Bridge geometric factors include the degree of flow contraction caused by the bridge restricting the flow area, the foundation geometry, the location of the bridge in relation to the channel bends and the presence of scour protection works. The geometry of the bridge piers can be described by the type, shape, length, width and alignment with the flow.

Although based on the above descriptions, several factors may be assumed as parameters influencing the local scour depth; according to Melville and Coleman (2000), the most important variables are summarised in Tab. 4.

**Tab. 4. Effective parameters for scouring at bridge piers**

$d_s$ : scour depth	$\sigma_g$ : geometric standard deviation of sediment size distribution
$\rho$ : water density	$\rho'_s$ : buoyant grain density ( $=\rho_s-\rho$ )
$\nu$ : water kinematic viscosity	$b$ : pier width
$B$ : top width of channel	$L$ : pier length
$S$ : channel slope	$e$ : pier roughness
$U$ : approach flow velocity	$K_s$ : a factor describing pier shape
$h$ : approach flow depth	$K_\theta$ : a factor describing pier alignment
$G$ : parameter describing the effect of secondary currents	$t$ : time
$g$ : gravitational acceleration	
$d_{50}$ : median grain size	

For a smooth circular pier in uniform and steady flow condition, in a rectangular straight channel, having a not too steep slope  $S$ , the application of Dimensional Analysis through the Buckingham's method (II theorem), choosing  $\rho$ ,  $d_{50}$  and  $g$  as basic variables leads to the following dimensionless function (Simarro *et al.*, 2007):

$$\frac{d_s}{b} = \Phi \left( \sigma_g, \Delta, \frac{B}{d_{50}}, \frac{b}{d_{50}}, \frac{h}{d_{50}}, \frac{g\Delta d_{50}^3}{v^2}, \frac{Ut}{d_{50}}, \frac{U}{\sqrt{g\Delta d_{50}}} \right) \quad (\text{E.8})$$

Since critical flow velocity for the beginning of sediment motion, i.e.,  $U_c$  is not independent from other variables included in Tab. 4, it cannot be directly introduced into Dimensional Analysis. Nevertheless, (E.8) can be rearranged in order to include  $U_c$ , as shown by Simarro *et al.* (2007), obtaining

$$\frac{d_s}{b} = \Phi \left( \sigma_g, \Delta, \frac{U}{U_c}, \frac{B}{d_{50}}, \frac{b}{d_{50}}, \frac{h}{d_{50}}, \frac{Ut}{d_{50}}, \frac{U}{\sqrt{g\Delta d_{50}}} \right) \quad (\text{E.9})$$

and rearranging the dimensionless groups for non-cohesive sediments having a certain relative submerged grain density (typically sand and gravel with  $\Delta = \rho'_s/\rho \approx 1.65$ ):

$$\frac{d_s}{b} = \Phi \left( \sigma_g, \frac{U}{U_c}, \frac{B}{b}, \frac{b}{d_{50}}, \frac{h}{b}, \frac{Ut}{b}, \frac{U}{\sqrt{gb}} \right) \quad (\text{E.10})$$

The parameters on the right-hand member of (E.10) take respectively into account the effects on the scour depth of sediment grading, flow intensity, side walls, sediment coarseness, flow shallowness, time and pier size, being  $U/(gb)^{0.5}$  the pier Froude number ( $Fr_p$ ).

The dimensionless pier Reynolds number ( $Re_p = Ub/v$ ) indicates the influence of water viscosity on pier local scouring. In general, most of researchers conducted their experiments by assuming fully developed turbulent flow around the pier. Monti (1994) carried out experiments on scouring at a circular pier and investigated the flow pattern around the cylinder. He concluded that the local scouring process is independent of  $Re_p$  when  $Re_p > 7000$ . In the following subsections the influences of each group on the scour depth will be analysed and commented on, by pointing out the limit values and conditions to avoid undesired influences.

### 2.3. Flow intensity and sediment grading

Uniform or graded sediment grain distributions can be distinguished through the geometric standard deviation [ $\sigma_g = (d_{84}/d_{16})^{0.5}$ ]. For  $\sigma_g < 1.3$  to 1.5, the sediment distribution can be assumed as uniform. However, as it will be explained in Chapter 5, a better value for this parameter is obtained when  $\sigma_g < 1.2$ . This classification is important as in non-uniform distributions, owing to armouring of the scour hole, lesser scour depth is generally expected (Florida Department of Transportation, 2005). The ratios  $U/U_c$  for uniform sediment and  $U/U_a$  for non-uniform sediments are employed to consider flow intensity,  $U_a$  being the mean approach flow velocity at the ‘‘armour peak’’. According to the literature (see, e.g., Melville and Coleman, 2000), in order to achieve the maximum scour depth, flow intensity should reach the threshold value ( $U/U_c = 1$ ) and uniform sediments ( $\sigma_g < 1.3$  to 1.5) should be used in experiments (Fig. 14). On the other hand, at the threshold condition of sediment motion, the grains start moving all over the bed; in order to avoid such problem, experiments should be carried out with flow intensity slightly below the threshold condition of sediment motion (e.g.,  $U/U_c = 0.90$  to 0.95).

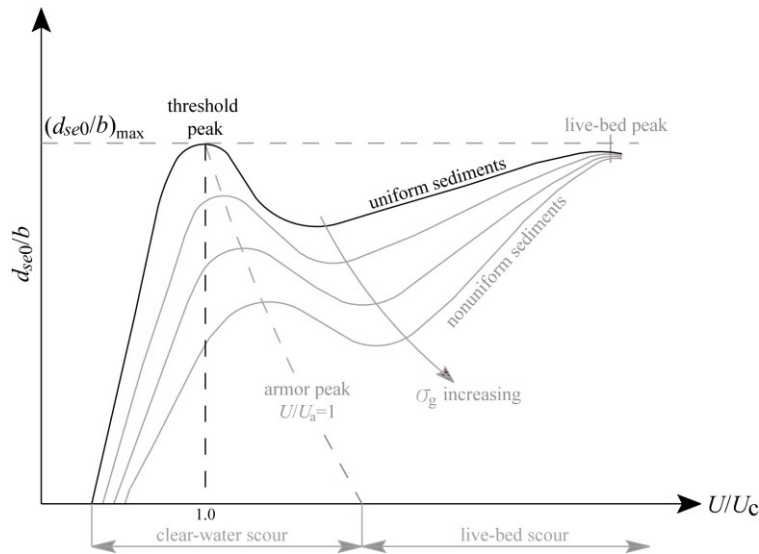


Fig. 14. Local scour depth variation with flow intensity (modified from Melville and Coleman, 2000)

## 2.4. Side walls

For bridge piers, a blockage ratio equal or more than 10, i.e.,  $B/b \geq 10$  was proposed to neglect the side wall effects and minimise pier blockage effect (Laursen and Toch, 1956; Chiew and Melville, 1987). In particular, Chiew (1984), performing live-bed tests, found that the blockage ratio of 8 proposed by Shen *et al.* (1966a) can produce significant wall effects.

Furthermore, the ratio of  $h$  with respect to  $B$  seems to be important. When  $B/h \leq 3$  the side walls significantly affect the velocity distribution (Fig. 15), which becomes three-dimensional (Graf and Altinakar, 1998). This condition, i.e.,  $B/h \leq 3$  is not common in natural rivers. Thus, it is recommended not to carry out local scour experiments at piers in narrow channels ( $B/h \leq 3$ ). Anyway, further research is required in order to show the effects of narrow channels on scour at piers.

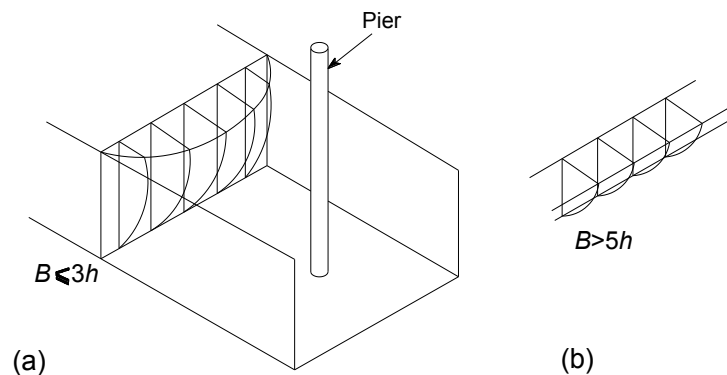


Fig. 15. Distribution of approaching flow velocity for: (a)  $B/h \leq 3$ ; (b)  $B/h > 5$  (modified from Graf and Altinakar, 1998)



## 2.5. Sediment size

Both coarse and fine sediment sizes may affect scour depth. Sediment coarseness effect is represented by the ratio  $b/d_{50}$ . For smaller values of this ratio, the sediment grains are large with respect to the pier dimension and, consequently, the erosion process is impeded. The best-fitting line in Fig. 16a (dashed line) by Chiew and Melville (1987) shows that for  $b/d_{50}=25$ , the sediment size corrective factor,  $K_d$ , can achieve the value of about 0.89. This value shows that sediment coarseness effects can be found to some extent when  $b/d_{50}=25$ . Melville and Sutherland (1988) in a design procedure also proposed  $b/d_{50} \geq 25$  to neglect sediment coarseness effect (Fig. 16a). Several researches (e.g., Breusers and Raudkivi, 1991; Chiew and Melville, 1987) proposed a more restrictive value: they showed that sediment size effects on scour depth can be neglected when  $b/d_{50} \geq 50$ . More recent studies in large-scale flumes and analysis of field data show that the ratio  $d_{se0}/b$  increases with  $b/d_{50}$  up to a specific limit value, beyond which it decreases (Sheppard *et al.*, 2004; Lee and Sturm, 2009). The corrective factor  $K_d$  proposed by Sheppard *et al.* (2004) is shown in Fig. 16b, where it can be noted that  $K_d$  decreases for values of  $b/d_{50}$  greater than about 50. On the other hand, on the basis of Lee and Sturm's results,  $K_d$  decreases for values of  $b/d_{50}$  greater than 25. It seems that the previous limit values of  $b/d_{50}$  (25 or 50) were defined through the analysis of datasets acquired in small scale experiments. Raudkivi and Ettema (1983) also believed that for values of  $b/d_{50} \geq 130$ ,  $d_{se0}/b$  is invariant of sediment size (Fig. 17a). However, it is possible that for  $b/d_{50} \geq 130$ ,  $d_{se0}/b$  varied with  $b/d_{50}$  as shown with red line in Fig. 17a. Although more investigations are needed in order to know accurately the effect of the sediment coarseness parameter, on the basis of the available researches its effect on scour depth should be neglected if  $25 \leq b/d_{50} \leq 130$ .

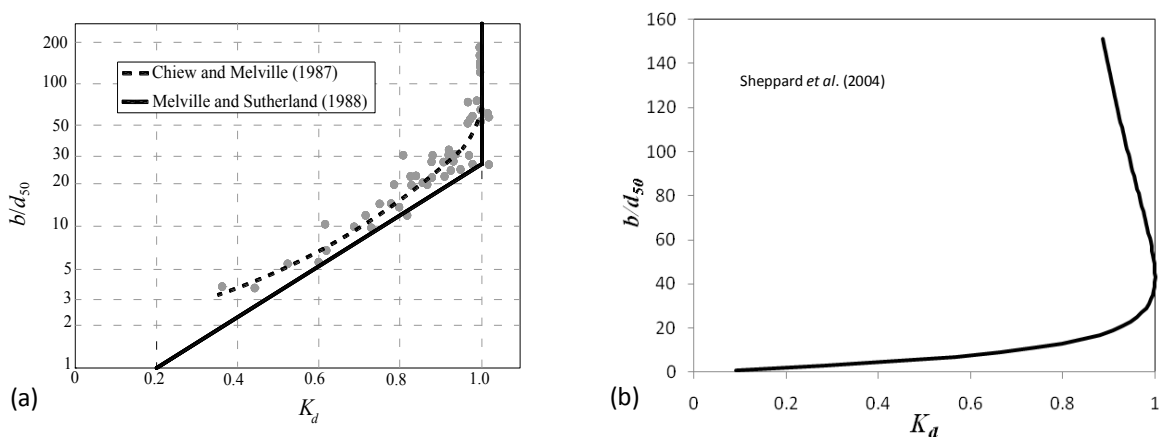


Fig. 16. Variation of the sediment size corrective factor with the sediment coarseness in different studies

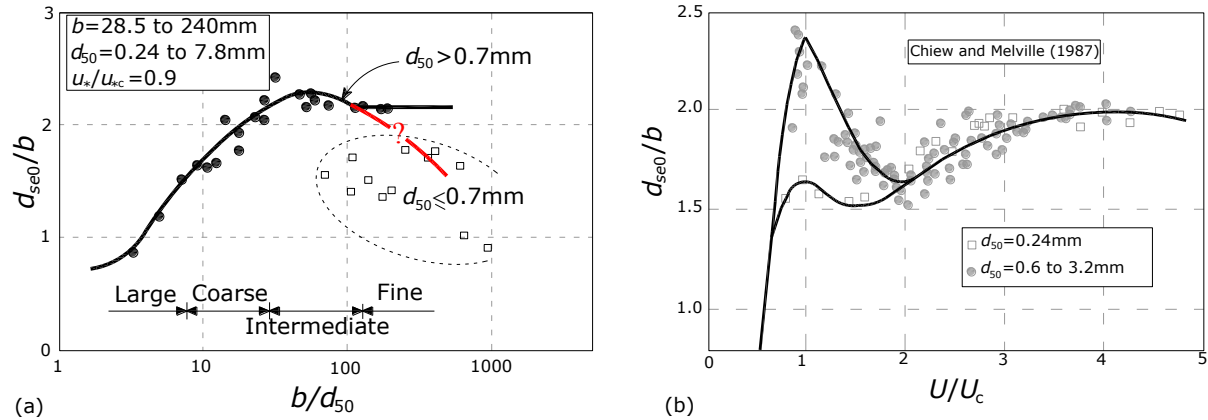


Fig. 17. Influence of sediment size on scour depth: (a) Raudkivi and Ettema (1983); (b) Chiew and Melville (1987)

On the other hand, a ripple-forming bed is expected when sediment sizes are less than 0.7 mm and  $u_* > 0.6u_{*c}$  (Breusers and Raudkivi, 1991), where  $u_*$  and  $u_{*c}$  are the shear velocity and the critical shear velocity for the initiation of sediment motion, respectively. In such condition, reduced scour depths will be achieved for flow intensity values around the threshold condition of sediment motion as shown in Fig.17b.

## 2.6. Flow depth

The scour depth at a pier foundation increases as the water depth increases up to a threshold value. Previous studies reveal that, to consider the flow shallowness effects on scour depth, both dimensionless parameters  $h/b$  and  $b/d_{50}$  should be taken into account (Raudkivi and Ettema, 1983; Chiew and Melville, 1987; Breusers and Raudkivi, 1991). Melville and Sutherland (1988) proposed  $h/b > 2.6$  (Fig. 18a) in a design procedure, in order to neglect shallowness effects when  $b/d_{50} \geq 50$ , although Fig. 18b shows that a value of about 4.3 is necessary to wholly eliminate the shallowness effects on scour depth. Breusers and Raudkivi (1991) indicated that for fine sediments the scour depth can be almost independent of flow depth when  $h/b \approx 2$  (Fig. 18b). According to Fig. 18b, values of about 0.89 and 0.92 are achieved for the flow depth corrective factor  $K_h$  when  $b/d_{50} = 50$  and  $b/d_{50} > 70$ , respectively. In fact, when  $b/d_{50} > 70$  a value of  $h/b \approx 2$  is enough to neglect shallowness effect ( $K_h > 0.9$ ); however, for  $b/d_{50} = 50$  a value of  $h/b = 2.5$  is more appropriate in order to obtain the same  $K_h$  as for  $b/d_{50} > 70$  and  $h/b = 2$ . The value  $h/b = 2.5$  is also assumed by Ettema (1980) to neglect the influence of approach flow depth. This value is also close to the value  $h/b = 2.6$  proposed by Melville and Sutherland (1988).

In summary, shallowness effect is a function of both  $b/d_{50}$  and  $h/b$ . For  $b/d_{50} \approx 50$ , it can be assumed as negligible for  $h/b \geq 2.5$ , whereas a minimum value of  $h/b \approx 4.3$  is required in order to eliminate it completely.

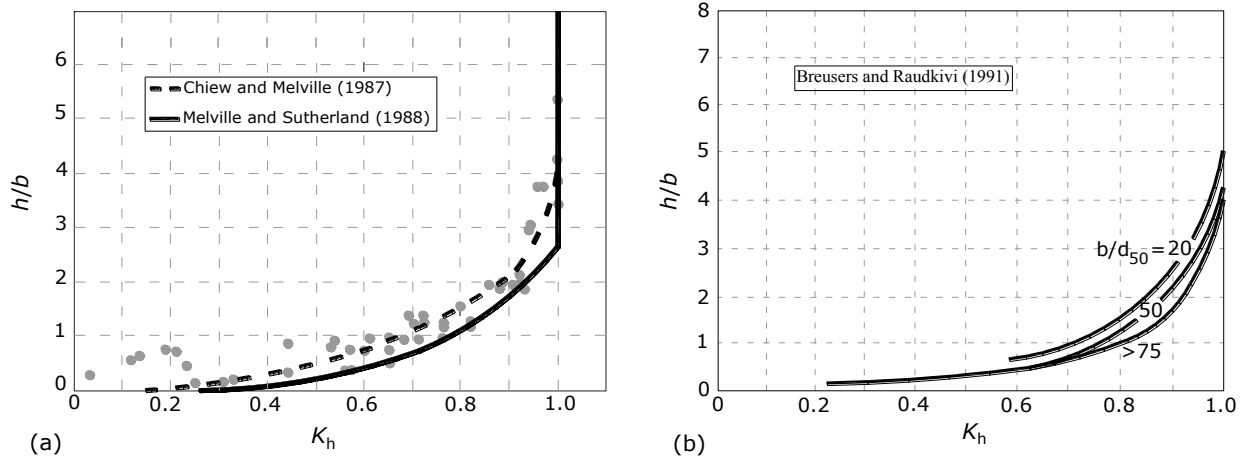


Fig. 18. Variation of the flow depth corrective factor with the flow shallowness

## 2.7. Time

Under clear-water scour conditions, the scour depth develops asymptotically towards the equilibrium state. In contrast, in live-bed scour condition the equilibrium depth is reached more quickly and then the scour depth oscillates, owing to the passage of bed forms. In order to achieve equilibrium conditions in small-scale laboratory experiments on clear-water scour depth development, it is necessary to run the experiments for several days. Melville and Chiew (1999) proposed that the equilibrium is reached if the variation of the scour depth is equal or less than 5% of the pier diameter in a period of 24 h. Grimaldi (2005) proposed the following procedure, in order to design the duration of equilibrium tests and verify if equilibrium is finally reached:

- 1) the test duration is computed *a priori* as  $2 \cdot 10^6 \cdot b/U$ , according to Franzetti *et al.* (1994);
- 2) the scour depth is plotted versus time in a semi-logarithmic graph and the equilibrium state is assumed as achieved if a slope change is identified (see Raudkivi and Ettema, 1983; Cardoso and Bettess, 1999);
- 3) the variation of the scour depth in 24 h is computed in order to verify if it is less than a little percentage of  $b$  ( $\Delta d_{s,24} \leq 0.05b/3$ ).

Conditions 2 and 3 were considered as mandatory, whereas the test duration was computed as a reference value (see Grimaldi *et al.*, 2009a and 2009b, for the application of the criterion).

Recently, Lança *et al.* (2010) performed five long tests, which lasted 24.9 to 45.6 days. Their results show that all the above methods may be erroneous. They proposed to adjust a 7 days-long test with a 6-parameters polynomial function and extrapolated the results to infinite time, in order to assess robust values of the equilibrium scour depth at single cylindrical piers. This method needs more attention and probably further investigation is necessary to be suggested as a robust method. In fact, the Author proposed 7 days on the base of experiments with piers of diameters  $b=6.3$  cm, 7.5 cm and 8 cm. The proposed required time, i.e. 7 days, probably should depend on the pier width  $b$  and the other experimental conditions. For example, longer test is required for wider piers and *vice versa*. Application of polynomial functions was also employed by Sheppard *et al.* (2004) in large scale tests when the scour at a circular pier significantly

reduces. In fact, results of Sheppard *et al.* (2004) shows that time to 90% of equilibrium scour depth may change based on the experimental conditions. Therefore, the base time required to equilibrium also should change and cannot be a fixed value as 7 days. The parameter related to time,  $Ut/b$  also shows that for a certain approach velocity at a certain time this parameter is greater in smaller pier. In other words scour rate in smaller pier is higher. Other parameters, e.g. flow intensity also influence on temporal evolution of scour (Melville and Chiew, 1999). Therefore, this proposed method needs more investigations.

Note that all these criteria were originally proposed for unprotected piers or protected piers with some types of countermeasures that have similar scour evolution to an unprotected pier and application of these methods may not be applicable for some countermeasures which slow down scour evolution and change the temporal evolution of scour depth respect to an unprotected pier. These limitations will be discussed in Chapter 4.

### 2.8. Pier size

Respecting all the above conditions for a single pier may often result in the maximum scour depth for a selected pier width. Raudkivi and Ettema (1983), Chiew and Melville (1987), and Melville and Sutherland (1988) indicated that the dimensionless maximum scour depth at equilibrium can reach the upper limit  $d_{se0}/b=2.3$  to 2.4; consequently, in such condition (E.8) reduces to  $d_{se0}/b=\Phi(Fr_p)$ . Note that the upper limit of 2.3 to 2.4 was found in most of the investigations; however, rarely higher values (also more than 3) were reported in some researches (e.g., Lee and Sturm, 2009).

The pier Froude number,  $Fr_p$ , is an important parameter indicating the effects of pier size (scale effect) on scour depth and it relates the ratio of stagnation head,  $H=U^2/(2g)$ , to pier width,  $b$ . Since  $H$  is independent of pier width, for two piers with widths equal to  $b_s$  and  $b$  ( $b>b_s$ ), in a certain flow, a certain value of  $H$  is expected (Fig. 19).  $H$  takes into account the flow gradient at pier. This fact results in strength of downflow and consequent horseshoe vortex respect to pier size increases at the pier foundation of smaller pier.

Furthermore, narrower piers generate stronger eddies at greater shading rates at the same flow velocity, producing greater relative scour depths,  $d_{se0}/b$  (Ettema *et al.*, 1998a; Ettema *et al.*, 1998b; Ettema *et al.*, 2006). Therefore, it is expected that the ratio of  $d_{se0}/b$  increases as  $b$  increases.

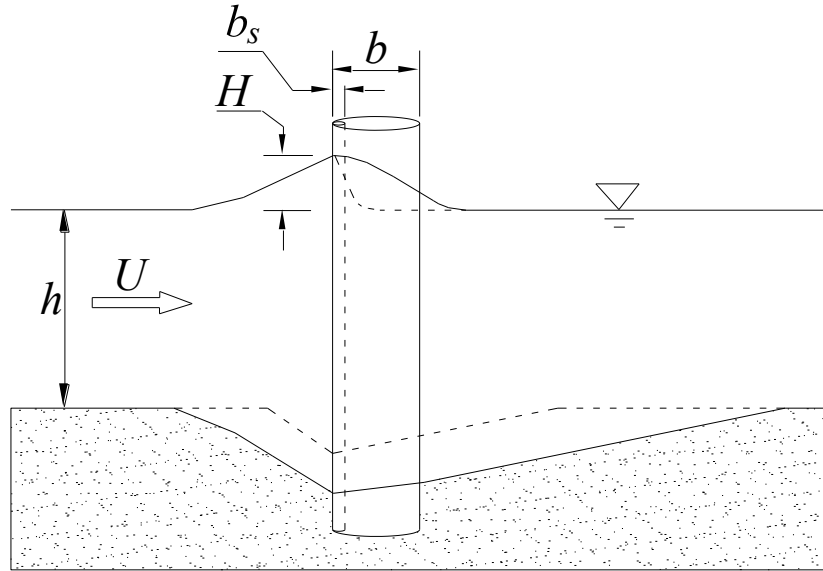


Fig. 19. Stagnation pressure head ( $H$ ) for two pier sizes in the same flow (Ettema *et al.*, 1998a)

Scaling from flume to field conditions needs similitude of all dimensionless parameters in Eq. (3). In general, laboratory experiments are performed by using particles of comparable size with respect to the field; therefore, in order to obtain the same flow intensity,  $U/U_c$ , larger values of  $U$  are set in flumes than those required by the Froude law for dynamic similitude, and the value of  $Fr_p$  (or  $H/b$ ) in laboratory experiments using small scale piers is higher than in field conditions (Ettema *et al.*, 1998a). In fact, increasing the pier size causes decreasing the ratio  $d_{se0}/b$  and a functional dependence as  $d_{se0}/b = \Phi(Fr_p)$  may occur for wider pier diameters. Such relation for a few tests was found by Ettema *et al.* (2006), as shown in Fig. 20. This functional relationship may also be due to the sediment size effect. In fact, the ratio  $b/d_{50}$  in Ettema *et al.* (2006) ranged from 61 to 387. Therefore, the decrease of  $d_{se0}/b$  vs. pier size could also be due to the increase of  $b/d_{50}$  (see Fig. 16b). More study in large scale flumes might clarify the influence of these two parameters ( $b/d_{50}$  and  $Fr_p$ ) on the maximum scour depth.

In fact, in order to obtain the influence of pier size or  $Fr_p$  on the experiments, it is necessary to perform the experiments in relatively wide flumes (e.g.,  $B=4\text{m}$ ) which is not available in most of laboratories. Results of available studies show that in general the experiments were carried out in small size flumes ( $B \leq 1\text{m}$ ). In this condition, piers with  $b \leq 10\text{cm}$  should be used in order to avoid side-wall effect. Therefore such relationship as shown in Fig. 20 may not be obtained. In present study, as it will be explained in Chapter 4, all the tests were performed in one condition. Therefore, the results will be valid only for the selected condition. However, such condition seems not be critical for the obtain results. In fact, as the pier size increases the strength of downflow and horseshoe vortex respect to pier size reduces. Therefore, It is expected that efficiency of countermeasure in application for larger piers will not reduce. However, more study is also needed to ensure about this statement.

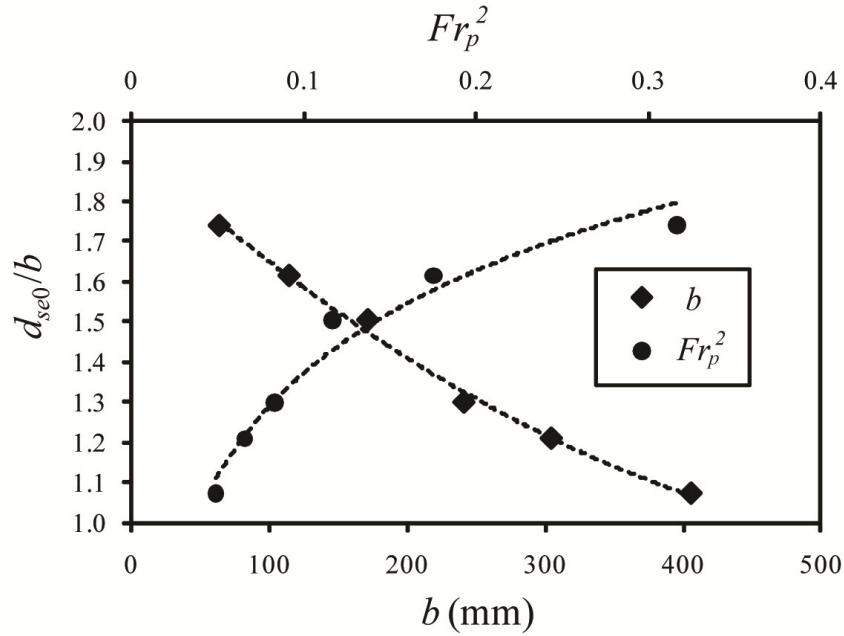


Fig. 20. Variation of  $d_{se0}/b$  with  $b$  and  $Fr_p$  for constant approaching flow velocity (Ettema *et al.*, 2006)

## 2.9. Required conditions to achieve the maximum scour depth at a pier

Based on the above consideration on dimensionless parameters, the required conditions to obtain maximum scour depth at a circular pier are summarised in Tab. 5. In order to achieve the maximum possible scour depth for a certain pier, all these conditions should be respected simultaneously. On the other hand, it is not so easy to respect all the conditions, since in some experiments respecting some of them may cause that other parameters fall out of the required ranges. For example, by increasing the flow depth, the flow shallowness effect decreases, but the side wall effect may increase. Therefore, for some parameters the two conditions *negligible* and *eliminated* are proposed. In fact, when a parameter is selected in a negligible range, its effect may remain in the experiments and lesser scour depth may result. Pier scouring is certainly a complex phenomenon and the experimental results are often scattered points and do not follow a defined line, as shown in some of the Figures presented in this paper and in several other Figures taken from the literature (e.g., Chiew and Melville, 1987). In other words, the criteria presented in this chapter only reflect the general behaviour of the maximum scour depth with respect to the known influencing parameters. In special conditions, measured values of  $d_{se0}/b$  higher than predicted values were also reported in the literature (e.g., Lee and Sturm, 2009), even if one or more influencing parameters did not range in the recommended variation intervals.

**Tab. 5. Required conditions to achieve the maximum scour depth at a circular pier**

Influencing factor	Required condition
Sediment grading	$\sigma_g \leq 1.3$ to 1.5
Flow intensity	$0.9 \leq U/U_c < 1$
Side walls	$B/b \geq 10$ and $B/h > 3.5$ to 5
Sediment size	(1) $d_{50} > 0.7$ mm; (2) $25 \leq b/d_{50} \leq 130$ to neglect sediment coarseness effect.
Flow depth	For $b/d_{50} \approx 50$ , $2.5 \leq h/b < 4.3$ or $h/b \geq 4.3$ in order to neglect or eliminate shallowness effect, respectively. For higher values of $b/d_{50}$ , lesser value of $h/b$ is required to assume scour depth as independent of flow depth.
Water viscosity	$Re_p > 7000$
Time to equilibrium	The composite method by <i>Grimaldi</i> (2005)

Note that the influences of these dimensionless numbers have been already investigated for unprotected piers and more study is necessary to investigate influence of these parameters in pier protected with a specific countermeasure. Assuming the effects of these parameter be same for the solid pier and the protected pier, in-line with Ettema (1980) and Chiew (1992), Vittal *et al.* (1994), Gimaldi *et al.* (2009a,b), etc., the ratio of  $d_{se}/b$  for protected pier with each countermeasure will be a function of  $Fr_p$  and certain dimensionless parameters related to the selected countermeasure. For each countermeasure these parameters will be presented in Chapter 5. In Chapter 3, based on these criteria, a preliminary evaluation of previous studies is presented and in Chapter 4, they will be used as a basis to design the experiments.





## Chapter 3

### REVIEW OF FLOW-ALTERING COUNTERMEASURES AGAINST LOCAL SCOUR AT BRIDGE PIERS

#### 3.1. Introduction

As indicated in Introduction, all the perceived engineering solutions in order to decrease local scouring at bridge piers can generally be categorised into two distinct groups; *bed-armouring* and *flow-altering countermeasures*. The idea behind bed-armouring countermeasures is the provision of a physical barrier against pier scour. In practice, the barriers are often in the form of large, heavy units that do not easily move with the flow. Examples of such units are riprap stones, Reno mattresses, cabled tied blocks, gabions etc. On the other hand, flow-altering countermeasures decrease the power of the eroding agents, e.g. downflow and horseshoe vortex, which are main factors in scouring at the piers (Parker *et al.*, 1998; Chiew and Lim, 2003). Note that in some cases, a countermeasure may have both influences on scour depth reduction. For example, tetrahedral frames proposed by Tang *et al.* (2009) as bridge scour countermeasure, although influence the flow around the pier, can be also assumed as a bed-armouring countermeasure. Riprap stones may influence the flow around the pier too; however, they mainly increase the stability of bed materials.

Although use of bed-armouring countermeasures in particular riprap is more common in practical purposes, they may be involved in some types of failures. According to Chiew (1995), Chiew and Lim (2000), Unger and Hager (2006), the mechanism of Riprap failure can be summarised into four major categories as *shear failure*, where the riprap is unable to withstand the down flow and the horseshoe vortex associated with the pier scour mechanism; *winnowing*

*failure*, where the underlying finer bed material escapes through the voids of the riprap; *edge failure*, where riprap material at the interface to the bed material slides into the scoured surface; *embedment failure*, which is caused by fluctuations of the sediment bed due to propagation of the bed features. Figure 21 shows these possible failure and extensive discussions about these types of failure are presented in indicated references. In fact, due to such problems the researchers tried to find some alternatives to bed-armouring countermeasures.

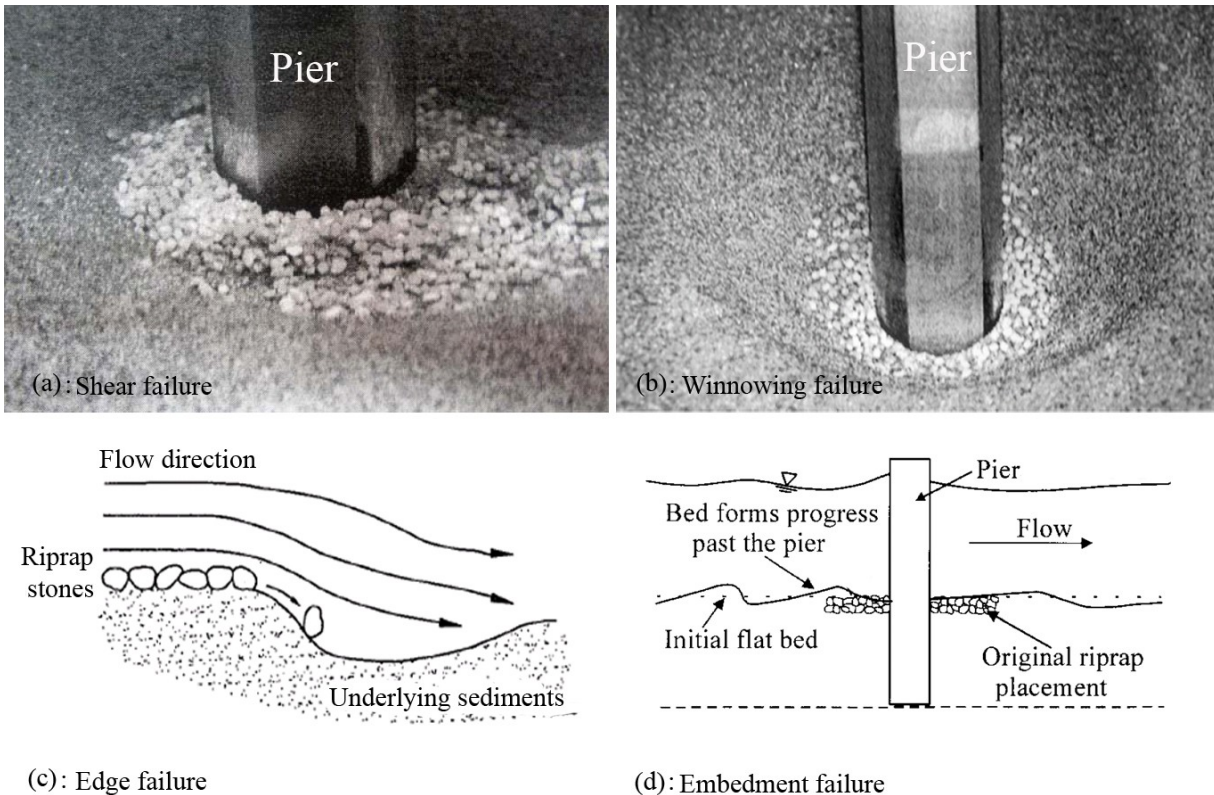


Fig. 21. Main types of riprap failure (Chiew, 1995; Lauchlan and Melville, 2001)

After extensive investigation in all proposed types of flow-altering countermeasures, four main categories, based on the shape and performance of each countermeasure, are identified: 1) openings through piers, 2) pier-attachments, 3) bed-attachments, and 4) other devices (Fig. 22). Each category will be analysed in detail in the following sections (Tafarjnoruz *et al.* 2010a).

## 3.2. Openings through the piers

In the first category of flow-altering countermeasures the downflow and horseshoe vortex strength is decreased by conveying a part of approach flow through the openings. In this case three major methods were proposed and investigated by researchers: internal connecting tubes, pier group and slot.

### 3.2.1. Internal connecting tubes

This type of countermeasure, also called *internal openings*, consists of connecting tubes in the

pier (Fig. 23). Several experiments on internal connecting tubes applied to circular piers embedded in a sand bed were performed by Abd El-Razek *et al.* (2003). Various connecting tubes arrangements were tested, by changing the inclination angle of the internal connecting tubes with respect to the approach flow direction,  $\alpha$ , the distance of the side openings with respect to the upstream opening,  $X_0$ , and the opening diameter,  $d$ , keeping constant the vertical spacing between openings,  $h_i=h/5$ , in flows with different Froude numbers,  $Fr$ .

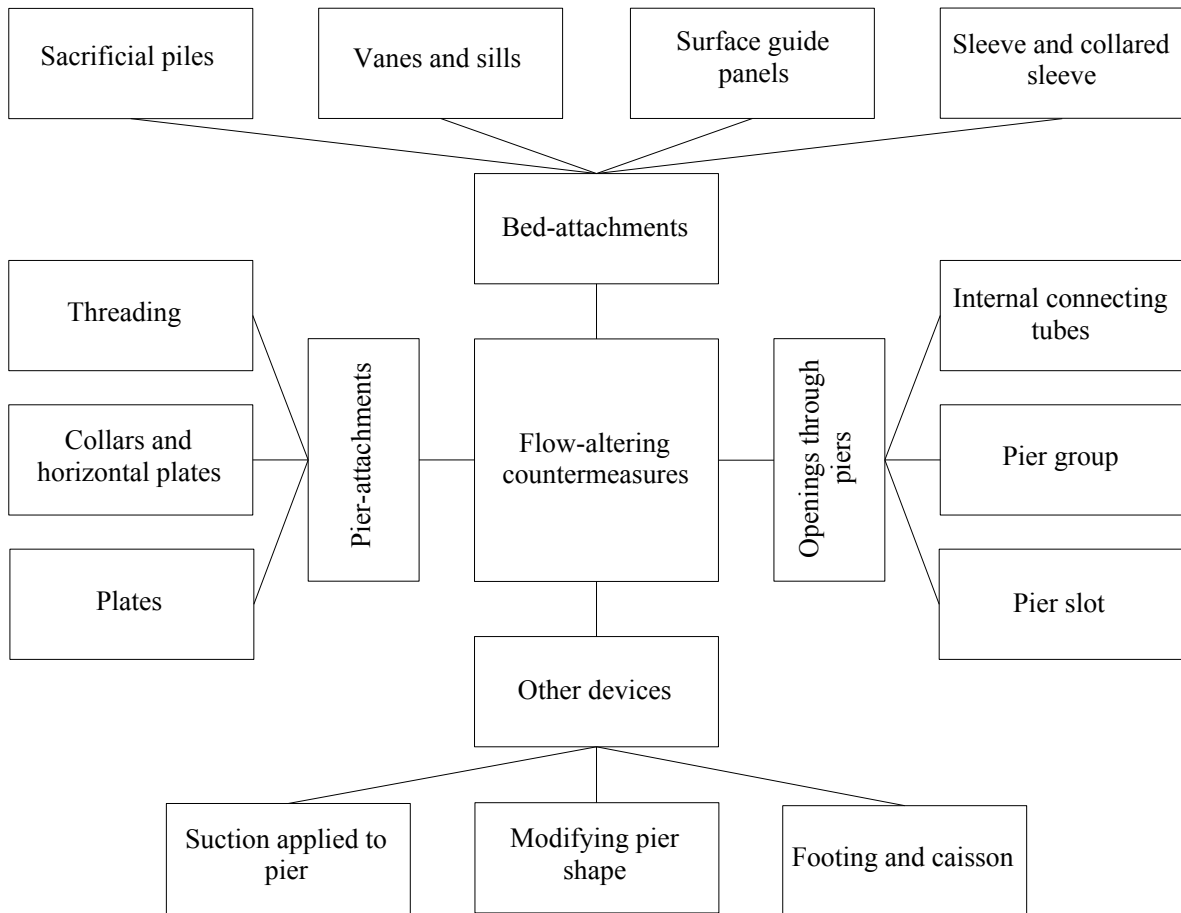


Fig. 22. Classification of flow-altering countermeasures against pier scouring

Efficiency of this countermeasure increased with  $d$  and reached 39% in the best configuration ( $d/b=0.25$ ,  $\alpha=90^\circ$  and  $X_0/b=0.5$ , for  $Fr=0.217$ ). However, the maximum scour volume reduction, computed with an analogous formula, was achieved for  $d/b=0.188$  and was equal to about 62%.

### 3.2.2. Pier group

In this countermeasure the pier will be replaced with smaller piers. This method was proposed by Vittal *et al.* (1994) by replacing a solid pier with three smaller piers in two configurations: *partial* and *full pier groups*. In the former, the solid pier may be replaced by a pier group extending only

partially into the flow depth, the rest of the pier remaining solid up to the bridge deck (Fig. 24a;  $y_L < h$ , where  $y_L$  is the height of the pier group above the bed). In the latter, a full pier group extends into the entire flow depth ( $y_L \geq h$ ).

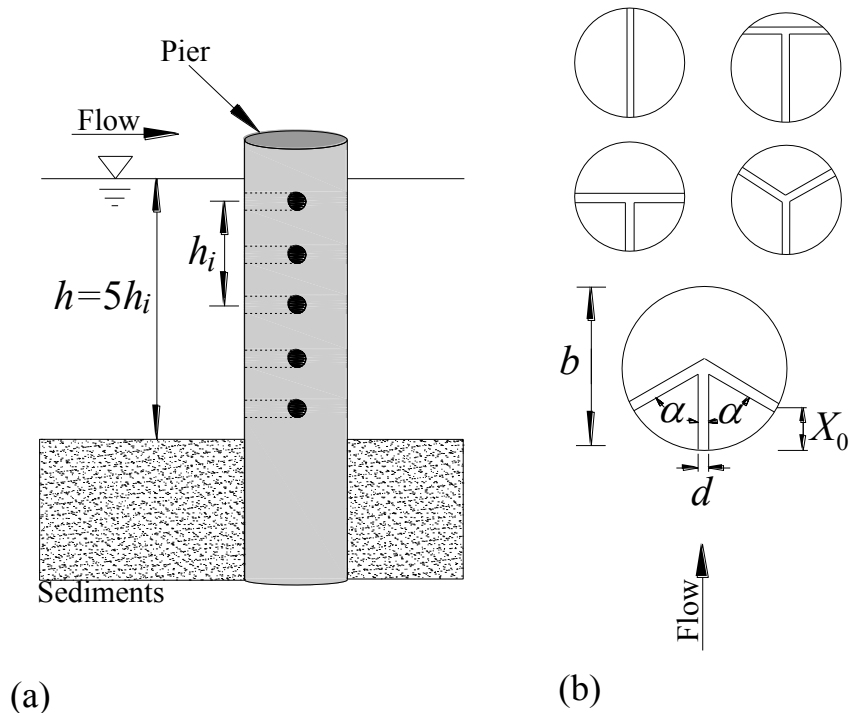


Fig. 23. Configuration of internal connecting tubes: (a) side view; (b) typical cross-sections (modified from Abd El-Razek *et al.*, 2003)

Vittal *et al.* (1994) conducted experiments using full pier groups at an angular spacing of  $120^\circ$  in the case that anyone of them can just pass through the gap between the other two, having diameter  $b_g$  (Fig. 24b).

Results of full pier group tests using different sediment sizes, water depths and orientations,  $\theta$ , showed that the results were obtained in the tests for  $\theta=30^\circ$ , with average scour reduction of about 39%.

Results of the experiments with partial pier groups showed that the scour reduction is less than in the case of full pier groups and decreases for decreasing  $y_L/h$ .

### 3.2.3. Pier slot

The basic principle of using a slot is to divert the downflow away from the bed, reducing the impinging effect on the bed. The slot width,  $w_s$ , length,  $l_s$ , and location are parameters influencing the performance of a slot in reducing the scour depth (Fig. 25a). Location of a slot can be described with the sinking depth of the slot,  $z_s$ , which is assumed to be positive for slots sunk in the bed and negative otherwise.

A slot near the bed diverts the downflow through its opening, thus reducing the erosive effects; in other words, the oncoming flow at the bottom boundary layer accelerates through the

slot as a horizontal jet. Since the downflow at the pier is perpendicular to the jet, the latter may deflect the downflow away from the bed, causing a scour reduction. In contrast, a slot near the water surface allows near-surface water to pass through the slot opening, thereby creating a similar effect as a lower flow depth (Chiew, 1992).

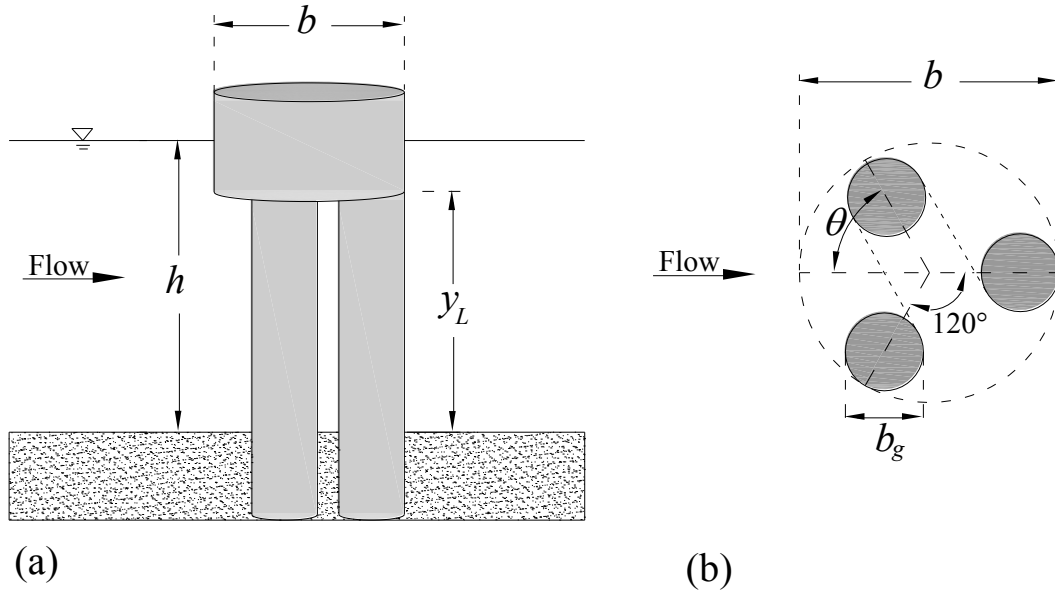


Fig. 24. Partial pier group ( $\theta=60^\circ$ ); (a) side view; (b) plan view (Vittal *et al.*, 1994)

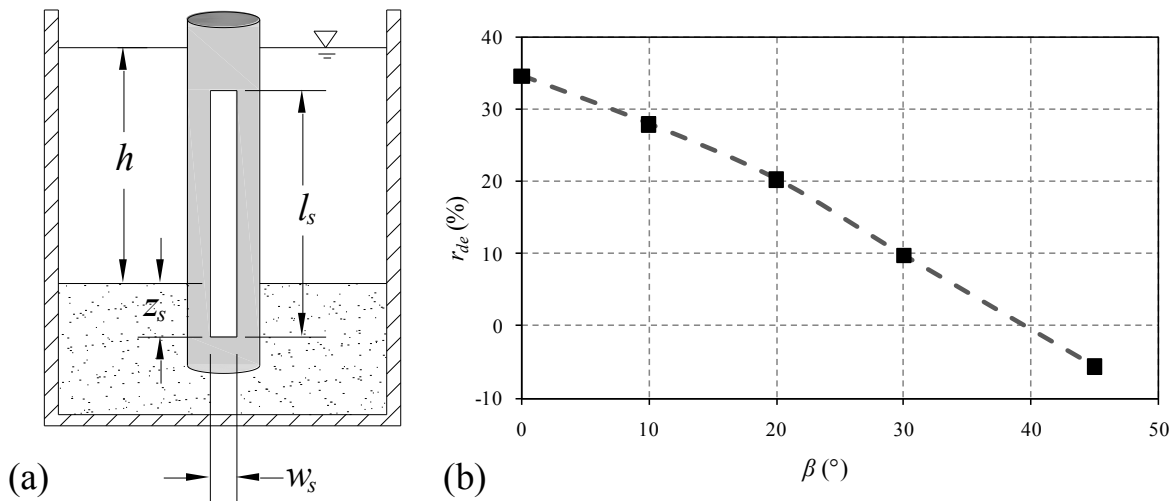


Fig. 25. (a) Configuration of a slot through a pier; (b) scour depth reduction versus angle of attack (modified from Kumar *et al.*, 1999)

Results of several researches by different investigators show that in general, by increasing slot length,  $l_s$ , and/or slot width,  $w_s$ , the efficiency of the slot in scour depth reduction will increase (Tanaka and Yano, 1967; Chiew, 1992; Kumar, *et al.* 1999; Moncada-M *et al.*, 2009). The experiments also indicate that a slot near the bed is more effective than a slot near the water surface (Tanaka and Yano, 1967; Chiew, 1992; Heidarpour, 2002; Moncada-M *et al.*, 2009) and

the efficiency of a slot may increase when it extends partly into the bed (Tanaka and Yano, 1967; Kumar *et al.*, 1999; Grimaldi *et al.*, 2009b).

Earlier researches about application of slot were conducted by Shen *et al.* (1966b) and Tanaka and Yano (1967). In tests by Shen *et al.* (1966b) the cylindrical pier split along the axis of symmetry. This type of slot is different with typical drilling slot through the pier and also can be classified as modifying pier shape.

Tanaka and Yano (1967) tested circular piers with two square slot sizes, i.e. 1 cm×1 cm ( $w_s/b=0.33$ ) and 2 cm×2 cm ( $w_s/b=0.67$ ), obtaining the maximum efficiencies of about 18.5% and 30%, respectively.

Circular piers with slots having  $w_s=0.25b$  and  $w_s=0.5b$  and various lengths were also tested by Chiew (1992), who reported a maximum reduction of the equilibrium scour depth equal to 20% and 30%, respectively. Similar results for the case of slots with  $w_s=0.25b$  were reported by Vittal *et al.* (1994).

Kumar *et al.* (1999) tested a circular pier with slots having  $w_s=0.25b$  and two slot lengths, i.e.  $l_s=h$  ( $z_s=0$ ) and  $l_s=h+d_{se0}$  ( $z_s=d_{se0}$ ). Results showed that the slot efficiency was greater for the sunk slot. Kumar *et al.* (1999) also carried out interesting experiments in order to investigate the effect of the angle of attack,  $\beta$ , using a circular pier with a slot extended into the bed (see Fig. 25b, in which  $d_{se}$  is the equilibrium scour depth in the case of pier with slot). Results showed that the scour depth reduction decreased significantly by increasing the angle of attack. For  $\beta \approx 20^\circ$ , the efficiency of a slot having  $l_s > h + d_{se0}$  decreased and was the same as in the case of a shorter slot ( $l_s=h$ ); for  $\beta \approx 40^\circ$ , the slot is not efficient and the pier behaves as an unprotected one. If  $\beta$  increases further, the scour depth exceeds  $d_{se0}$ .

Heidarpour (2002) considered the effect of two slots (having  $w_s=0.25b$  and  $l_s=b$  or  $2b$ , respectively) on scour reduction. Circular and round-noised piers were used, with the slots near the bed and near the water surface. Results showed that the slots near the water surface had no influence on the equilibrium scour depth for the circular pier, and scour reduction was negligible (less than 10%) for the round-noised pier. The maximum scour reduction (10% to 18%) occurred for piers with  $l_s=2b$  close to the bed.

Heidarpour *et al.* (2003) tested slots with  $w_s=0.25b$  and  $l_s=2b$  in-line pier groups (aligned streamwise). The Authors used groups of two or three circular piers, with pier spacing  $s=2b$  and  $4b$  and  $\beta=0^\circ, 5^\circ, 10^\circ$  and  $15^\circ$ . Figure 26 shows the influence of pier spacing and angle of attack on the scour reduction, in the case of groups of three piers. Heidarpour *et al.* (2003) concluded that the slot efficiency increases as  $s$  increases and/or  $\beta$  decreases.

Grimaldi *et al.* (2009b) conducted several tests to consider the behaviour of a slot with  $l_s/h=1$ ,  $w_s=0.25b$  and  $z_s/h=0, 1/6, 1/3, 1/2$  and 1. Results showed that the efficiency of the slot was lower for  $z_s/h=0$  and 1, higher for  $z_s/h=1/6, 1/3$ , and  $1/2$  with maximum scour reduction at equilibrium of about 30% in terms of depth and 70% in terms of area and volume.

A high efficiency of about 88% was found by Moncada-M *et al.* (2009) in experiments with a slot having  $w_s=0.25b$ . The Authors showed that, in general, the greater the slot length,  $l_s$ , the smaller the scour hole sizes, and that the best location of a slot is near the bed.

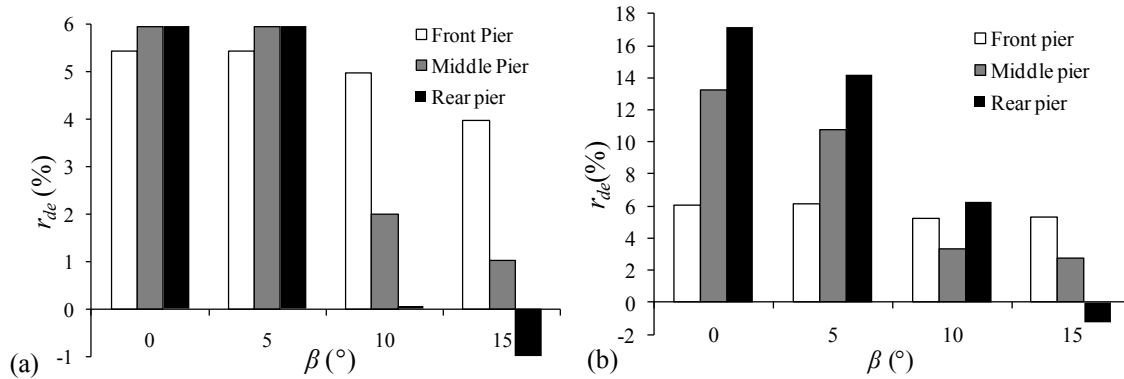


Fig. 26. Equilibrium scour reduction versus angle of attack for an in-line pier group of three circular piers with slots; (a)  $s/b=2$ ; (b)  $s/b=4$  (modified from Heidarpour *et al.*, 2003)

### 3.3. Pier-attachments

In the second category of flow-altering countermeasures the power of downflow and horseshow vortex can be decreased by attaching some devices to the piers. Threading, horizontal plates and collars, and pier-attached plates are the major types in this category.

#### 3.3.1. Threading

Threading was suggested by Dey *et al.* (2006) as an economic and easy to install countermeasure against local scouring at piles and piers (Fig. 27). In this method, cables wrapped spirally forming threads on pile or pier help to weaken the downflow and horseshoe vortex. Dey *et al.* (2006) conducted laboratory experiments using synthetic cables with diameter  $d_c=1, 1.5$  and  $2$  cm wrapped spirally on the surface of a  $20$  cm diameter pile, in order to form circular threads with two thread angles ( $\alpha_t=15^\circ$  and  $30^\circ$ ). For each combination of synthetic cable size and thread angle, three threaded piles (with single, double and triple threading, respectively) were tested. In the best configuration, the maximum scour reduction was  $46.3\%$ , which was obtained for the triple threaded pile with  $\alpha_t=15^\circ$  and the  $d_c/b=0.1$ . Results showed that the scour reduction increased as the cable diameter and the number of threads increased and the thread angle decreased.

A close observation of the flow field, performed by using an acoustic Doppler velocimeter (ADV), revealed that the cable not only reduced the magnitude of the downflow, but also deflected the horseshoe vortex further away towards upstream, resulting in a relatively flat base of the scour hole without any groove; consequently, with this countermeasure scour is considerably reduced (Dey *et al.*, 2006).

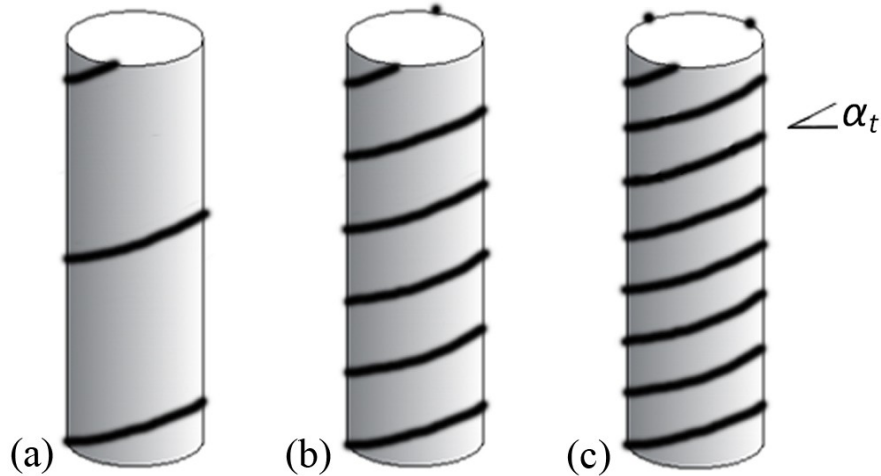


Fig. 27. Application of (a) single, (b) double and (c) triple threading as pier scour countermeasure (Dey *et al.*, 2006)

### 3.3.2. Collars and horizontal plates

A collar consists of a thin horizontal plate around the pier, whereas a horizontal plate (see, e.g., Kim *et al.*, 2005) may be attached just to the front pier face (Parker *et al.*, 1998; Lauchlan, 1999). A collar generally consists of a circular disk; however collars with other shapes were also applied in limited experiments [see, e.g., the Joukowski collar in Dargahi (1987) or a quadrangular collar attached to a circular pier in Sani Khani *et al.* (2008)] (Fig. 28). Collars and horizontal plates as pier scour countermeasures were early investigated by Schneible (1951), Chabert and Engeldinger (1956), Laursen and Toch (1956) and later by Tanaka and Yano (1967) and Thomas (1967).

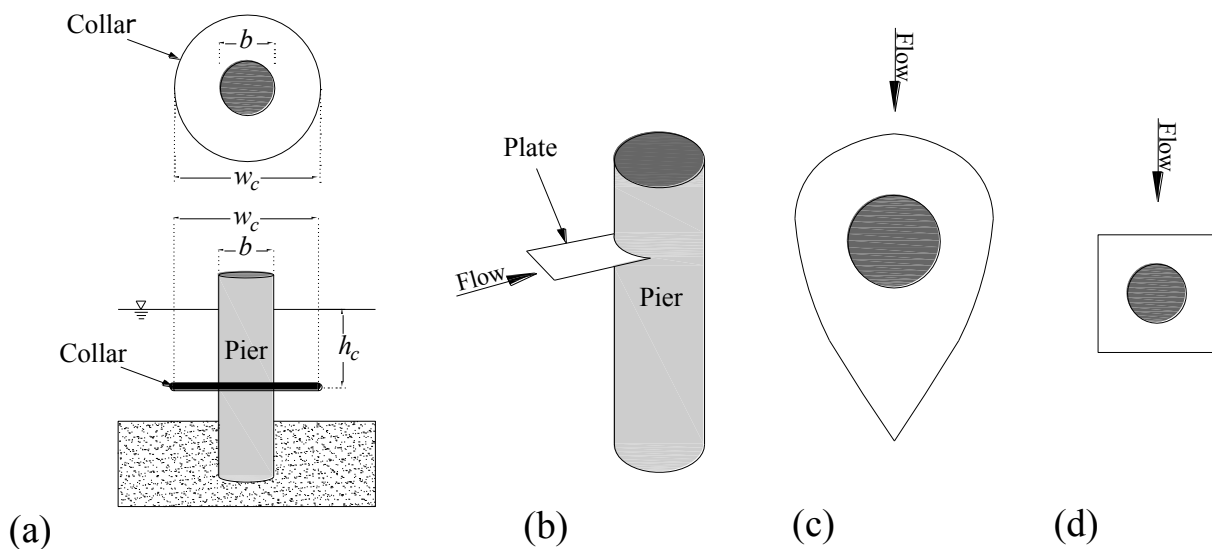


Fig. 28. Configurations of collars or plates attached to a circular pier: (a) circular collar; (b) horizontal plate (Kim *et al.*, 2005); (c) Joukowski collar (Dargahi, 1987); (d) quadrangular collar (Sani Khani *et al.*, 2008)



A collar located at a certain level above the bed divides the flow into two regions: above and below the collar, respectively. In the former region, the countermeasure acts as an obstacle against the downflow, which loses its strength by impinging on it. In the latter region, the downflow and horseshoe vortex strengths are consequently reduced (Zarrati *et al.*, 2006).

Tanaka and Yano (1967) carried out an extensive campaign of experiments on collars, showing that their efficiency increased as the width,  $w_c$ , and/or the distance from the water surface,  $h_c$ , increased, as confirmed by several researches of other Authors (e.g., Chiew, 1992; Zarrati *et al.*, 2004; Kayatürk *et al.*, 2005; Moncada-M *et al.*, 2009). Nevertheless, the construction of collars wider than  $3b$  seems to be impracticable (Zarrati *et al.*, 2006). Results of several tests by Moncada-M *et al.* (2009) showed that the maximum collar efficiency can be reached when the countermeasure is placed at the bed level or slightly below it, depending on the flow conditions and collar size. In particular, in the case of a collar placed below the streambed level, although the scour depth in front of pier may reduce with respect to the case of a collar set at the bed level (*ceteris paribus*), the extension of the scour hole around the pier and the scour depth downstream of it may increase (Zarrati *et al.*, 2004). Chiew (1992) and Singh *et al.* (2001) found 100% scour depth reduction by using collars around a circular pier, with  $w_c=3b$  and  $2.5b$ , respectively; the former Authors used uniform medium sand (median diameter:  $d_{50}=0.33$  mm), whereas the latter used non-uniform medium sand ( $d_{50}=0.285$  mm; geometric standard deviation of the grain size distribution:  $\sigma_g=2.51$ ). A scour depth reduction of 100% in very coarse sand ( $d_{50}=1.4$  mm) was also reported by Moncada-M *et al.* (2009), who used a  $3b$ -wide collar, set at the bed level, in tests of about 6 h.

Efficiency of a collar is also related to its thickness,  $t_c$ . The collar thickness is generally negligible; for large values of  $t_c/b$ , the effective pier diameter will increase and an increase in scour depth will result (Dargahi, 1990).

The development of the scour hole around a pier with a collar is different from that of an unprotected pier or a pier with other kinds of countermeasures. At the beginning of experiments on a collar placed at the streambed level, Zarrati *et al.* (2006) observed the scouring evolution at the rear and at both sides of the pier. In this phase the wake vortices developed, but no scour was caused by the downflow and horseshoe vortex; therefore, the grooves at both sides of pier moved around the collar rim, until they joined each other at the front edge of the collar. When flow penetrated below the collars, upstream to the piers, scouring intensified in this region. Since this process takes time, there was a delay in scouring around the pier perimeter, and the scouring development is considerably slowed down (e.g., Mashahir and Zarrati, 2002; Mashahir *et al.*, 2004; Alabi, 2006). For instance, Mashahir *et al.* (2004), in the case of a collar with  $w_c/b=3$  and  $h_c=h$ , attached to a circular pier, showed that the maximum scour depth at equilibrium was achieved in front of the pier after 90 h and was equal to about 67.5 mm (Fig. 29), whereas for the unprotected pier it was reached after about 44 h and was equal to about 92 mm. The Authors also showed that the collar is more effective than a circular pier foundation with the same width and flush with the bed. In a recent study, Masjedi *et al.* (2010) found that the time needed to reach a given scour depth decreases as the flow intensity increases.

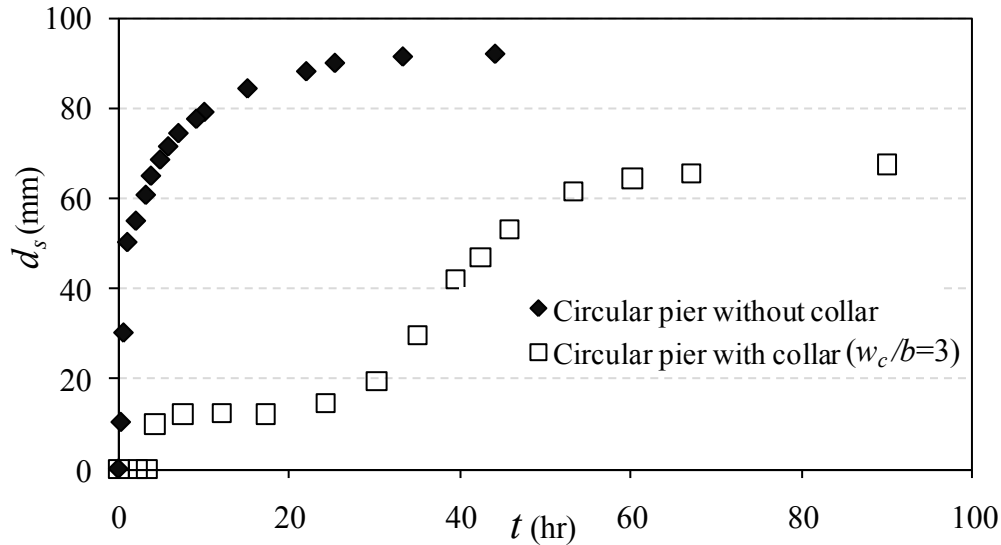


Fig. 29. Time evolution of the scour depth for an unprotected pier and a pier with collar (modified from Mashahir *et al.*, 2004)

Furthermore, the scouring rate increased as the flow intensity,  $u^*/u_{*c}$  (where  $u^*$  and  $u_{*c}$  are shear velocity and shear velocity at initiation of sediment motion, respectively), increased in clear water condition (Mashahir *et al.*, 2007).

Zarrati *et al.* (2006) tested a  $3b$  wide collar set at bed level and observed that the maximum scour depth occurred in front of the pier. Kumar *et al.* (1999) indicated that the deepest scour occurs at the upstream face of the pier for smaller-sized collars placed at higher elevations, and in the wake for larger-sized collars placed at lower elevations. This statement seems to be incorrect, the maximum scour depth location being influenced by both flow conditions and collar parameters. Further research is needed in order to investigate the location of the maximum scour depth around a pier with a collar.

Kumar *et al.* (1999) developed the following empirical formula, based on both original and literature data, which gives the percent scour depth reduction:

$$r_{de} (\%) = \frac{d_{se0} - d_{se}}{d_{se0}} \cdot 100 = 0.057 \left( \frac{w_c}{b} \right)^{1.612} \left( \frac{h_c}{h} \right)^{0.837} \cdot 100 \quad (\text{E.11})$$

Richardson and York (1999) applied several small size collars, as roughness elements with uniform spacing, in order to decrease the downflow strength and consequently the local scour depth at a pier (Fig. 30a). Results showed that, when collars are closely spaced, scour depth was not significantly reduced; vice versa, when collars are largely spaced, the scour depth decreases with respect to the unprotected pier, obtaining a scour reduction equal to 30% in the best configuration. Zarrati *et al.* (2004) also observed an increase of scour reduction by adding a second collar ( $h_c=h-0.6b$  and  $w_c=2b$ ) to a pier protected with a collar ( $h_c=h-0.2b$  and  $w_c=3b$ ).

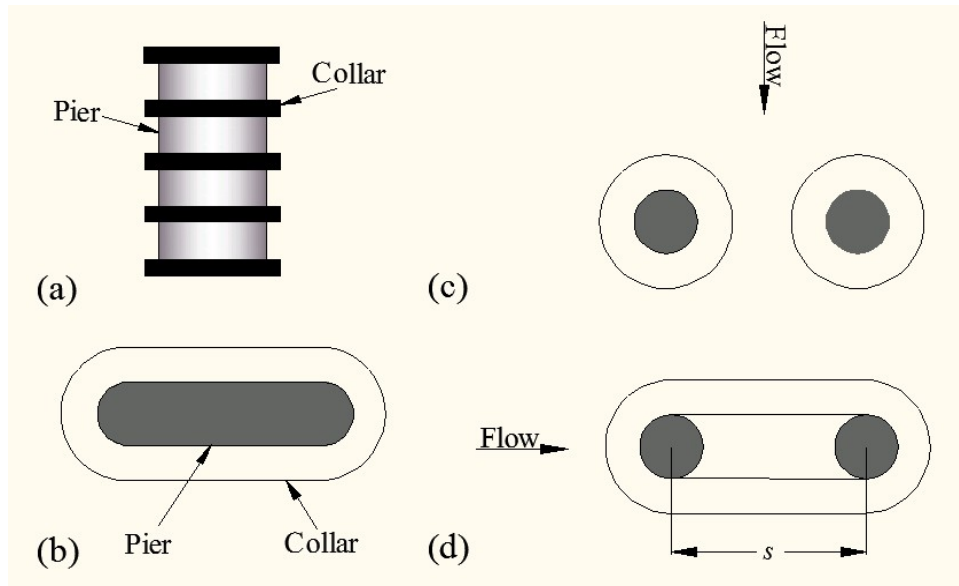


**Fig. 30.** (a) side view of attachment of several collars to a pier (Richardson and York, 1999); (b) plan view of attachment of a collar to a rectangular pier with circular nose and tail (Zarrati *et al.*, 2004); (c) plan view of independent collars for a transverse group of two circular piers; (d) plan view of a continuous collar for an in-line group of two circular piers (Zarrati *et al.*, 2006)

Results of tests on a collar applied to a rectangular pier with circular nose and tail (Fig. 30b) showed that the countermeasure was highly effective (maximum scour reduction of about 74%); however its effectiveness was reduced as the pier skewness with respect to the flow direction increased (Zarrati *et al.*, 2004).

Several tests were devoted to the investigation of collars applied to in-line and transverse pier groups (Heidarpour and Afzalimehr, 2005; Zarrati *et al.*, 2006). Figure 30c shows in-line and transverse pier groups with independent or continuous collars. Results of applications of independent collars on groups of 2 or 3 piers in-line with the flow showed that installing the collar on the rear pier is more effective than on the front pier, and pier spacing and collar size have a more significant influence on the scour at the rear pier than that at the front pier (Heidarpour and Afzalimehr, 2005).

Zarrati *et al.* (2006) considered the effects of continuous or independent collars on in-line or transverse pier groups under clear water conditions. The experimental results relative to in-line groups of two piers revealed that independent collars have a better efficiency compared to continuous collars (about 30% versus 25% at the front pier, and about 75% versus 35% at the rear pier, respectively); however, collars were not effective in the case of transverse pier groups. It was also shown that in a similar test condition the efficiency is greater in the case of a collar applied to a rectangular pier with circular nose and tail aligned with the flow (Fig. 30b) than in the case of an equivalent in-line group of two circular piers with a continuous collar (Fig. 30d).

### 3.3.3. Plates

Plates (or vanes) were tested as bridge pier countermeasures in different shapes and configurations. When a vane is added to a pier, this will divert the streamlines from the pier and reduce the power of horseshoe vortex (Ghorbani and Kells, 2008).

An early study of pier-attached plates was probably conducted by Maza (1967) using an inclined plate as shown in Fig. 31a. Scour began at the edges of the plate; however, when the plate was exposed, the scour could not proceed deeper. It was recommended to set the plate at a slope of 3:1, which provides a 70 to 80% in scour reduction.

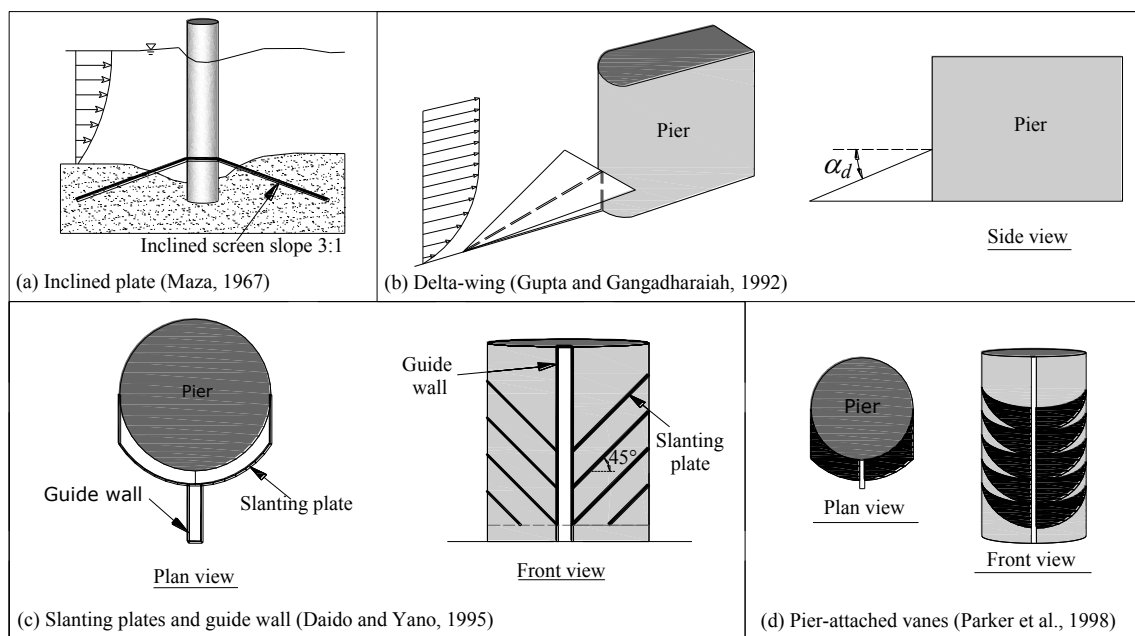


Fig. 31. Different types of pier-attached plates and vanes

Delta-wing is another type of pier-attached vanes. This countermeasure consists of a thin delta-wing-like plate; along the axis of symmetry of its lower face, a thin vertical spinal rib is attached. The spinal rib height decreases to zero at the delta vertex (Gupta, 1987). Figure 31b shows a delta-wing attached to a pier at a conventionally negative angle of attack ( $\alpha_d$ ), which has two effects on horseshoe vortex modification: first, by acting as a barrier to the vortex build-up at the leading edge of the pier foot, and second, by generating a pair of counter-rotating vortices whose sense of rotation is opposite to that of the original horseshoe vortex (Gupta, 1987). In general, the local maximum scour depths along the pier sides occur farther away from the pier side walls and the near wake regions of the pier show deposits of sand when the pier is protected with the delta-wing-like passive device. A maximum local scour depth reduction of 67% under clear water condition and a minimum scour depth reduction of 32% at the end of unsteady flow (hydrograph test) were reported by Gupta and Gangadharaiah (1992) in application of a delta-wing to a rectangular pier with round nose embedded in a fine sand ( $d_{50}=0.16$  mm) bed.

Daido and Yano (1995) installed slanting plates directly on a circular pier (Fig. 31c). A

vertical guide wall also was applied so that it extends upstream from the centre of the pier. On both sides of the guide wall a series of vanes are attached to the surface of the pier, stacked vertically and inclined upward at an angle of  $45^\circ$ . Both guide wall and slanting plates were applied to disrupt and decrease the power of downflow and horseshoe vortex. Daido and Yano (1995) reported reductions in scour depth as high as 90% in clear water condition. Results of laboratory tests about two forms of pier-attached vanes in live-bed conditions are reported by Parker *et al.* (1998). The first form was similar to that used by Daido and Yano (1995); the second form was similar to the previous one, except that vanes were angled downward at  $45^\circ$  in the streamwise-vertical plane (Fig. 31d). Results showed a maximum scour reduction of 50%, which was significantly less than the 90% reported by Daido and Yano (1995) in clear-water condition. This result indicates that such configurations are ineffective in natural rivers in flood condition (Parker *et al.*, 1998).

Some special forms of flow-altering devices were proposed by, e.g., Vysotsky (2001 and 2005) and Kim *et al.* (2005), but they need more attention and deeper investigation in order to evaluate their performances under different flow conditions.

### 3.4. Bed-attachments

These methods aim at diverting or weakening the approach flow or modifying its boundary layer. Consequently, downflow and/or horseshoe vortex will be decreased in power. In this category, several techniques were proposed, which can be classified into four major groups as follows.

#### 3.4.1. Sacrificial piles

Sacrificial piles are single or multiple piles in front of a pier, in order to modify and divert the approach flow away from it, and consequently reduce the scour depth. The piles, which themselves may be subjected to substantial scour, protect the pier from scouring by deflecting the high-velocity flow and creating a lower velocity wake region behind them with lesser erosive force (Melville and Hadfield, 1999; Chiew and Lim, 2003; Haque *et al.*, 2007).

The effectiveness of this countermeasure depends on piles characteristics (number, size relative to the pier dimension, protrusion – partly or fully submerged –, geometric arrangement in relation to each other and to the pier) and flow features (intensity, angle of attack or skewness) (Melville and Hadfield, 1999).

The earliest study on sacrificial piles was probably conducted by Charbet and Engeldinger (1956), who placed the piles in a triangular pattern upstream to the pier and reported up to a maximum scour depth reduction of 50% by changing number, layout and position of the piles.

Also a single pile placed upstream to a pier can reduce the scour depths, depending on the pile diameter and the placement distance upstream to the pier (Shen *et al.*, 1966b). Results of application of a single circular pile upstream to a rectangular pier by Haque *et al.* (2007) showed that when a single pile is placed at a distance of  $4b_p$  from the pier (where  $b_p$  is the projected width of the pier facing downstream of the piles) the maximum depth and volume of the scour hole

increase, whereas, when the same pile is placed at the closer distance of  $2b_p$ , they start decreasing.

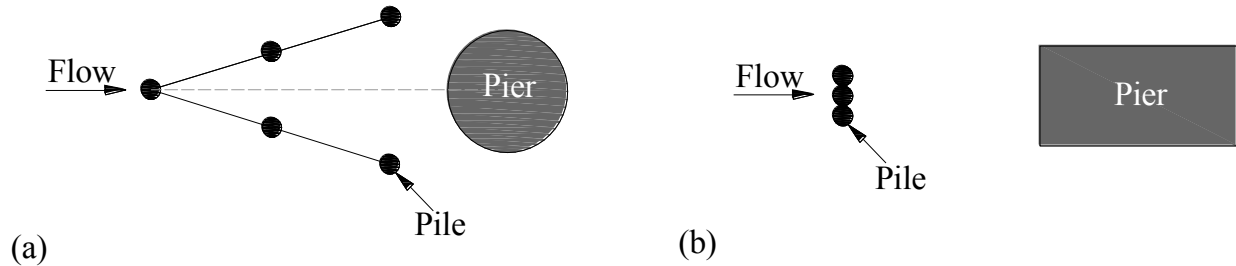


**Fig. 32. (a) General arrangement of a triangular array of sacrificial piles upstream to a circular pier (Melville and Hadfield, 1999); (b) configuration of transverse sacrificial piles upstream to a rectangular pier (Haque *et al.*, 2007)**

Chang and Karim (1972) conducted both laboratory and field studies on sacrificial piles. *In situ*, they placed three protective circular piles upstream to a cylindrical pier for a bridge crossing the Big Sioux River, South Dakota, and scour depths were reduced up to 44%.

Paice and Hey (1993) carried out experiments using a variety of sacrificial pile arrays in laboratory and at three different field sites. Just in one bridge, which was on a tidal reach of the Severn River, some preliminary data gathered over five tidal cycles support the claim that sacrificial piles reduce scour at bridge piers. The other sites were not flooded during the observation time period.

Single and multiple piles were also tested by Herbertson and Ibrahim (1992), Wang (1994), Singh *et al.* (1995) and Kayatürk *et al.* (2005). One of the most comprehensive researches about application of sacrificial pile in a triangular array, with the apex of the triangle pointing upstream (Fig. 32a), was carried out by Melville and Hadfield (1999), who tested circular and rectangular piers under both clear-water and live-bed conditions, for different flow skew angles. Their results showed that the countermeasure efficiency was greater in clear-water than in live-bed conditions, and decreased by increasing flow skewness. The Authors concluded that sacrificial piles are not effective unless the flow remains aligned and its intensity is relatively small; under such conditions, submerged and full depth piles have the same efficiency. However, in most tested cases, the Authors reported that submerged piles are slightly more effective than full depth piles, and, for a circular pier, the scour depth reduction in the best configurations was 56% and 17.5% in clear-water and live-bed conditions, respectively.

Haque *et al.* (2007) observed that, if the pile arrangement is such that the sediments scoured around the sacrificial piles fill in the scour hole upstream to the pier, sediments are trapped inside the scour hole, owing to the low velocity close to pier and also because of downflow. In this case, the effectiveness of piles in scour reduction depends on their arrangement and percentage of blockage provided by them. The Authors performed several pile arrangement tests in front of a rectangular pier under clear-water condition in different pile arrangements (Fig. 32b). The

optimum arrangement (producing the maximum scour reduction) occurred when three piles were placed at a distance of  $2b_p$  from the pier, with reduction of scour volume and maximum scour depth up to 61% and 50%, respectively.

### 3.4.2. Vanes and sills

Submerged vanes in form of Iowa vanes have been developed originally for sediment control in rivers. The vanes are small flow training structures, which modify the flow pattern and redistribute flow and sediment transport within the channel boundaries (Fig. 33a). Vanes generate secondary flow circulation, altering the magnitude and direction of bed shear stresses and modifying velocity distribution, depth and sediment transport (Odgaard and Wang, 1991a). Odgaard and Wang (1991a, 1991b) discussed theory and application of submerged vanes, leading to the development of design criteria. The major controlling parameters are vane height ( $h_v$ ), aspect ratio ( $h_v/l_v$ ), angle with respect to the approach flow ( $\alpha_v$ ), spacing ( $e_v$ ), displacement from the upstream pier face ( $X_v$ ), lateral spacing between vanes ( $z_v$ ), vane submergence, channel resistance and sediment Froude number. An increase in any of these parameters causes the induced changes in bed elevation to increase (Lauchlan, 1999).

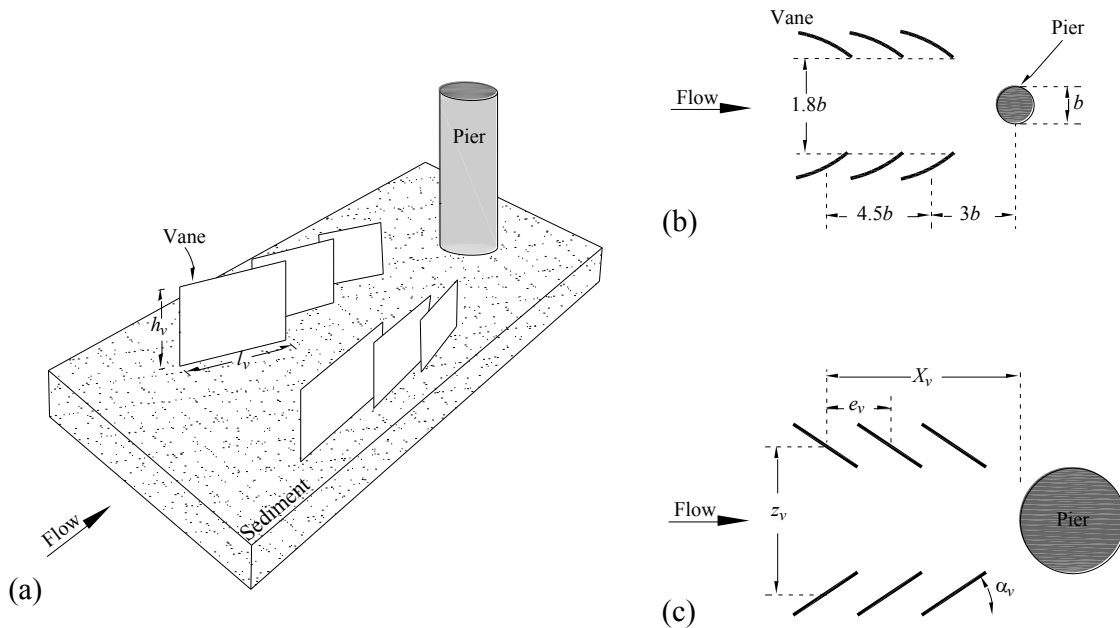
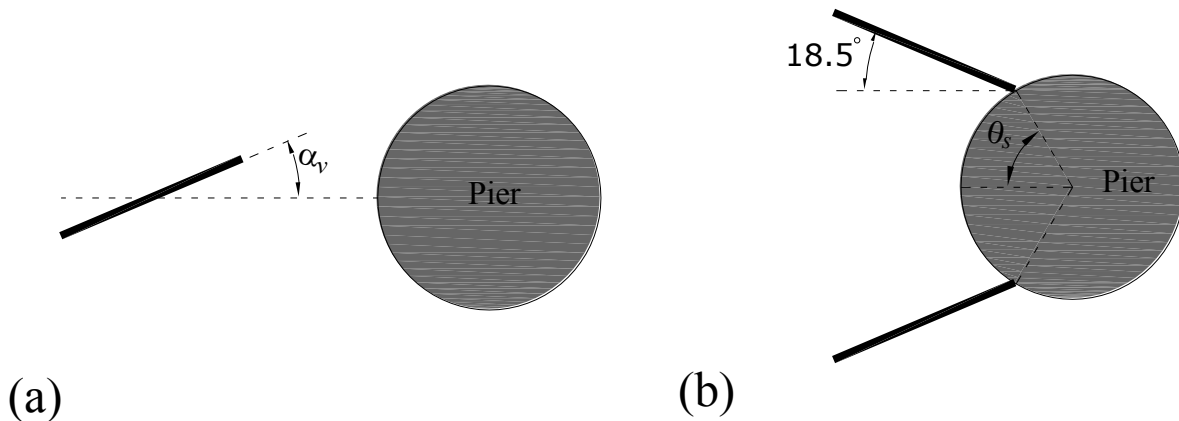


Fig. 33. Submerged vanes (Iowa vanes): (a) general configuration; (b) curve vanes (Odgaard and Wang, 1987); (c) flat plates (Lauchlan, 1999)

Submerged vanes were applied as pier scour countermeasure as both curve vanes (Odgaard and Wang, 1987) and flat plates (Lauchlan, 1999). Result of experiments by Odgaard and Wang (1987) shows a 36% in maximum scour depth reduction in application of submerged vanes (Fig. 33b). In this case, an extensive experiment was performed by Lauchlan (1999) in several configurations for two type of vanes ( $l_v/h_v < 1$  and  $l_v/h_v > 1$ ) in both clear-water and live-bed conditions (Fig. 33c). Type I vanes ( $l_v/h_v < 1$ ) performed to disrupt the flow system ahead of the pier and reduce the strength of the downflow and horseshoe vortex systems at the pier and around

it, whereas type II vanes ( $l_v/h_v > 1$ ) interacted with the sediment bed rather than the approach flow to reduce local scour depth. Lauchlan (1999) found that Type II vanes offer greater potential for scour protection than Type I vanes, and in the best configuration under live-bed condition a maximum scour reduction of 34.4% and an average of 50.4% were achieved for Type II vanes. Results also showed that the ability of vanes in maximum scour depth reduction under live-bed conditions is lesser than under clear-water condition. The most important parameters affecting vane performance were recognised to be the vane angle with respect to the approach flow ( $\alpha_v$ ); increasing the vane angle from  $15^\circ$  to  $30^\circ$ , the effective width of the vane and the streamwise spacing between the vanes ( $e_v$ ) increased; increasing the spacing, the vane performance improves significantly (Lauchlan, 1999).

Several tests were performed by Ghorbani and Kells (2008) in application of a single vane at a short distance in front of a pier and double vanes attached to the pier (Fig. 34). The main result of their experiments is that in some cases, especially when the vanes height is greater than zero ( $h_v > 0$ ) vanes may increase the scour depth. Their results also show that double vanes (Fig. 34b) seem to be much more effective on scour reduction than single vane (Fig. 34a). The Authors believe that the reason may be related to the reduction of the downflow power, entrapping the eroded sediments between the vanes and preventing the scour hole from extension.



**Fig. 34. Configuration of (a) single and (b) double submerged vanes (Ghorbani and Kells, 2008)**

Permeable and impermeable sheet piles, and upstream or downstream bed-sills were investigated by some researchers. A sheet pile or a bed-sill, when placed upstream to a pier with a low height, acts as a flow deflector in order to decrease the approach flow velocity near the bed and, consequently, the horseshoe strength. An impermeable bed-sill (or sacrificial sill protection system) upstream to the pier consists of a completely rigid wall. Therefore, it may be considered to be equivalent to a sheet pile or an array of a few standard piles arranged in a row; unlike the sacrificial pile system proposed in the literature, in this case there is no gap between the piles, in order to shelter the pier from erosion (Chiew and Lim, 2003). In contrast, permeable (porous) sheet piles upstream to a pier can weaken the horseshoe vortex near the bed, by diverting part of the near-bed flow away from the bridge pier, and decreasing the approach velocity of the remaining near-bed flow (Parker *et al.*, 1998). On the other hand, application of a rigid bed-sill at



a short distance downstream of a pier affects on the lower part of the wake vortex system and in the case that the sill is adjacent to the pier, the bed-sill totally excludes the wake vortex system from the scour volume around the pier and alters the flow field, probably influencing also the horseshoe vortex (Grimaldi *et al.*, 2009a).

Levi and Luna (1961) used an impermeable sheet pile upstream to a pier under clear-water conditions. More recently, Chiew and Lim (2003) carried out an extensive experiment by applying a sacrificial sill upstream to a pier in both clear-water and live-bed conditions (Figs. 35).

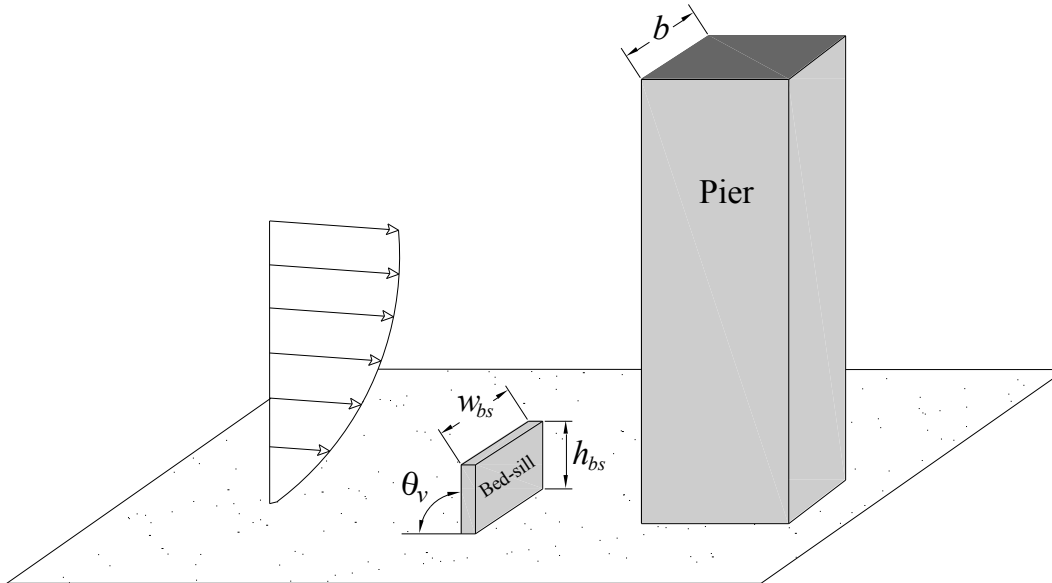


Fig. 35. Application of a sacrificial sill upstream to a square pier (Chiew and Lim, 2003)

Results showed that flow skewness reduces the effectiveness of the sacrificial sill, which becomes completely ineffective for  $\beta=15^\circ$  and  $20^\circ$ , respectively for circular and square pier. Bed-sill height above the bed ( $h_{bs}$ ) is only important in affecting scour depth reduction when  $h_{bs}/h \leq 0.3$  under clear-water conditions; beyond this limit value, the scour depth reduction remains essentially constant. The sill is efficient in reducing the equilibrium clear-water scour depth, reaching a maximum percentage reduction of pier scour depth of approximately 50% when the sacrificial sill is vertical ( $\theta_v=90^\circ$ , where  $\theta_v$  is the vertical inclination of the bed-sill); the bed-sill height above the bed ( $h_{bs}$ ) is larger than 0.3 times the depth of flow ( $h_{bs}/h \geq 0.3$ ); the clear distance between the pier and bed-sill is 4.4 times the pier width, and the angle of attack ( $\beta$ ) is zero. The efficiency of the sill decreased under live-bed conditions, and the scour depth reduction reduced from 41% at  $U/U_c=0.74$  down to 15.1% at  $U/U_c=2.6$ .

The porous (permeable) sheet pile should be founded in the bed and should be short enough to minimize interference with the approach flow. The sheet pile permeability would increase the efficiency of the countermeasure, by encouraging the deposition of sediment downstream of it, in a zone that would otherwise be scoured. Results of several tests with permeable sheet piles as a countermeasure for circular and rectangular piers under completely submerged and barely

emerged conditions are reported by Parker *et al.* (1998). The sheet piles were designed with two panels forming an arrow shape pointing upstream (Fig. 36).

In test series (a), the panels formed an angle of  $90^\circ$ , in order to be effective also for skewed flows. Each panel was made up of wooden slats evenly spaced, with a percentage area of the openings equal to 50% (Fig. 36a). In test series (b) and (c), two triangular horizontal panels were installed within the slats in order to prevent downwelling of the flow toward the pier (Fig. 36b,c). In addition, in test series (c) the slats were raised of  $10^\circ$  upward, in order to further suppress flow downwelling near the pier. Results showed a scour reduction under live-bed conditions, less than 50% also in the best configuration (type c).

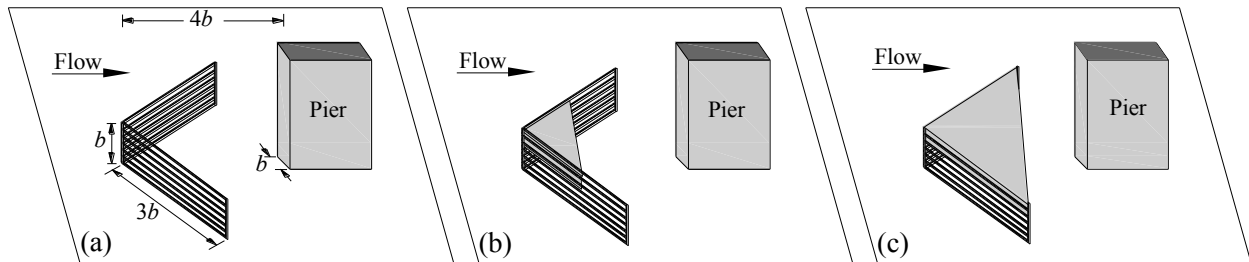


**Fig. 36. Permeable sheet piles; (a) uncovered; (b) partially covered with plates; (c) completely covered with plates (Parker *et al.*, 1998)**

Application of a bed-sill as a scour countermeasure downstream of a pier (Fig. 37) was proposed by Grimaldi *et al.* (2009a). The bed-sills used in the tests were 20 mm thick maritime-wooden plates, as wide as the working cross section width ( $B$ ) with zero height ( $w_{bs}=B$  and  $h_{bs}=0$ ), where  $w_{bs}$  is the bed-sill width. Long-term (equilibrium) laboratory experiments were designed in order to evaluate the effectiveness of a sill downstream of a pier for variable distance between pier and sill. Results showed that the smaller the distance between bed-sill and pier, the larger the scour reduction, with maximum scour depth reduction (about 26%) when the sill were adjacent to the pier. In this configuration, the maximum depth of the scour hole may occur in front of the bed-sill instead of the pier. The study of the scour depth time evolution showed that the downstream bed-sill started to be effective after an initial time,  $t^*$ , equal to about 10 min to 6 h in the performed tests, dependent on the bed-sill location.

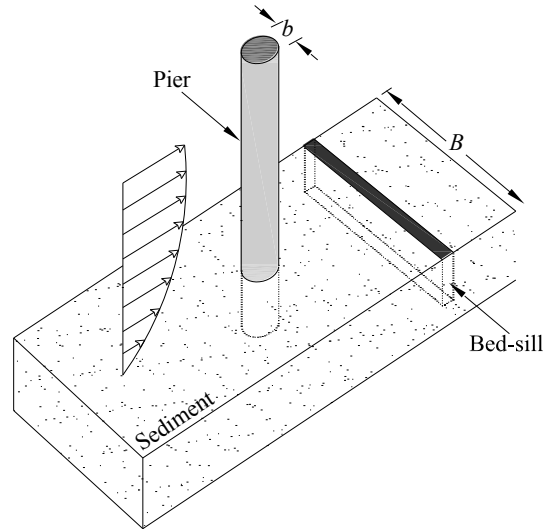


Fig. 37. Configuration of a downstream bed-sill (Grimaldi *et al.*, 2009a)

### 3.4.3. Surface guide panels

In this method, two vertical panels with some interior angle and leading opening locate at a distance in front of a pier (Fig. 38).

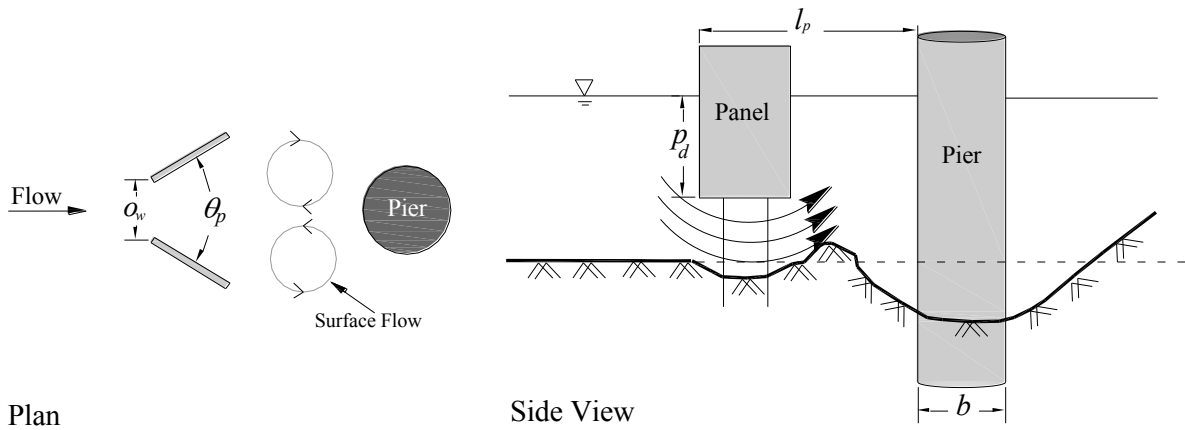


Fig. 38. Configuration of surface guide panels (Huang *et al.*, 2005)

When the surface guide panels is set up in front of the pier the flow divides into two parts, namely, the upper layer of fluid guided by surface guide panel and the lower without being guided. It was observed that the upper flow entering through the leading opening of panels will separate and generate two wake vortices at the rear of panels near the free surface. In addition, the lower unguided flow tends to go upward across the bottom ends of the panels into the inner region ahead of the pier (Fig. 38). Moreover, on the movable sand bed a deposition dune following the local scour hole at the guide panels site also enforces the upward flow motion near bottom (Fig. 38). Therefore, the downflow motion along the front face of pier can be weakened by

this upward flow. Surface guide panels has two major effects on scour reduction at the pier; at first, the upward flow motion below the panels results in a smaller shear flow near bottom when it approaches to the pier. Consequently, the horseshoe vortex has less energy to develop scour around the pier. Secondly, the local deposition at the location of the panels also aids in delivery of sediment into the downstream pier scour hole. Both effects will reduce the scour at the pier (Huang *et al.*, 2005).

Results of several tests on various parameters of surface guide panels including the interior angle ( $\theta_p$ ), leading opening ( $\sigma_w$ ), distance between panel and pier ( $l_p$ ), submerged depth of panel ( $p_d$ ), pier diameter ( $b$ ) and water depth ( $h$ ) led to a best performance on decrement of the maximum scour depth at pier up to 90% with ignorable side effects on the surface guide panels scour (Huang *et al.* 2005).

#### 3.4.4. Sleeve and collared sleeve

A sleeve consists of a larger diameter cylinder encircling the pier (e.g.,  $D_s=1.5b$  to  $2.5b$ , where  $D_s$  is diameter of the sleeve). The underlying mechanism of scour reduction with a sleeve is to confine the scouring vortex inside the annular space between pier and sleeve. A sleeve is analogous to an open well, which will contain the horseshoe vortex system and restrict its size and propagation (Singh *et al.*, 2001; Garg *et al.*, 2008). Experiments on sleeves show two distinct locations of the maximum scour depth: one inside the sleeve and the other outside of it (Singh *et al.* 2001). To reduce the problem of outside scour, a collar plate may be installed around the sleeve to improve the performance of the device (“collared sleeve”, Fig. 39; Garg *et al.*, 2008). Scour was completely eliminated with a collared sleeve ( $D_s=1.5b$ ,  $w_c=2b$ ), in which the upper face of the sleeve was placed at the depth of  $b/4$  in the sediment bed and sealed. The device gave no inside nor outside scour under uniform as well as unsteady flow conditions (Singh *et al.* 2001).

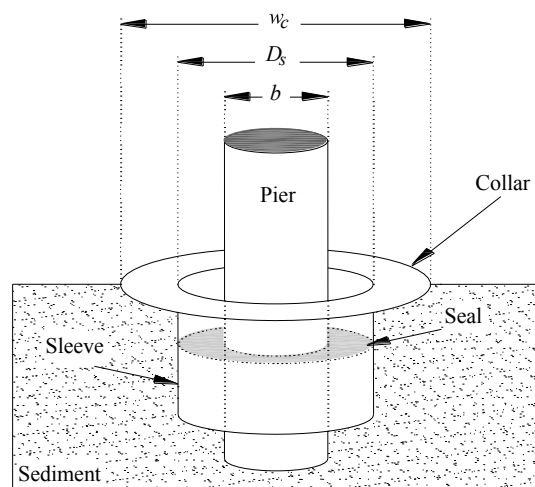


Fig. 39. Configuration of a collared sleeve (Singh *et al.*, 2001)

### 3.5. Other methods

#### 3.5.1. Suction applied to the pier

This method was tested successfully by Rooney and Machemehl (1977). The lower embedded part of a circular pier ( $b=114$  mm) was drilled with thirty 0.5-in-diameter holes (six holes per each of five levels, ranging from just above the sediment bed to below the bed surface), from which water could be extracted by pump suction (Fig. 40). Results showed that the sand bed completely guarded from scour by pumping suction at high pumping rate (about 5 gal/min), and only few scour holes with very low depth appeared in the wake of the cylinder.

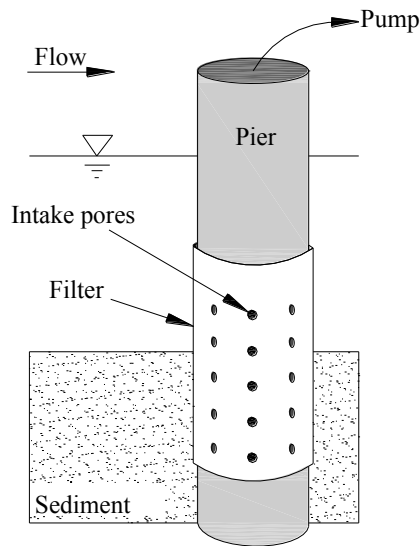
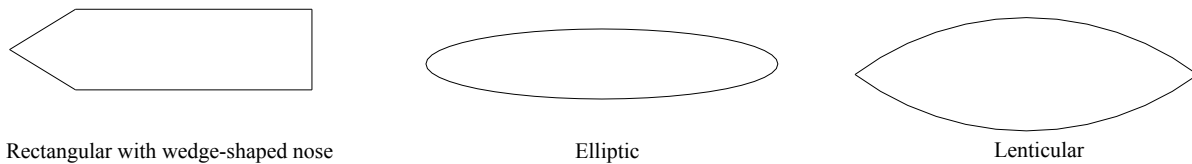


Fig. 40. Suction applied to a circular pier (modified from Parker *et al.*,1998)

#### 3.5.2. Modifying pier shape and texture

Modifying pier shape and texture may affect local scouring around a pier. Blunt nosed pier has a strong horseshoe vortex system at the upstream face. In contrast, sharp nosed pier acts to reduce the drag exerted by flow, and high portion of approach flow conveys from around the pier and less downflow and consequently weaker horseshoe vortex develops. In this case, Schneible (1951) presented interesting results with regard to streamlining of pier shapes to reduce scour levels. Chabert and Engeldinger (1956) conducted an experimental study of pier scour on a variety of pier shapes. Another influential study of pier shapes was undertaken by Laursen and Toch (1956), who investigated local scouring around bridge piers. Results of previous researches (e.g., Tison, 1940; Laursen and Toch, 1956; Venkatadri, 1965 and Dietz, 1972) showed that, by modifying the pier shape, the shape factor,  $K_s$ , may be reduced to values less than 0.7 in special cases of triangular or parabolic nose, elliptic and lenticular piers (Fig. 41). Such shape factors indicate that more than 30% reduction in scour depth may be achieved by modifying pier shapes. It should be noted that furthermore modifying the pier nose, pier length,  $L$ , or the ratio  $b/L$  affects  $K_s$  and scour depth reduction. Also variations of the angle of attack can have a significant

detrimental influence on scour depths of streamlined piers. More explanations about pier shapes and alignment can be found in Breusers and Raudkivi (1991) and Melville and Coleman (2000).



**Fig. 41. Some of the most effective pier shapes for local scour depth reduction**

Shen *et al.* (1966b) carried out some tests on a pier with a roughened upstream face and apron, but no significant reduction in scour was observed. In this case, Parker *et al.* (1998) indicated that modified pier texture does not appear to be promising as a means of suppressing pier scour.

### 3.5.3. Footing and caisson

Effect of footing or caisson was considered by several researchers (e.g., Chabert and Engeldinger, 1956; Jones *et al.*, 1992; Fotherby, 1992; Parola *et al.*, 1996; Melville and Raudkivi, 1996). The most important results of previous research are that, when the top elevation of a caisson or foundation (generally employed with a larger diameter cylinder,  $b_f$ ) is located above the average bed level, the scour depth increased. In contrast, when the top elevation is located in the scour hole, below the initial average bed level, a decreasing in scour depth occurs. In this case, a comprehensive research was performed by Melville and Raudkivi (1996). They also considered previous data from experiments about footing (Fig. 42). Their results showed that the maximum scour depth reduction was achieved for  $y_f/b \approx 1$  to 1.5, where  $y_f$  is the depth of the foundation top face below the initial bed level.

Chiew (1984) conducted scour experiments in live-bed conditions using a caisson with diameter  $2b$ , which embedded the pier below the bed level. Results showed that the equilibrium scour depths were essentially same as for the unprotected pier, i.e. caisson lost its protective effect in live-bed condition.

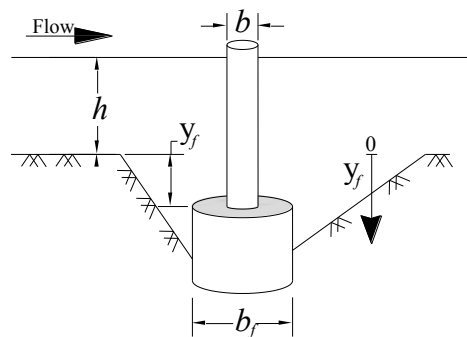


**Fig. 42. Configuration of a circular pier with a foundation**

### 3.6. Combination of countermeasures

#### 3.6.1. Slot and collar

Combined tests using collar and slot were conducted by Chiew (1992), employing a slot in the pier and two collars of dimensions  $w_c=2b$  and  $3b$ , respectively, attached to the cylinder in different positions. The combined countermeasure increases the efficiency of scour reduction. In most of the combinations, scour was eliminated. A similar 100% reduction of scour depth was achieved by Moncada-M *et al.* (2009) by combining a slot and a  $2b$ -wide collar placed at the original bed level.

#### 3.6.2. Collar and pier group

Vittal *et al.* (1994) used a combination of a full depth pier group with a collar ( $w_c=2b$ ). The tested combination was equivalent to a collar wider than  $6b$  on a solid pier. A collar attached to a pier group is more effective than a collar attached to a solid pier.

#### 3.6.3. Permeable sheet piles and riprap

A combination of permeable sheet piles with riprap as scour countermeasure for circular and rectangular piers was tested by Parker *et al.* (1998). A performance of up to 91% was achieved in live-bed scour conditions. Sheet piles can help to reduce the flow velocity near the pier and consequently to stabilize the riprap, which otherwise would be displaced.

#### 3.6.4. Suction and riprap

Tests were performed by Chiew and Lu (2005) to determine the effects of another mode of suction on the riprap stability around a pier. This suction type was applied through three pipes at the immediate upstream end of the riprap layer. The suction effect on riprap stability depends on the type of riprap failure, suction rate and flow intensity. Suction reduces the threat of winnowing failure by decreasing the level of turbulence intensity in the vortices induced by the pier. However, in a dune-bed, where destabilization of a riprap layer by the propagation of dunes past the pier is the dominant failure mode, the dune height increases by suction, resulting in an increase of bedform-induced failure. In contrast, turbulence intensity reduces in the presence of suction and the overall effect depends on the relative magnitude of these two opposing effects (Chiew and Lu, 2005).

#### 3.6.5. Collar and riprap

Zarrati *et al.* (2006) tested a combination of continuous collars and a riprap in clear-water scour conditions. In the experiments, the space inside the continuous collar and between two in-line piers was covered by riprap placed on the streambed. Previously, it was observed that scour developed quickly in this region, and the scour hole extended upstream in the absence of a riprap. With  $s/b=3$ , a combination of continuous collar and riprap resulted in the largest scour depth reduction of about 50 and 60% in the vicinity of the front and rear piers, respectively, whereas continuous collars reduce the scour depth at the front and rear piers by about 25 and 35%,

respectively. The size and extent of stable riprap around rectangular piers protected with collar were also studied (Mashahir *et al.*, 2010). In another study by Zarrati *et al.* (2010), combination of riprap and collar with  $w_c=2b$  and  $3b$  was examined. The Authors employed riprap stones downstream of a  $3b$ -wide collar where the scouring initiates. However, for  $2b$ -wide collar, the riprap layer should be extended from downstream to upstream of the collar. The Authors also reported that the examined combination permits reducing the volume of required riprap stones.

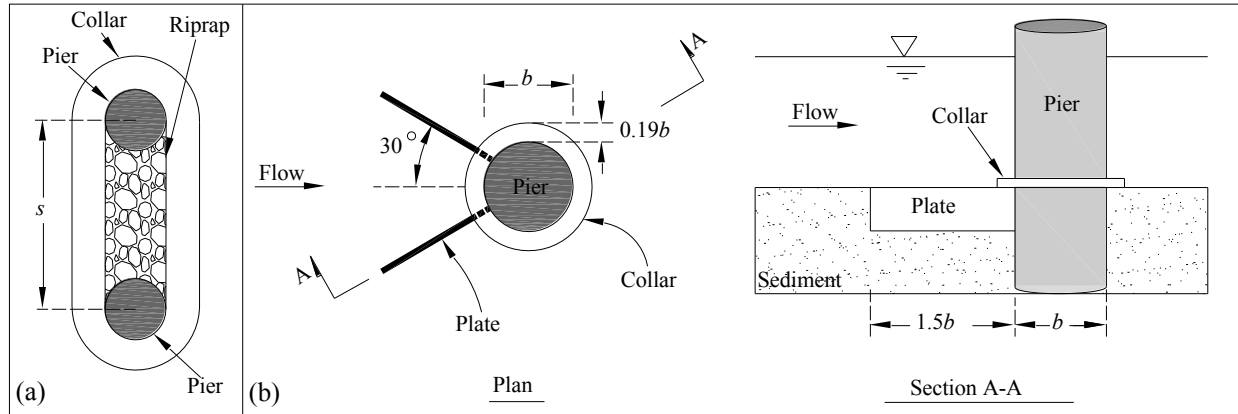


**Fig. 43. (a) Combination of riprap and collar (Zarrati *et al.*, 2006); (b) combination of pier plates and collar (Odgaard and Wang, 1987)**

### 3.6.6. Slot and bed-sill

Grimaldi *et al.* (2009b) tested a combination of downstream bed-sill and slot, both in their best configuration, obtaining a scour reduction in front of the pier of about 45%.

### 3.6.7. Submerged vanes and bed-sill

Mansueto (2009) showed that a combination of submerged vanes and bed-sill is not a proper combination, since its efficiency may be improved less than 2% in comparison to a sole bed-sill when a vane with  $l_v=b$  is used. The results also showed that the efficiency may reduce respect to efficiency of a single bed-sill when the  $l_v$  increases.

### 3.6.8. Other combinations

Combinations of collar and submerged vanes, in the form of Iowa vanes, and pier-attached plates were studied by Odgaard and Wang (1987). Figure 43b shows this combination. If each countermeasure was applied separately, up to 36% scour depth reduction was achieved. However, the scour depth reduction increased to 64 and 45% by using combinations of submerged vanes and collar or pier plates and collar, respectively. Limited tests on the combinations of various flow-altering countermeasures were conducted by Garg *et al.* (2008). Combinations of two devices could change their combined behaviour for better or worse. It is possible that the performance of combined countermeasures decreases with respect to the single protection. For



instance, Garg *et al.* (2008) found that if a collar was combined with a delta-wing, the combined efficiency was less than that of a single collar alone.

### **3.7. Evaluation of the experiments**

Previous experiments were critically examined in terms of laboratory test conditions. In most of the studies, laboratory conditions were not detailed. The test conditions were therefore analysed to verify whether the effects of side-walls, sediment size, flow shallowness and time were negligible. Note that these conditions were originally defined for a single unprotected pier and further research is needed to evaluate them if applied to protected piers, owing to the presence of countermeasures. Below a preliminary discussion of previous researches is presented with respect to the limit values of the dimensionless groups defined for a single pier and describing the aforementioned effects. In all the experiments available in the literature, the efficiency of a pier protected with a countermeasure is calculated with respect to the scour measured for the unprotected pier.

#### **3.7.1. Side-wall effect**

It was indicated in Chapter 2 that for piers, the condition  $B/b \geq 10$  was proposed to neglect side-wall effects and to minimize the pier blockage effect (Laursen and Toch, 1956; Chiew and Melville, 1987). A review of previous research shows that the results of laboratory tests (e.g. Abd El-Razek *et al.*, 2003; Dey *et al.*, 2006; Haque *et al.*, 2007; Moncada-M *et al.*, 2009) are possibly influenced by the sidewall effect ( $B/b=7.4, 4.5, 7$  and  $6.85$ , respectively).

#### **3.7.2. Sediment size effect**

A ripple-forming bed is expected if  $d_{50} < 0.7$  mm and  $u_* > 0.6u_{*c}$  (Breusers and Raudkivi, 1991). Alabi (2006) observed the formation of ripples in experiments on collars by using fine sediments with  $d_{50}=0.53$  mm in clear-water scour conditions. Test results based on fine sediments are also available from Chiew (1992), Singh *et al.* (2001), Dey *et al.* (2006) and Garg *et al.* (2008) with  $d_{50}=0.33, 0.285, 0.26$  and  $0.28$  mm, respectively.

#### **3.7.3. Flow shallowness effect**

In order to consider the flow shallowness effect on scour depth, the two dimensionless parameters  $h/b$  and  $b/d_{50}$  should be considered (Raudkivi and Ettema, 1983; Chiew and Melville, 1987; Breusers and Raudkivi, 1991). For fine sediments, the scour depth may be almost invariant of  $h$  for  $h/b \geq 2$ , whereas for relative coarse sediments a higher value is required to overcome the flow shallowness effect (Breusers and Raudkivi, 1991). A better value for this dimensionless number proposed in Chapter 2 as  $h/b \geq 2.5$ . A review of previous studies shows that influence of flow shallowness can be found in some researches. For instance, the test results of Huang *et al.* (2005) could be influenced by the shallowness effect ( $h/b=1.5-1.85$  and  $b/d_{50}=32.26$ ). Ghorbani and Kells (2008) reported for this case the high efficiency of 88% in applying submerged vanes. However, this was obtained in a test with low flow intensity and shallow flow depth ( $U/U_c=0.69$ ,

$h/b=0.88$  and  $b/d_{50}=200$ ). New tests by Mansueto (2009) showed that this countermeasure lose its efficiency in higher flow intensity and flow depth. The results showed that when  $h/b=2.5$  and  $U/U_c=0.95$  the efficiency as low as 12.4% may be obtained.

#### **3.7.4. Time effect**

To achieve equilibrium scour condition in typical laboratory experiments, an essential prerequisite is to run tests for several days (Grimaldi *et al.*, 2006). The duration of equilibrium tests and the shape of the time evolution curves of scour can be influenced by the presence of countermeasures. Long-term tests showed that a collar may delay the scour depth development (Mashahir *et al.*, 2004). A downstream bed-sill may affect the scour evolution after a certain time period (Grimaldi *et al.*, 2009a). In such cases, short-duration tests may lead to erroneous results. For instance, Moncada-M *et al.* (2009) reported high scour depth reductions by using a collar (96 and 100% for  $w_c=2b$  and  $3b$ , respectively), although the test duration was only 6 h; also other researchers reported results of tests having a duration of only a few hours (Gupta and Gangadharaiyah, 1992; Vittal *et al.*, 1994; Huang *et al.*, 2005; Ghorbani and Kells, 2008 and Garg *et al.*, 2008).

### **3.8. Limitations and difficulties in practical applications**

Field applications of flow-altering countermeasures seem to have several problems, which may limit their practical use. Parker *et al.* (1998) indicated several advantages and disadvantages of flow-altering countermeasures. The most important limitations of such devices are summarised below.

#### **3.8.1. Debris flow**

Debris flow may affect the performance of countermeasures. For instance, floating debris during floods may block the gaps between piers of a pier group (Vittal *et al.*, 1994) or may partially block a slot opening, thus reducing the efficiency of the countermeasures (Chiew, 1992). Such a problem may also affect the internal connecting tubes. Collars can potentially collect debris flow, and large amounts of debris may render a porous sheet pile ineffective (Parker *et al.*, 1998). The performance of suction through a pier can decrease as well, owing to the intake holes being blocked by debris. However, more research is required to assess the effect of debris flow on the efficiency of flow-altering countermeasures (Parker *et al.*, 1998).

#### **3.8.2. Flow obliqueness**

A slot may lose its efficiency significantly in an oblique flow (Kumar *et al.*, 1999; Heidarpour *et al.*, 2003), and this phenomenon can also occur for other types of openings through piers (e.g. pier group). A slot or a pier group acts by diverting part of the downflow through its opening. For a slot or a pier group, the projected opening area (which is the main parameter in diverting the downflow) decreases. Consequently, the performance of these countermeasures in scour reduction decreases. The efficiency of sacrificial piles or a sill upstream of a pier can decrease in

the case of oblique flow (Melville and Hadfield, 1999; Chiew and Lim, 2003). The efficiency of a collar attached to a rectangular pier also decreases with an increase in flow obliqueness (Zarrati *et al.*, 2004). Although modified pier shape may result in a scour depth reduction, changes in the angle of attack seem to have an unsafe effect on scour depth at a streamlined pier (e.g. lenticular shape). The performance of a streamlined pier in an oblique flow decreases as the approach flow cannot pass smoothly around the pier, forming stronger downflow and horseshoe vortex.

### 3.8.3. High flow intensity

Experiments on caissons under live-bed conditions by Chiew (1984), pier-attached vanes by Parker *et al.* (1998), sacrificial piles by Melville and Hadfield (1999), submerged vanes by Lauchlan (1999) and sacrificial sill upstream of a pier by Chiew and Lim (2003) revealed that these flow-altering countermeasures lose their efficiency to a large extent under high flow velocities, i.e. for  $U > U_c$ . Furthermore, the stability of countermeasures during floods should also be noted. Stability of a sill, especially if the sill top is above the initial bed level, may be undermined. During floods, the stability of surface guide panels seems to be difficult, since this countermeasure consists of two large panels of height comparable to the water depth and therefore highly exposed to the approach flow. In addition, collars, horizontal plates and pier-attached plates (e.g. delta wing vane) may flutter during floods.

### 3.8.4. Other problems

Suction needs a permanent pumping system. The system requires regular monitoring and maintenance. Parker *et al.* (1998) emphasised possible aesthetic disadvantages using sacrificial piles at bridge sites. Their use may also have problems in navigation channels. It seems that the problems related to the navigation channels are critical also for high-wide downstream or upstream bed-sills especially for transportation during low flow and in channels subject to dredging. Furthermore, openings through piers (slots, internal connecting tubes and pier groups) are difficult to be employed for already existing piers, as their use affects the pier structure. Application of openings through piers may also decrease the buckling strength of a pier.

## 3.9. Conclusions

According to difficulties and limitations in field applications, various types of flow-altering countermeasures can be divided into two categories: (1) countermeasures which are difficult to install in the field or may exhibit a low efficiency, and (2) countermeasures which are applicable, but require more research to prove their adequacy and reliability. For the first category, a survey on countermeasures indicates that some have serious problems in field applications. These problems should be investigated before further research is carried out. All tested countermeasures in live-bed conditions showed lower efficiency with respect to clear-water conditions. Among them, the sacrificial sill upstream of a pier and triangular arrangement of sacrificial piles showed efficiencies as low as 15% in live-bed tests. These countermeasures cannot be reliable during typical flood conditions. Although a 100% scour depth reduction was reported in applying

suction in laboratory tests, its use in the field requires permanent pumping units. Use of surface guide panels seems to be impractical, since stability of large size panels in front of piers during floods is not guaranteed, and a strong structure is necessary for ensuring stability. Based on the available research, the other countermeasures can be classified into the second category. They may be used at bridge piers under certain field conditions, especially if debris flow and flow obliqueness are not dominant, but more research (long test durations under both clear-water and live-bed conditions) is anyway required to confirm their performance and adequacy. Furthermore, performance of these countermeasures in cohesive and also non-uniform sediments is needed. Among them, a combination of slanting plates and guide wall showed good efficiencies in both clear-water and live-bed scour conditions. However, further investigation is needed to ascertain the adequacy of this configuration in the presence of debris-flow and high-flow obliqueness. Collars are other types of countermeasure, which seem to be effective for rectangular piers and also in the field. For these two countermeasures more investigations are recommended to find a reliable efficiency before field application, especially under live-bed scour conditions. Furthermore, combinations of flow-altering countermeasures may also result in higher efficiency and a more reliable combination is obtained if a flow-altering countermeasure is combined with a bed-armouring countermeasure. Therefore, further research on combinations of flow-altering and bed-armouring countermeasures might help to find optimum and safe methods to mitigate pier scour to a great extent.

## Chapter 4

### EXPERIMENTAL FACILITIES AND PROCEDURE

#### 4.1. Introduction

As mentioned before, the experimental part of this study, which is the main part of it, focuses on performance and possible combination of flow-altering countermeasures. All the experiments were carried out at the *Laboratorio di Grandi Modelli Idraulici, Università della Calabria, Italy*. In the following sections the experimental apparatus and the procedure to perform the experiments are explained.

#### 4.2. Flume and related facilities

The experiments were carried out in a 9.66 m-long, 48.5 cm-wide rectangular tilting flume with a constant longitudinal slope of 0.06%. Figure 44 shows a general view of the flume. The left wall of the flume is made of PVC, whereas the right wall is made of glass panels, in order to allow the direct observation of the hydrodynamic and scouring phenomena. The flow was supplied and measured respectively by an electric pump and a Thomson weir (see Appendix A for details of flow measurement).

A 1.5m-long, 20.5 cm-deep recess box is located at about 6.05 m from the flume inlet (see Figs. 45 to 47a). This recess box was filled with the selected bed materials and the same bed materials were also glued on the false floors in order to avoid any change in water profile due to change in bed roughness. The depth of flow was also controlled with an adjustable tailgate (Fig. 47b).



Fig. 44. General view of the flume

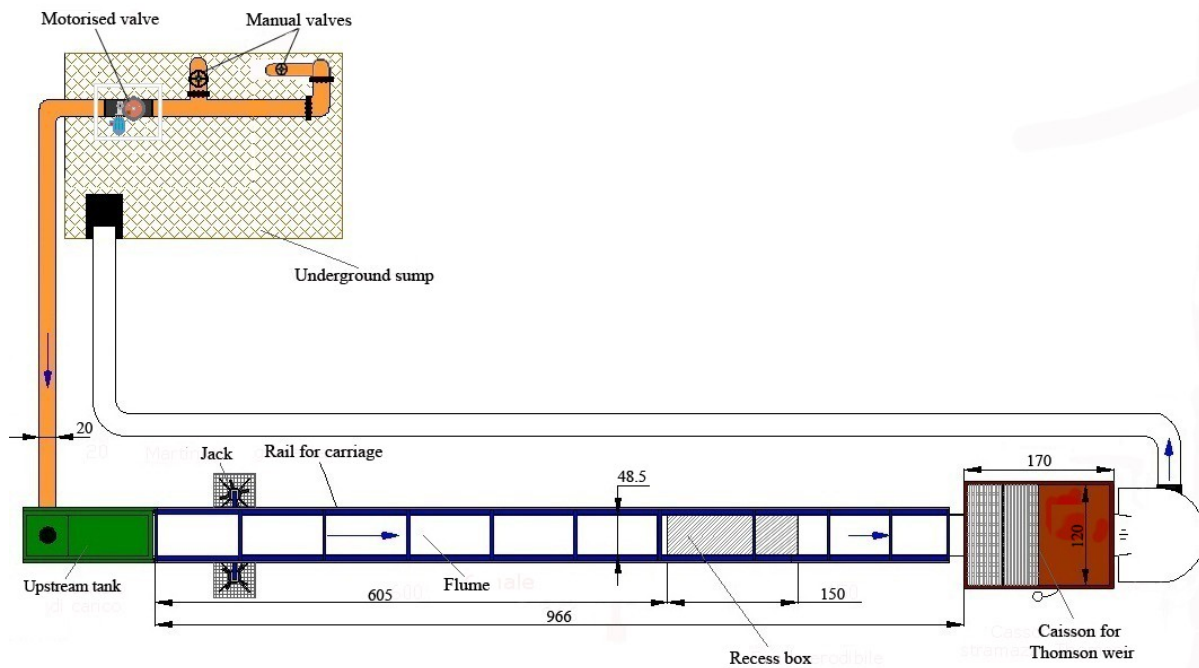


Fig. 45. Plan-view of the flume and other facilities (units: cm)

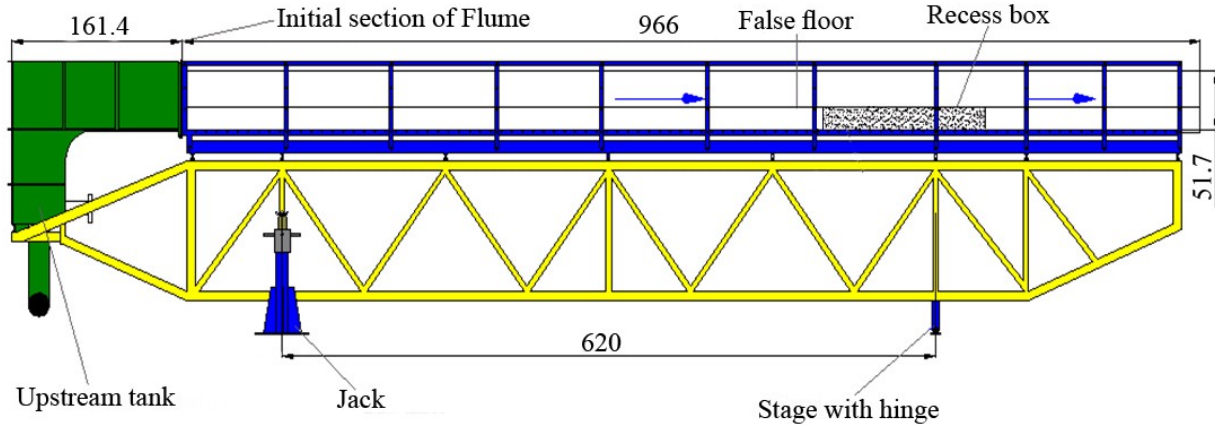


Fig. 46. Side-view of the flume (units: cm)

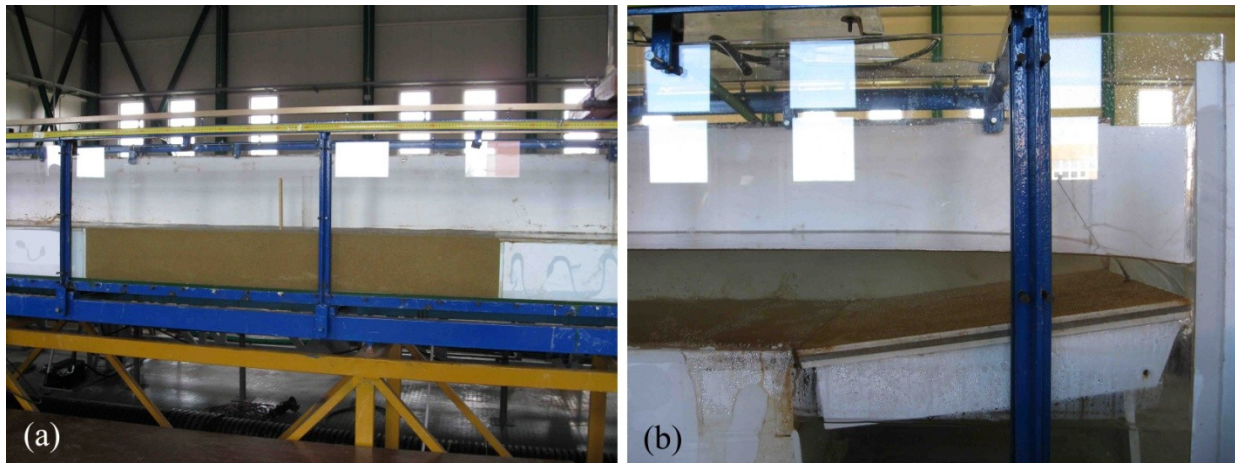


Fig. 47. (a) Recess box; (b) and adjustable tailgate

#### 4.2.1. Bed longitudinal slope

In order to have a uniform flow in an open channel, the energy slope and flow surface slope should be the same as the channel bed slope,  $S$ . In this condition, when  $h$ ,  $U$  and  $d_{50}$  are enclosed as independent variables in (E.8), bed slope cannot be reported as an independent variable (see, e.g., Manning or Chézy equations). The channel slope was modified using two jacks (Fig. 48a) and a simple method was used to estimate the channel slope as follows:

1. the tail gate was raised up in order to store about 20 cm water in channel;
2. the border of the tailgate was sealed with Silicone sealant as shown in Fig. 48b in order to prevent water leakage;
3. the channel was filled with flow from upstream and the upstream valves were closed to reserve the flow in the flume. It was observed that by this method the water level in flume is constant for a period of about 1 minute;
4. using a point gauge with needle-shaped tip and decimal vernier, two points, the former upstream and the latter downstream of the channel, were measured quickly in a short time

period (less than about 30 s). The longitudinal slope was calculated as the difference between the two water depths with respect to the distance of the two measured points.

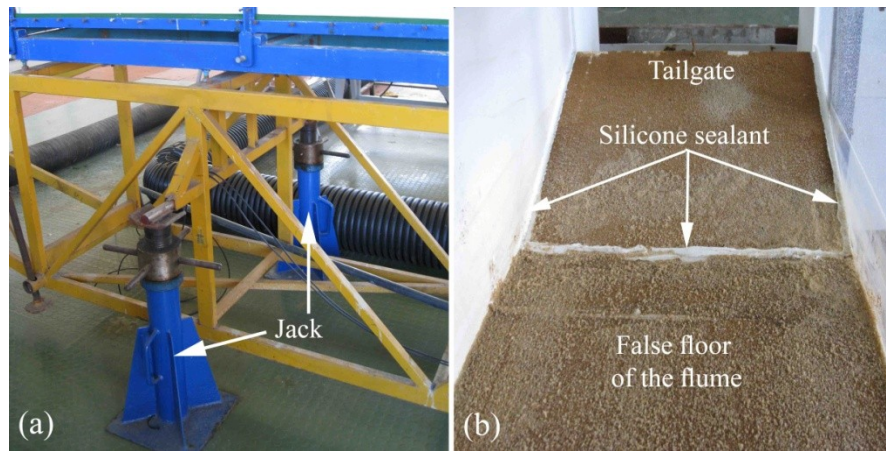


**Fig. 48. (a) Jacks; (b) caulking the borders of the tailgate**

Several attempts were made to regulate the channel slope. At the last attempt, when the distance of the two points was 6.7 m, the difference between the two water depths was 3.9 mm. Therefore, a slope of 0.06% was obtained for the flume bed. It should be noted that this method is only applicable for low values of bed slope, since the point gauge is perpendicular to the bed and not to the horizontal plane.

For the selected slope, the water depth at these two points differs by only a few millimetres. In this condition, more attempts to reduce the bed slope might result in a negative slope or non-accuracy in slope estimation.

Dade and Friend (1998) analysed about 120 alluvial rivers. Their results show a range of  $10^{-5}$  to  $10^{-2}$  for longitudinal slope. Therefore, the selected bed slope value for the experiments is also in the range of natural alluvial rivers.

### 4.3. Design of the tests

In the present study, the tests were designed on the basis of Tab. 5. Since the channel width is 48.5 cm, the pier width,  $b$ , should be less than 4.8 cm in order to satisfy the condition  $B/b \geq 10$ . The result of a single circular pier test by Mansueto (2009) showed that with a 4.8 cm width pier a part of the scour hole border reached the channel walls; therefore, in the present study a smaller pier, i.e. a smooth transparent Perspex<sup>®</sup> cylinder with  $b=4$  cm was employed for the experiments.

A approach flow depth of 10 cm was selected for the experiments in order to satisfy the condition  $h/b \geq 2.5$  and neglect the shallowness effect in the experiments. It was regulated with the tailgate and measured at a distance of about 1 m upstream to the pier, in order to avoid the influence of turbulence flow near the pier on approach flow depth. On the other hand, the ratio of  $B/h=4.8 > 3$  shows that the experiments are not performed in narrow channel conditions.

The water temperature of 19.3°C was measured with a digital thermometer. This value results in a kinematic viscosity of water of about  $1.02 \cdot 10^{-6}$  m<sup>2</sup>/s and consequently the value of



$Re_p=Ub/v=10275>7000$  is obtained. Therefore, it can be assumed that the flow around the pier is fully turbulent.

As mentioned in Chapter 2, in order to neglect the influence of sediment size on the experiments, the condition of  $25 \leq b/d_{50} \leq 130$  should be respected. Furthermore, two other conditions, i.e.  $d_{50} > 0.7$  mm and  $\sigma_g < 1.5$ , are also required in order to avoid development of bed-forms upstream to the pier and significant influence of bed-armouring on the scour hole.

The sediment used in the present study is sand with a specific gravity of 2.67 and grain-size distribution as in Tab. 6. Table 7 shows that, although the value of  $d_{50}$  of the available sand is proper for the experiments, the value of  $\sigma_g$  is greater than 1.5 ( $\sigma_g=1.58$ ). In order to reduce  $\sigma_g$ , a part of sand with diameters smaller than  $d_{50}$  was separated using a sieve with mesh dimension of 0.707 mm. Table 6 shows the results of sediment grading analysis for two samples of the sieved sands. The average values of passed weight of the two samples were used as characteristic values of bed sediments for the experiments (Tab. 6). Therefore, the bed material consisted of cohesionless, uniform sand with  $d_{50}=0.76$  mm,  $\sigma_g=1.46 < 1.5$  and specific gravity of 2.67. Figure 49 shows the size distribution curve of the bed sediment.

**Tab. 6. Grain-size distribution of the sand before and after sieving**

diameter (mm)	Percent finer by weight			
	Available sand	After sieving-S1	After sieving-S2	After sieving-Average
2.36	100	100	100	100.00
1.18	100	99.9	100	99.95
0.6	37.39	24.51	23.14	23.83
0.3	0.25	0.36	0.29	0.33
0.15	0	0.04	0	0.02
2.36	100	100	100	100

**Tab. 7. Grain-size distribution of the sand before and after sieving**

Parameter	Available sand	After sieving-Average
$d_{16}$ (mm)	0.4	0.47
$d_{50}$ (mm)	0.79	0.76
$d_{84}$ (mm)	1	1
$\sigma_g$	1.58	1.46

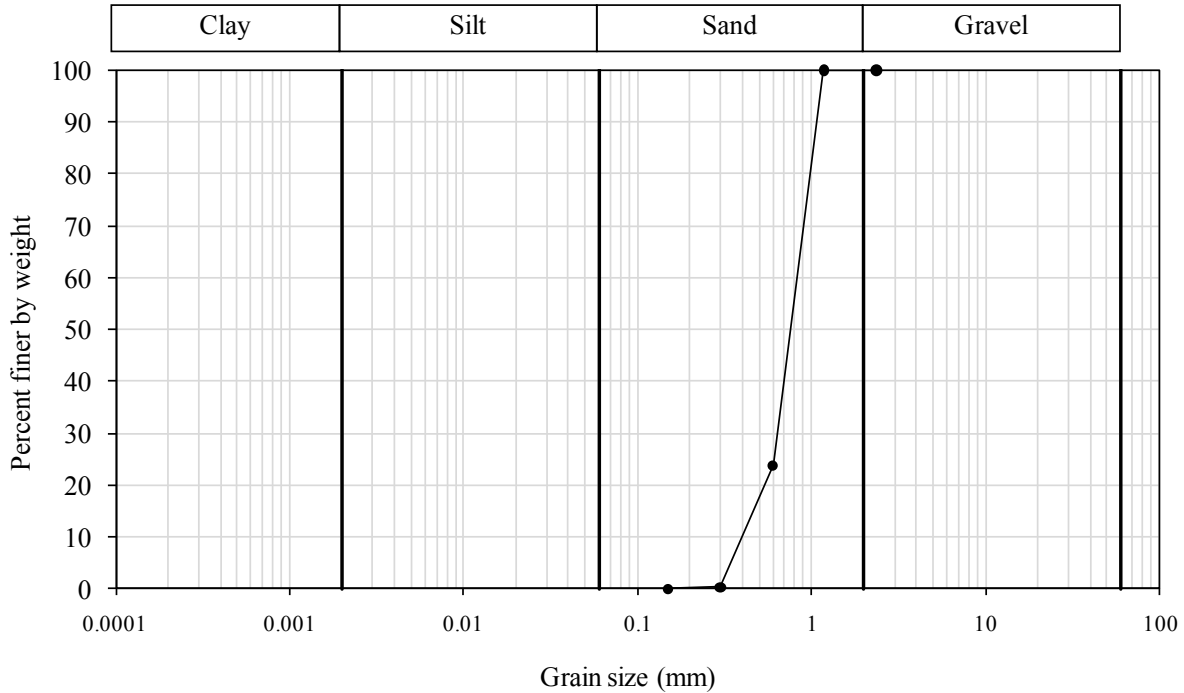


Fig. 49. Size distribution curve of bed sediment

As discussed in Chapter 2, the maximum scour depth in clear-water tests is expected when the approach flow velocity,  $U$ , is near the value of threshold condition of sediment movement,  $U_c$ . In general, in order to prevent particle movement during the experiments, the flow intensity should be selected in the range  $U/U_c=0.9$  to  $0.95$ . A preliminary estimation of  $U_c$  using the following empirical formulae by Goncharov (1964) and Garde (1970) gave  $U_c=0.258$  m/s and  $0.3$  m/s, respectively:

$$\text{Goncharov (1964): } U_c = \log\left(8.8 \frac{h}{d_{50}}\right) \sqrt{\frac{2}{3.5} g \Delta d_{50}} \quad (\text{E.12})$$

$$\text{Garde (1970): } U_c = \left(0.5 \log \frac{h}{d_{50}} + 1.63\right) \sqrt{g \Delta d_{50}} \quad (\text{E.13})$$

A more accurate estimation of  $U_c$  was also carried out by direct observation of particle movement. In this case, a test series was performed without pier. In these tests the tailgates was raised up and after measuring the discharge,  $Q$ , the tailgate was slowly pushed down to establish an approach flow depth of 10 cm in the channel. In fact, all the tests presented in Tab. 8 were

performed with  $h=10$  cm and different approach velocities. After each observation, the discharge was increased and the tailgate was again pushed down to regulate the 10 cm approach flow depth.

Kramer (1935) indicated four different bed shear stress conditions for sedimentary bed:

1. no particles are in motion, termed *no transport*;
2. a few of the smallest particles are in motion at isolated zones, termed *weak transport*;
3. many particles of mean size are in motion, termed *medium transport*;
4. particles of all sizes are in motion at all points and at all times, termed *general transport*.

In Table 8, terms proposed by Kramer (1935) also were presented for each observation. In fact, for  $U=28.4$  cm/s, particle motion in isolated zones of movable bed with size of about  $d_{50}$  was observed. Therefore, the value of  $U_c=28.4$  cm/s is assumed in the present study. The average predicted value of  $U_c$  by Goncharov (1964) and Garde (1970) is equal to 27.9 cm/s and is near to the observed value.

As mentioned before, the experiments should be performed in clear-water conditions with  $U$  slightly less than  $U_c$ . Table 8 shows that the values  $U=27.8$  cm/s or 26.7 cm/s are probably high for the experiments, since in this condition a major part of the bed materials will be transported during the experiments that lasted for more than 3 days. In the present study,  $U=26.2$  cm/s was selected for the tests in clear-water conditions. This value indicates that the experiments performed with flow intensity of  $U/U_c=0.92$ .

It was observed that with this approach velocity only during the first few hours the sediment grain smaller than  $d_{50}$  moved for short distances from the movable bed surface and during the following hours and days such movements were negligible.

**Tab. 8. Observations of the tests to estimate critical velocity of sediment movement**

$U$ (cm/s)	Observation	Terms proposed by Kramer (1935)
14.9	No sediment movement	No transport
25.0	No sediment movement	No transport
25.4	Few very small particles could jump and rotate for distance less than 2 cm and then stopped	weak transport
26.2	Few very small particles could jump and rotate for distance less than 2 cm and then stopped	weak transport
26.7	Few very small particles could jump and rotate for distance about 5 cm	weak transport
27.8	Particles smaller than median sediment size could move frequently	weak transport
<b>28.4</b>	<b>Sediment transport of sand in forms of jumping and rotating grains of size equal to about or less than the median diameter</b>	<b>medium transport</b>
30.2	Sediment transport in wide range of particles (also greater than median size)	general transport

The experimental conditions of the present study for the steady flow tests in clear-water condition (tests S0 to S23, where “S” means “steady”) are presented in Tab. 9. In the present

study also a few preliminary tests were carried out in unsteady flow conditions. Among them, the peak flow of only one test, U00 (where “U” means “unsteady”), occurred in clear-water condition, i.e. in the same conditions as in the steady flow tests (Tab. 9).

**Tab. 9. Experimental conditions of tests S0 to S23 and at the peak flow of test U00**

$b$ (cm)	$B$ (cm)	$d_{50}$ (mm)	$h$ (cm)	$U$ (m/s)	$U_c$ (m/s)	$U/U_c$	$b/d_{50}$	$B/b$	$Re_p$	$Fr_p$
4	48.5	0.76	10	0.262	0.284	0.92	52.63	12.13	10275	0.42

In this study, nine preliminary tests were performed in unsteady live-bed condition (Tests U0 to U8). In these tests, experimental conditions at peak flow are presented in Tab. 10.

**Tab. 10. Experimental conditions at the peak flow of tests U0 to U8**

$b$ (cm)	$B$ (cm)	$d_{50}$ (mm)	$h$ (cm)	$U$ (m/s)	$U_c$ (m/s)	$U/U_c$	$b/d_{50}$	$B/b$	$Re_p$	$Fr_p$
4	48.5	0.76	10	0.312	0.284	1.1	52.63	12.13	12735	0.5

#### 4.4. Experimental procedure

The first phase of the experiments consists in the bottom preparation, positioning the pier and the countermeasures and then levelling the bottom. After filling the recess box with sediments, the bed was compacted manually and then an aluminium bar and two trowels were employed to level the sand bed at the same elevation of the false floors (Fig. 50).

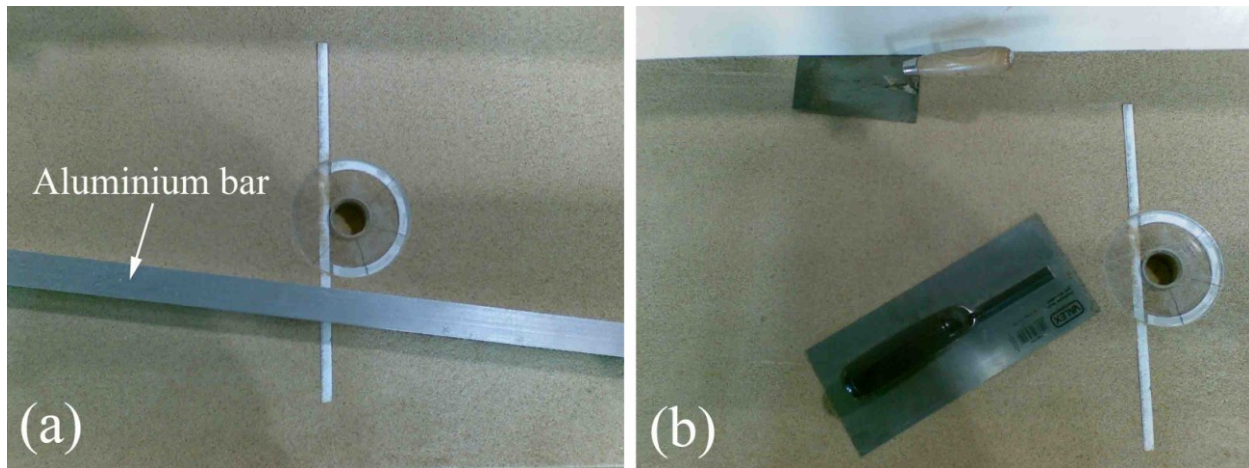


**Fig. 50. (a) Aluminium bar and (b) trowels used to level the sediment bed**

Starting the test is one the most important phases of the experiments, since during the first minutes of the experiments the local scouring rate at the pier is high. In order to avoid any disturbance of bed sediments by the first surge of the flow, the flume was fed slowly from downstream as shown in Fig. 51a. Afterwards, the flume was fed by gradually opening of manual

valves. In the unsteady flow tests, the flow was increased by gradually opening the motorised valve.

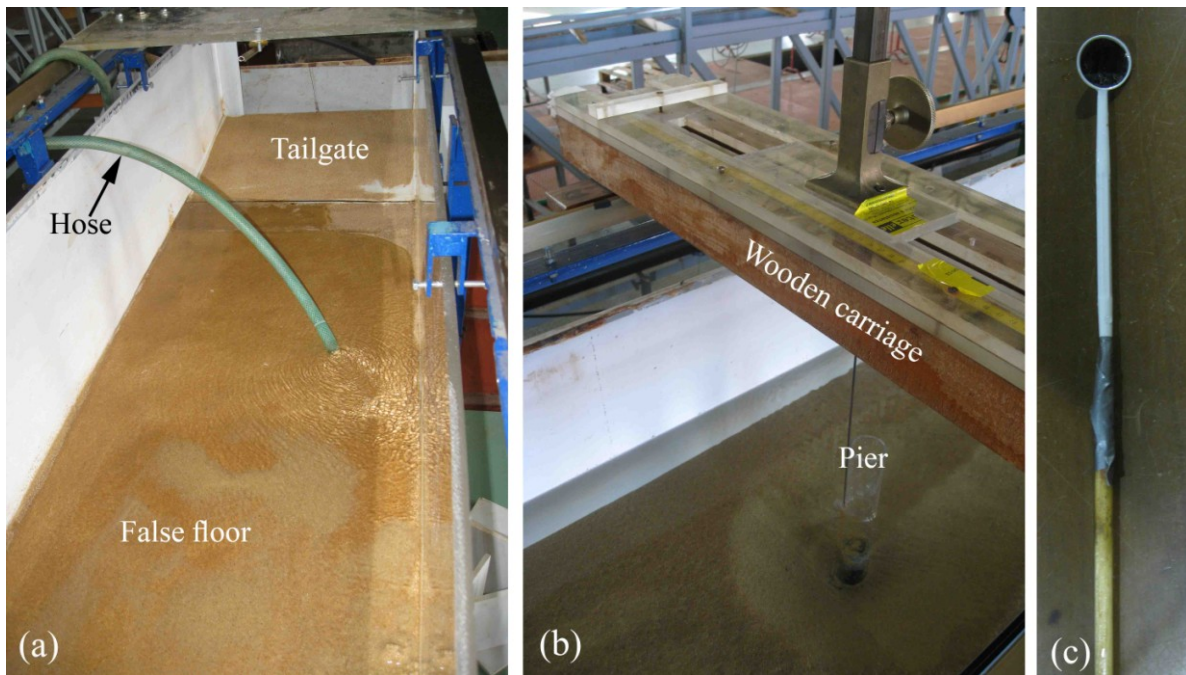


**Fig. 51. (a) Hose to fill the flume from downstream; (b) point gauge; (c) dental mirror to control the level of point gauge tip in collar tests**

In this study, except for the pier slot tests and the threading test (see §5.2.4 and §5.2.5), a two-part pier was employed for the experiments (Fig. 52a). The lower part was located inside the recess box flush with the bed. As the flow condition of Tab. 9 was achieved, the upper part of the pier was placed at its location and the experiment started. The application of a two-part pier also has two other advantages: first, levelling of the bed is performed easily with higher quality (Fig. 50a); second, the upper part of pier acts as a troublemaker in the acquisition with a 3D laser scanner; in fact, when merging the images around the pier a notable area around the pier should be eliminated from the images if the upper part of the pier is present. Details of the 3D laser scanner used to acquire the bed surface are presented in Appendix B.

In pier slot tests and threading test, the two-part pier could not be used, since the slot sank under the initial bed level and threads should be continuous in both the entire flow depth and the scour hole (see §5.2.4 and §5.2.5). In the tests related to these countermeasures, the tailgate was adjusted to regulate a 12.7 l/s discharge with  $h=10$  cm. In these tests, after feeding the flume from downstream, the flow gradually increased by opening the valve up to the condition  $h=8$  cm. Because of the use of the tailgate, the flow intensity in the case of  $h$  less than about 8 cm was not so high to initiate the scouring phenomenon. Afterwards, the valve was opened quickly and the flow depth reached 10 cm. Note that this method may not be applicable for wider channels or higher flow depths.

During all the experiments, the maximum scour depth in one or more locations was measured with a point gauge with needle-shaped tip and decimal vernier (Fig. 51b). In the test with a collar, the tip of the point gauge was positioned inside the pier and a small dental mirror was employed to control the level of the point gauge tip with respect to the bed materials in front of the pier (Fig. 51c). Previously, Mashahir *et al.* (2004) installed a periscope inside the pier to measure the development of the scour hole around the pier. Recently, Defanti *et al.* (2010) applied combination of laser ray and high resolution camera to measure scour in the plane of symmetry at a pier protected with a collar.

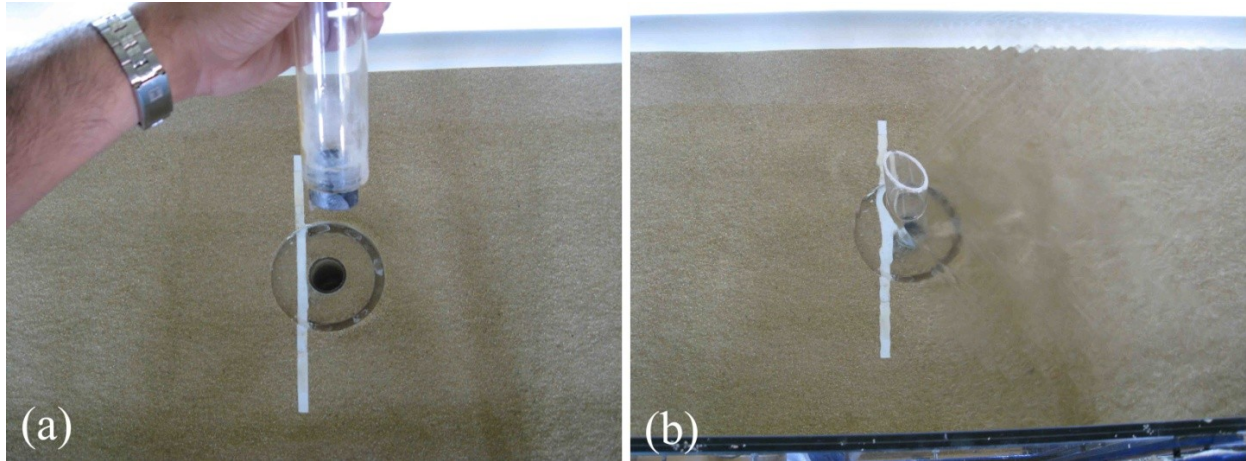


**Fig. 52. Application of two-part pier (a): before and (b): after starting the test**

As mentioned before, nine tests were performed in unsteady flow with the peak flow in live-bed conditions. In general, the live-bed flume tests are conducted in sediment feed or sediment recirculating flumes. In the live-bed tests of the present study, owing to the fact that only for a short period flow intensity is slightly greater than 1, a thin layer (about 2-3 mm) of sand was put on the false floor upstream and adjacent to the recess box, in order to avoid probable erosion upstream to the pier during live-bed periods (Fig. 53a). Afterwards, this sand layer was levelled with the sand in the recess box. The results of the experiments show that this method is adequate to avoid unusual erosion in movable bed. Figures 53b,c show the sparse sand layer on the false floor upstream to the pier after an unsteady flow test.

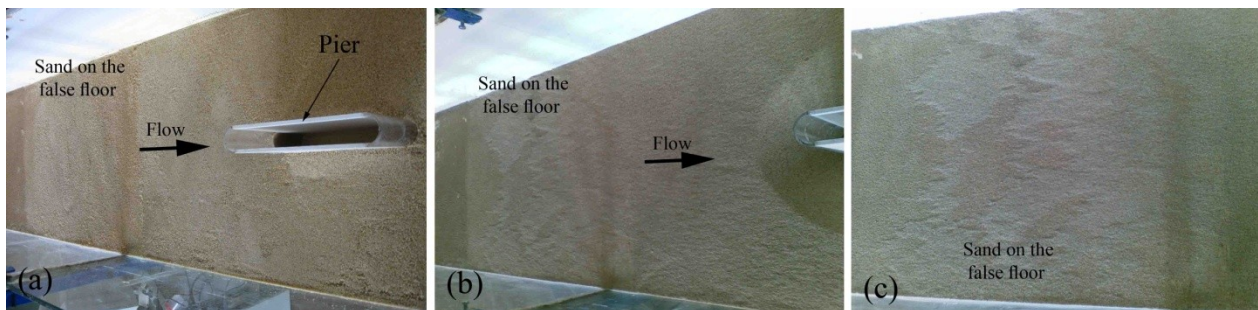


**Fig. 53. (a) Sand coverage on the false floor before and (b, c) after a test with peak flow in live-bed conditions**

To reproduce a flood hydrograph, a valve located at the supply pipe of the flume was equipped with two gears and an electromotor (Fig. 54a). The rotation velocity of the electromotor is regulated with an electrical current regulator (Fig. 54b).

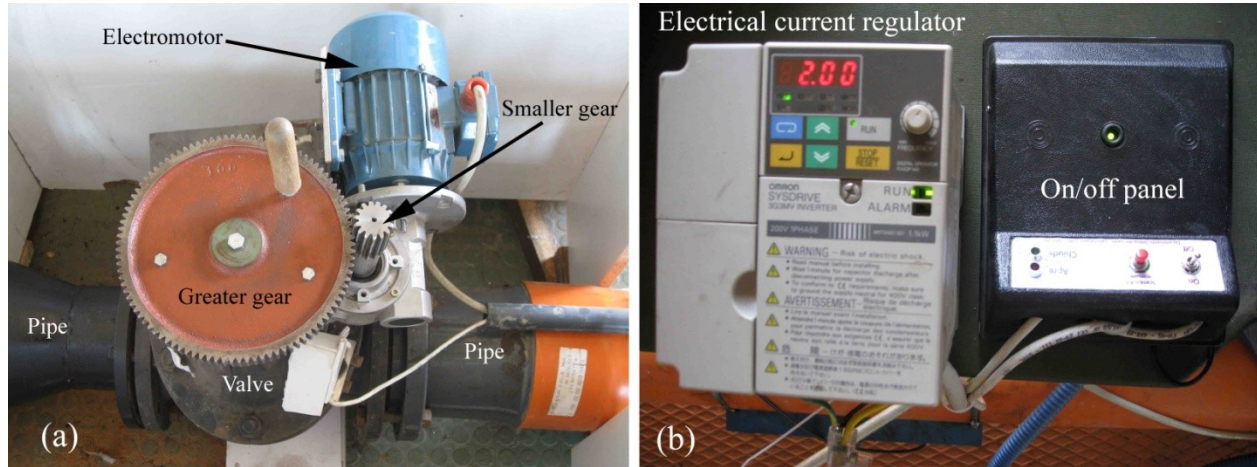


Fig. 54. (a) Motorised valve; (b) electrical current regulator

The rotation frequency of the electromotor was adjusted to open the valve at about 1 h and close it at 4 h and 20 min (total duration of 260 min), in order to simulate schematically a typical hydrograph of a Calabrian watercourse with the return period of 200 years requested by the Calabrian regional law for the study of inundation areas and bridge safety (Cardoso *et al.*, 2010). As mentioned before, the flow peaks of all unsteady tests, except one preliminary test, were in live-bed condition, with a flow intensity value slightly greater than 1 ( $U/U_c=1.1$ ). The hydrograph peak discharge of the preliminary test was equal to that of the steady flow test. Figures 55 and 56 show the hydrographs with the peaks in clear-water (test U00) and live-bed conditions (test U0), respectively. During the hydrograph with the peak in live-bed condition, approach flow depth and flow discharge were also measured simultaneously. The result is presented in Fig. 57, along with the regression power law and the coefficient of determination,  $R^2$ . Using these data, another relation between mean approach flow velocity and flow discharge is derived (Fig. 58). Based on the relationship between flow discharge and approach flow depth, variation of approach flow depth versus time is shown in Fig. 59. Critical flow velocity for sediment motion was estimated by empirical formulae. Figure 60 shows flow intensity value during imposing hydrograph, with a maximum of 1.13 for flow intensity slightly greater than the established value of 1.1. In fact, this difference was expected, since the  $U_c$  was only estimated by empirical formulae and approach flow depth and velocity were also estimated by regression-based equations. Figure 60 also shows that after about 25 min from initiation of the hydrograph and until 150 min (i.e., for a period of about 125 min) the flow remains in live-bed condition.

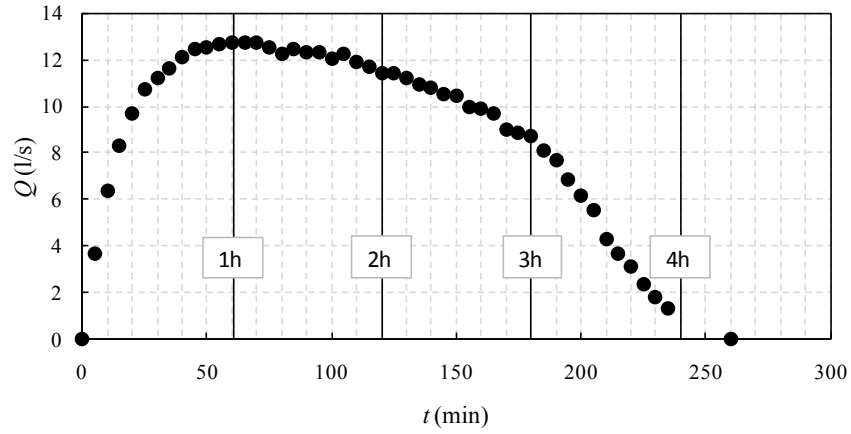


Fig. 55. Imposed hydrograph with the peak in clear-water condition (test U00)

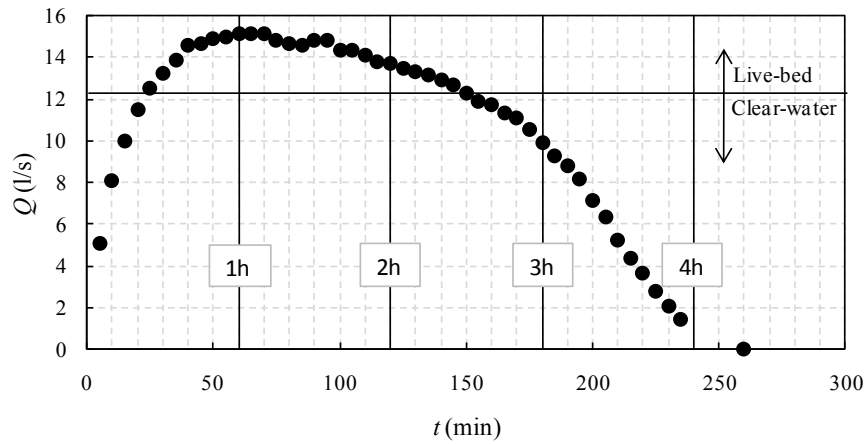


Fig. 56. Imposed hydrograph with the peak in live-bed condition (test U0)

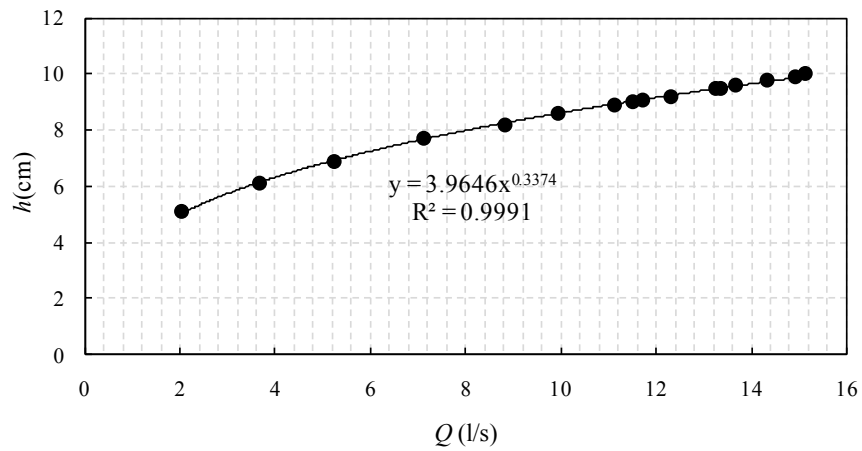


Fig. 57. Relation between flow discharge and approach flow depth



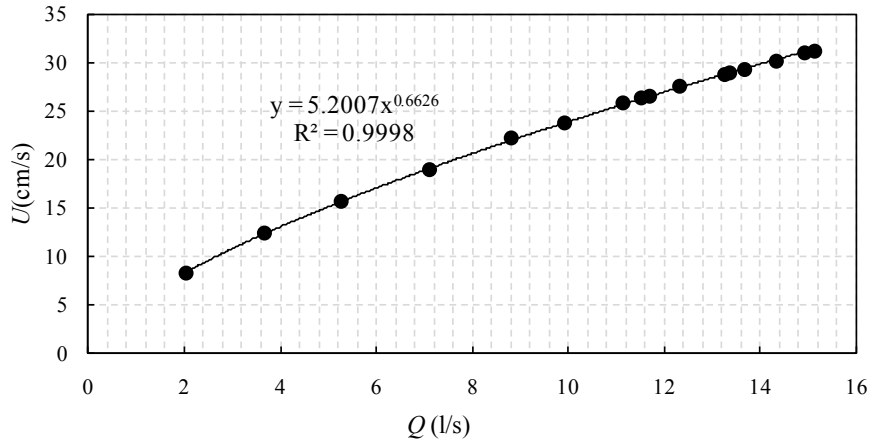


Fig. 58. Relation between flow discharge and approach flow velocity

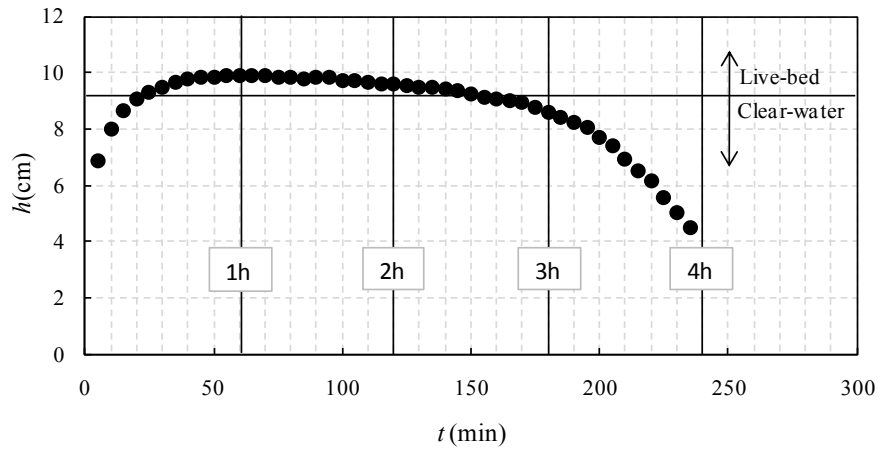


Fig. 59. Variation of approach flow depth during hydrograph test

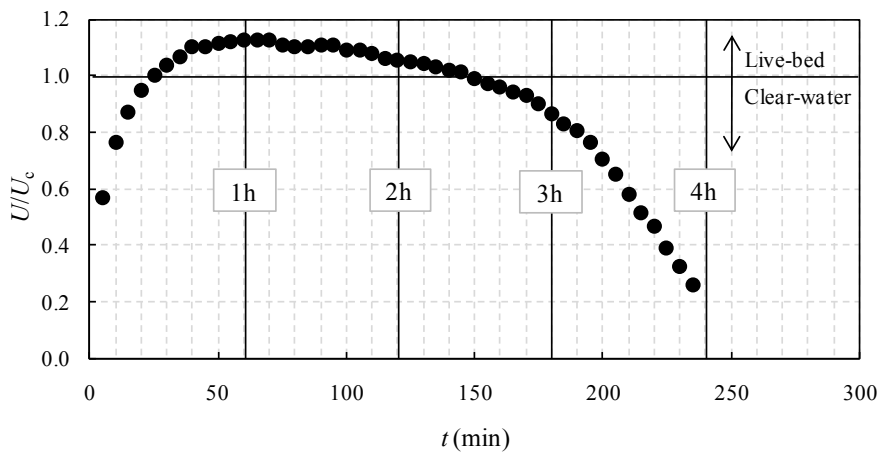


Fig. 60. Variation of flow intensity during hydrograph test

## 4.5. Locations and time-schedule to measure scour depth

### 4.5.1. Steady flow tests

Owing to the fact that the collars slow down strongly the scour evolution around the pier, the scour depth measurements were divided into two categories: tests with and without using a collar.

In the second group, a notable scour is obtained in front of the pier during the first hours of the scouring process, and the maximum scour depth in front of the pier was measured in accordance with the following time-schedule during the first day of the test: 2; 5; 8; 11; 14; 17; 20; 23; 26; 30; 35; 40; 45; 50; 55; 60; 70; 80; 90; 105; 120; 140; 160; 180; 210; 240; 270; 300; 360 min. Only 3 measurements per day were taken during the successive days of the test.

In tests with application of the collar, only 3 measurements per day were taken during the test, and the location of the expected maximum scour depth was monitored during the experiments. Furthermore, if the scour reached the pier, this scour was also measured during the test from inside the pier. However, only in two tests, although scour with small depth reached the pier, owing to the use of a border around the collar, it could not be observed and measured during the test; it was therefore measured only after the test.

### 4.5.2. Unsteady flow tests

In these tests, the maximum scour depth was measured with intervals of 10 min in different zones around the pier where separated scour holes could be distinguished.

## 4.6. Equilibrium criterion

In §2.7, a procedure proposed by Grimaldi (2005) was presented in order to verify that equilibrium is achieved. Although that procedure seems to be a proper criterion to ensure the equilibrium condition for an unprotected pier or for a pier protected with a slot through it, it may be impractical or encounter serious difficulties when applied to some countermeasures which slow down the temporal evolution of scour depth or are applied to small size piers.

In fact, the first criterion proposed by Grimaldi (2005), i.e. the test duration is computed *a priori* as  $2 \cdot 10^6 b/U$ , cannot be used for a pier protected with some types of countermeasures such as a collar. In Chapter 5, it will be shown that a longer test period is needed for a pier protected with a collar to obtain equilibrium condition. This criterion may be adequate in some conditions for single pier tests or a protected pier with a slot or bed-sill which do not significantly slow down the scour process.

Application of semi-logarithmic graph seems to be applicable for temporal evolution of some particular countermeasures (e.g. pier slot and sacrificial piles). However, its application may be questionable in the case of a pier protected with a collar. For example, in test S14 (that will be shown in the next chapter) maximum scour depth *in proximity to* the pier and in movable bed were simultaneously monitored during the test. These two values were measured in front of the pier and downstream of the bed-sill, respectively. Note that in this study “*in proximity to*” refers to maximum scour depth adjacent to the pier body or at a distance of a few millimetres (less than 5 mm) around it. Figures 61 and 62a show this configuration and temporal evolution of

the maximum scour depth at these two locations. Figure 62a shows that although the maximum scour in the movable bed stopped increasing and a slope change in temporal evolution is clearly observed, the scour beneath the collar shows a different behaviour. Figure 62b is a close up of the scour depth temporal evolution at this point for values of  $Ut/b > 10^6$ . This Figure shows that a collar may influence the scour evolution beneath it and in semi-logarithmic graph the typical straight line may not be obtained during the principal phase of scour evolution.

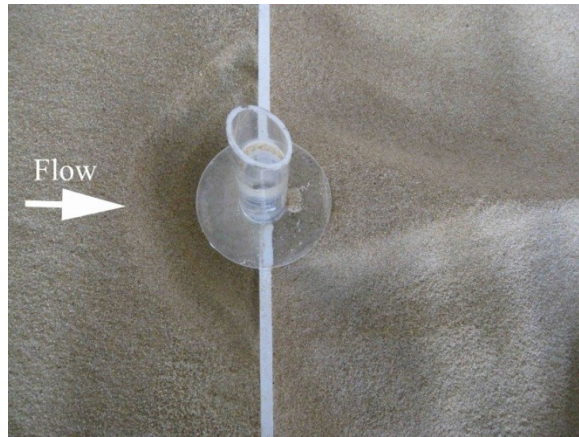


Fig. 61. Configuration and scour hole at the end of test S14

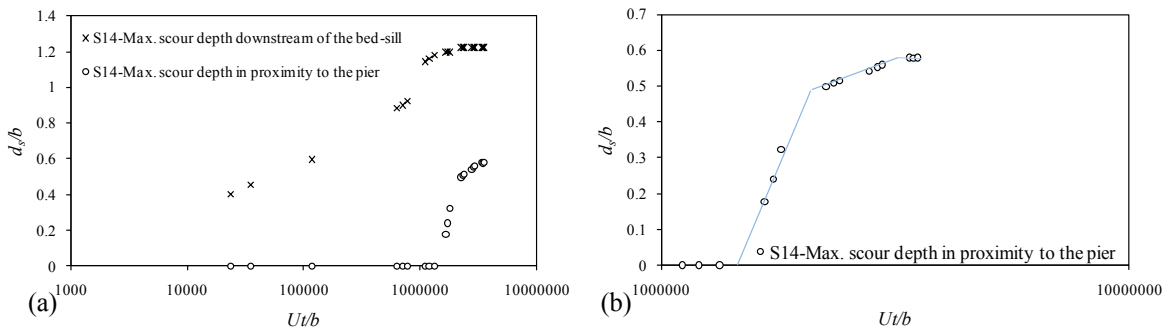


Fig. 62. (a) Temporal evolution of the maximum scour depth at two locations in test S14; (b) close up of the maximum scour depth temporal evolution for values of  $Ut/b > 10^6$

Note that the final value of  $Ut/b$  for this test is greater than  $3.5 \cdot 10^6$ . This value is much greater than that generally measured in pier tests performed in most laboratories. Although the slope of the line in Fig. 62b changes and during the last 24 h of the experiment the variation in scour depth in proximity to the pier was negligible (about 0.8 mm), there is a doubt in application of Cardoso and Bettess (1999) method for a pier protected with a collar.

Irrespective of the scour conditions (clear-water or live-bed), the curves relating the scour depth with time may be subdivided into three reaches corresponding to three phases of the scouring process:

- o the initial phase, where scour depth increases very quickly (lasting minutes in laboratory conditions);

- the principal phase, where the scour hole systematically increases in depth and plan extent at a progressively decreasing rate;
- the equilibrium phase, where the scour depth practically does not increase anymore.

According to Ettema (1980), the initial phase is characterised by the fast scour rate produced by the downflow at the pier face. The principal phase begins when the horseshoe vortex starts to dominate the scouring process. However, at the equilibrium phase, the scour depth “practically” does not increase anymore.

In general, these three phases can be identified, according to Fig. 63, on the basis of slope changes displayed on logarithmic plots of the scour depth against time. In most practical situations, the slope associated with the initial phase is not easily distinguishable from the slope of the principal phase. The onset of the equilibrium phase may also be difficult to identify due to the logarithmic nature of the plot. For this reason, the definition of time needed to reach time to equilibrium,  $t_e$ , is a matter of controversy. For example, Fig. 64 shows the difficulty in definition of time to equilibrium, since the location of change in slope of the principal phase cannot be distinguished easily.

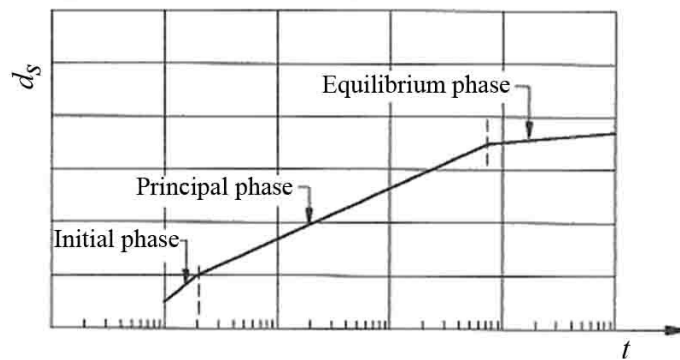


Fig. 63. Identification of phases in scouring process

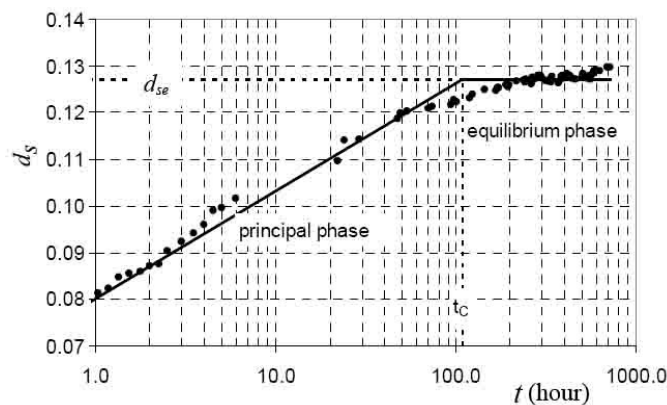


Fig. 64. Definition of time to equilibrium according to Cardoso and Bettess (1999) for a single pier test (modified from Lança *et al.*, 2010)

In the use of a collar, the initial phase of scouring cannot be observed, since downflow action is blocked by the collar. The influence of collar on downflow results in an influence on the horseshoe vortex, which is the main factor in the principal scouring phase. Therefore, this method may be not useful as in a single pier test. Radice *et al.* (2002) also claimed that this approach may fail, since after the observation of a long-lasting horizontal plateau scouring can be triggered again. It seems that this method needs more investigations before suggesting for a pier protected with flow-altering countermeasures, since these countermeasures influence scour progress by impacting on downflow and horseshoe vortex.

The other criterion proposed by Grimaldi (2005) is, in fact, an improved version of that proposed by Melville and Chiew (1999). As mentioned in Chapter 2, Grimaldi (2005) calculated the variation of the scour depth in 24 h to verify whether it is less than a small percentage of  $b$  ( $\Delta d_{s,24} \leq 0.05b/3$ ). In the present study, in the use of a 4 cm-wide pier, the value  $0.05b/3 = 0.67$  mm is obtained. It should be noted that although the point gauge with decimal vernier may have the accuracy of  $\pm 0.1$  mm, when it is employed to measure the maximum scour depth, such accuracy may not be obtained, owing to that the visual control of the point gauge tip under the flow from the lateral glass is not easy: in fact, it is not sure that the tip of the point gauge only touches the sediment surface or touches and slightly (in the order of less than 1 mm) pushes it down! On the other hand, the exact location of the maximum scour depth cannot be observed with an accuracy of less than 1 mm. Therefore, to speak about accuracies less than 1 mm in the use of a manual point gauge is questionable.

Grimaldi (2005) employed piers with widths in the range of 7.5 to 12 cm, and the value of  $0.05b/3$  ranged from 1.3 to 2 mm. In this case, scour measurements with such accuracies using a manual point gauge are obtainable.

In summary, the criterion proposed by Franzetti *et al.* (1994) is not adequate to be applied to all the countermeasures tested in the presented study, and the method proposed by Cardoso and Bettess (1999) is not adapt to all the countermeasures (however, it was applicable in most scour measurements of the present work).

The third criterion proposed by Grimaldi (2005) was originally proposed by Melville and Chiew (1999) as  $\Delta d_{s,24} \leq 0.05b$ . The value of  $0.05b$  in the present study is equal to 2 mm, and therefore this criterion was selected; nevertheless, the tests were carried out with longer durations and results will show that the value of  $\Delta d_{s,24}$  ranged from 0 to 1.3 mm with an average of 0.8 mm, which is significantly smaller than  $0.05b = 2$  mm.

In fact, more study is needed to find a proper criterion for each countermeasure. Owing to the fact that the results of Lança *et al.* (2010) show that for a single pier test the duration of about one month or more than it may not be enough to achieve equilibrium, tests should probably be performed for several months for those countermeasures which particularly slow down the scour progress.

Figures 65 and 66 show a comparison of temporal evolution of the maximum scour depth at an unprotected pier (present study) with data by Grimaldi (2005) and Lança *et al.* (2010). These figures show that the rate of scouring in the present study is almost similar to those two studies and at the end test, the maximum scour depth is in the range of Grimaldi's results. However, it

seems that based on Lança *et alii*'s data, the scour depth may increase after this period. In test S0, during the period from 46.5 to 72 h (more than 1 day) the scour depth evolution in front of the pier stopped and the slope change was clearly observed: therefore, the test was stopped at  $t=72$  h. Figure 66 shows that in tests #3 to #5 performed by Lança *et al.* (2010) the slope of the scouring progress line changed for  $Ut/b > 10^6$  and the increase in scour depth rate was significantly reduced. Although after this period scour depth slightly increased in those three tests, it is possible to assume the scour process enters the equilibrium phase (see also Fig. 63). In particular, in those three tests and in test S0 of the present study the increase in scour depth almost finished during similar  $Ut/b$  ranges (see Fig. 66 for  $10^6 < Ut/b < 1.3 \cdot 10^6$ ). Owing to the similar temporal evolution of the maximum scour depth for  $10^6 < Ut/b < 1.3 \cdot 10^6$  in the present study and in test #5 by Lança *et al.* (2010), a comparison of the two data series is presented in Fig. 67.

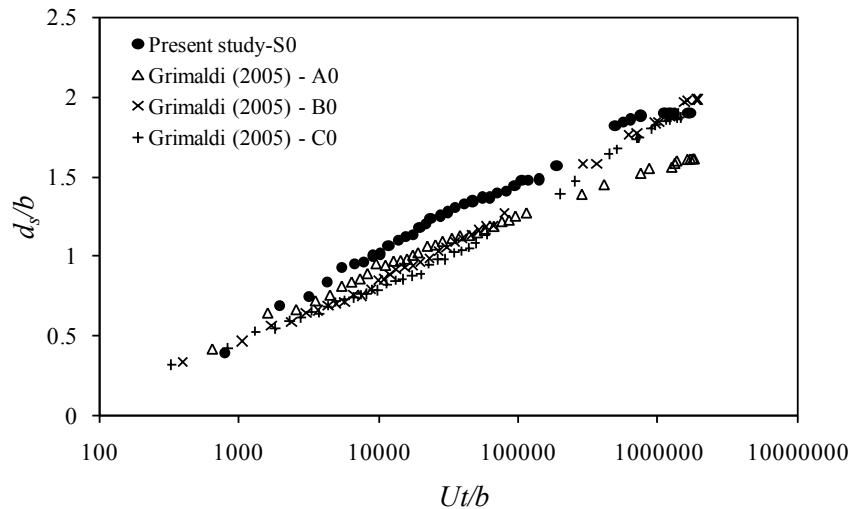


Fig. 65. Temporal evolution of scour depth in front of pier in tests S0 and Grimaldi (2005)

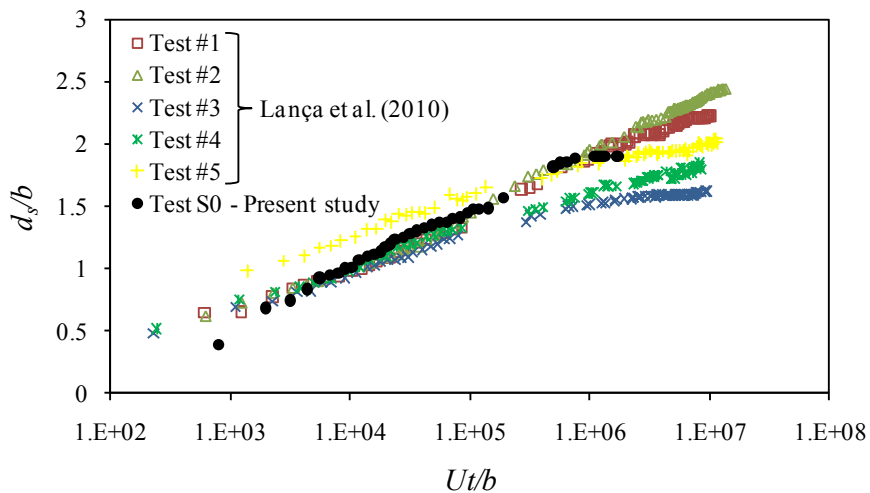


Fig. 66. Temporal evolution of scour depth at the pier in tests S0 and Lança *et al.* (2010)

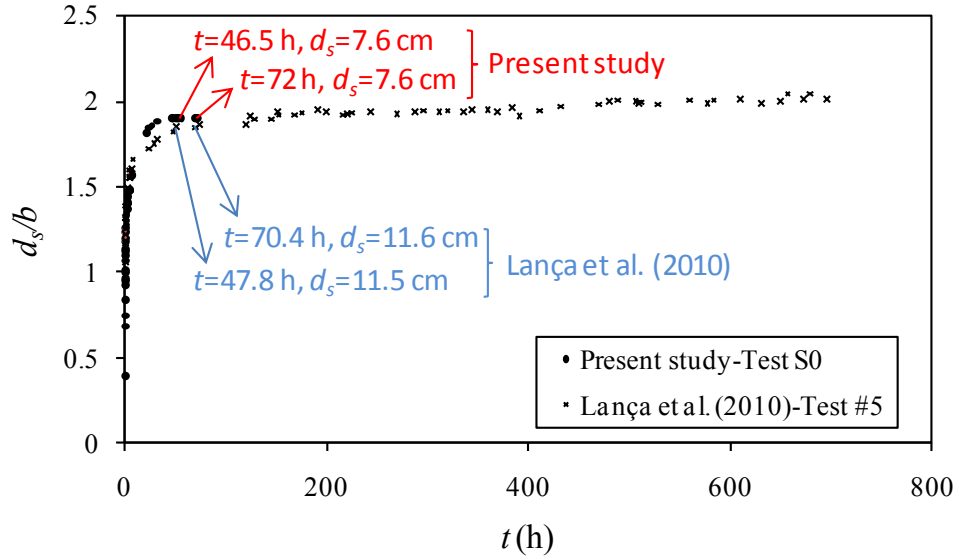


Fig. 67. Comparison of unprotected pier test (S0, present study) with test #5 by Lança *et al.* (2010)

Figure 67 shows that during a similar time period (3<sup>rd</sup> day) in both tests the scour almost stopped. Lança *et al.* (2010) suggested the use of a 6-parameters polynomial function (E.14) to extrapolated scour depth to infinite time. In their equation,  $p_1$  to  $p_6$  are parameters obtained by regression analysis:

$$d_s = p_1 \left( 1 - \frac{1}{1 + p_1 p_2 t} \right) + p_3 \left( 1 - \frac{1}{1 + p_3 p_4 t} \right) + p_5 \left( 1 - \frac{1}{1 + p_5 p_6 t} \right) \quad (E.14)$$

In (E.14), when  $t \rightarrow \infty$ , then  $d_{se0} = p_1 + p_3 + p_5$ . It should be noted that application of regression for this equation may result in more than one solution for  $p_1$  to  $p_6$ . Therefore, more research is necessary in the application of this equation to estimate the end scour depth.

Equation (E.14) was applied to test S0 of the present study, as shown in Fig. 68. The value of  $d_{se}$  based on the summation of  $p_1$ ,  $p_3$  and  $p_5$  is equal to 8.12 cm, only about 6% greater than the observed scour value at the end of 3 days. In fact, the scour process in test S0 of the present study after about 46.5 h entered to the equilibrium phase; however, the end scour depth may be greater than the measured scour depth at the time when the test was stopped.

The dimensionless ratio  $d_s/d_{se0}$  vs.  $t/t_e$  is presented in Fig.69a for test S0. According to Melville and Chiew (1999), depending on the approach flow velocity the scour depth after 10% of the time to equilibrium is between about 50% and 80% of the equilibrium scour depth (Fig. 69b). Figure 69a shows that about 78% scour depth was observed in 10% of the time to equilibrium, which confirms the statement of Melville and Chiew (1999); this value was expected, since the approach flow velocity was near the threshold of the sediment movement.

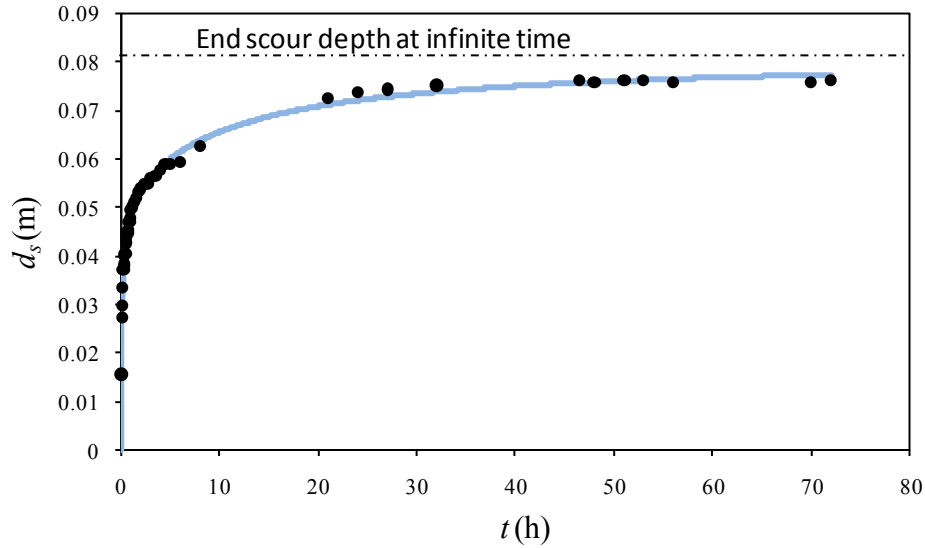


Fig. 68. End scour depth based on data of test S0 and (E.14)

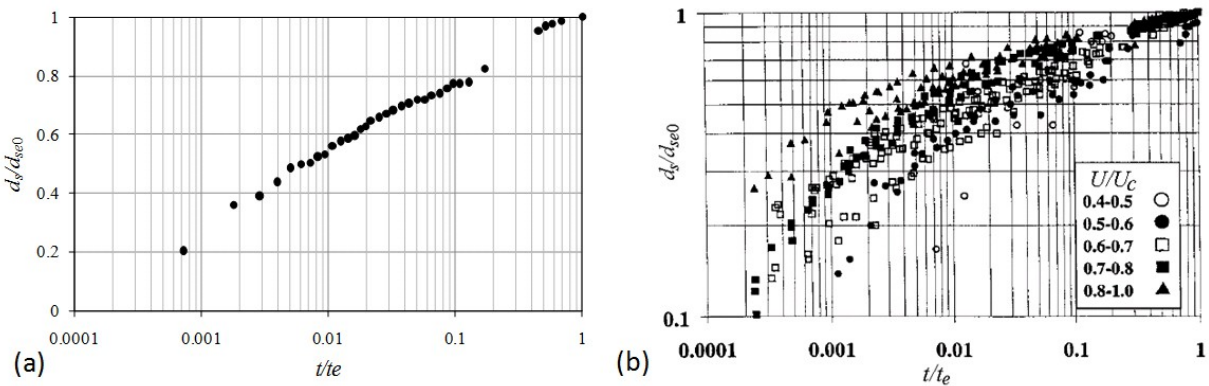


Fig. 69. Dimensionless ratio  $d_s/d_{se0}$  vs.  $t/t_e$ ; (a) test S0; (b) from Melville and Chiew (1999)

Eventually, the application of a polynomial function has been recently proposed for unprotected piers and more study is needed to check the adequacy of this method. Furthermore, the performance of a flow-altering countermeasure in the long-period tests is unknown. In particular, the writer is not sure about the application of this method to flow-altering countermeasures that significantly impact on the temporal evolution of the scour depth. Therefore, in the present study the scour depth measured at the end test was used to calculate the efficiency of the countermeasures, as explained in the following section.



#### 4.7. Calculation of efficiency

Generally, the maximum scour depth for a single unprotected circular pier is located in front of the pier. Also if a pier is protected with some countermeasures (e.g., pier slot) the maximum scour depth is in front of the pier. Therefore, calculation of scour depth reduction based on maximum scour depth which is near the pier foundation properly shows the efficiency of the countermeasure as follows:

$$r_{de} (\%) = \frac{d_{se0} - d_{se}}{d_{se0}} \cdot 100 \quad (E.15)$$

where  $d_{se}$  and  $d_{se0}$  are the equilibrium scour depths in proximity to the protected and unprotected pier, respectively.

The application of some other pier countermeasures (e.g., combination of a collar and a bed-sill) may result in changing the location of maximum scour depth. In this case, although the scour depth that reached the pier body may be negligible, a deep scour may be observed in front of the upstream bed-sill adjacent to the pier. In this case, the bed-sill cannot be a reliable protector against pier instability. Figure 70a shows a pier adjacent to a bed-sill with a scour in front of it. In this case, the horizontal component of stress under the pier that is the result of the vertical weight of the bridge pier may destroy the bed-sill and consequently the pier will collapse. Furthermore, the bed-sill may also be unstable due to deep scour in front of it. In this condition, small scour in proximity to the pier downstream of the bed-sill cannot be assumed as a proper criterion to estimate the efficiency of this countermeasure. In this case, maximum scour depth in front of the bed-sill which is also the maximum scour in the movable bed at equilibrium condition,  $d_{sem}$ , is used in (E.15) instead of  $d_{se}$ .

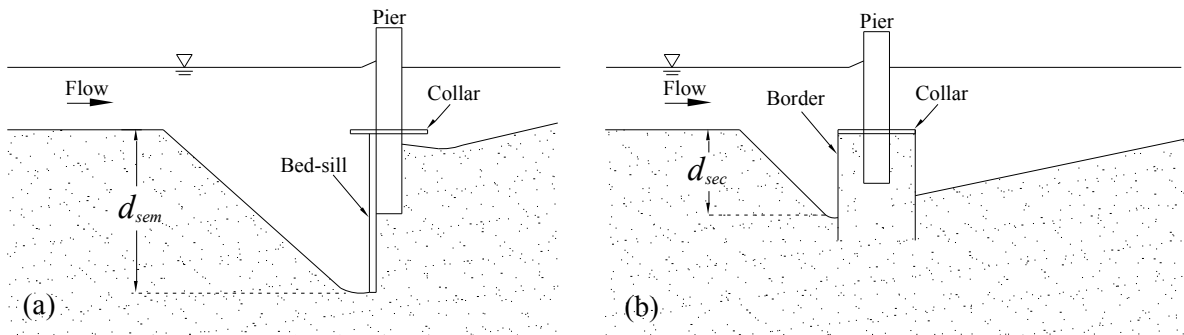


Fig. 70. (a) Schema to illustrate the scour in front of a bed-sill and (b) around a bordered-collar

In the combination of collar and bed-sill, the scour may not reach to the upstream part of the bed-sill, however, it may intrude beneath the collar and major parts of bed-materials under the collar are eroded. In practical applications, the collar may collapse in this condition. Therefore, as it will be explained in the next Chapter, a border was attached around the collar to prevent the intrusion of scour under the collar. In this condition, although the bed materials under the collar

and adjacent to the pier are intact, the bed-material under the collar cannot protect the pier foundation. For example, Fig. 70b shows a pier protected by a collar, around which a border was attached to protect the bed materials under it. This configuration is similar to a pier with a wider foundation as explained in the previous Chapter. In this case, the maximum scour will be observed in front of the border; although the bed-materials under the collar in proximity to the pier are intact, they cannot transmit the stress due to pier and bridge weight, since they are disconnected from the other bed-materials. In fact, assuming 100% efficiency for this countermeasure based on maximum scour depth in proximity to the pier is not correct. In this condition, if the scour intrudes beneath the collar, the maximum scour depth under the collar or, if a part of border is exposed, the maximum scour depth adjacent to the border,  $d_{sec}$ , is used instead of  $d_{se}$  in order to calculate  $r_{de}$  with (E.15).

Although scour volume and scour area around the pier foundation are not the most important factors in pier design, they were also measured in order to have an idea about scour extension and volume in the application of some countermeasures. The scour area and volume reduction,  $r_{Ae}$  and  $r_{Ve}$  respectively, can be calculated as follows:

$$r_{Ae} (\%) = \frac{A_{e0} - A_e}{A_{e0}} \cdot 100 \quad \text{and} \quad r_{Ve} (\%) = \frac{V_{e0} - V_e}{V_{e0}} \cdot 100 \quad (\text{E.16})$$

where  $A_{e0}$  and  $V_{e0}$  are the equilibrium scour area and volume at the unprotected pier, whereas  $A_e$  and  $V_e$  are the equilibrium scour area and volume at the protected pier, respectively.

In the next Chapter, the results of the present work will be compared with those of some previous studies. In some studies the experiments were performed in steady flow conditions for a period so short that probably the equilibrium condition was not achieved. Also in unsteady flow tests of the present work, equilibrium was not reached. In these cases, the efficiency,  $r_{ds}$ , will be calculated on the basis of the maximum scour depth, which occurred at the end of the steady flow tests or during the unsteady flow tests, as follows:

$$r_{ds} (\%) = \frac{d_{s0} - d_{sp}}{d_{s0}} \cdot 100 \quad (\text{E.17})$$

where  $d_{sp}$  and  $d_{s0}$  are the maximum scour depth in proximity to the protected and unprotected piers, respectively, measured during the test. In tests with the application of a collar, the maximum scour depth adjacent to the collar border or beneath the collar during test period,  $d_{scb}$ , is employed instead of  $d_{sp}$  to estimate the efficiency of the countermeasure.

## Chapter 5

### RESULT ANALYSIS AND DISCUSSION

#### 5.1. Introduction

The aim of the present study is to analyse the efficiency of five flow-altering countermeasures which seem to be of practical use, as well as some possible combinations of selected countermeasures. In the first part of the present chapter, the efficiencies of countermeasures are evaluated on the basis of long-term steady-state tests (considered practically in equilibrium condition). Afterwards, the selected countermeasures are tested in unsteady live-bed conditions.

#### 5.2. Steady flow tests

In this part of the thesis, the results of a test for an unprotected pier (S0) and 23 tests with various flow-altering countermeasures (S1 to S23) are presented.

##### 5.2.1. Unprotected pier: test S0

Test S0 was performed with an unprotected pier and then used as a reference test in order to evaluate the performance of tests with countermeasures. As mentioned before, a smooth circular pier with diameter  $b=4$  cm was employed in this study. A detailed explanation about the temporal evolution of scour in this test was presented in §4.6. The maximum scour depth in this test was 7.62 cm and occurred in front of the pier. Figure 71 shows a photo at the end of this test. A 3D pattern of scour around the pier and the contour line plot of the scour are presented in Figs. 72 and 73. The scour area and volume at the end of this test were  $1050.4 \text{ cm}^2$  and  $2806.4 \text{ cm}^3$ , respectively.



Fig. 71. Scour hole at the end of test S0

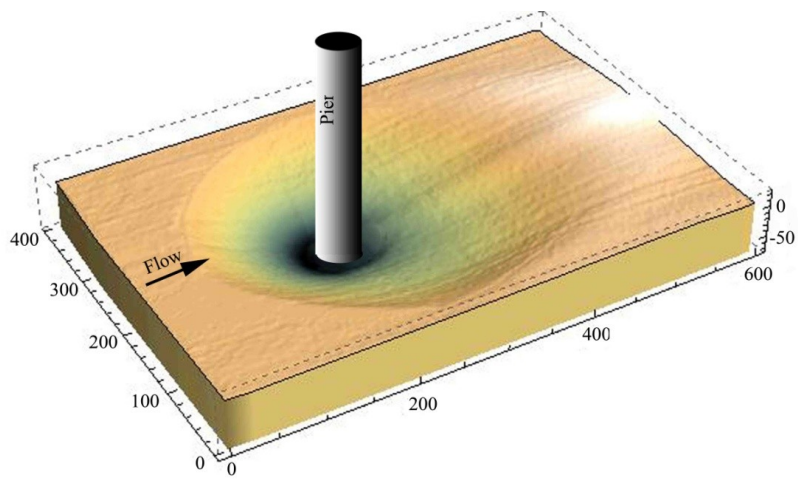


Fig. 72. 3D pattern of scour in test S0 at equilibrium (units: mm)

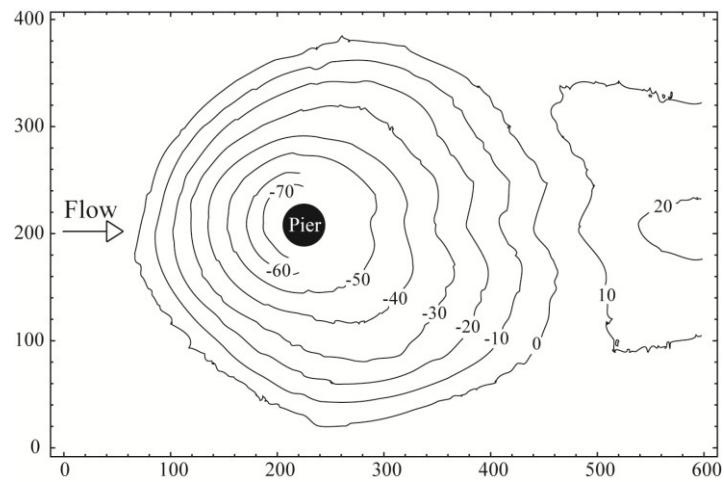


Fig. 73. Contour lines of equilibrium scour hole in test S0 (units: mm)

The influence of sediment grading in scour depth is presented in Fig. 74. This figure shows that for  $\sigma_g \approx 1.5$  the value of the sediment grading adjustment factor,  $K_\sigma$ , is about 0.9, and influence of this parameter can be assumed to be negligible; however, its influence was not eliminated. The selected flow intensity,  $U/U_c = 0.92$ , may also reduce the maximum scour depth with respect to  $U/U_c = 1$ . The ratio  $h/b = 2.5$  results in  $K_h \approx 0.92$  (Fig.18b). In this condition, although the influence of each parameter is negligible, the influence of both parameters results in a more than 10% reduction in maximum scour depth. Therefore, for these two reasons the maximum scour depth ( $d_{se0} = 1.9b$ ) is about 21% less than maximum possible scour depth which is about  $d_{se0} = 2.4b$ .

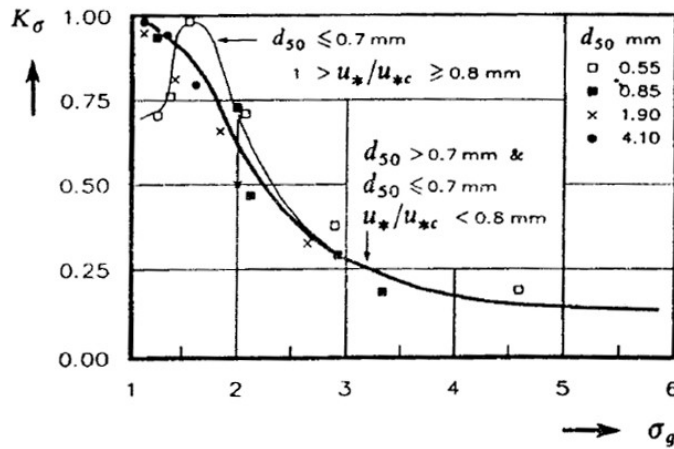


Fig. 74. Coefficient  $K_\sigma$  as a function of  $\sigma_g$  ( Breusers and Raudkivi, 1991)

At the downstream portion of the scour holes the propagation of bed forms was observed (Fig. 75a). Such bed forms and turbulent flow field near them probably affected the scour hole. Figures 72 and 73 show that the scour hole in test S0 is more similar to a bowl with a round border; however, in conditions that such bed forms did not develop, the downstream border of the scour hole propagates more towards downstream. Such bed forms were not observed by Mansueto (2009) and Grimaldi (2005). Contour lines of equilibrium scour hole at the end of those two studies are shown in Figs. 76 and 77, in which the development of the scour hole in the downstream direction is clearly apparent. In contrast, such bed forms were also observed downstream of the scour hole in the test by Melville and Raudkivi (1977) (Fig. 75b) and the downstream part of the scour hole did not develop as much as shown in Figs. 76 and 77.

On the other hand, the value of  $d_{se}/b$  in Mansueto (2009) is equal to 1.88 and in Grimaldi (2005) ranges from 1.62 to 1.87. Note that in those two studies the experimental conditions and dimensionless groups are almost similar to those of the present study (Tab.11). In fact, values of  $d_{se}/b$  of the present study are similar to those by Grimaldi (2005) and Mansueto (2009) and therefore bed forms probably do not affect the maximum scour depth, owing to the prevailing action of the horseshoe vortex and wake vortices in the scouring phenomenon.

## Chapter 5. Result analysis and discussion

In Table 11 the results of a test performed by Mashahir *et al.* (2004) are presented,  $t_d$  being the test duration. In that test a circular cylinder with  $b=4$  cm (the same diameter as in the present study) was employed. Their results show that  $d_{se0}/b$  is equal to 2.3, which is significantly higher than the value obtained in the present study and in the other tests in Tab. 11; however, their test period was less than the other tests. In this case, probably the higher value of  $h/b$  and the lesser value of  $\sigma_g$  justify this result.

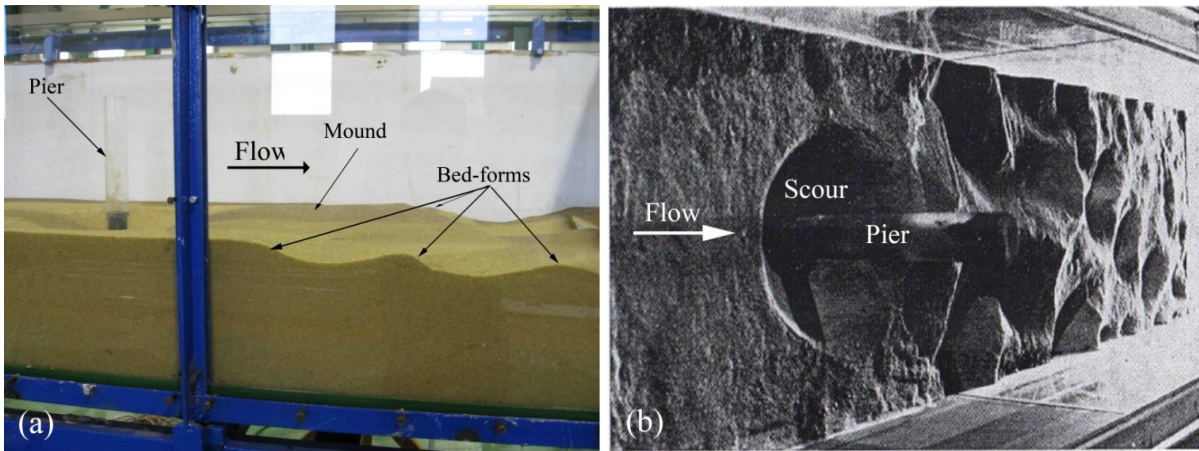


Fig. 75. Bed-forms downstream of the pier scour; (a) test S0; (b) Melville and Raudkivi (1977)

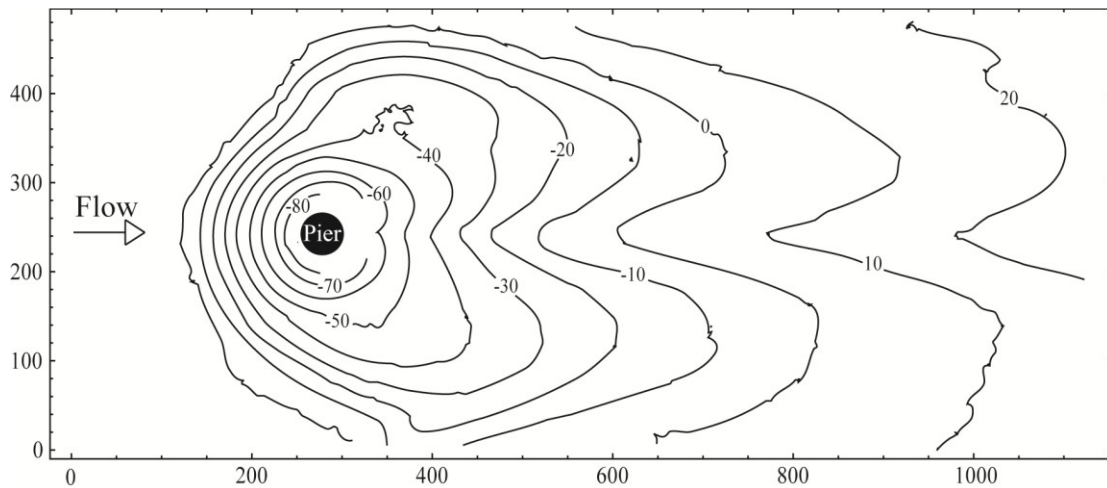


Fig. 76. Contour lines of equilibrium scour hole at unprotected pier (Mansueto, 2009) (units: mm)

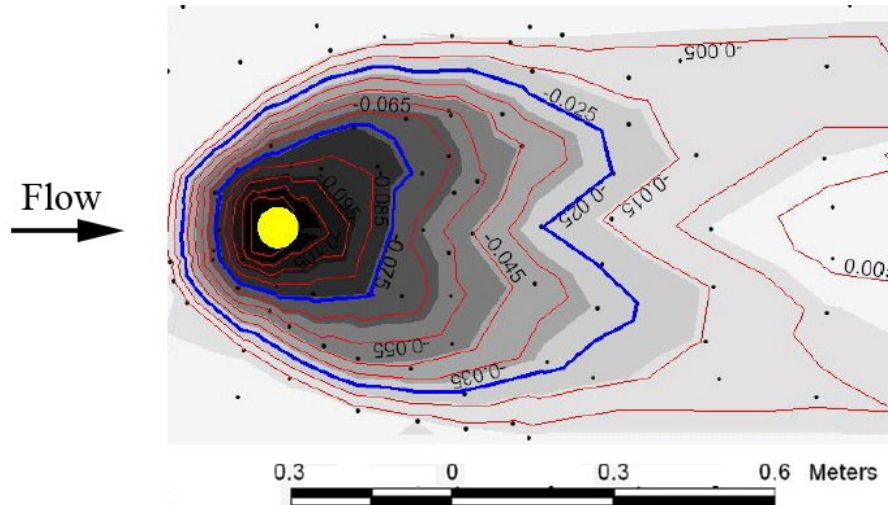


Fig. 77. Contour lines of equilibrium scour hole in test A0 by Grimaldi (2005) (units: m)

Tab. 11. Comparison of experimental conditions and results of test S0 with some other tests

Test	$B$ (cm)	$b$ (cm)	$t_d$ (h)	$\sigma_g$	$d_{50}$ (mm)	$U$ (m/s)	$U_c$ (m/s)	$h$ (cm)	$d_{se0}$ (cm)
S0	48.5	4	72	1.46	0.76	0.262	0.284	10	7.62
Mashahir <i>et al.</i> (2004)	75	4	44	<1.2	0.95	28.9	-	12	9.2
Grimaldi <i>et al.</i> (2005)-A0	80	7.5	96	1.46	1.3	0.4	0.4	15	12.14
Grimaldi <i>et al.</i> (2005)-B0	200	9	147.9	1.44	0.7	0.33	0.33	25	17.9
Grimaldi <i>et al.</i> (2005)-C0	200	12	146.1	1.44	0.7	0.33	0.33	25	22.46
Mansueto (2009)	48.5	4.8	70.8	1.42	0.78	0.27	0.28	12	9

Tab. 11. (continued)

Test	$Ut_d/b$	$B/b$	$b/d_{50}$	$h/b$	$U/U_c$ or $u^*/u^*_c$	$Fr_p$	$d_{se0}/b$
S0	$1.7 \cdot 10^6$	12.1	52.6	2.5	0.92	0.42	1.9
Mashahir <i>et al.</i> (2004)	$1.14 \cdot 10^6$	18.75	42.1	3	0.92	0.46	2.3
Grimaldi <i>et al.</i> (2005)-A0	$1.84 \cdot 10^6$	10.7	58.6	2	1	0.47	1.62
Grimaldi <i>et al.</i> (2005)-B0	$1.95 \cdot 10^6$	22.2	132.2	2.8	1	0.36	1.99
Grimaldi <i>et al.</i> (2005)-C0	$1.45 \cdot 10^6$	16.7	176.2	2.1	1	0.31	1.87
Mansueto (2009)	$1.43 \cdot 10^6$	10.1	61.5	2.5	0.95	0.39	1.88

### 5.2.2. Transverse sacrificial piles

When transverse sacrificial cylindrical piles are used as countermeasure, three other dimensionless numbers, i.e.  $b_r=N_p \cdot D_p/b_p$ ,  $X_p/b_p$  and  $b_p/D_p$  should be considered,  $b_r$ ,  $N_p$ ,  $D_p$ ,  $X_p$  and  $b_p$  being the blockage ratio, the number of piles, the pile diameter, the distance from the transversal axis of the pile group to the upstream pier face and the pier width projected on the transversal axis of the pile group, respectively. As mentioned in §3.4.1, according to Haque *et al.* (2007) transverse sacrificial piles give the optimum performance when 3 piles ( $N_p=3$ ) with 60% blockage ratio ( $b_r=0.6$ ) are placed at a distance of  $2b_p$  from the pier. Note that for cylindrical piers  $b_p=b$ . This configuration is considered in this section. In order to obtain 60% blockage with 3 piles, 8mm-diameter wooden sticks were employed in test S1 ( $N_p=3$ ,  $b_p/D_p=5$ ). These piles were located at a distance equal to  $X_p=2b_p=8$  cm from the pier face as shown in Fig. 78a. The geometric parameters of this configuration are presented in Tab. 12.

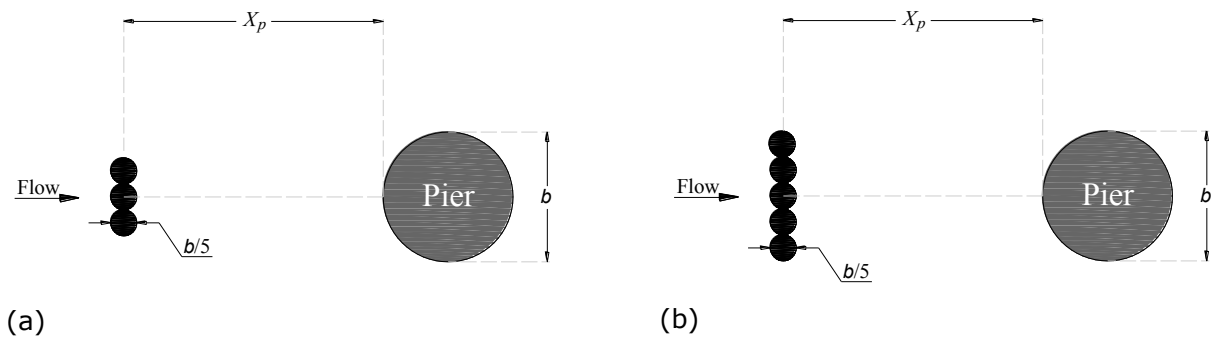


Fig. 78. Configuration of transverse sacrificial piles; (a) test S1; (b) test S2

Tab. 12. Geometric parameters of configurations in tests S1 and S2

Test	$N_p$	$b_r$	$b_p$	$X_p$
S1	3	0.6	$b$	$2b$
S2	5	1	$b$	$2b$

In test S1, during the first 2 min ( $Ut/b=786$ ) the scoured sediments around the piles were deposited at the pier location and during this period this accumulation could overcome the scouring of bed materials around the pier. However, during this period a scour equal to 1.56 cm ( $d_s/b=0.39$ ) was observed in front of the unprotected pier (test S0; Fig. 79), even if the eroded bed material around the piles moved towards the pier. A portion of eroded material was deposited around the pier and the other part was transported downstream and outside of the pier scour hole by turbulent flow around the pier. Figure 80a shows that sediments scoured around the piles were transported to the pier scour hole. At the end of the test, maximum scour depths of 5.17 and 6.65 cm ( $d_{se}=5.17$ ,  $d_{sem}=6.65$  cm) were observed in front of the pier and in front of the piles, respectively (Figs. 80b, 81 and 82). Based on maximum scour depth in proximity to the pier,  $d_{se}$ , the efficiency of 33.4% is obtained for this test (Tab. 13).



Tab. 13. Results of tests S1 and S2

Test	$t_d$ (h)	$Ut_d/b$	$d_{se}$ (cm)	$d_{sem}$ (cm)	$A_e$ (cm <sup>2</sup> )	$V_e$ (cm <sup>3</sup> )	$r_{de}$ (%)	$r_{Ae}$ (%)	$r_{Ve}$ (%)
S1	90.1	$2.12 \cdot 10^6$	5.17	6.65	781.7	1870.4	32.2	25.6	33.4
S2	72	$1.7 \cdot 10^6$	7.2	9.98	1628.8	5151.2	5.5	-55.1	-83.6

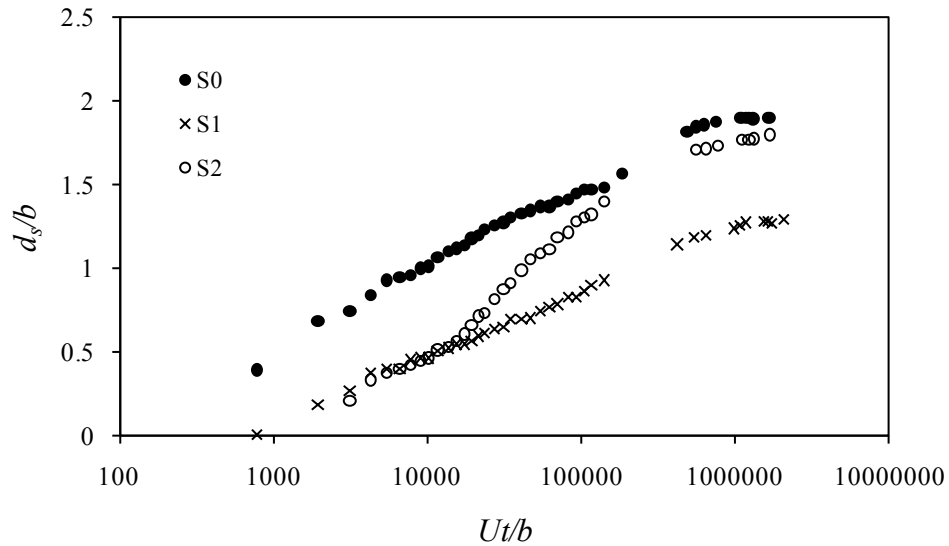


Fig. 79. Temporal evolution of scour depth in front of the pier in tests S0, S1 and S2

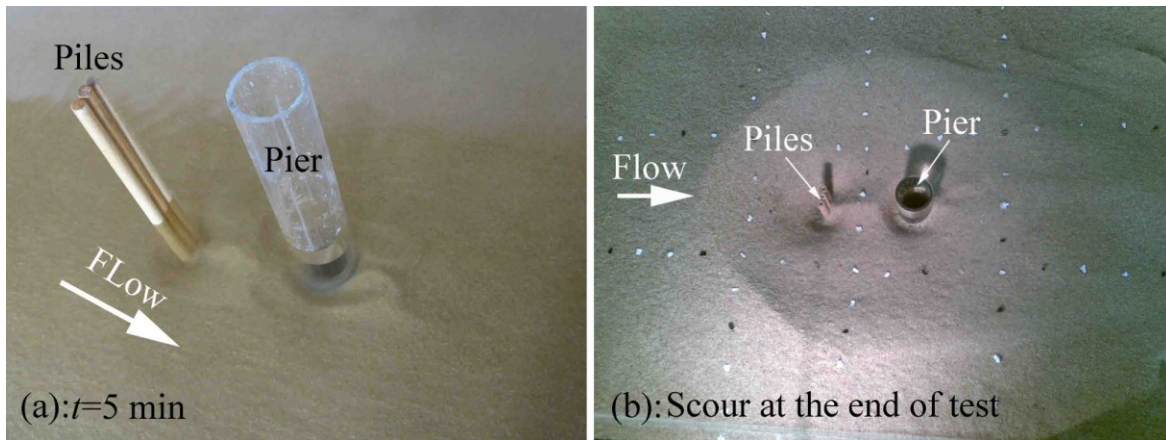


Fig. 80. Scour around the pier in test S1; (a) filling the pier scour by sediments eroded around the piles; (b) scour hole at the end of test

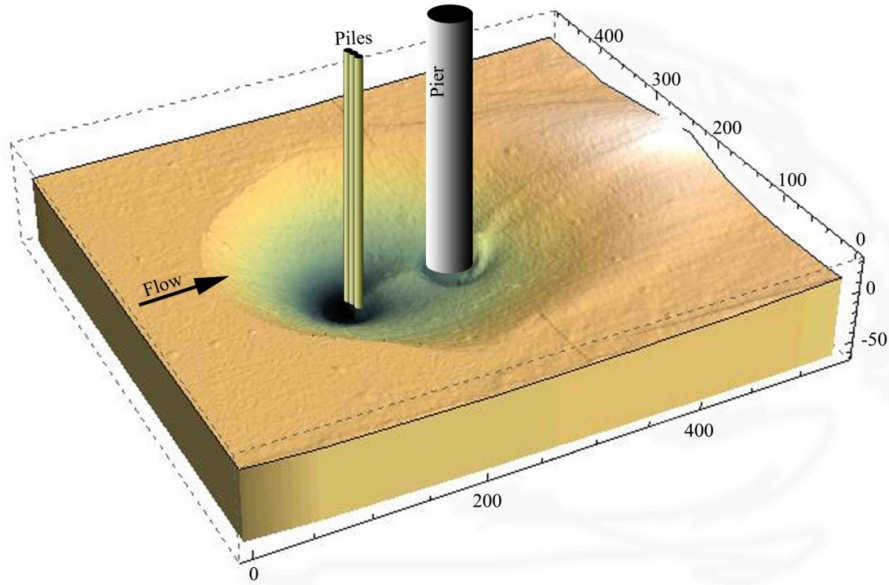


Fig. 81. 3D pattern of equilibrium scour hole in test S1 (units: mm)

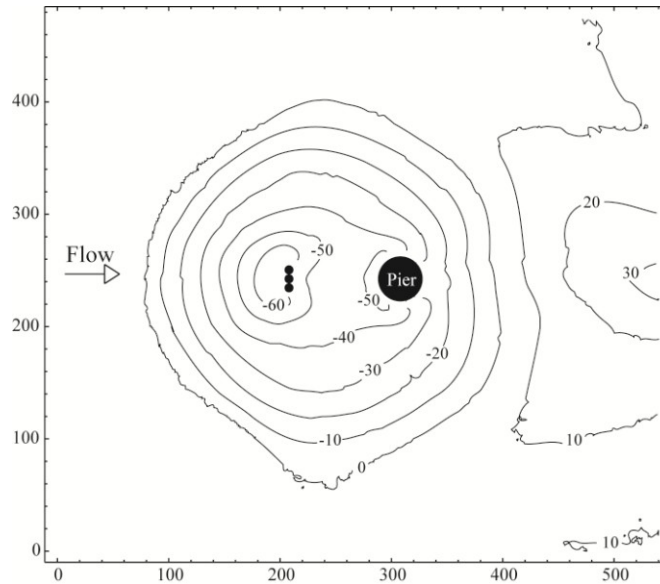


Fig. 82. Contour lines of equilibrium scour hole in test S1 (units: mm)

In test S2, the number of piles increased to 5 in order to increase the blockage ratio ( $N_p=5$ ,  $b_r=1$ ); however, the other parameters of this configuration are the same as in test S1 (Fig. 78b and Tab. 12). In test S2, the strength of the horseshoe vortex and wake vortices around the piles is stronger with respect to the previous test, since the piles have a wider width subjected to the flow. Figure 83a shows the bed materials downstream of the piles scattered by wake vortices. This phenomenon was clearly observed owing to strong wake vortices downstream of the piles, whereas in the previous test S1 this phenomenon was not so apparent.

During the first 5 min of test S2, the rate of accumulation around the pier of bed materials scoured around the piles was higher than the scouring rate in front of the pier, and therefore an increase of bed level in front of the pier was observed. After this period and up to about 30 min ( $Ut/b=11790$ ), the scoured bed material at piles filled in the pier scour hole and the scouring rate around the pier in test S2 was similar to that in test S1 (Fig. 79). After this period, the scouring rate in front of the pier in test S2 was higher than in test S1. This observation indicates that the influence of deeper scour around the piles and the erosion of bed materials between piles and pier overcome the deposition of eroded sediments around the pier.

At the end of the test, a more extensive scour was observed around the pier and the piles with respect to test S1. As Tab. 13 shows, the scour depth, area and volume of this test is much greater than tests S1. The scour volume and scour area are also greater than for the unprotected pier, resulting in a negative efficiency in scour area and scour volume reductions. Figures 83b, 84 and 85 also illustrate such an extensive scour in test S2.

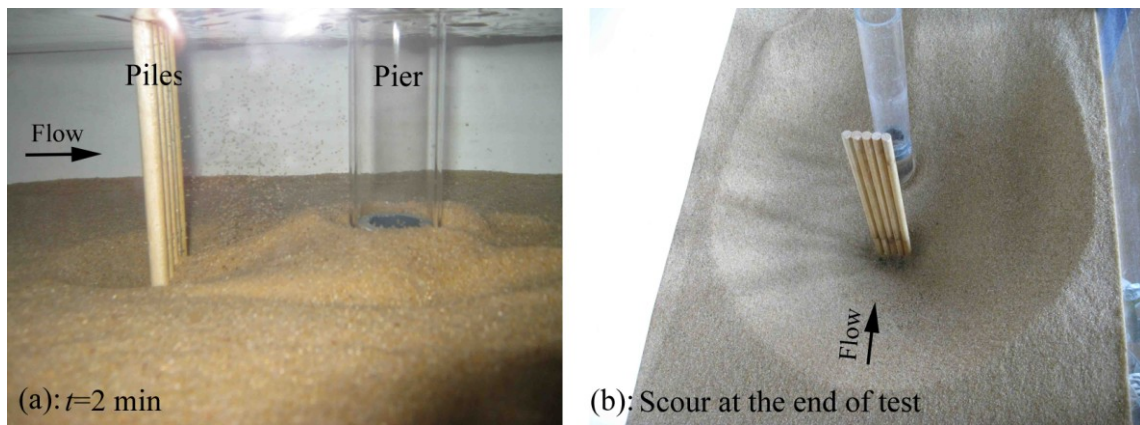


Fig. 83. (a) Scour after 2 min; (b) scour hole at the end of test S2

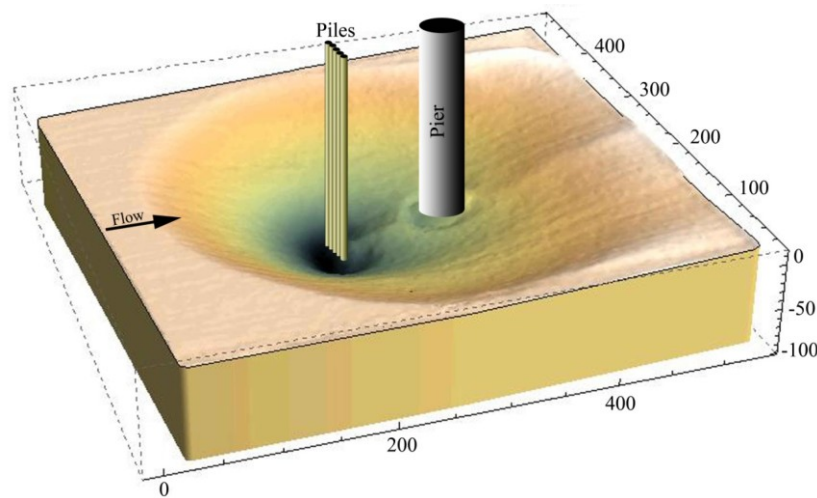


Fig. 84. 3D pattern of equilibrium scour hole in test S2 (units: mm)

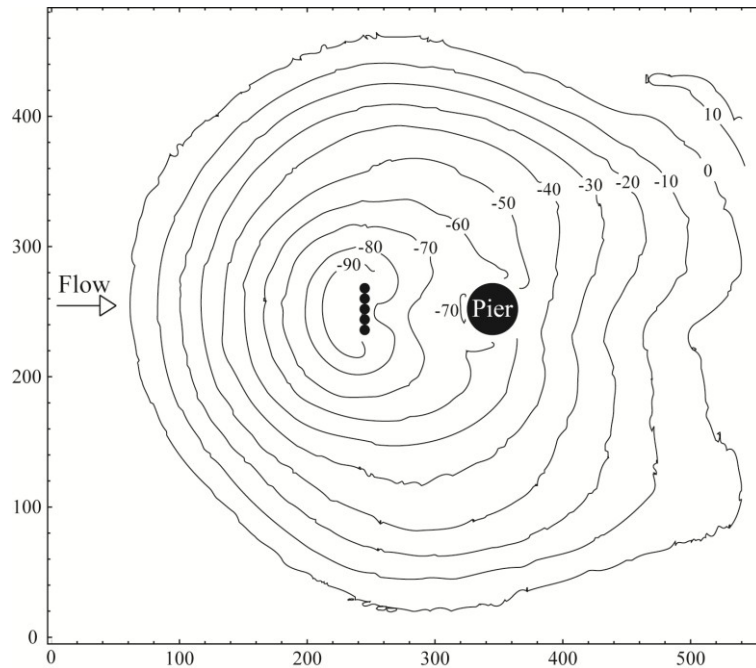


Fig. 85. Contour lines of equilibrium scour hole in test S2 (units: mm)

The maximum scour depth in movable bed in test S2 was observed in front of the piles ( $d_{sem}=9.98$  cm). This value is also greater than the maximum scour depth in front of a circular unprotected pier (test S0); however, the five piles forms a single obstacle subjected to the flow with the same width of the unprotected pier. In fact, the five piles act as a single round-end rectangular pier (having width  $b$  and  $L=b/5$ ) rather than a circular pier.

The influence of the rectangular pier on wake vortices was considered by Ettema *et al.* (1998b). They stated that “as the streamwise length of a pier increases from the condition of a flat plate to that of an elongated rectangular, the wake vortex system is augmented by separation vortices at the leading corners” (p. 759), as shown in Fig. 86. In a private communication that the writer had with the first Author of the paper, he confirmed that this statement is not correct in all conditions. Figure 87, also presented in the same article, clarifies that in general the ratio  $d_{se0}/b$  reduces as the ratio  $L/b$  increases.

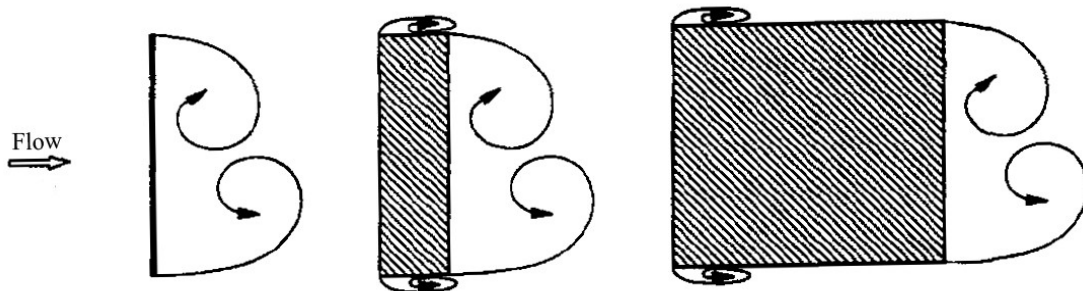


Fig. 86. Plan view of separation vortices for rectangular piers (modified from Ettema *et al.*, 1998b)

Based on studies by Dietz (1972) for a rectangular pier, the scour depth is 1.22 times the scour depth at a circular pier (see Melville and Coleman, 2000, p. 505). According to Fig. 87,  $d_{se0}/b=2.24$  for a rectangular pier with  $L/b=1$ . This value is equivalent to  $d_{se0}/b=1.84$  for a circular pier that is also close to the result of test S0 in the present study. In other words, experimental conditions and results of the present study are compatible with the graph presented in Fig. 87.

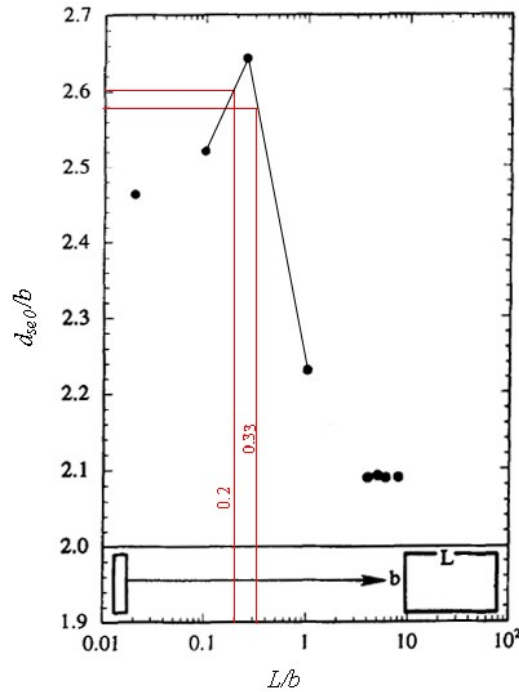


Fig. 87. Dimensionless ratio  $d_{se0}/b$  versus  $L/b$  for rectangular piers (modified from Ettema *et al.*, 1998b)

Although there is a lack of data in this figure for values of  $L/b$  both greater and less than  $1/4$ , for a preliminary estimation of scour depth in front of single obstacles including three and five piles the three data points for  $L/b=0.1, 1$  and  $0.25$  were connected by straight lines in order to interpolate and obtain the following values:  $d_{se0}/b=2.58$  for  $L/b=0.33$  and  $d_{se0}/b=2.6$  for  $L/b=0.2$ . As Table 13 shows, the observed  $d_{sem}$  values were 6.65 cm and 9.98 cm for three and five piles, respectively. These values result in  $d_{sem}/b=2.77$  and  $2.5$  and they are close to the values obtained from Fig. 87 (the differences are less than 7%).

In fact, although by increasing the number of piles in a transverse piles system  $b_r$  increases and more bed materials are scoured from the pile foundation and piled up near the pier, at the same time the scour hole around the piles is deeper, longer and wider, and consequently it extends to the pier location, as verified in test S2.

According to Haque *et al.* (2007), one or two piles have less efficiency in reduction of the scour depth with respect to three piles. A four piles system was also tested by Haque *et al.* (2007), and their result shows that scour depth increases at the pier and consequently lesser efficiency with respect to the three pile system is obtained. Therefore, based on the results of the present study for  $b_r=60\%$  and  $100\%$  and those performed by Haque *et al.* (2007), a three piles

system ( $b_r=0.6$ ) is assumed as the optimum number of piles, for which in the present study the efficiency was 33.4%. This value is actually less than that reported by Haque *et al.* (2007) for a three pile system (Tab. 14). Although the Authors reported a 50% scour depth reduction, their experiments were affected by the side-walls ( $B/b<10$ ).

**Tab. 14. Experimental conditions and best efficiency of transverse sacrificial piles by Haque *et al.* (2007)**

Test	$N_p$	$b_r$	$b_p$	$X_p$	$d_{50}$ (mm)	$t_d$ (h)	$B/b$	$b/d_{50}$	$h/b$	$u*/u_{*c}$	$r_{de}$ (%)
Haque <i>et al.</i> (2007)	3	0.6	$b$	$2b$	0.7	-	7	142.8	2	0.85	50

Furthermore, test S1 was performed with better values of  $h/b$ ,  $b/d_{50}$  and flow intensity. Above all, Haque *et al.* (2007) employed a rectangular pier. In fact, the efficiency of a countermeasure may vary as the pier shape changes. For instance, Zarrati *et al.* (2004) showed that a collar is more effective with rectangular piers rather than with circular ones.

### 5.2.3. Collar

As indicated in §3.3.2, collar width  $w_c$ , with respect to pier width,  $w_c/b$ , and the distance of the collar below water surface  $h_c$ , with the respect to the flow depth,  $h_c/h$ , affect the efficiency of a collar in scour depth reduction. Furthermore, collar thickness,  $t_c$ , is another parameter whose influence on scouring is still unknown.

In this study, a  $3b$ -wide, 5 mm-thick transparent Perspex<sup>®</sup> collar ( $w_c/b=3$ ) flush with the bed ( $h_c/h=1$ ) was selected in order to obtain maximum possible efficiency for a practical collar size. In fact, although wider collars result in higher efficiencies, collars with  $w_c>3b$  seems to be impracticable (Zarrati *et al.*, 2006). In addition to the higher efficiency of  $3b$ -wide collars with respect to smaller sized ones, Mashahir *et al.* (2004) showed that a  $3b$ -wide collar also has a better influence on the reduction of the scouring rate with respect to a  $2b$ -wide collar (Fig. 88). Table 15 shows the geometric parameters of this countermeasure for test S3.

Configuration and scour around the pier protected with a collar (test S3) before and during the test are shown in Figs. 89 and 90. Two grooves, which are the results of wake vortices, were developed at the downstream part of the collar during about the first 50 min after starting the test (see Figs. 89 and 90b,c,d). After this period, two grooves extended in about 10 min to the upstream part of the collar, around the rim of the collar, and reached point A in Fig. 89. Then, the scour penetrated beneath the collar and after about 5 h the scour reached the upstream face of the pier (point B in Fig. 89). In test S3 the temporal evolution of the scour depth in front of the pier was monitored (Fig. 91). At the end of test, maximum scour depth in movable bed was found in front of the pier (see Figs. 90g,h, 92 and 93). In this test, the efficiency in scour depth reduction about 29% was obtained using this countermeasure.

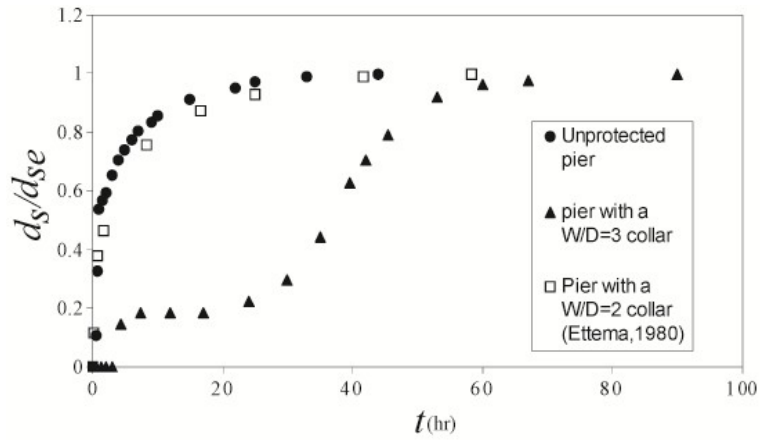


Fig. 88. Comparison of temporal evolution of scour depth at piers protected with  $2b$  and  $3b$  collars flush with the initial bed level (modified from Mashahir *et al.* 2004)

Tab. 15. Geometric parameters of countermeasure of test S3

$w_c$	$h_c$	$t_c$
$3b$	$h$	$b/8$

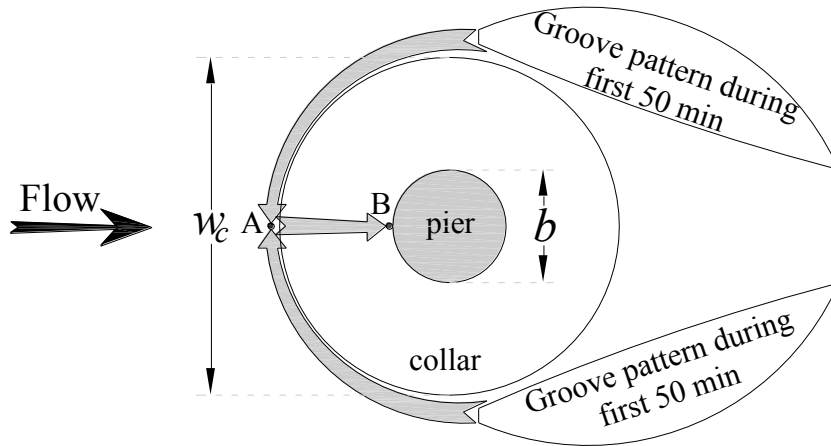


Fig. 89. Schematic pattern of scour development around a collar ( $w_c=3b$ )

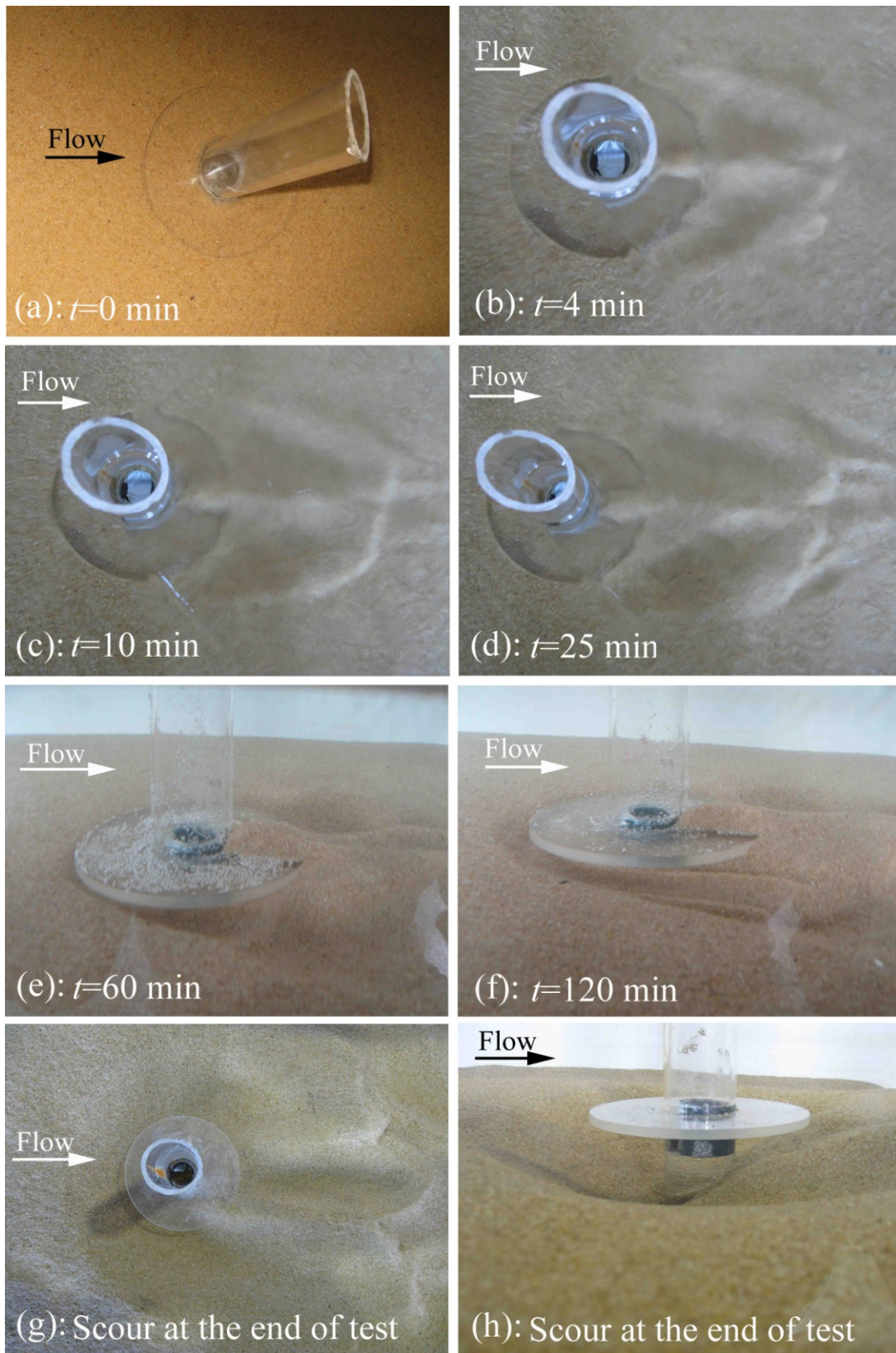


Fig. 90. Scour evolution around pier protected with collar (test S3)



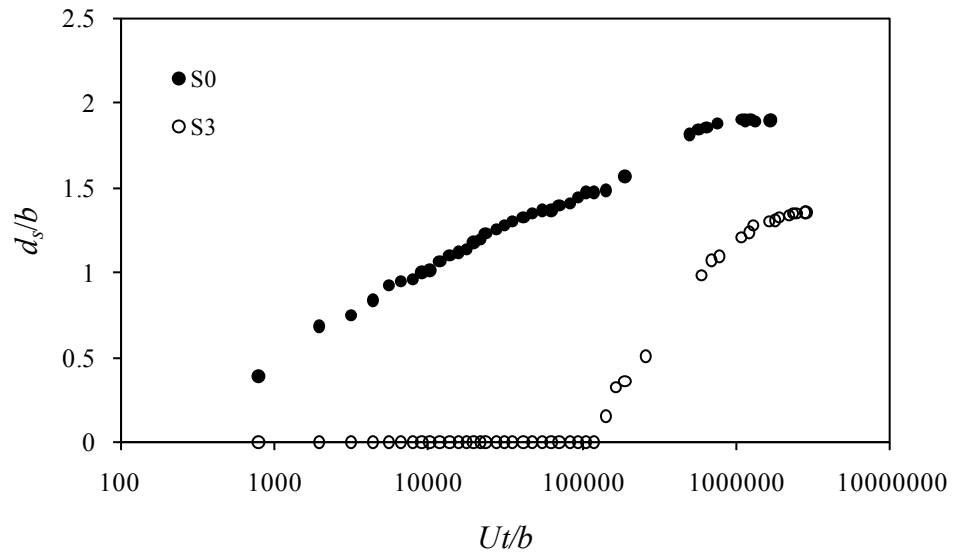


Fig. 91. Temporal evolution of scour depth in front of the pier in tests S0 and S3

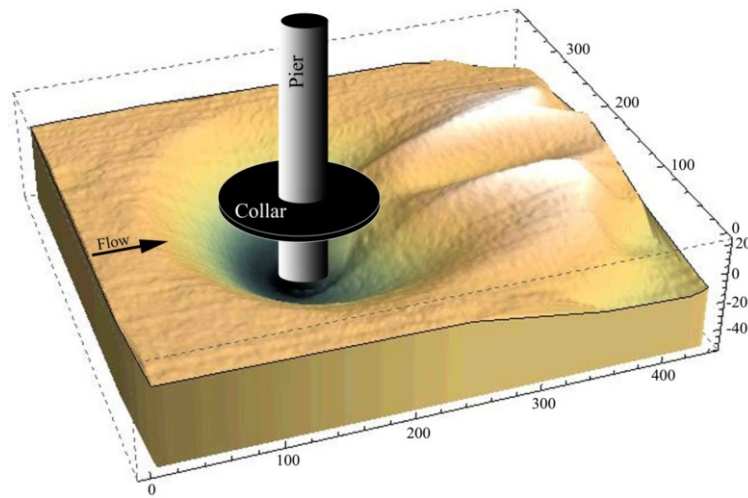


Fig. 92. 3D pattern of equilibrium scour hole in test S3 (units: mm)

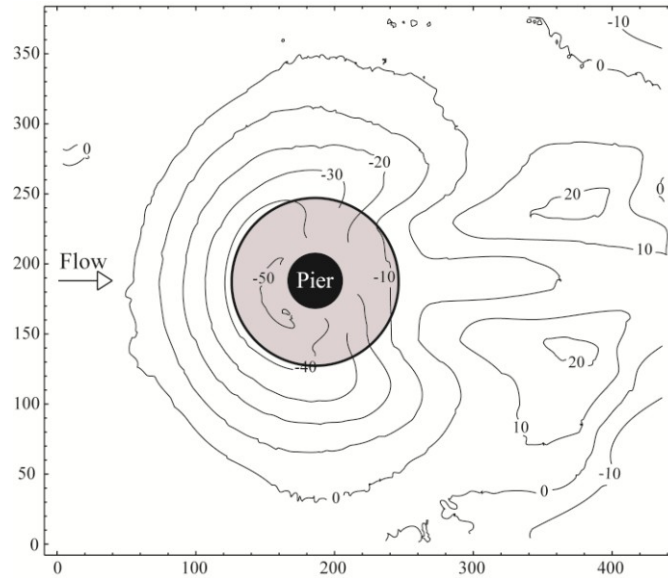


Fig. 93. Contour lines of equilibrium scour hole in test S3 (units: mm)

According to Mashahir *et al.* (2004), those two grooves (Figs. 89b and 90) at the rear of the collar are formed under the action of wake vortices. In fact, the action of the horseshoe vortex upstream to the pier seems to be blocked, since during development of the two grooves no sign of scour upstream to the pier was observed. The reason is probably due to the size of the primary horseshoe vortex in front of the pier. In this case, Kothyari *et al.* (1992) proposed the following equation to estimate the diameter of the primary vortex,  $D_v$ :

$$\frac{D_v}{h} = 0.28 \left( \frac{b}{h} \right)^{0.85} \quad (\text{E.18})$$

Based on equation (E.18), the diameter of the primary vortex for this study is about 1.3 cm, which is less than the collar extension in front of the pier, equal to 4 cm.

Another study on horseshoe vortex characteristic was performed by Muzzammil and Gangadhariah (2003). In their study, the vortex size,  $D_v$ , is assumed to be the average of the maximum and minimum axes of an elliptically-shaped vortex (Fig. 94).

Muzzammil and Gangadhariah (2003) prepared Fig. 95 using their data along with data taken from literature. They gave an explanation about the scattered data: specially, data by Garde (1989) belong to the case of  $h/b \leq 1$ , where the size of the horseshoe vortex may be affected by the interference of the bow wave developed on the water surface ahead of the pier with the horseshoe vortex.

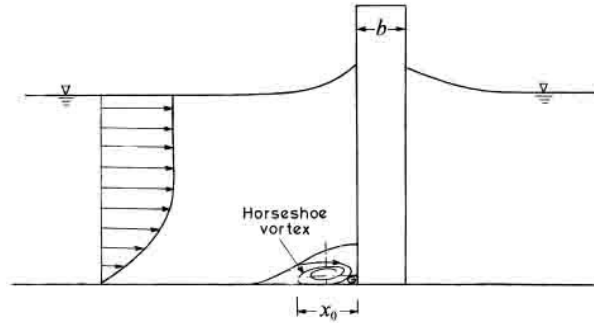


Fig. 94. Sketch of horseshoe vortex on a rigid flat bed (modified from Muzzammil and Gangadhariah, 2003)

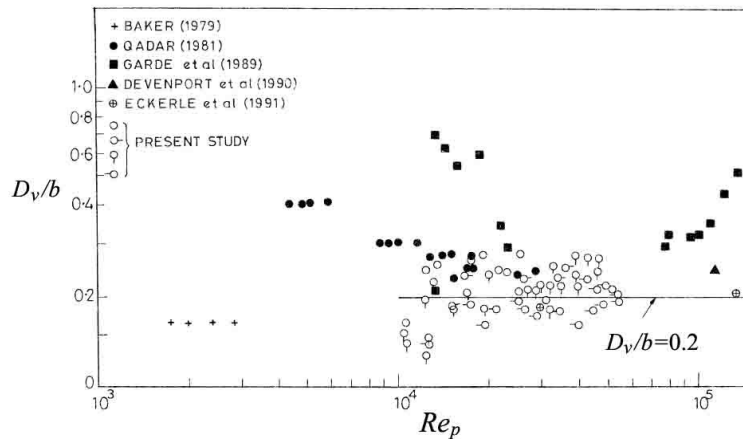


Fig. 95. Vortex size on a rigid bed (modified from Muzzammil and Gangadhariah, 2003)

Muzzammil and Gangadhariah (2003) proposed the average value  $D_v/b \approx 0.2$  for  $Re_p \geq 10000$  and the horizontal dimension of the vortex,  $x_0$ , was found to be approximately equal to  $2D_v$ . In this case, if in Fig. 95 Garde's (1989) data is neglected, based on available data  $D_v/b$  reaches a maximum of 0.4. In other words,  $x_0$  may reach a value of  $0.8b$ . Although this value is less than  $b$ , which is the protrusion of a  $3b$ -wide collar around the pier, it is greater than  $0.5b$ , which is the protrusion of a  $2b$ -wide collar around the pier. In fact, a  $2b$ -wide collar is not safe in its upstream part, owing to the action of the primary horseshoe vortex, whereas a  $3b$ -wide collar can be protected by it.

Therefore, there is a doubt over the performance of collars for low values of  $h/b$ , when the bow wave interacts on the primary vortex, since experimental data by Garde (1989) in Fig. 95 indicates that  $D_v$  may be greater than  $0.5b$  and consequently  $x_0 > b$ . For this condition, more study is required to consider the performance of the collars.

In contrast, Unger and Hager (2007) believed that the primary vortex (initial vortex) is a non-scouring vortex (see Fig. 6), since the scour always starts at an angle of about  $75^\circ$  from the channel axis. They also considered that the  $D_v/b$  may not be a constant and it may have a decreasing trend as  $Re_p$  increases (Unger and Hager, 2005). In addition, according to Ettema

(1980) the initial phase is characterised by the fast scour rate produced by the downflow at the pier face and the horseshoe vortex acts later in the principal phase of scouring.

Anyway, in the case that the primary vortex system, which may also be included in more than one vortex as shown in Fig.4, is a non-scouring system, the result of test S3 shows that a  $3b$ -wide collar is adequate to prevent the upstream part of the collar from scouring.

Note that, in addition to the test for low  $h/b$  values, tests in higher flow intensities are also recommended to consider the performance of collars. In particular, in live-bed conditions the performance of collars is not clear.

Tables 16 and 17 show the results of the present test and some of those available in the literature.

**Tab. 16. Results of test S3**

$t_d$ (h)	$Ut_d/b$	$d_{se}$ (cm)	$d_{se}/b$	$A_e$ (cm <sup>2</sup> )	$V_e$ (cm <sup>3</sup> )	$r_{de}$ (%)	$r_{Ae}$ (%)	$r_{Ve}$ (%)
120	$2.83 \cdot 10^6$	5.43	1.36	581.8	937.4	28.7	44.6	66.6

**Tab. 17. Experimental conditions and results in application of a  $3b$ -wide collar at the bed level**

Test	$d_{50}$ (mm)	$t_d$ (h)	$Ut_d/b$	$B/b$	$b/d_{50}$	$h/b$	$U/U_c$ or $u^*/u^*_c$	$r_{ds}$ or $r_{de}$ (%)
Tanaka and Yano (1967)	-	-	-	10	-	3.33	-	22
Mashahir <i>et al.</i> (2004)	0.95	90	$2.34 \cdot 10^6$	18.75	42.1	3	0.92	26.6
Alabi (2006)	0.53	955	$5.83 \cdot 10^6$	10.6	217	2	0.7	58
Moncada-M <i>et al.</i> (2009)	1.4	about 6	-	6.85	52.14	2.61	-	100
Defanti <i>et al.</i> (2010)	0.8	24	$0.9 \cdot 10^6$	16.67	37.5	7.2	0.92	about 20

Table 17 shows that a wide range of efficiencies are available for a collar with  $w_c/b=3$  and  $h_c/h=1$ . Although Tanaka and Yano (1967) found the efficiency almost near that of the present study, experimental conditions of their experiments are not clear. Mashahir *et al.* (2004) performed the experiment in proper conditions and obtained 26.6% scour depth reduction. As mentioned before, they also found a proper result for unprotected pier test and could find equilibrium conditions with  $d_{se0}/b=2.3$ . A long test (about 40 days) was performed by Alabi (2006). At the end of this test, the Author found that the scour did not reach the pier body; however, this test was performed under relatively low flow intensity ( $u^*/u^*_c=0.7$ ). The Author also reported observation of ripples due to the use of small sediment sizes. The results of the present study and the test by Mashahir *et al.* (2004) clarify that since a collar slows down the scour rate, tests with collars should be much longer than with an unprotected pier in order to achieve the equilibrium condition. Table 17 shows that in test S3 the ratio  $Ut_d/b$  is about  $2.83 \cdot 10^6$  and is much more than for an unprotected pier ( $Ut_d/b=1.7 \cdot 10^6$ ). In this case, the results of Moncada-M *et al.* (2009) are based on non-equilibrium conditions after a few hours. The influence of a low  $B/b$  ratio is also significantly found in tests by Moncada-M *et al.* (2009). Results of Defanti *et al.* (2010), although are based on non-equilibrium conditions, clarify the

importance of the flow intensity value in collar tests. The Authors performed tests with flow intensity ranging from 0.69 to 0.92. Their results show that, as the flow intensity increases, the risk of scour intrusion to the upstream part of the collar increases and the scour reaches the upstream face of the pier in a shorter period. The Authors found that for flow intensities of 0.69 and 0.77 the scour did not reach the upstream part of the collar and occurred only at the downstream part. This findings confirm that the test with collar by Alabi (2006) is not proper to evaluate a collar efficiency. All the above experiments clarify that tests with a collar should be performed in appropriate conditions in order to obtain reliable results.

As indicated in §3.3.2, a formula was proposed by Kumar *et al.* (1999) to estimate the performance of a collar (E.11). For a collar with  $w_c/b=3$  and  $h_c/h=1$ , (E.11) furnishes an efficiency equal to 33%, which is near to the result of the present study.

#### 5.2.4. Threading

Test S4 with threading was carried out on the basis of the optimum configuration suggested in the only available study by Dey *et al.* (2006). The optimum configuration consists of a triple threading with a thread angle  $\alpha_t=15^\circ$  and  $d_c/b=0.1$  (Fig. 27). Configurations before starting the test and at the end of it are presented in Fig. 96a,b. Figure 97 shows the temporal evolution of the scour depth in front of the pier protected with a triple threading and in front of an unprotected pier. Figures 98 and 99 show 3D pattern and contour lines of scour around the pier protected with triple threading. The results and experimental conditions of test S4 and the best configuration of Dey *et al.* (2006) are presented in Tabs. 18 and 19.

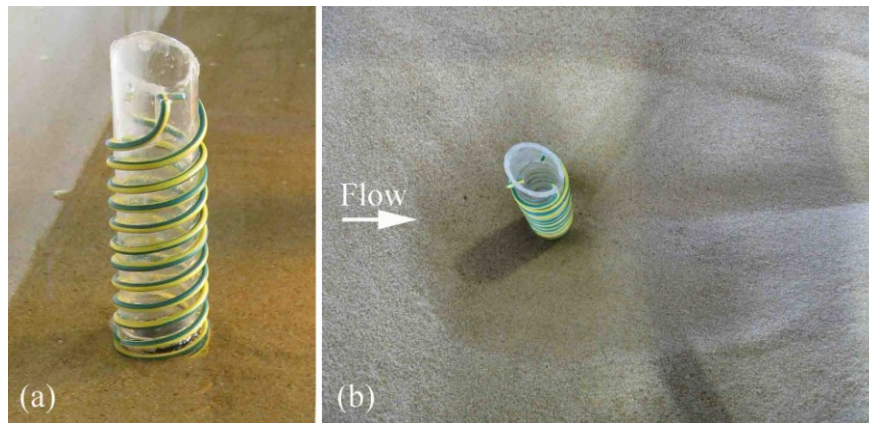


**Fig. 96. (a) A pier protected with threading; (b) scour hole at the end of test S4**

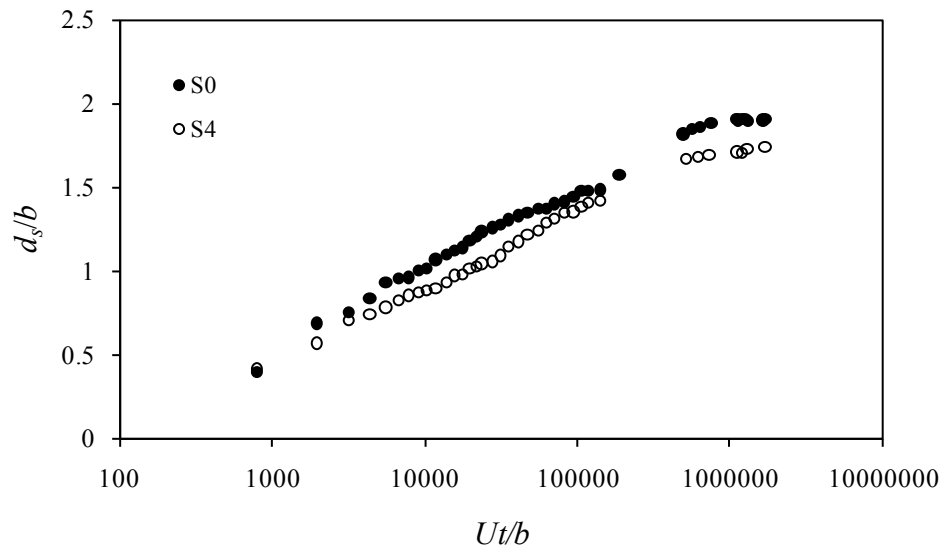


Fig. 97. Temporal evolution of scour depth in front of the pier in tests S0 and S4

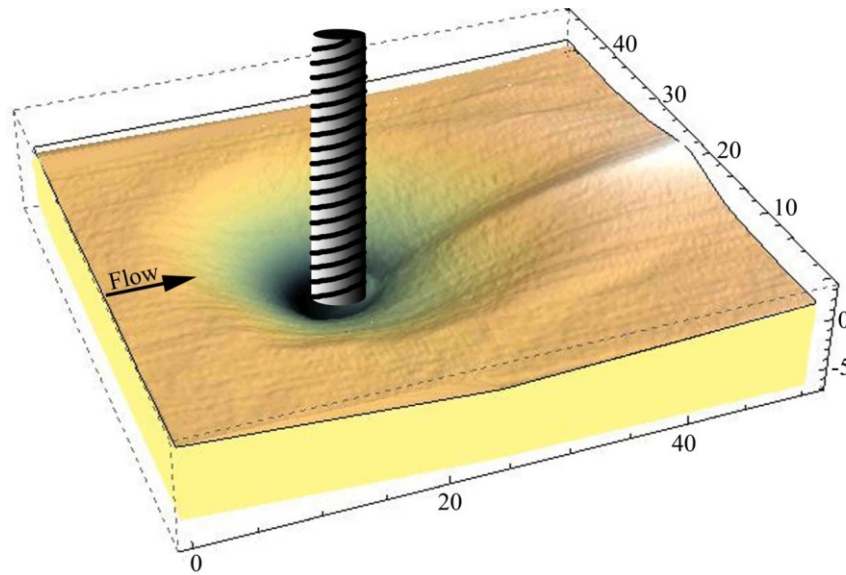


Fig. 98. 3D pattern of equilibrium scour hole in test S4 (units: mm)

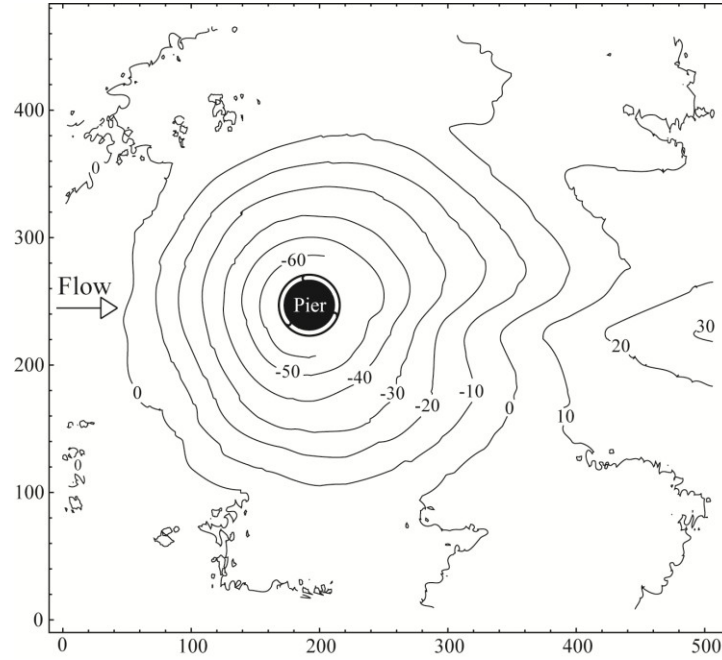


Fig. 99. Contour lines of equilibrium scour hole in test S4 (units: mm)

Tab. 18. Configuration and results of test S4

Threading type	$\alpha_t$ (°)	$d_c/b$	$t_d$ (h)	$Ut_d/b$	$d_{se}$ (cm)	$d_{se}/b$	$r_{de}$ (%)
Triple	15	0.1	72	$1.7 \cdot 10^6$	6.96	1.74	8.7

Tab. 19. Experimental conditions and results of optimum configuration of threading by Dey *et al.* (2006)

Threading type	$\alpha_t$ (°)	$d_c/b$	$d_{50}$ (mm)	$t_d$ (h)	$Ut_d/b$	$B/b$	$b/d_{50}$	$h/b$	$U/U_c$	$d_{se0}/b$	$r_{ds}$ (%)
Triple	15	0.1	0.26	48	$0.23 \cdot 10^6$	4.5	769	1.5	0.9	0.475	46.3

The comparison of results of test S4 with those obtained by Dey *et al.* (2006) in the same configuration puts in evidence a notable difference between the efficiencies. Table 19 shows that, although the experiments by Dey *et al.* (2006) were performed with a flow intensity slightly less than 1 ( $U/U_c=0.9$ ), i.e. under the threshold condition of sediment movement, the ratio  $d_{se0}/b$  for the unprotected pier is small ( $d_{se0}/b=0.475$ ); therefore, the experiments were not performed in proper conditions. Another problem is the sediment size, which is significantly less than 0.7 mm, with possible ripple formation (see §2.5). Further, the ratio  $b/d_{50}=769$  is greater than 50. As indicated in §2.5, on the basis of recent studies values of  $b/d_{50}$  greater than about 50 lead to reduction in scour depth. In particular, when this ratio is greater than about 130, its influence may not be neglected. In addition, the ratio  $B/b=4.5$  is much less than the value of 10, and consequently side walls affect on the scour depth. The ratio  $Ut_d/b$  is also relatively low and probably the equilibrium condition was not achieved for this test. Note that although the ratio  $h/b=1.5$  is less than 2.5, the influence of flow depth on scour depth is probably negligible, since

the ratio of  $b/d_{50}=769$  is relatively high. In this case, Fig.100 shows that for the experimental conditions of Dey *et al.* (2006)  $K_h$  is greater than 0.9.

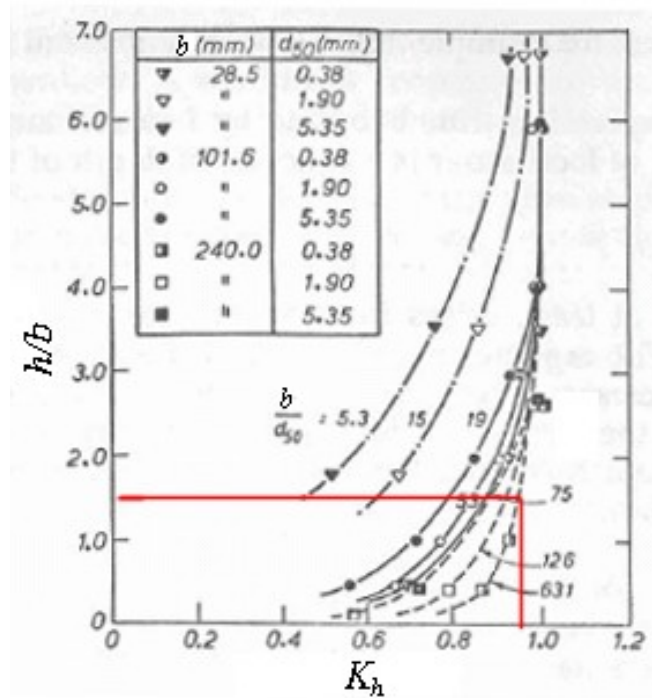


Fig. 100. Flow depth adjustment factor (modified from Raudkivi and Ettema, 1983)

### 5.2.5. Pier slot

As indicated in Chapter 5, according to Grimaldi *et al.* (2009b) the optimum condition for a slot with  $l_s=h$  is obtained when  $z_s=h/3$  or  $h/6$  or  $h/2$ , and it is not clear which configuration can be proposed as the best one. In this study, these three configurations are compared with a pier slot extended from water surface to the minimum bed elevation (corresponding to the maximum scour depth). The result of each configuration in scour depth reduction is presented in Tab. 20, which clarifies that the scour efficiency of a slot partially sunk in the bed varies from 24.7% to 35% in configurations of tests S5 to S7. In these experiments the maximum scour depths in front of the pier were monitored (Fig.101). Figure 102 shows that the rate of scour depth increasing in the present study is almost in the same range as those of Grimaldi's (2005, 2009b) tests. When the slot covers total approach flow and scour depth, as in test S8, maximum efficiency is obtained. However, test S5 shows that for a shorter slot length ( $l_s$  in test S5 is about 2/3 of  $l_s$  in test S8), the efficiency reduces down to about 2%. Figures 103 to 111 show 3D scour pattern and contour lines of equilibrium scour hole at the end of each test. As these Figures show the general scour shape of a pier protected with a slot is similar to an unprotected pier.



**Tab. 20. Results of experiments with slot (tests S5 to S8)**

Test	$z_s$	$w_s$	$l_s$	$t_d$ (h)	$Ut_d/b$	$d_{se}$ (cm)	$d_{se}/b$	$r_{de}$ (%)
S5	$h/2$	$b/4$	$h$	72	$1.7 \cdot 10^6$	5.09	1.27	33.2
S6	$h/3$	$b/4$	$h$	72	$1.7 \cdot 10^6$	5.37	1.34	29.5
S7	$h/6$	$b/4$	$h$	73	$1.72 \cdot 10^6$	5.74	1.44	24.7
S8	$d_{se}$	$b/4$	$h+d_{se}$	72	$1.7 \cdot 10^6$	4.95	1.24	35.0

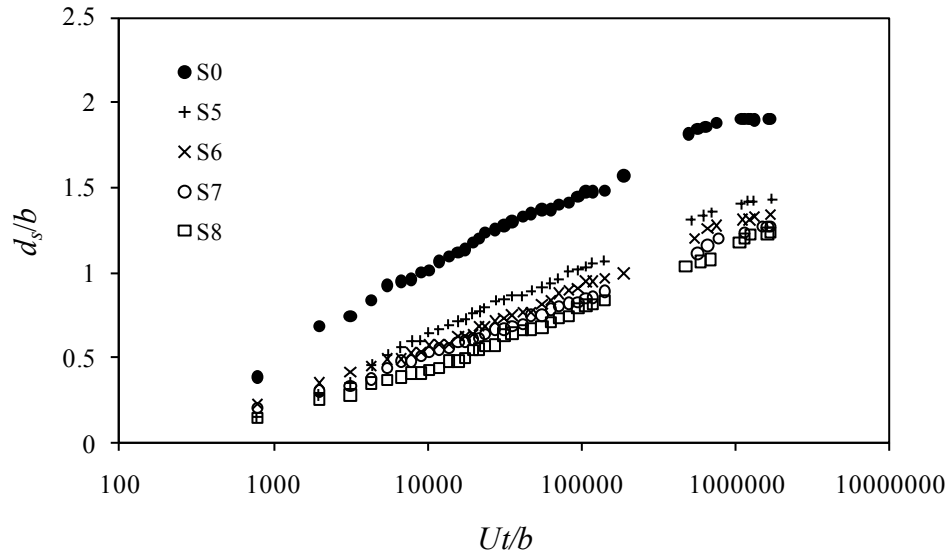


**Fig. 101. Temporal evolution of scour depth in front of the pier in tests S0 and S5 to S8**

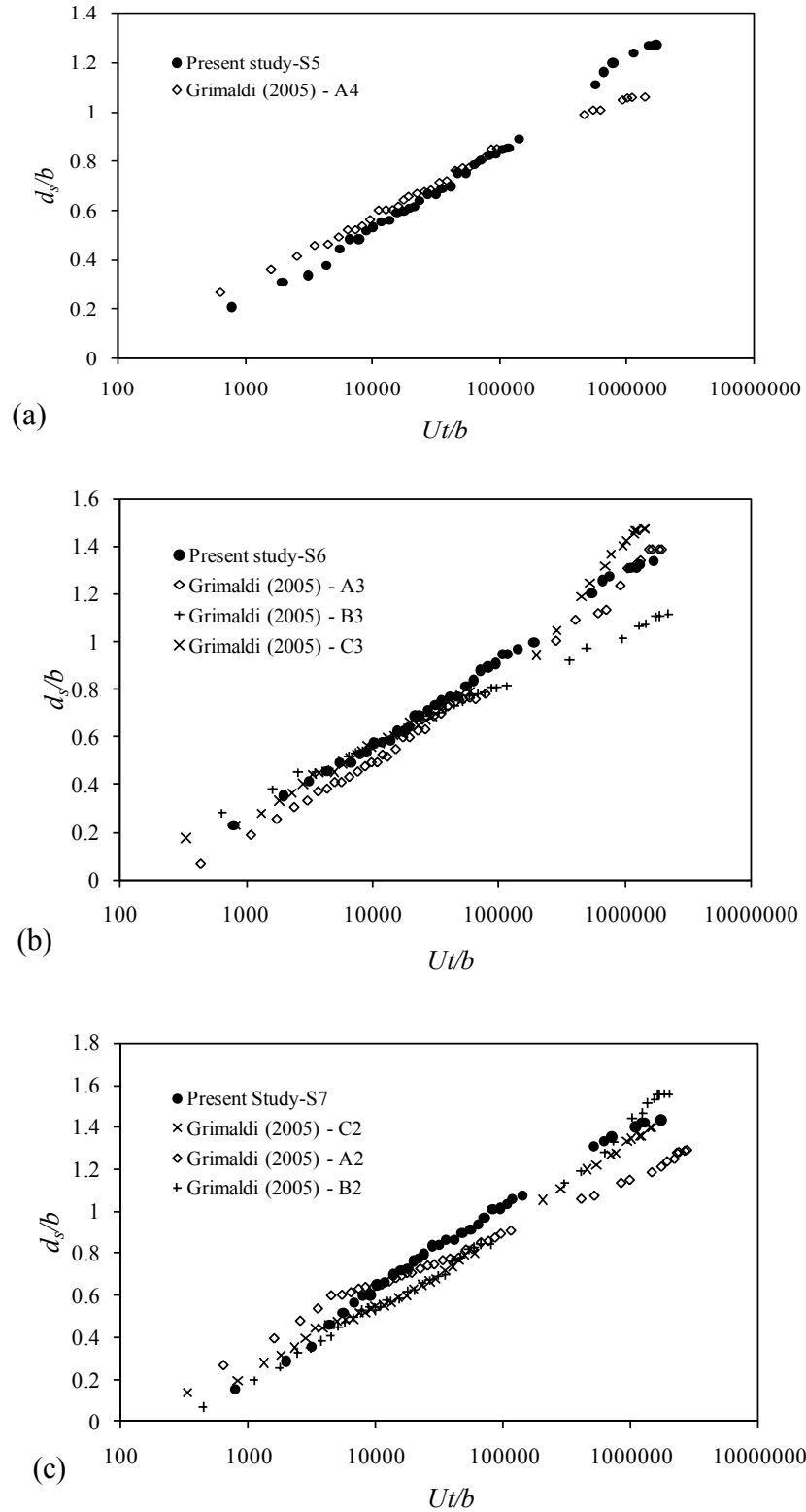


Fig. 102. Comparison of scour depth evolution in present study with Grimaldi's (2005) data in pier slot tests

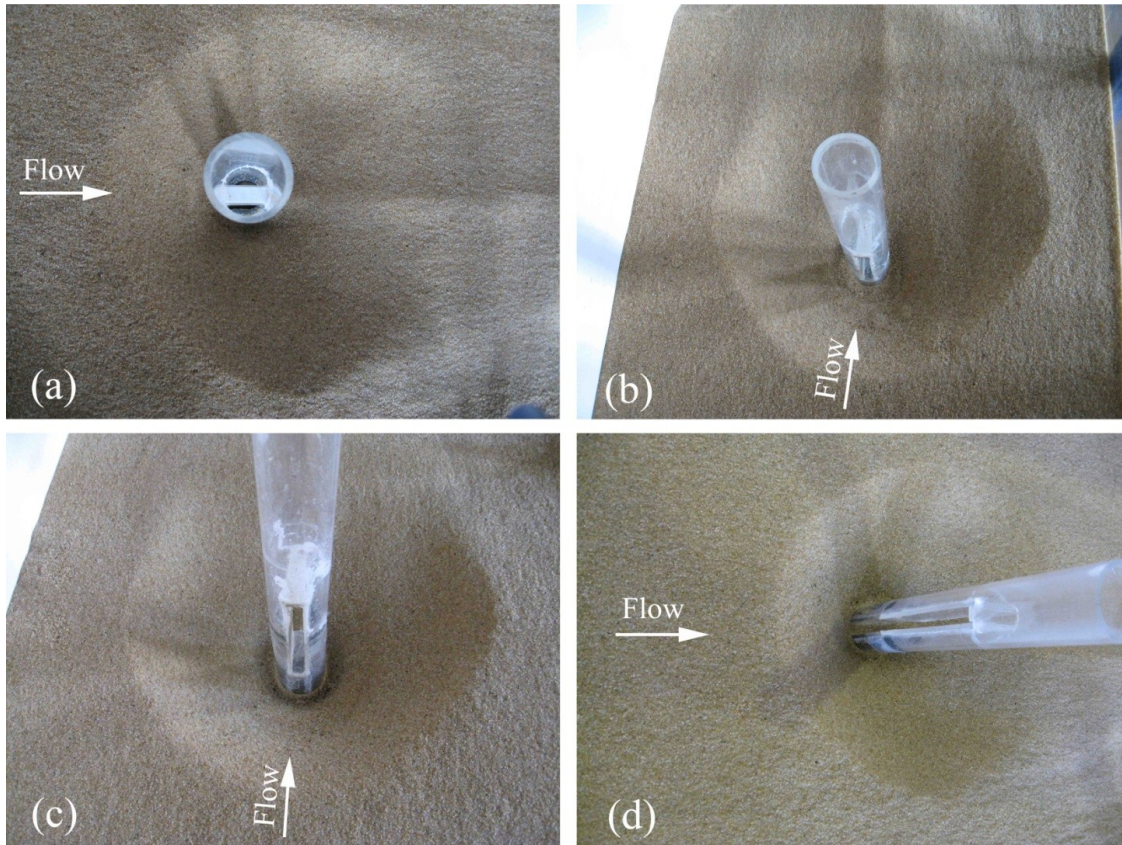


Fig. 103. Scour hole at the end of tests (a) S5; (b) S6; (c) S7; (d) S8

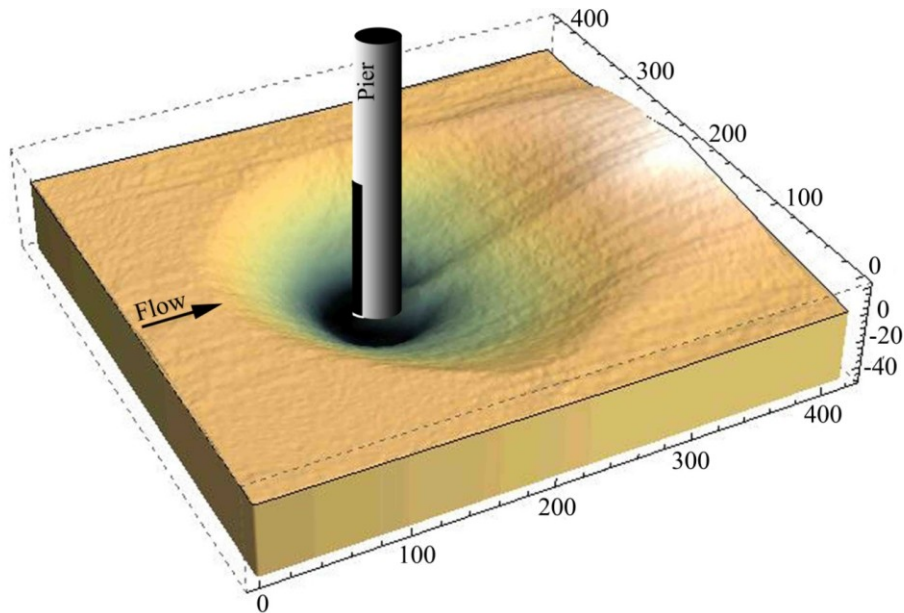


Fig. 104. 3D pattern of equilibrium scour hole in test S5 (units: mm)

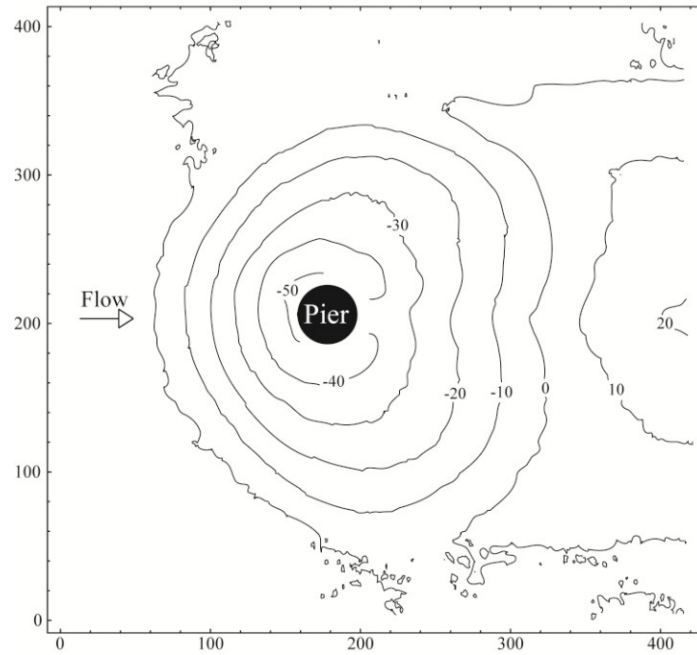


Fig. 105. Contour lines of equilibrium scour hole in test S5 (units: mm)

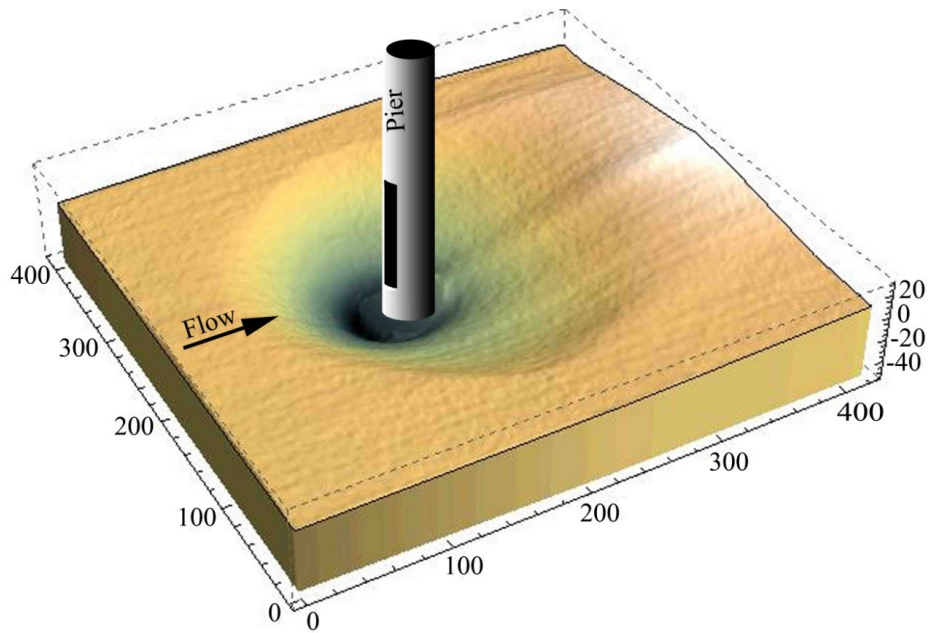


Fig. 106. 3D pattern of equilibrium scour hole in test S6 (units: mm)

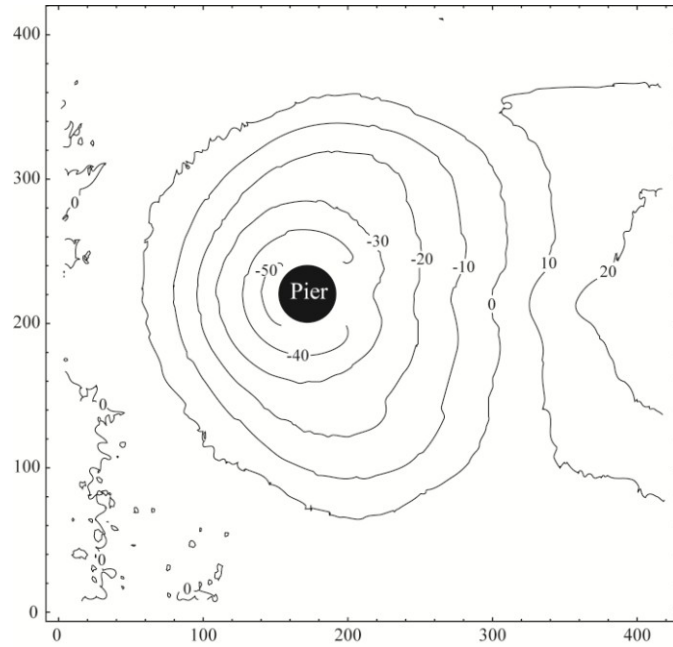


Fig. 107. Contour lines of equilibrium scour hole in test S6 (units: mm)

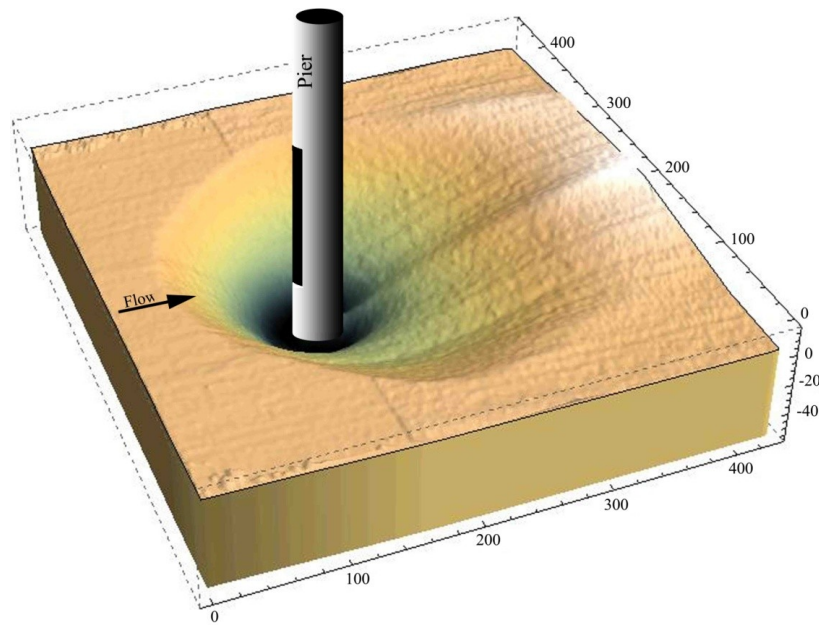


Fig. 108. 3D scour pattern around the pier in test S7 (units: mm)

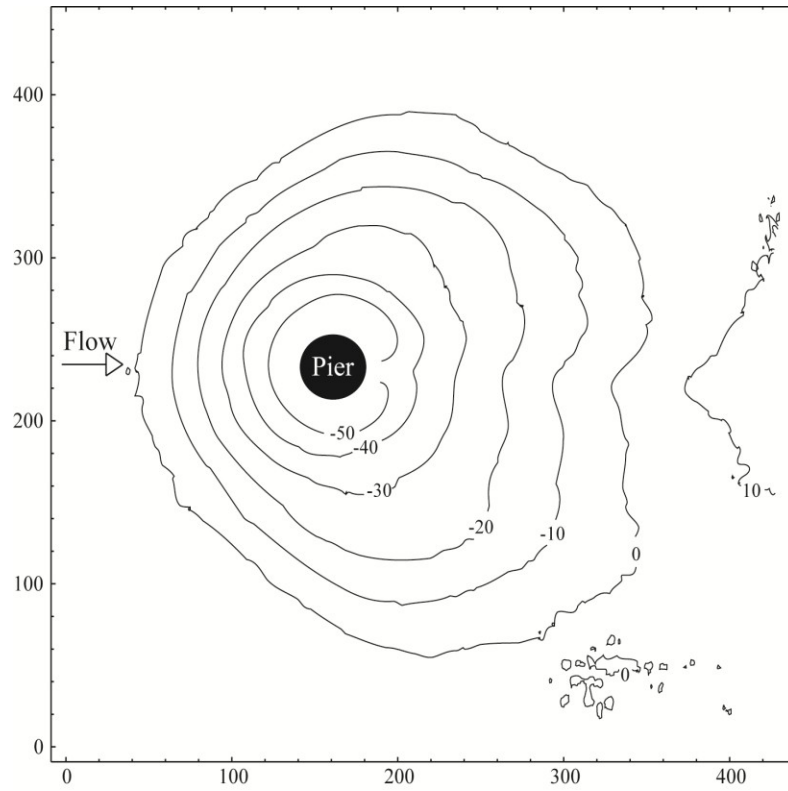


Fig. 109. Contour lines of equilibrium scour hole in test S7 (units: mm)

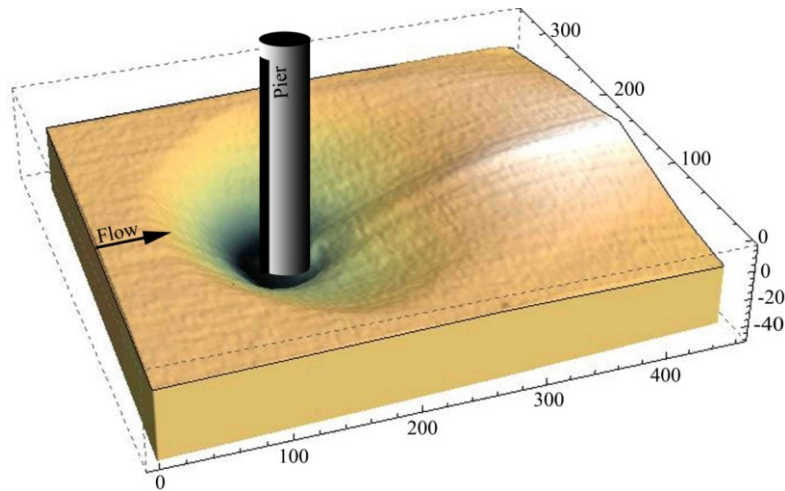


Fig. 110. 3D scour pattern in test S8 (units: mm)

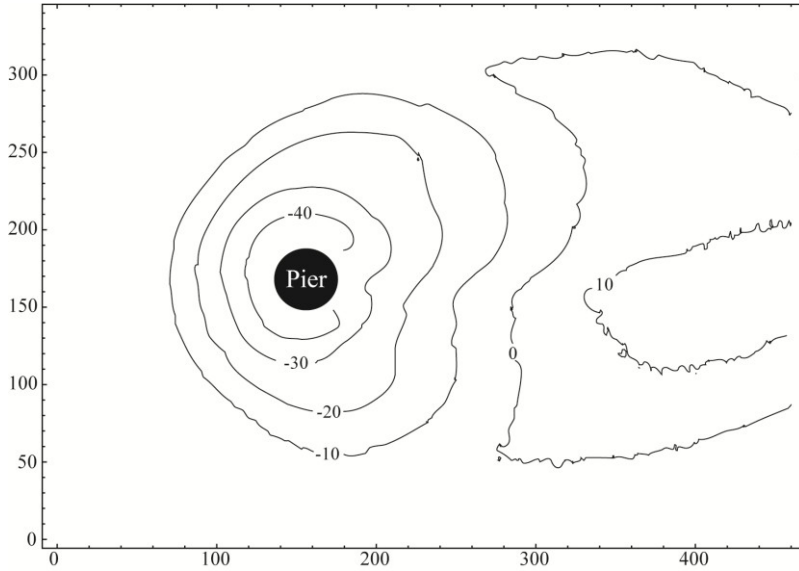


Fig. 111. Contour lines of equilibrium scour hole test S8 (units: mm)

Table 21 shows results of the tests performed by Grimaldi (2009b). In order to compare scour depths and efficiencies of this study with Grimaldi’s data, Fig. 112, according to result of present study, and Figs. 113 to 115 were prepared based on the results of Grimaldi’s (2005) experiments.

Tab. 21. Experimental conditions and results of tests with slot ( $l_s=h$ ) by Grimaldi *et al.* (2009b)

Test	$b$ (mm)	$h$ (cm)	$z_s$ (cm)	$z_s/h$	$d_{se}$ (mm)	$r_{de}$ (%)
A1	75	15	0	0	109.4	9.9
A2	75	15	2.5	1/6	96.9	20.2
A3	75	15	5	1/3	83.8	31.0
A4	75	15	7.5	1/2	79.5	34.5
A5	75	15	10	2/3	87.5	27.9
A6	75	15	15	1	84.7	30.2
B1	90	25	0	0	144.7	19.2
B2	90	25	4.17	1/6	140.2	21.7
B3	90	25	8.33	1/3	125.2	30.1
B4	90	25	25	1	133.1	25.6
C1	120	25	0	0	185.5	17.4
C2	120	25	4.17	1/6	167.9	25.2
C3	120	25	8.33	1/3	177.1	21.1
C4	120	25	25	1	170.6	24.0

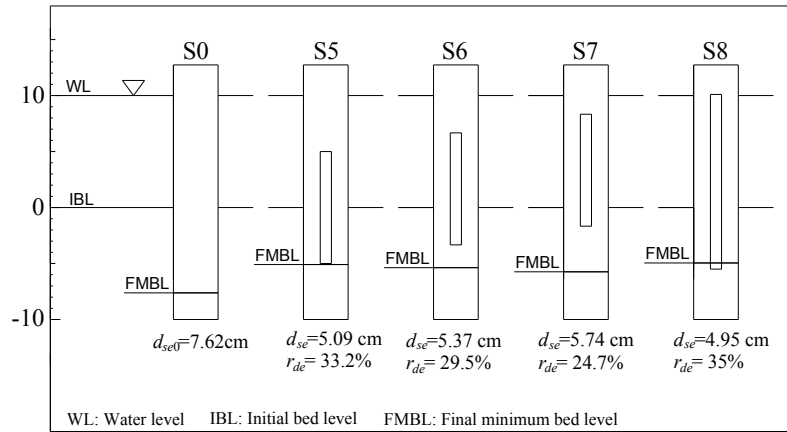


Fig. 112. Configuration of tests S5 to S8 (units: mm)

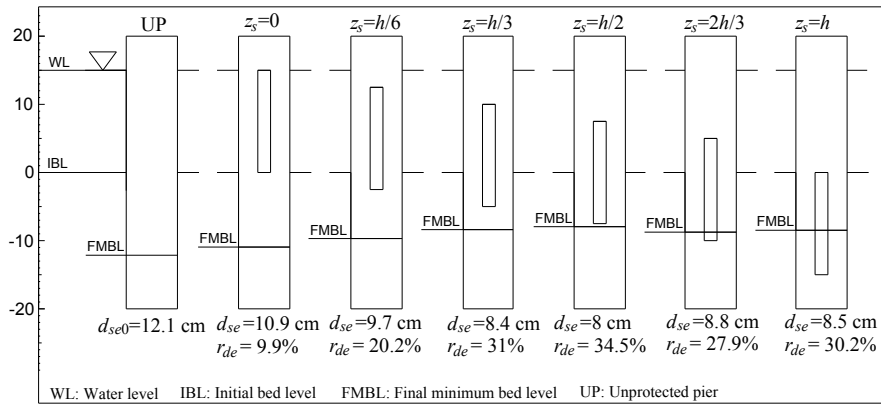


Fig. 113. Configuration of test series A by Grimaldi *et al.* (2009b) (units: mm)

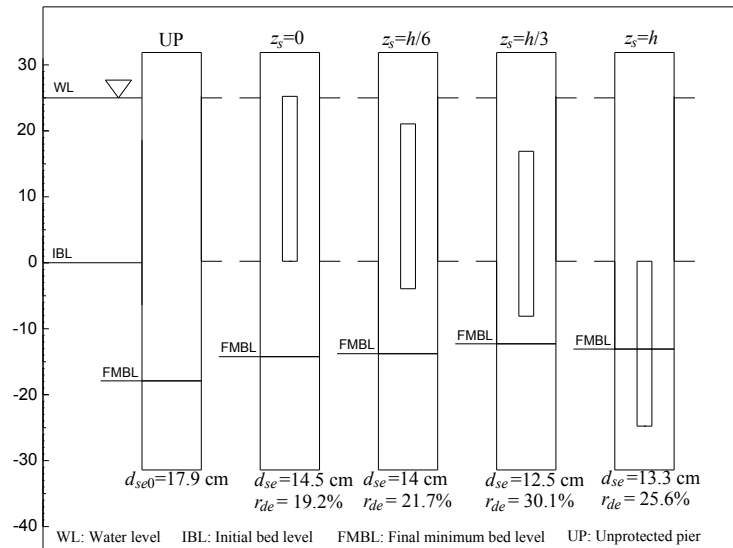


Fig. 114. Configuration of test series B by Grimaldi *et al.* (2009b) (units: mm)



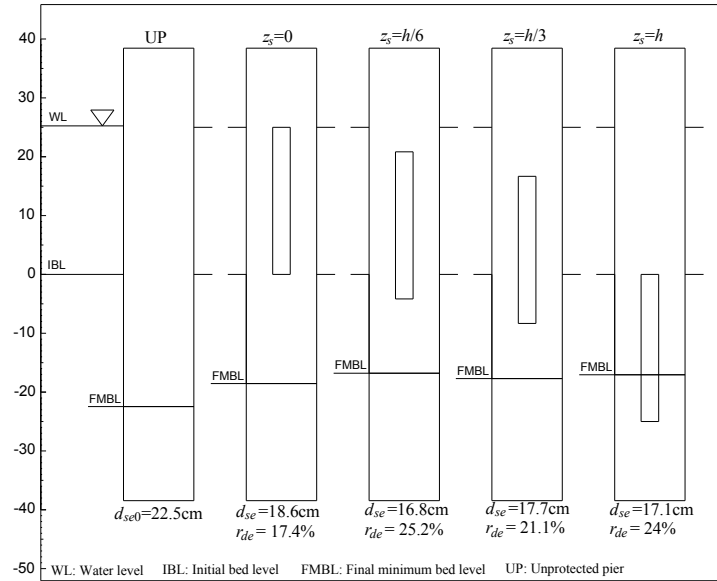


Fig. 115. Configuration of test series C by Grimaldi *et al.* (2009b) (units: mm)

The results show that when a slot extends from bed level to maximum scour depth ( $z_s=h$ ,  $l_s=h$ ) is much more effective with respect to the condition when the slot extends from bed level to water surface ( $z_s=0$ ,  $l_s=h$ ); however, in the former case, the effective slot length (equal to  $d_{se}$ ) is smaller. Figures 113 to 115 show that the efficiency of a slot drilled only under the initial bed level is just a few percent less than that in the best configuration proposed by Grimaldi; however, effective slot length in the former case is significantly lower. Figure 116 was prepared based on results of the present study and by Grimaldi *et al.* (2009b).

Figure 116 shows the efficiency of a slot in scour depth reduction versus  $(d_{se}-z_s)/b$ . In all these data the slot length is as long as the approach flow depth,  $l_s=h$ . As this figure shows, by extending the slot to the total scour depth the efficiency increases. These comparisons clarify the importance of drilling the total length of the pier located under the bed level (inside the scour). In fact, there is a problem in proposing the best configuration as defined by Grimaldi *et al.* (2009b), since the slot length  $l_s$  is defined only based on the approach flow depth. For a certain approach flow condition (e.g., flow depth, flow intensity, etc.), the slot length and location ( $l_s$  and  $z_s$ ) are the same for two piers of different width; however, deeper scour is expected for a wider pier. In particular, deeper scour at a pier with a slot partially sunk into the bed results in a greater portion of not drilled pier exposed to the flow; as mentioned before, this part is an important part and generally the efficiency of a slot increases as the slot extends further under the initial bed level and covers the full pier part inside the scour. Although scatter points in Fig. 116 clarify that such statement is not always correct, the negative slope of the best-fit line in this figure indicates that a better efficiency is generally expected when the slot portion which is sunk into the bed is greater than the final scour depth at the pier. The best efficiency (34.5%) in the tests by Grimaldi (2005, 2009b) was found in test A4 for  $z_s/h=0.5$ . This value is near those of test S5 and also S8 with highest efficiencies. Figures 112 and 113 show that in these three tests the slot extended to all the

pier part inside the scour. However, in other tests (Figs. 113 to 115), with a slot as long as the approach flow depth and partially sunk into the bed, the maximum efficiency is lower and probably the slot may potentially decrease the scour depth if positioned in a better location.

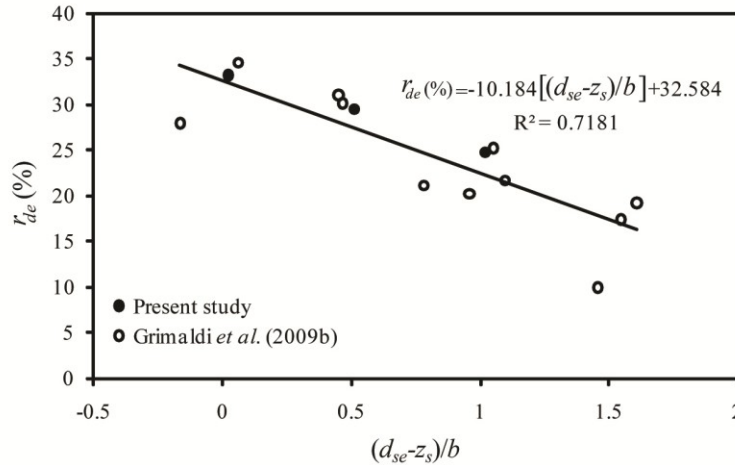


Fig. 116. Relationship of  $r_{de}$  versus  $(d_{se} - z_s)/b$

In fact, the result of tests by Chiew (1992) shows that with a slot as long as  $h/2$  positioned near the water surface the efficiency is significantly less than with a slot as long as  $h$  positioned above the initial bed level (5÷7% compared to 20%; see Fig. 117).

The results of other researches performed by Tanaka and Yano (1967) and Heidarpour (2002) confirm that a slot near the water surface is less effective than a slot near the bed. The results of the present study also show that the difference between the efficiencies in tests S5 and S8 are negligible. In fact, a slot extending from the water surface to beyond the final bed level may not significantly improve the efficiency of the countermeasure (see results of test S8 with respect to those of test S5 in Fig. 112).

The best configuration of a slot can be then defined as  $l_s = d_{se} + h/2$  and  $z_s = d_{se}$  (see results of test S5 in Fig. 112). The results of the present study and literature works clarify that the efficiency in scour depth reduction is about 30% to 35% in the best configurations of a pier slot. Therefore, in order to preliminary design a slot based on the predicted pier scour depth, it can be assumed  $d_{se} \approx 0.7d_{se0}$ . In this case, the slot can be design as  $l_s = 0.7d_{se0} + h/2$  and  $z_s = 0.7d_{se0}$ .

Note selecting the configuration of test S5 rather than that of test S8 has the two following advantages for practical purposes:

1. the slot length in test S5 is about 2/3 of that in test S8. As mentioned in §3.8.4, slots may reduce the buckling strength of a pier. This problem may be enhanced with longer slots;
2. floating debris may less likely block the slot in the proposed configuration of test S5, with respect to the configuration of test S8 or similar configurations in which the slot is located near the water surface.

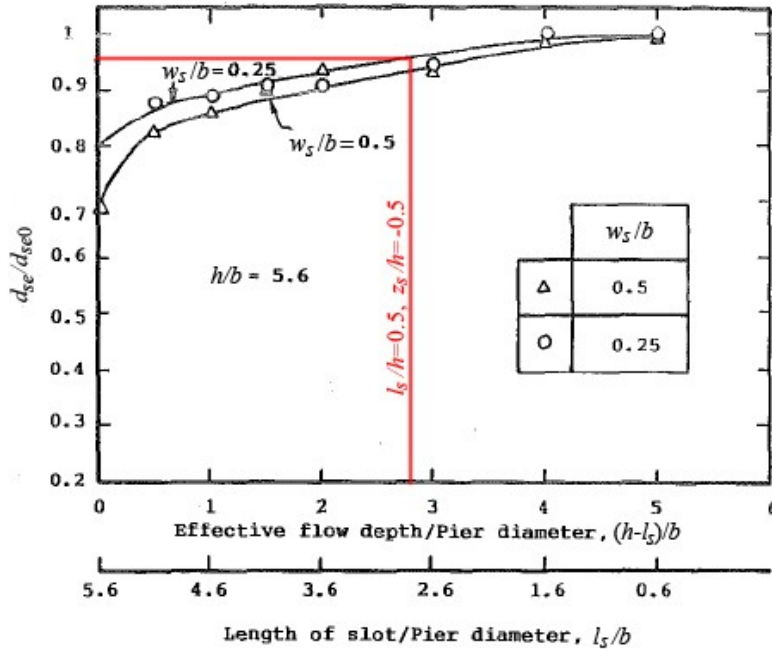


Fig. 117. Effect of a slot positioned near the water surface on scour depth (Chiew, 1992)

### 5.2.6. Combination of a collar with pier slot

In the previous tests of the present work, the efficiency in terms of scour depth reduction was always less than 35%. Therefore, combinations of countermeasures will be considered hereinafter.

In test S9 the best configuration of a pier slot was combined with a collar flush with the bed. The geometric parameters of this combined countermeasure are presented in Tab. 22. In test S9 only the scour depth downstream of the collar, which is the maximum scour depth in the movable bed, was monitored (Fig. 118).

Since the slot was extended inside the bed, the bed materials inside the slot, upstream and downstream of the pier and beneath the collar were partially removed through the slot opening. In this test, owing to difficulties in measuring the scour depths in different inaccessible locations, the equilibrium condition was only verified on the basis of the scour depth downstream of pier. At the end of the test, the scour downstream of the collar was considered (Figs. 119a and 120). In comparison to the case of pier protected with collar only, the scour downstream of the collar extended more; however, the scour could not extend upstream to the collar to intrude under it as in test S3. As Figure 120 shows, the maximum scour depth was observed inside the slot ( $d_{se}=1.39$  cm). Table 23 shows that the efficiency of this configuration is about 81.8%. In this table and similar subsequent tables, the value used for calculation of efficiency is underlined. In order to prevent scour intrusion beneath the collar from inside the slot, test S10 was performed with the geometric parameters shown in Tab. 22. In this test, only the  $h/2$ -high part of pier above the bed was drilled. At the end of test S10, a scour similar to that of test S9, with the same maximum

depth, was observed (Fig. 119 and Tab. 23); however, the scour could not intrude beneath the collar through the slot. This combination was previously tested by Chiew (1992) and Moncada-M *et al.* (2009), and 100% scour depth reduction was also reported by the Authors. Based on the results of the present study, the recommendation is that the slot should not sink under the initial bed level. Up to now, several researchers as Chiew (1992) and Grimaldi *et al.* (2009b) described the influence of a slot in scour depth reductions; however, they only paid attention to the role of a slot as a method to reduce the strength of downflow and horseshoe vortices. It seems that the outflow through the slot also affects the wake vortices by deviating the wake vortices downstream. Furthermore, as the preliminary sketch in Fig. 121 shows, the outflow of the slot is in the opposite sense of the wake vortices. As mentioned before, the scour around the collar starts from downstream of the collar, owing to the action of the wake vortices. Probably the interaction of slot outflow reduces the strength of the wake vortices and deviates the wake vortices downstream. In this case, the scour extends downstream rather than moving to the upstream part of the collar; more research is anyway needed by measuring the flow field around the pier with a slot in order to consider this phenomenon.

Tab. 22. Geometric parameters of countermeasures of tests S9 and S10

Test	$w_c$	$h_c$	$t_c$	$z_s$	$w_s$	$l_s$
S9	$3b$	$h$	$b/8$	$0.7d_{se0}$	$b/4$	$h/2+0.7d_{se0}$
S10	$3b$	$h$	$b/8$	0	$b/4$	$h/2$

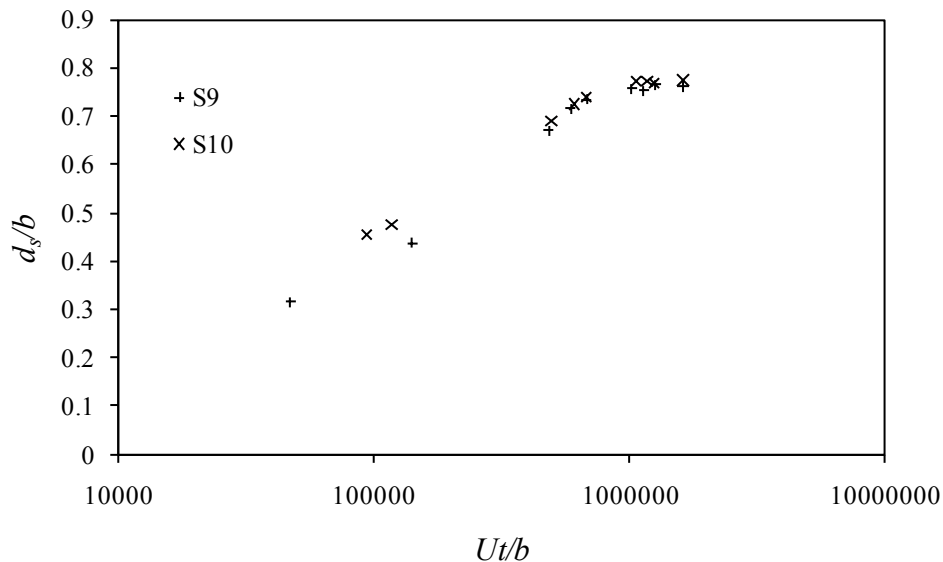


Fig. 118. Temporal evolution of scour depth downstream of collar in tests S9 and S10

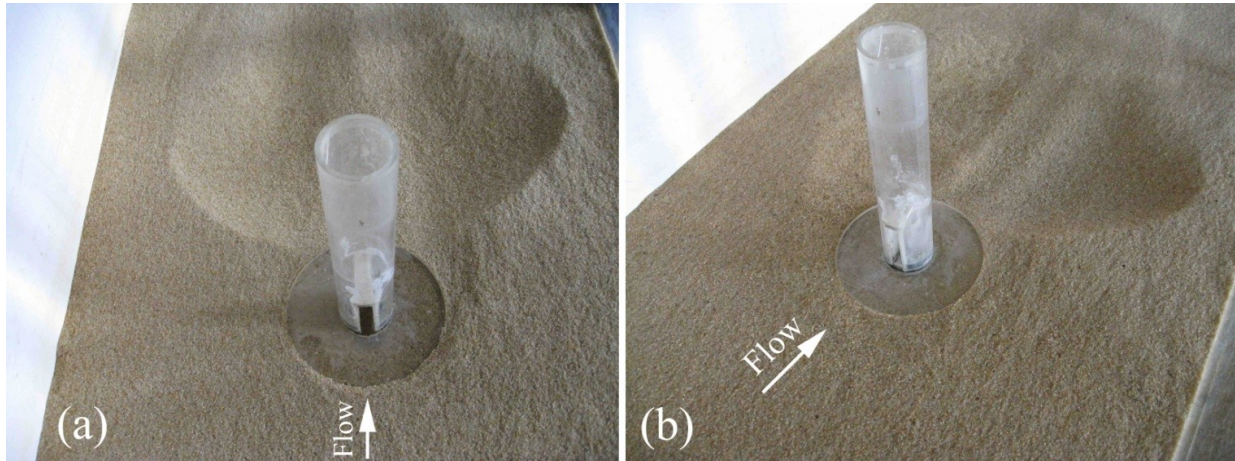


Fig. 119. Scour hole at the end of tests (a) S9 and (b) S10

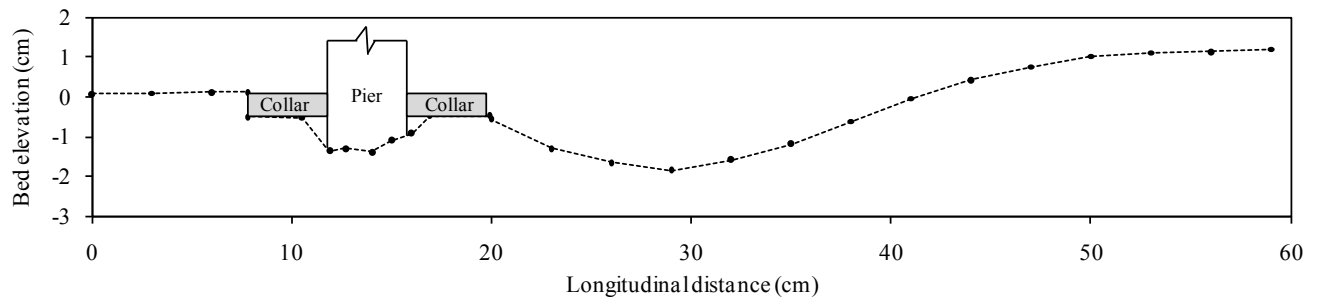


Fig. 120. Longitudinal profile of the scoured bed in test S9

Tab. 23. Results of tests S9 and S10

Test	$t_d$ (h)	$Ut_d/b$	$d_{se}$ (cm)	$d_{sec}$ (cm)	$d_{sem}$ (cm)	$r_{de}$ (%)
S9	68.9	$1.62 \cdot 10^6$	<u>1.39</u>	1.36	3.05	81.8
S10	69	$1.63 \cdot 10^6$	<u>0</u>	0.5	3.1	100

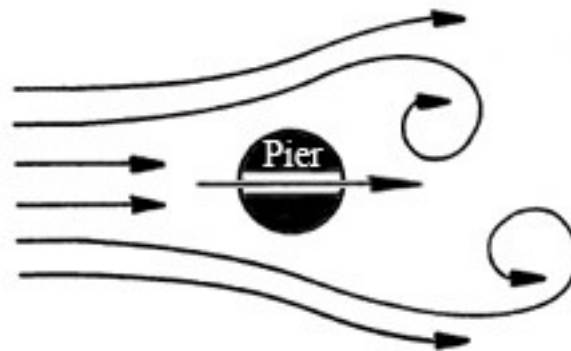


Fig. 121. Schema of passage flow through the pier slot

### 5.2.7. Combination of a pier slot with sacrificial piles

In test S11 a combination of the best configurations of sacrificial piles and pier slot was evaluated (Fig. 122a and Tab. 24). During the test, scour depth in front of pier was monitored and compared with those of an unprotected pier and of a pier with each single countermeasure (Fig. 123). The efficiencies of this countermeasure in terms of scour depth, area and volume are presented in Tab. 25. Figure 122b shows the scour hole shape at the end of the test. 3D pattern and contour lines of the equilibrium scour hole are presented in Figs. 124 and 125. These last two figures clarify that the maximum scour depth in the movable bed was found in front of the piles, as also observed in previous tests with sacrificial piles. In fact, the efficiency of this combination in terms of scour depth is negligible with respect to the application of each single countermeasure, being only about 5÷6% greater than in the case of slot or sacrificial piles. In conclusion, this combination is not proposed for efficient pier scour reductions.

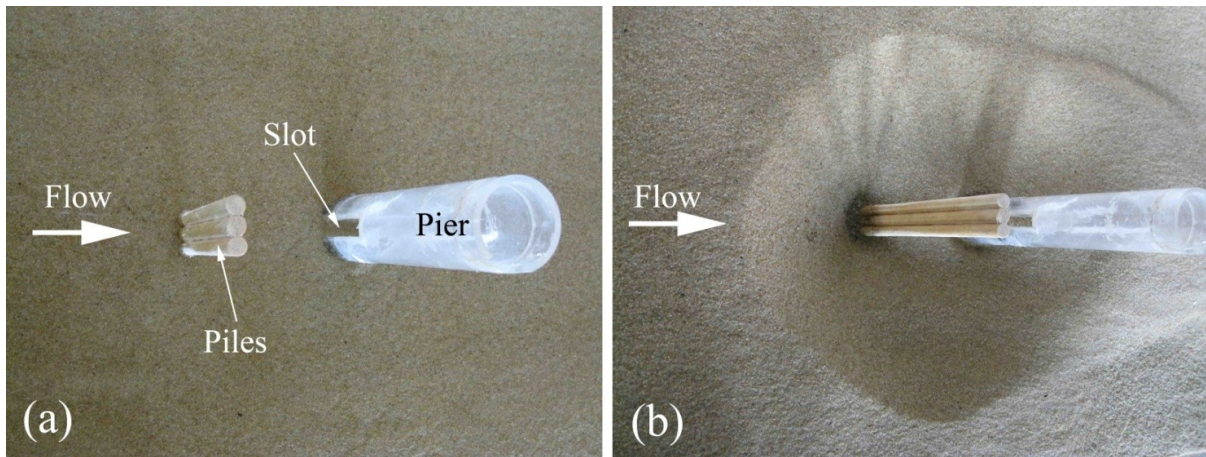


Fig. 122. (a): Configuration of test S11 before starting the test and (b): scour hole at the end of test S11

Tab. 24. Geometric parameters of countermeasures in test S11

Slot			Sacrificial piles			
$z_s$	$w_s$	$l_s$	$N_p$	$b_r$	$b_p$	$X_p$
$0.7d_{se0}$	$b/4$	$h/2+0.7d_{se0}$	3	0.6	$b$	$2b$

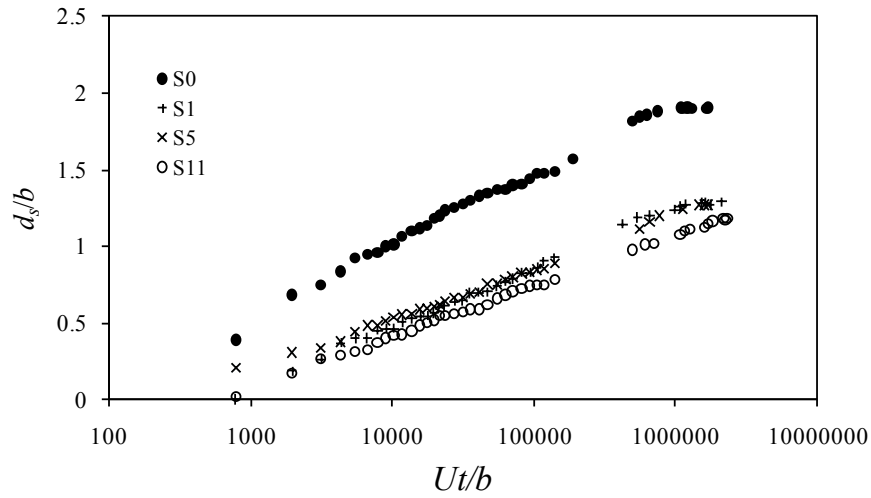


Fig. 123. Temporal evolution of scour depth in front of the pier in tests S0, S1, S5 and S11

Tab. 25. Results of test S11

$t_d$ (h)	$Ut_d/b$	$d_{se}$ (cm)	$d_{sem}$ (cm)	$A_e$ (cm <sup>2</sup> )	$V_e$ (cm <sup>3</sup> )	$r_{de}$ (%)	$r_{Ae}$ (%)	$r_{Ve}$ (%)
99	$2.33 \cdot 10^6$	4.72	6.63	795.1	1834	38.1	24.3	34.6

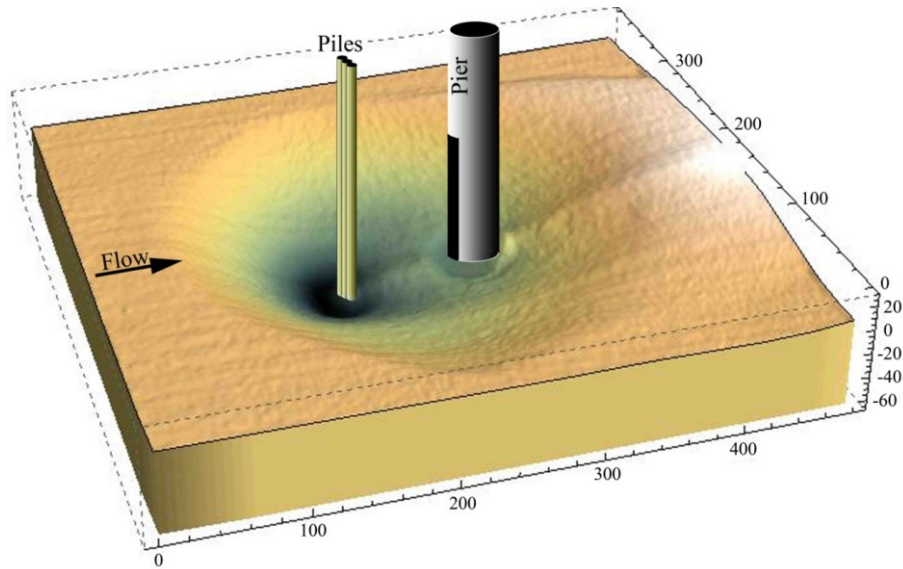


Fig. 124. 3D pattern of equilibrium scour hole in test S11 (units: mm)

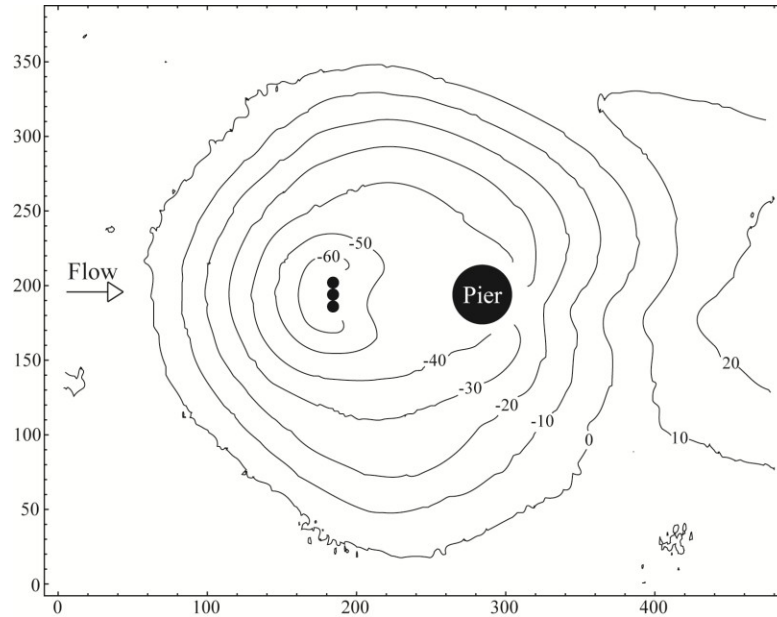


Fig. 125. Contour lines of equilibrium scour hole in test S11 (units: mm)

### 5.2.8. Combination of a collar with sacrificial piles

In test S12 a combination of the best configurations of transverse sacrificial piles and collar was considered (Tab. 26). After starting the test, the scour around the piles developed quickly and, although scoured sediments buried the collar for a few minutes (less than 5 min), the scour downstream of the piles intruded to beneath of the collar from upstream of the collar (Fig. 126a). The scour upstream to the collar developed with a high rate and after about 30 min the scour reached the pier face from the upstream part of the pier. Then the scour extended beneath all the parts of the collar. In fact, one of the most important advantages of the collar, i.e. slowing down the scour rate, did not occur in this configuration. Figure 127 shows the comparison of results; a single collar may slow down the scouring process better than this combination. In addition, the improvement in efficiency of this combination with respect to the individual application of each countermeasure is negligible: as Tab. 27 shows, the combination efficiency is 36.2%, only about 7% and 4% greater than with a collar or sacrificial piles, respectively. Therefore, also this combination cannot be suggested as a convenient countermeasure against pier scour. The 3D pattern of scour and contour lines of equilibrium scour hole are shown in Figs. 128 and 129. In test S12 the maximum scour depth in the movable bed was observed in front of the piles, being almost equal to 6.5 cm, as in the other tests with 3 piles (S1 and S11).



Tab. 26. Geometric parameters of countermeasures in test S12

Collar			Sacrificial piles			
$w_c$	$h_c$	$t_c$	$N_p$	$b_r$	$b_p$	$X_p$
$3b$	$h$	$b/8$	3	0.6	$b$	$2b$

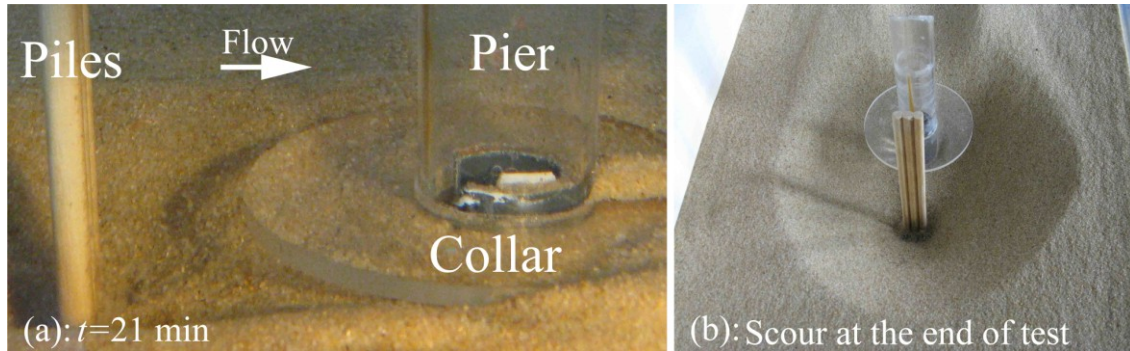


Fig. 126. (a) Scour intrusion from upstream of the collar; (b) scour hole at the end of test S12

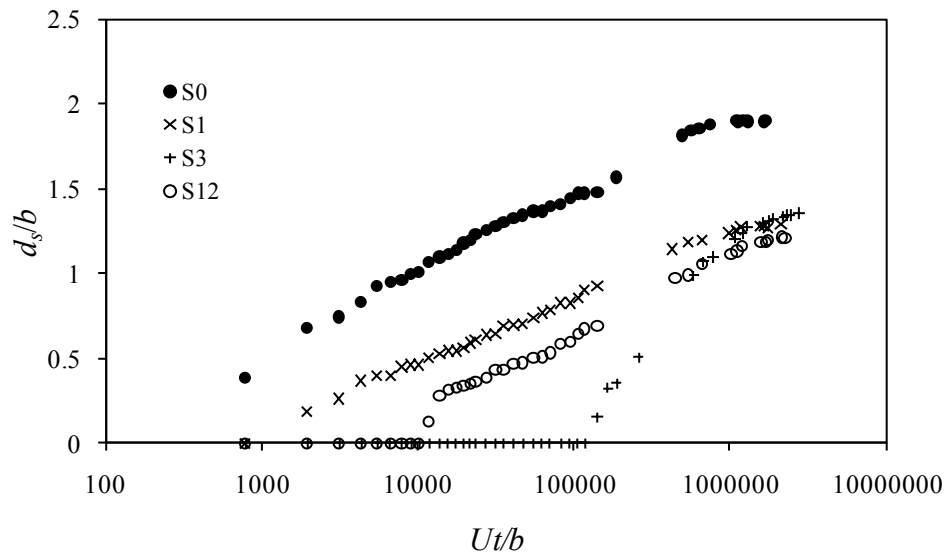


Fig. 127. Temporal evolution of scour depth in front of the pier in tests S0, S1, S3 and S12

Tab. 27. Results of test S12

$t_d$ (h)	$Ut_d/b$	$d_{se}$ (cm)	$d_{sem}$ (cm)	$A_e$ (cm <sup>2</sup> )	$V_e$ (cm <sup>3</sup> )	$r_{de}$ (%)	$r_{Ae}$ (%)	$r_{Ve}$ (%)
95.33	$2.25 \cdot 10^6$	4.86	6.54	750.3	1686.3	36.2	28.6	39.9

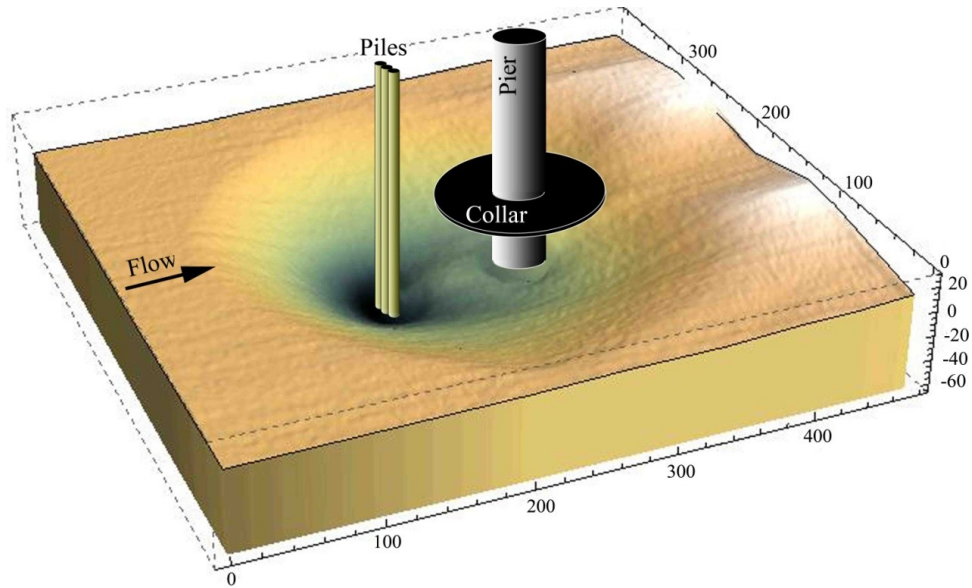


Fig. 128. 3D pattern of equilibrium scour hole in test S12 (units: mm)

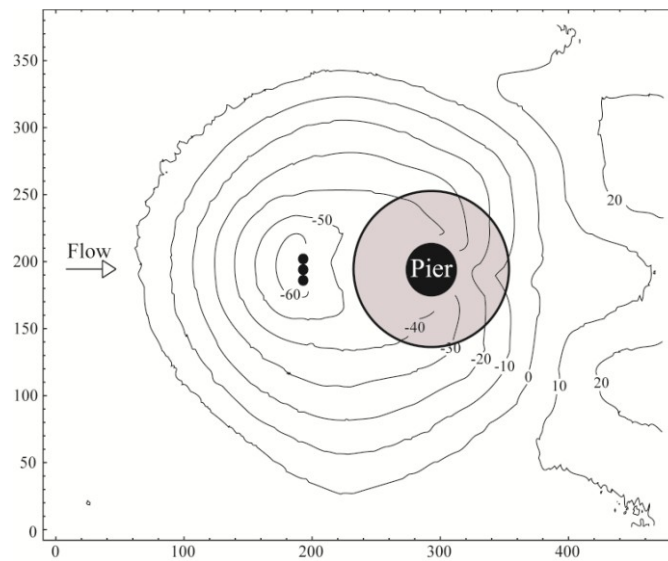


Fig. 129. Contour lines of equilibrium scour hole in test S12 (units: mm)

## 5.2.9. Combination of collar with bed-sill as scour countermeasure

### 5.2.9.1. Location of bed-sill respect to pier

As mentioned in §5.2.3, two grooves at a pier protected with a collar initiate from downstream of the collar and extend upstream of it, and then excavate the bed sediments beneath it. The main idea behind the combination of a bed-sill and a collar is to block the development of the two grooves extending to the upstream part of the collar and consequently washing away bed

materials beneath the collar and around the pier. In the application of a bed-sill flush with the mobile bed, neglecting roughness of the bed-sill, three other dimensionless numbers, i.e.  $l_{bs}/b$ ,  $t_{bs}/b$  and  $w_{bs}/b$ , can be assumed to play a non-negligible role, where  $l_{bs}$  is the centre-to-centre distance between pier and bed-sill, positive when the bed-sill is located upstream to the pier, negative otherwise (Fig. 130);  $w_{bs}$  and  $t_{bs}$  are bed-sill width and thickness, respectively. In some tests also two side-walls were added at the bed-sill ends to prevent scour intrusion at the upstream part of the bed-sill. In this case,  $l_{sw}/b$  can be assumed as another important dimensionless number,  $l_{sw}$  being the side-wall length.

According to Grimaldi *et al.* (2009a), a bed-sill located downstream of a pier has the maximum efficiency when it is adjacent to the cylinder. In test S13 the bed-sill was located downstream of and adjacent to the pier [ $l_{bs}=(b+t_{bs})/2$ ] protected with a  $3b$ -wide and  $b/8$ -thick transparent Perspex<sup>®</sup> collar ( $w_c=12$  cm and  $t_c=5$  mm) flush with the mobile bed ( $h_c=h=12$  cm; Fig. 130). The bed-sills used in this test was a 10 mm-thick PVC plate as wide as the working cross-section ( $t_{bs}=b/4$  and  $w_{bs}=48.5$  cm $\approx 12b$ ). In all the following tests of the present study the bed-sills are set flush with the bed, as is usually used as a countermeasure against general bed degradation.

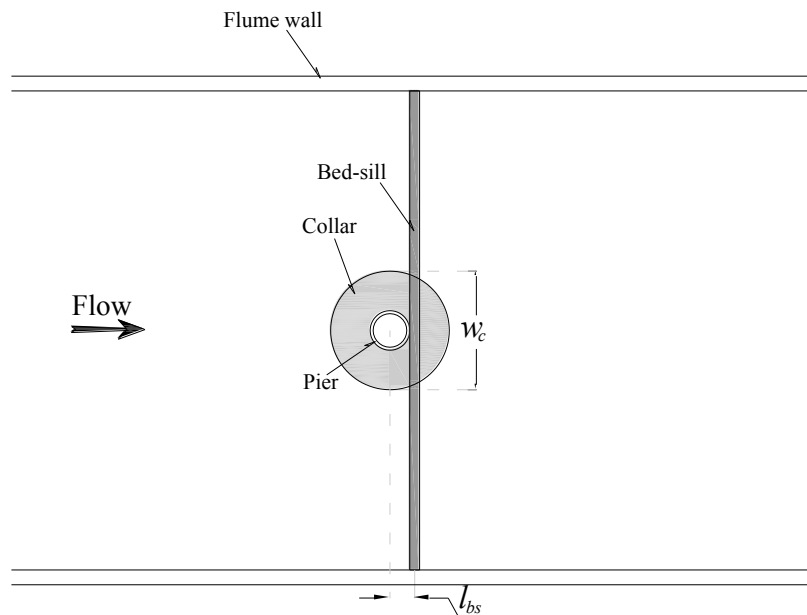


Fig. 130. Configuration of test S13

Figure 131 shows the temporal evolution of the scour depth in front of the pier, where at the end of the test the maximum scour depth was observed (adjacent to the pier). This figure also shows the temporal evolution of the maximum scour depth downstream of the bed-sill.

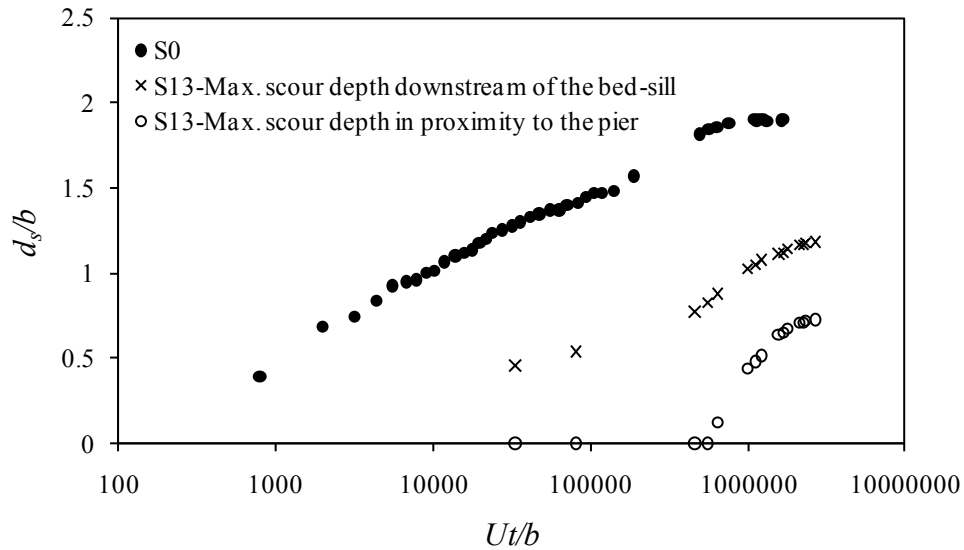


Fig. 131. Temporal evolution of the maximum scour depth in tests S0 and S13

The initial part of the scour development in test S13 was similar to that of test S3 with a single collar. In fact, two grooves started from downstream of the collar (Fig. 132b) and then they were blocked for a relatively long period up to 17 h (see, e.g., Fig. 132c). After this period the scour moved around the collar rim upstream of the bed-sill (Fig. 132d). Owing to the presence of the bed-sill, the scour development slowed down significantly and after about 27 h the scour reached the pier face from the upstream part of the pier; then, the scour developed slowly and continuously. When the maximum scour depth in proximity to the pier and in front of it was in equilibrium condition, the test was stopped (Figs. 132e,f and 133). In this condition the maximum scour depth in the movable bed was found downstream of the bed-sill ( $d_{sem}=4.74$  cm); however, a slightly smaller scour depth was also found under the collar upstream to the bed-sill ( $d_{sec}=4.1$  cm). Table 28 shows the results of each test in the combination of collar and bed-sill. In all the tests of the present study, a  $3b$ -wide collar flush with the bed was combined with the bed-sill and the efficiencies were calculated as in §4.7. The efficiency of this combination (46.2%) is almost the same as in the best configuration of combined slot and bed-sill (45%; see Grimaldi *et al.*, 2009b); however, the combination of test S13 has an important problem for practical purposes. In fact, since a major part of the bed materials under the collar are removed, it could probably collapse.

An interesting finding of test S13 is that, although the grooves pass the bed-sill and reach the pier, the bed-sill prevented the scour from extending longitudinally beneath the collar downstream of the pier. In other words, the bed sediments under the collar at the rear of the pier and bed-sill remained intact.

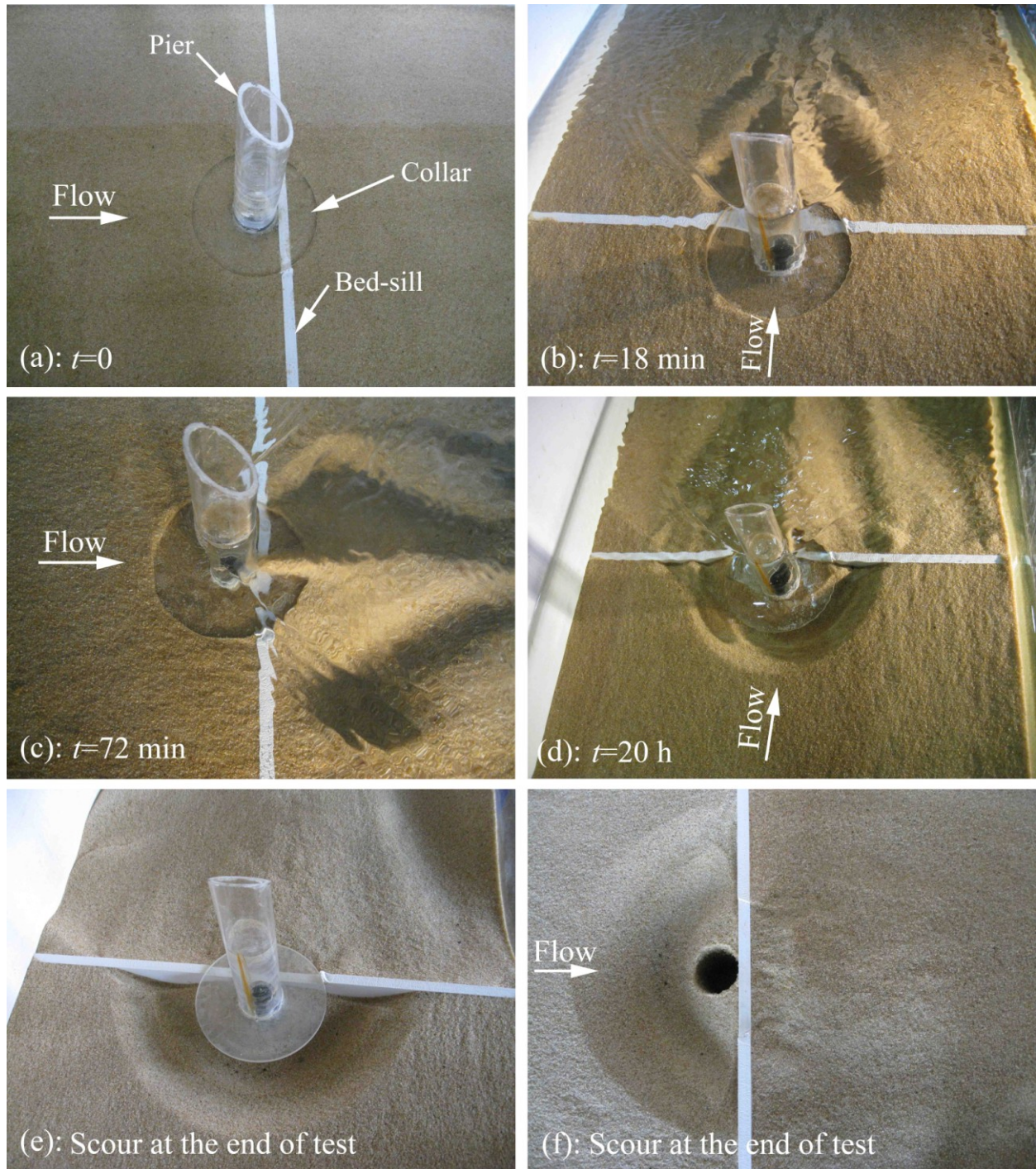


Fig. 132. Scour hole at different time instants in test S13

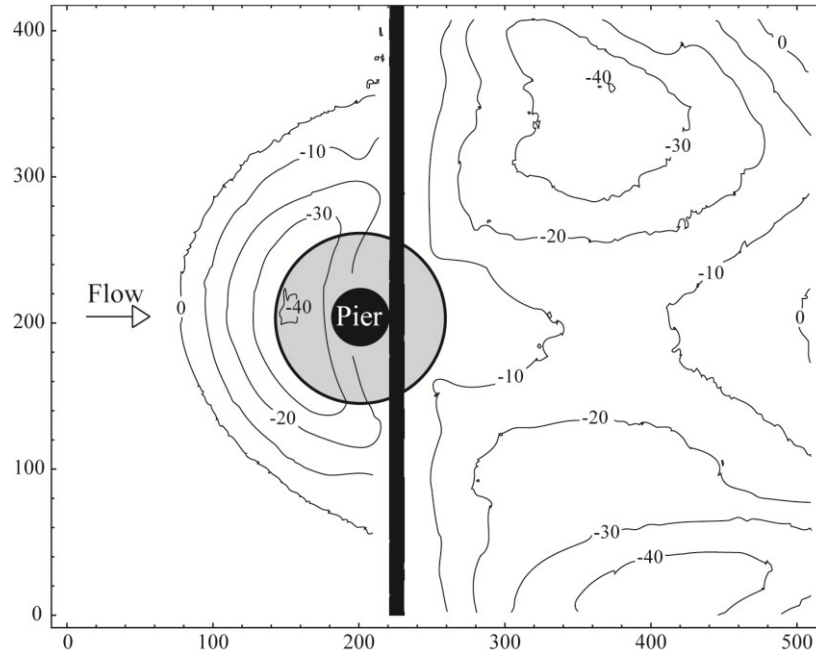


Fig. 133. Contour lines of equilibrium scour hole in test S13 (units: mm)

Tab. 28. Configurations and efficiencies in the combinations of a bed-sill and a collar

Test	$t_d$ (h)	$Ut_d/b$	$t_c$	$w_{bs}$	$t_{bs}$	$l_{bs}$	$l_{sw}$	$t_{cb}$	$d_{sem}$ (cm)	$d_{sec}$ (cm)	$d_{se}$ (cm)	$r_{de}$ (%)
S13	114	$2.69 \cdot 10^6$	$b/8$	$B \approx 12b$	$b/4$	$-(b + t_{bs})/2 = -5b/8$	-	-	4.74	<u>4.1</u>	2.91	46.2
S14	150	$3.54 \cdot 10^6$	$b/8$	$B \approx 12b$	$b/4$	0	-	-	4.89	<u>3.9</u>	2.32	48.8
S15	91.2	$2.15 \cdot 10^6$	$b/8$	$B \approx 12b$	$b/4$	$(b + t_{bs})/2 = 5b/8$	-	-	4.64	<u>1.8</u>	0.8	76.4
S16	96.2	$2.27 \cdot 10^6$	$b/8$	$B \approx 12b$	$b/4$	$b + t_{bs}/2 = 9b/8$	-	-	4.91	<u>2.8</u>	1.2	63.3
S17	126	$2.97 \cdot 10^6$	$b/4$	$4b$	$b/4$	$(b + t_{bs})/2 = 5b/8$	-	$b/2$	<u>7.93</u>	7.93	3.66	-3.9
S18	147	$3.47 \cdot 10^6$	$b/4$	$6b$	$b/4$	$(b + t_{bs})/2 = 5b/8$	-	$b/2$	<u>9.26</u>	-	1.3	-21.5
S19	56	$1.32 \cdot 10^6$	$b/4$	$7b$	$b/4$	$(b + t_{bs})/2 = 5b/8$	-	$b/2$	The test was suspended before equilibrium			
S20	81	$1.91 \cdot 10^6$	$b/4$	$9b$	$b/4$	$(b + t_{bs})/2 = 5b/8$	-	$b/2$	The test was suspended before equilibrium			
S21	52.2	$1.23 \cdot 10^6$	$b/4$	$6b$	$b$	$(b + t_{bs})/2 = b$	-	$b/2$	The test was suspended before equilibrium			
S22	102.4	$2.41 \cdot 10^6$	$b/4$	$6b$	$b$	$(b + t_{bs})/2 = b$	$b$	$b/2$	5.17	<u>2.7</u>	0	64.5
S23	104.4	$2.46 \cdot 10^6$	$b/4$	$B \approx 12b$	$b$	$(b + t_{bs})/2 = b$	-	$b$	5.31	<u>2.4</u>	0	68.5

In test S14 two bed-sills were located at both sides of the pier ( $l_{bs}=0$ , see Figs. 134 and 135a). In this combination, the scour started from the downstream of the collar (Fig. 135b); however, as soon as the grooves reached the bed-sill, the progress to the upstream part of the

collar was suspended for a relatively long period. At about 27 h the scour developed from the lateral sides of the collar towards its front; later the hole deepened and extended to the upstream side of the collar (Fig. 135c). After this period, the scour both developed continuously upstream and downstream of the bed-sill (Fig. 135d). At 70 h the scour reached the pier from the upstream part of the collar. At the end of the test in equilibrium condition, the zone beneath the collar downstream of the pier was almost intact.

In test S14, both the scour depths downstream of the bed-sill (i.e., the maximum scour depth in the movable bed) and in proximity to (adjacent to) the pier were monitored. Figure 136 shows that equilibrium condition was obtained downstream of the bed-sill before than upstream of it. Note that the equilibrium condition adjacent to the pier (Fig. 136) of this test was discussed in §4.6. The results of test S14 show that two scour holes downstream of the bed-sill (Fig. 134) originally started as two grooves (Figs. 135b) and then deepened during the test; however, they have less influence on the region beneath and downstream of the collar, and at the end of the test (Fig. 135d) an triangular area less influenced by the two scour holes was observed (Figs. 135e,f). The efficiency of the combined countermeasure was calculated based on the maximum scour depth beneath the collar ( $r_{de}=48.8\%$ , Tab. 28). Although this efficiency is close to that of test S13, a greater area beneath the collar remained intact in test S14.

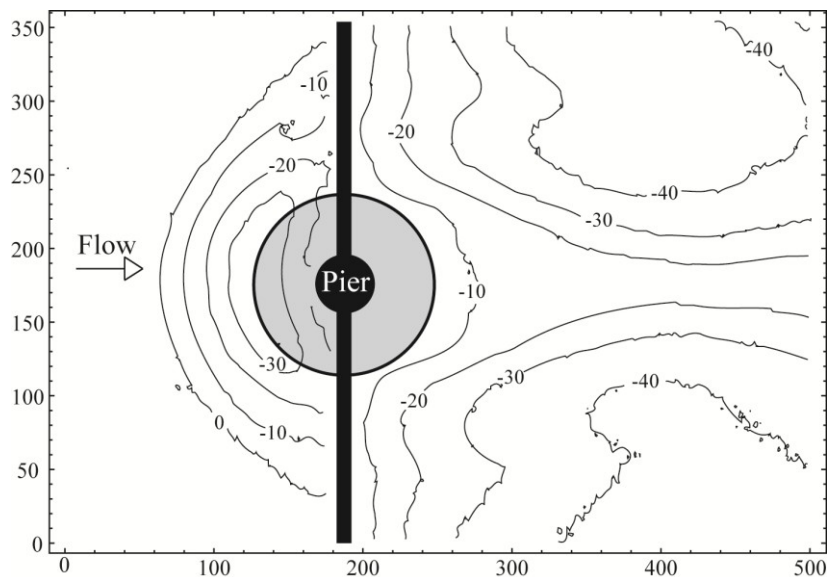


Fig. 134. Contour lines of equilibrium scour hole in test S14 (units: mm)

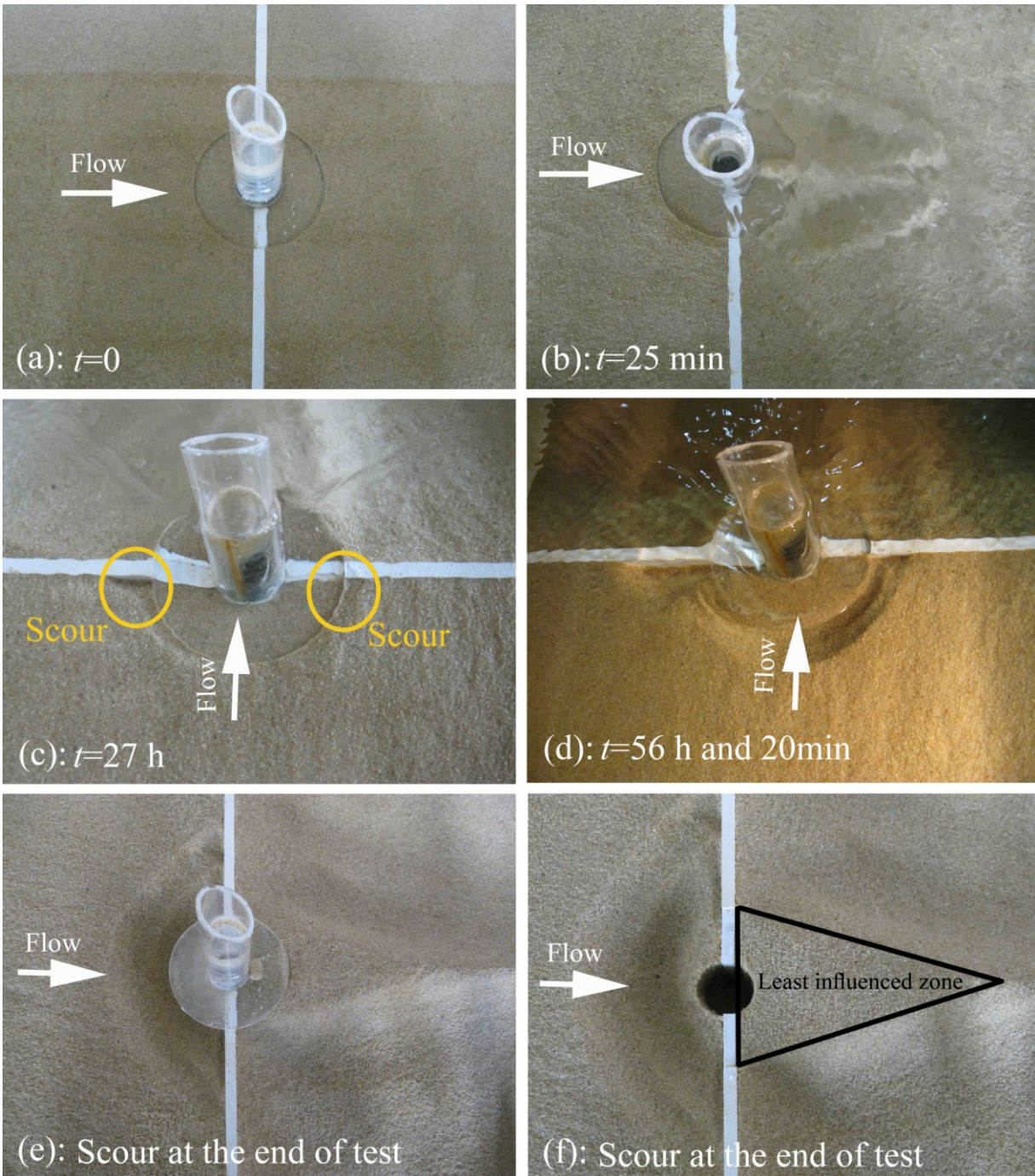


Fig. 135. Scour hole at different time instants in test S14



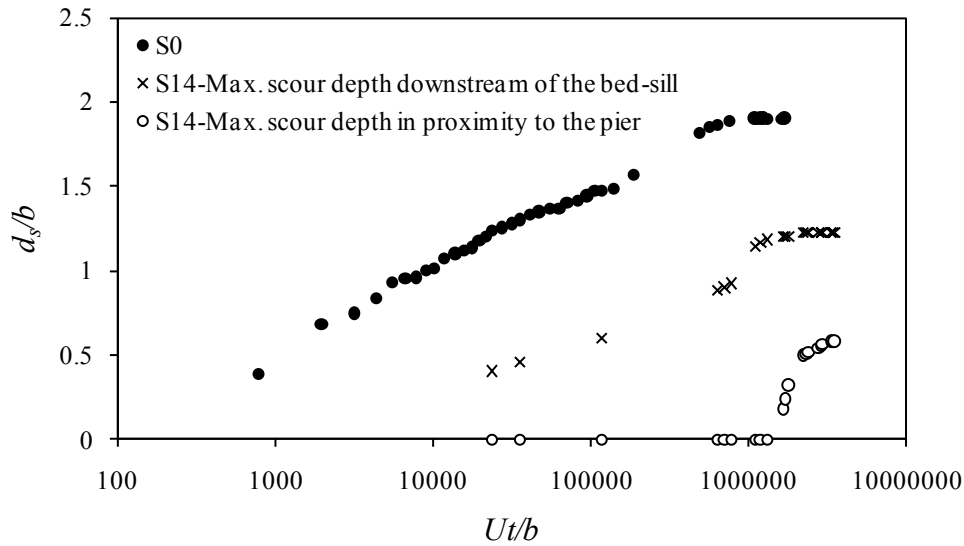


Fig. 136. Temporal evolution of the maximum scour depth in tests S0 and S14

In test S15, the collar and bed-sill dimensions were the same as in test S13; however, the bed-sill is located adjacent to the upstream face of the pier (Figs. 137a and 138). As soon as the test started, two grooves developed around both sides of the downstream part of the collar (Fig. 137b). The behaviour and development of these two grooves during the short term period were similar to those of the previous tests with collar and bed-sill or collar alone (tests S3, S13, S14); however, as soon as they reached the bed-sill, their intrusion to the upstream part of the collar was blocked. These two grooves continuously extended laterally and vertically (Fig. 137c) and their maximum depth moved away from the collar (Fig. 138).

At the end of test S15, downstream of the bed-sill the maximum scour depth under the collar was 1.8 cm, whereas the scour depth adjacent to the pier was as low as 3 mm ( $d_{se}=3 \text{ mm}+t_c=8 \text{ mm}$ , with  $t_c=b/8=5 \text{ mm}$ ) (Figs. 137d and 138). The maximum scour depth in the movable bed was measured over time downstream of the bed-sill outside the collar and was equal to 4.64 cm at the end of the test (Fig. 139). Based on the maximum scour depth under the collar, the efficiency was about 76.4% for this combined countermeasure.

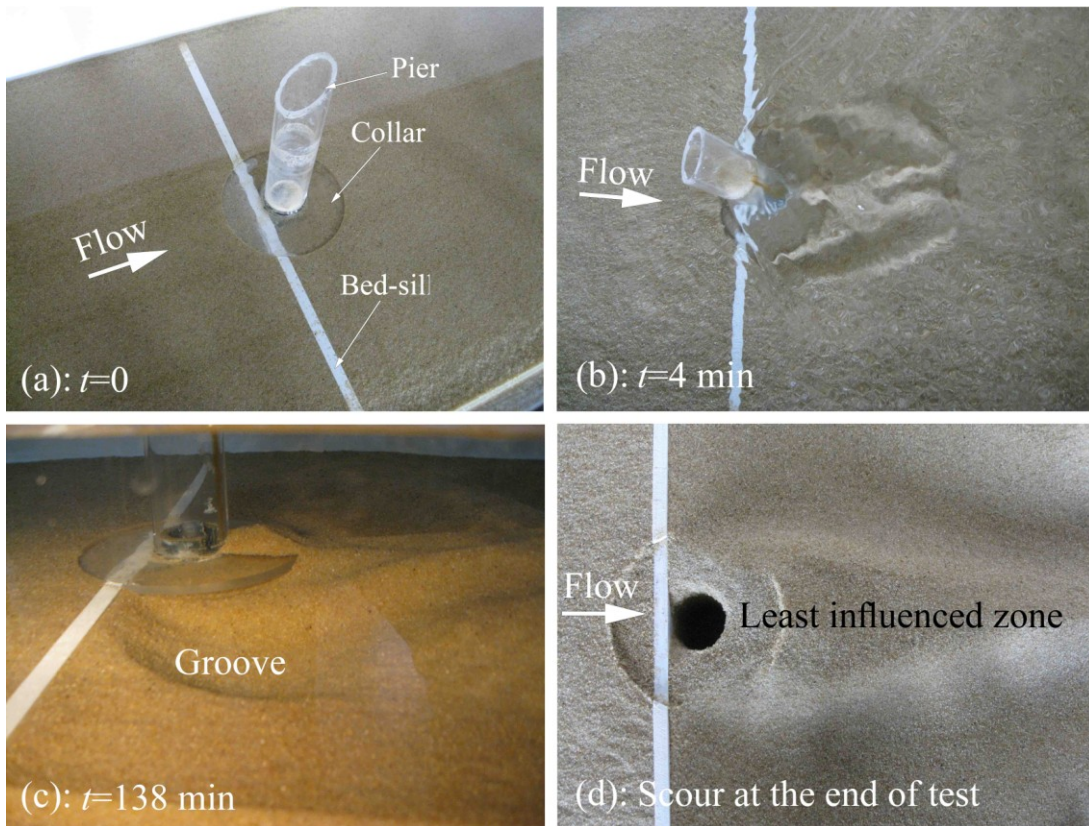


Fig. 137. Scour around the pier in test S15

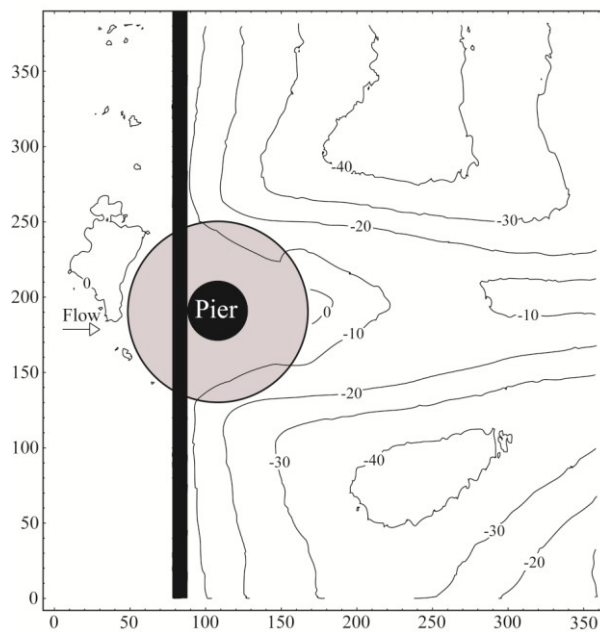


Fig. 138. Contour lines of equilibrium scour hole in test S15 (units: mm)

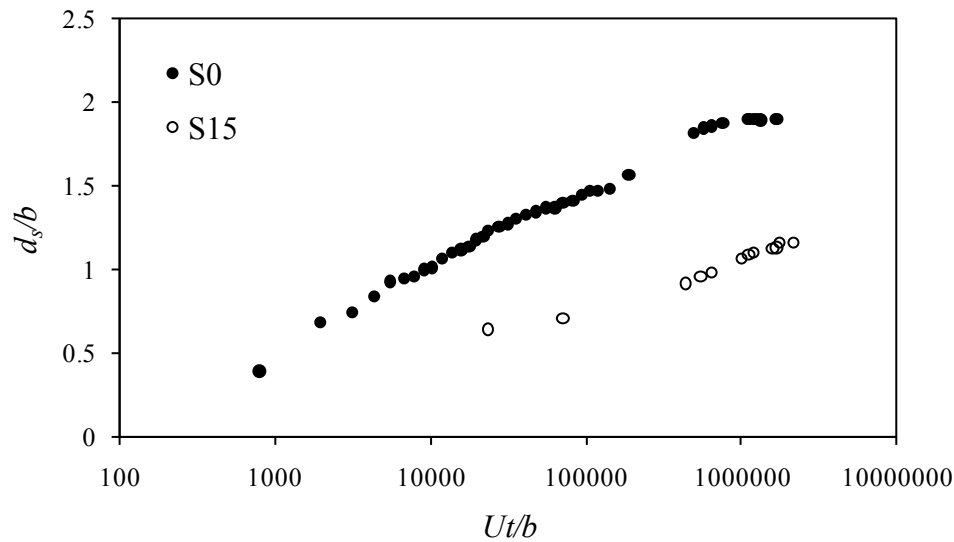


Fig. 139. Temporal evolution of the maximum scour depth in the movable bed in tests S0 and S15

In test S16, the bed-sill was located upstream of the pier at a distance of  $l_{bs}=b+t_{cb}/2=9b/8$ , as shown in Figs. 140a and 141. The start up and development of the grooves were similar to the previous test and the scour hole could not reach the upstream of the bed-sill; however, in this test the scour hole extended more under the collar. The test was stopped at equilibrium condition (Fig. 142). At the end of the test, a maximum scour equal to 7 mm was found under the collar at the side of the pier ( $d_{se}=0.7 \text{ cm}+t_c=1.2 \text{ cm}$ ); however, the maximum scour depth in the movable bed was found downstream of the bed-sill ( $d_{sem}=4.91 \text{ cm}$ ). In test S16 also the least influenced zone was observed; owing to further intrusion of scour beneath the collar, this area was narrower under the collar (Fig.140b). Based on the maximum scour depth beneath the collar, the efficiency of this configuration was about 63.3%.

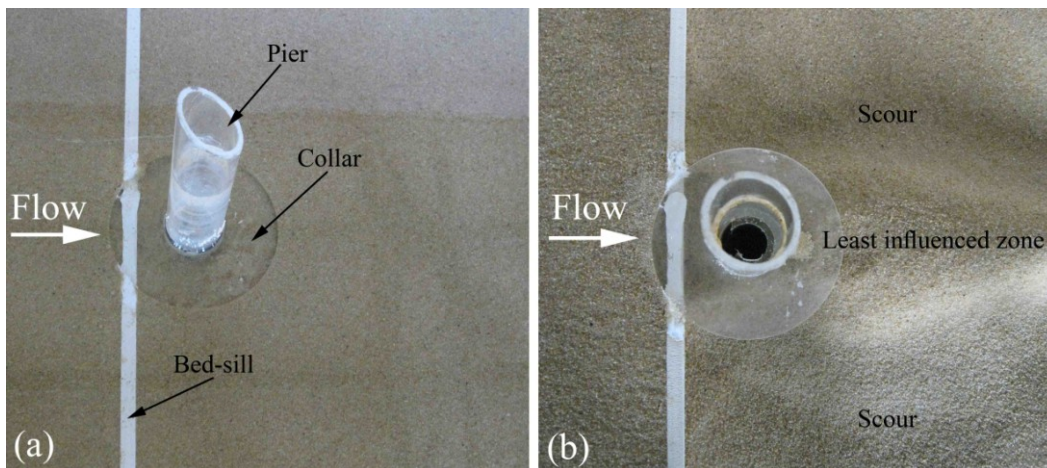


Fig. 140. (a) Initial configuration of test S16; (b) scour hole at the end of the test

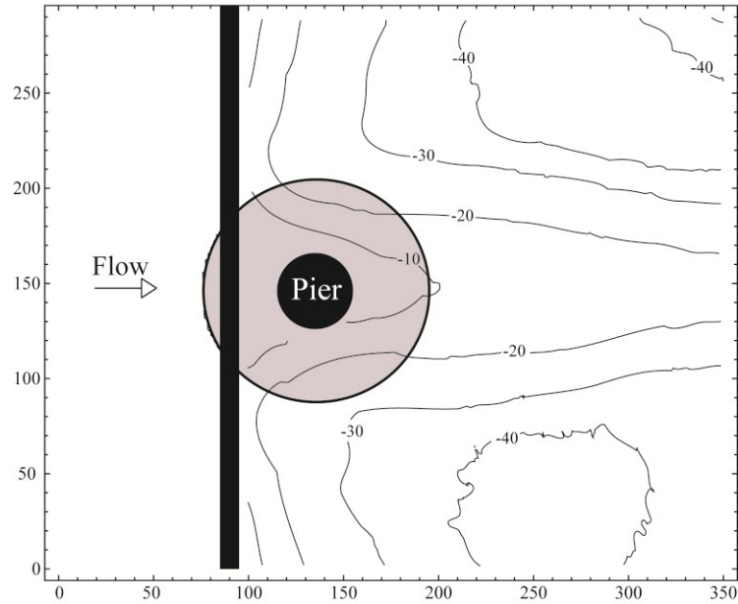


Fig. 141. Contour lines of equilibrium scour hole in test S16 (units: mm)

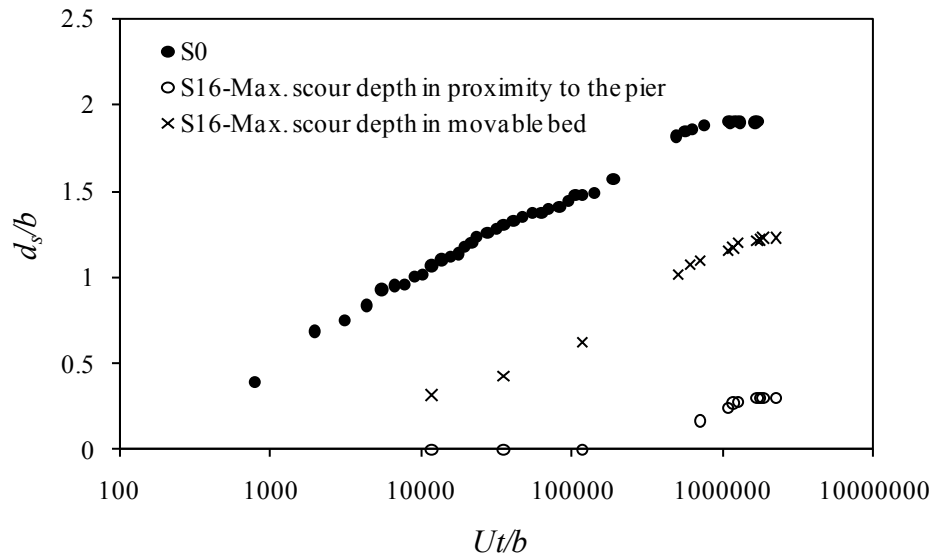


Fig. 142. Temporal evolution of the maximum scour depth in tests S0 and S16

The results of the previous tests show that the location of a bed-sill with respect to a pier protected with a collar plays an important role in the scour development around the pier. As the bed-sill moves from downstream to upstream of the collar, its efficiency increases, i.e. the risk of scour passage above the sill reduces. In contrast, the scour intrusion beneath the collar from downstream of the bed-sill increases. The maximum efficiency was obtained in the best configuration, namely when the bed-sill was adjacent to the upstream face of the pier.

### 5.2.9.2. Dimensions of bed-sill

In previous experiments, the bed-sill was as wide as the flume. In real applications, the constructions of a bed-sill as wide as the watercourse may present some difficulties, in particular for wide rivers. In the following experiments the influence of the bed-sill width on the scour around the pier is considered.

In test S17, the location of the bed-sill was upstream and adjacent to the pier as in test S15, but with  $w_{bs}=4b$ . In this test, the collar configuration was improved by adding a 1 cm-thick and wide border around and under a portion of the 1 cm-thick collar ( $t_c=1$  cm), in order to reduce the intrusion of scour beneath it. The total thickness of the collar in its bordered portion was  $t_{cb}=b/2$ , as shown in Fig. 143.

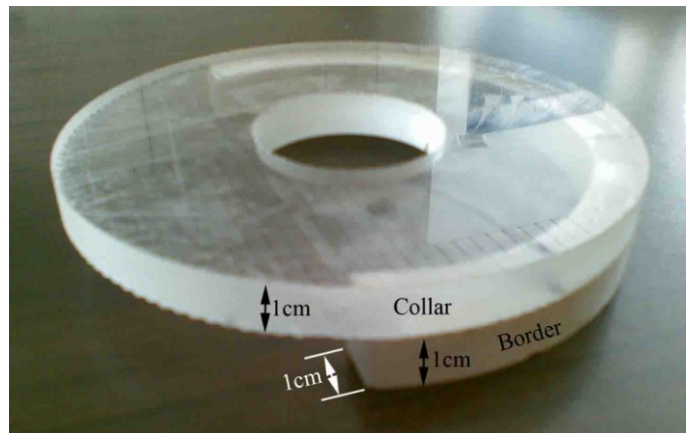


Fig. 143. Configuration and dimensions of the bordered-collar used in tests S17 to S22

The configuration of this countermeasure is shown in Fig. 144. In this test, the scour started from downstream of the collar (Fig. 145a) and then extended to the bed-sill during the first hour (Fig. 145b). After about 4 h, the scour extended to the upstream part of the collar (Fig. 145c) and then intruded under the collar and reached the bed-sill. After this period the scour increased in front of the bed-sill with a higher rate with respect to the scour in front of the unprotected pier (Fig. 146) and at the test end an extensive scour area was observed around bed-sill and pier (Figs.145d and 147a). Note that owing to application of a border, the scour in proximity to the pier was observable when it was greater than a value of about 3 cm under the initial bed level.

In contrast to previous tests, maximum scour in this test was found in front of the bed-sill (Fig. 148) which was greater also than that of the unprotected pier. The reason is probably due to the fact that a bed-sill much wider than the pier width is subjected to the approach flow. The vortices in front of the bed-sill and wake vortices at the lateral rims of the bed-sill play an important role in washing the bed materials in the front and lateral sides of the bed-sill. The locations of these clearly visible vortices are shown in Fig. 145d. The results of this test show that although a 2 cm-deep bordered-collar is probably enough to protect the intrusion of scour beneath the collar in a configuration of test S15, owing to deeper scour around the bed-sill in test

S17, it is not adequate for this configuration. In this test, the scour was laterally reached the pier and a maximum scour depth ( $d_{se}=3.66$  cm) was found at equilibrium condition (Fig. 147b).

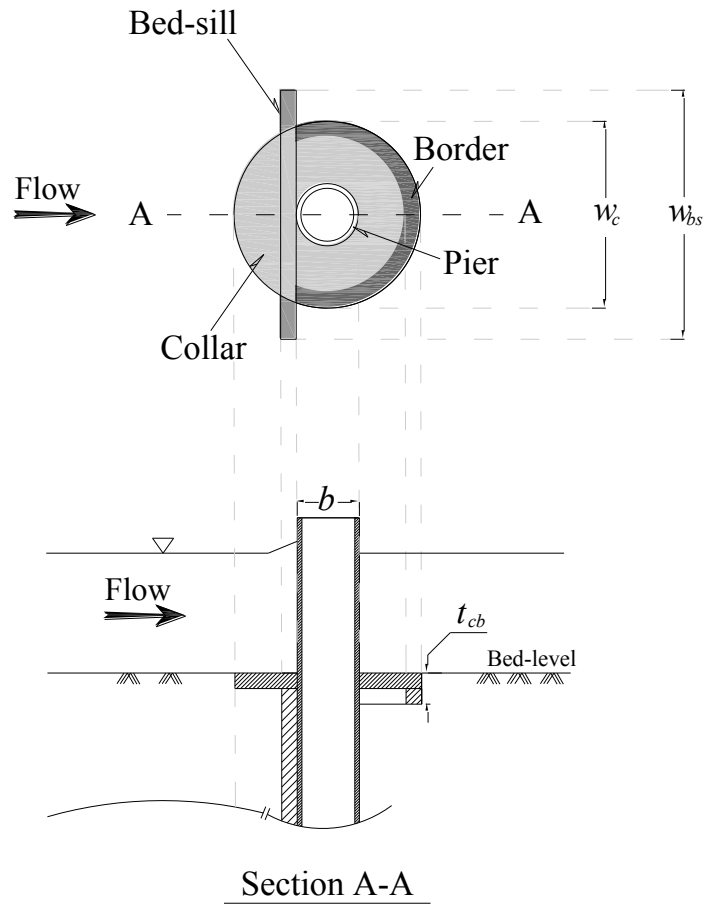


Fig. 144. Configuration of test S17

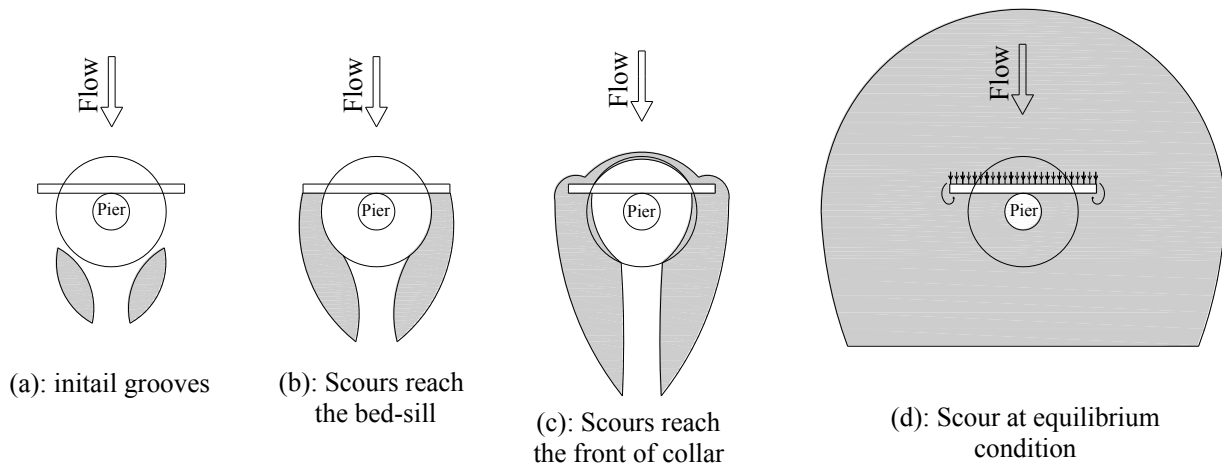


Fig. 145. Scour progress in test S17

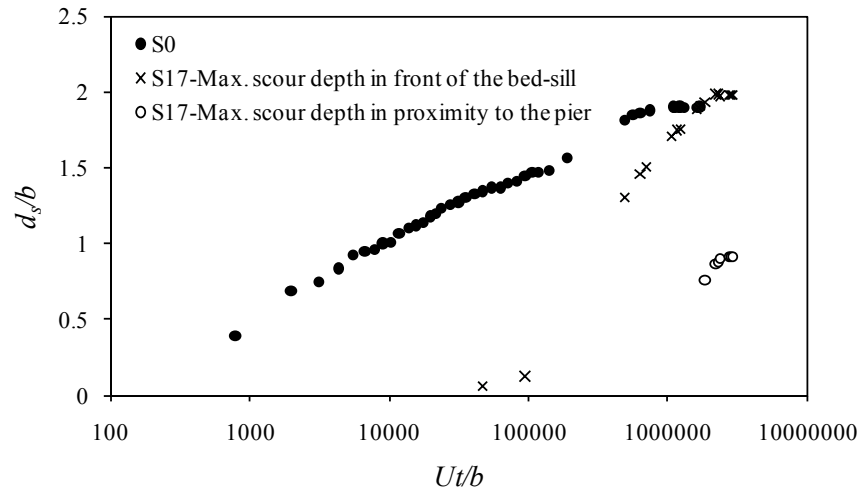


Fig. 146. Temporal evolution of the maximum scour depth in tests S0 and S17

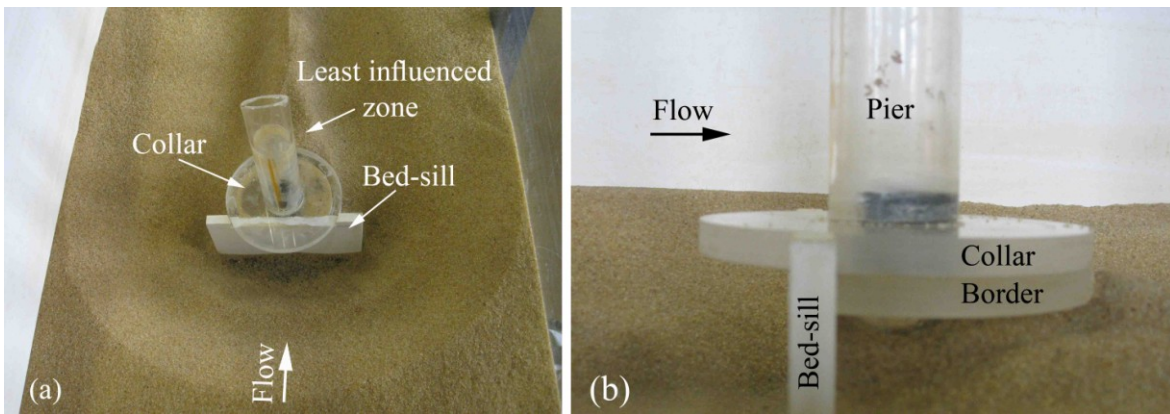


Fig. 147. Scour hole at the end of test S17

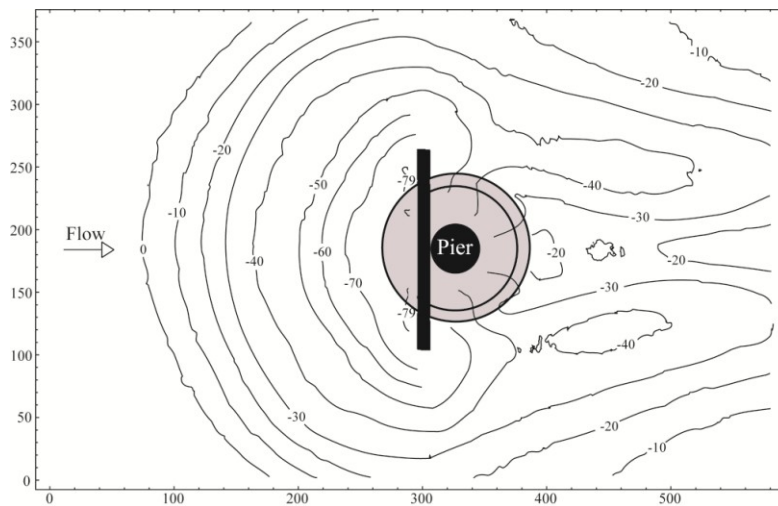


Fig. 148. Configuration and contour lines of equilibrium scour hole in test S17 (units: mm)

The configuration of test S18 is the same as in test S17, but with wider bed-sill ( $w_{bs}=6b$ ). The scour initiation and process was similar to test S17. In this test, during the first 22 h the scour was not found at the upstream part of the bed-sill; however, at 27 h small scour holes (only 3 mm-deep) were observed upstream and adjacent to the bed-sill near its edges. These scour holes developed rapidly and reached the collar and then the bed-sill part under the collar. As in the previous test, in test S18 the maximum scour depth in the movable bed was measured in front of the bed-sill ( $d_{sem}=9.26$  cm). In both tests the scour holes extended to the upstream part of the bed-sill, although in test S17 they extended to the upstream quicker and the maximum scour depth upstream of the bed-sill was less than in test S18. In contrast, in test S17, deeper scour was found adjacent to the pier ( $d_{se}=3.66$  cm with respect to 1.3 cm in test S18). In other words, in test S18, although a deep and extensive scour hole was found in front of the bed-sill, a better protection of the bed sediments around the pier at the rear of the bed-sill was obtained (Fig. 149). In test S18, the scour adjacent to the pier was only 3 mm under the collar and was not monitored during the test; the criteria for equilibrium condition was based on the maximum scour depth in front of the bed-sill, which is the maximum scour depth in the movable bed at the end of test (Fig. 150). The efficiency of the combined countermeasure of test S18 was also calculated on the basis of the maximum scour depth in front of the bed-sill and was negative ( $r_{de}=-21.5\%$ ). In fact, the deepest scour depth occurred in front of the bed-sill owing to the fact that its width is greater than the pier width (i.e., the combined countermeasure acts as an equivalent pier of width greater than  $b$ ); therefore, the bed-sill could be undermined and this configuration could be unsafe. A comparison of tests S15, S17 and S18 (Tab. 28) shows that the scour near pier and collar reduces as the bed-sill length increases; however, wider bed-sill results in deeper scour in front of it.

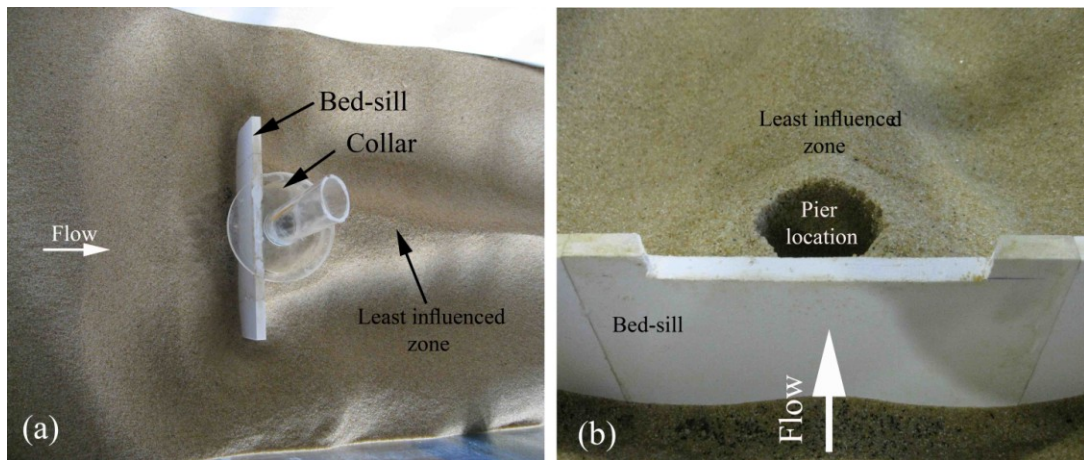


Fig. 149. Scour hole at the end of test S18



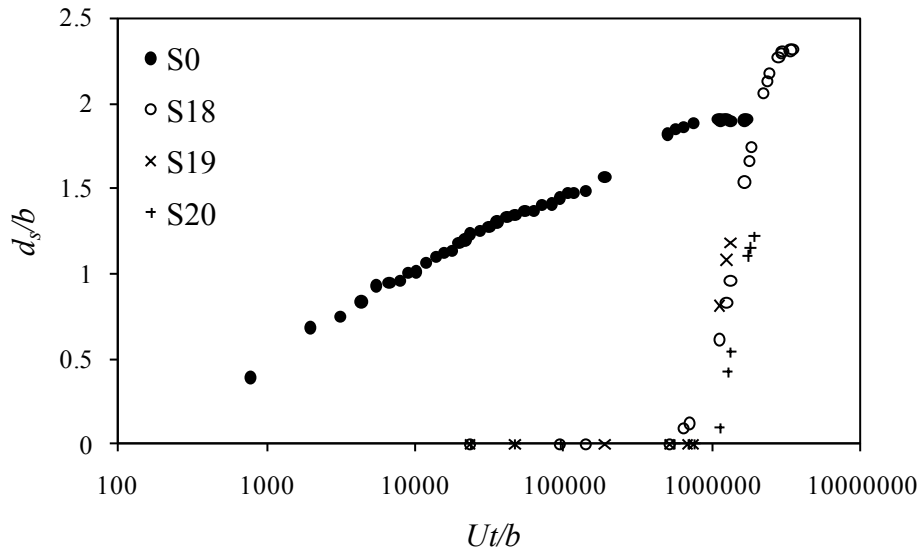


Fig. 150. Temporal evolution of scour depth in front of the bed-sill in tests S18, S19 and S20

In tests S19 and S20, the same combined countermeasure as in test S18 was investigated, but with wider bed-sills ( $w_{bs}=7b$  and  $9b$ , respectively). The initiation and development of scouring were similar to those of test S18. In fact, in both tests S19 and S20 the scour could intrude towards the upstream part of the bed-sill from its lateral edges. The temporal evolution of scour depth upstream of the bed-sill in these two tests is shown in Fig. 150. This figure put in evidence that increasing the bed-sill width only produced an increase of the lag time of the scour reaching the upstream of the bed-sill. However, as the scour intrudes towards the upstream of the bed-sill, the scour depth increases with a high rate. This problem significantly reduces the stability of the bed-sill and consequently restricts the application of this combination when the bed-sill is not as wide as the flume. Tests S19 and S20 were suspended respectively after 56 and 81 h, before the equilibrium condition. Figure 151 shows the initial configuration and the scour hole at the end of test S19, whereas Fig. 152 the scour hole after 1 day and at the end of test S20.

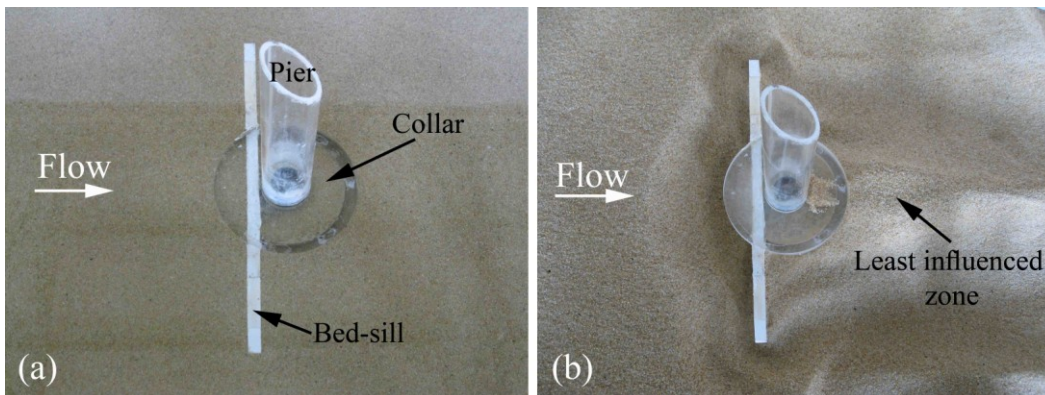


Fig. 151. (a) Initial configuration of test S19; (b) scour hole at the end of the test

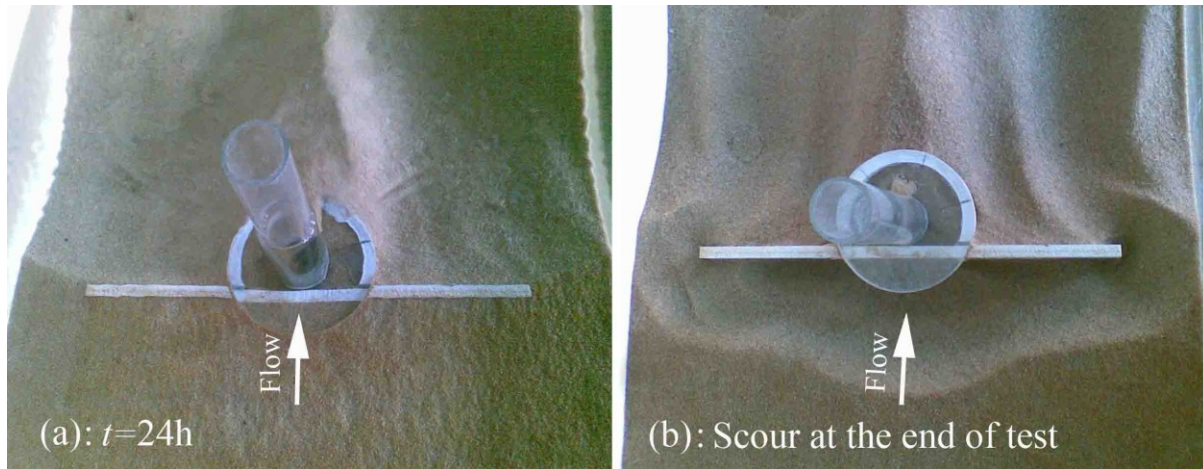


Fig. 152. (a) Scour hole after 1 day for test S20; (b) scour hole at the end of the test

In test S21 the performance of a  $6b$ -wide bed-sill with greater thickness was considered. In fact, the results of tests S15 to S20 (Tab. 28) showed that, when the bed-sill cannot be as wide as the watercourse for practical reasons, a good compromise is represented by the width of  $6b$ , for which the maximum scour depth adjacent to the pier was not too high than in the case of full width. The thickness of the bed-sill was selected equal to the pier width  $b$  due to the following reasons:

1. the results of tests S14 and S15 show that the bed-sill may protect scour intrusion to upstream of the bed-sill as the distance between bed-sill and pier slightly increases. In fact, this phenomenon is sensitive to that distance and it is probable that in higher flow intensities the bed-sill in the configuration of test S15 cannot prevent scour intrusion upstream of the bed-sill from the rim of the collar as shown in Fig. 153a. This phenomenon was observed in tests S13 and S14. Therefore, by increasing the bed-sill thickness these zones will be a part bed-sill as shown in Fig. 153b;
2. the edges of bed-sill provide better resistance against scour intrusion upstream of the bed-sill, since the grooves need to extend more in order to reach the upstream of the sill.

Also in test S21 the scour began in the form of two grooves downstream of the collar, as shown in Fig. 154a; an observation after about 42.7 h showed that the scour intruded to the upstream part of the bed-sill. The test was stopped after about 52.17 h, before achieving the equilibrium condition (Fig. 154b). In this test, the maximum scour depth in the movable bed which was observed downstream of the bed-sill as well as the scour depth in front of the bed-sill were monitored (Fig. 155). Although the maximum scour depth in the movable bed was observed downstream of the bed-sill during the test and at its end, owing to the high scouring rate in front of the bed-sill it is highly probable that the maximum equilibrium scour depth can be found in front of the bed-sill, as in tests S17 and S18.

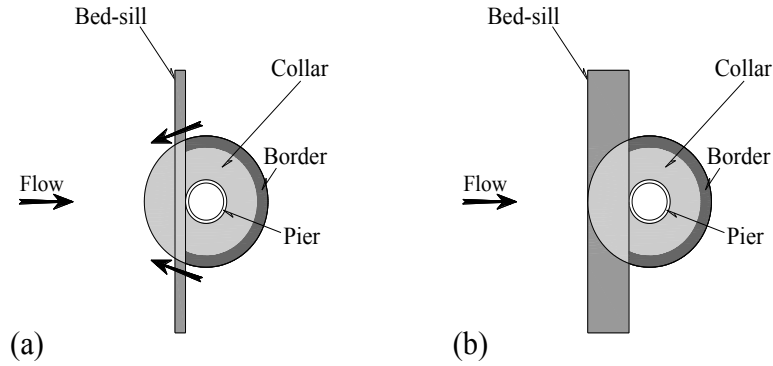


Fig. 153. (a) Location of possible passage of scour towards upstream of the bed-sill; (b) improved configuration in test S21

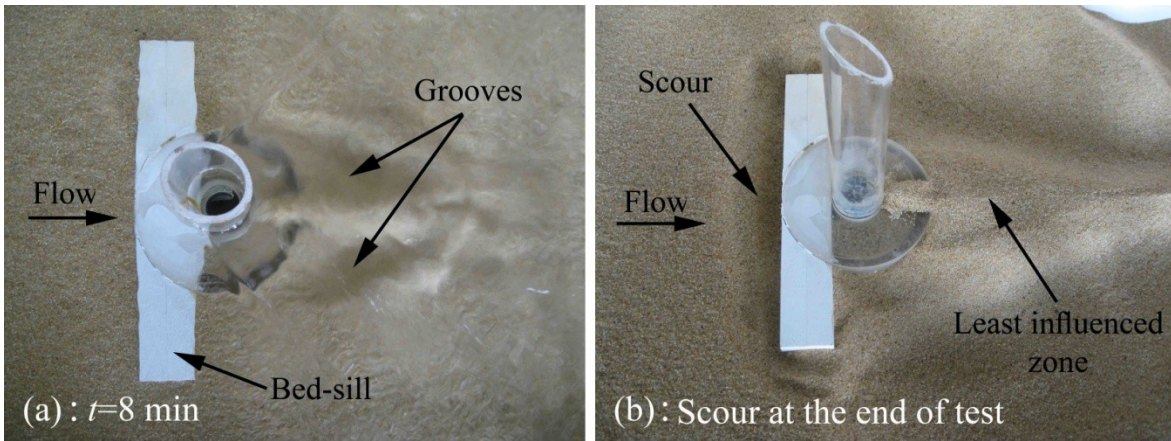


Fig. 154. (a) Grooves at  $t=8$  min in test S21; (b) scour hole at the end of the test

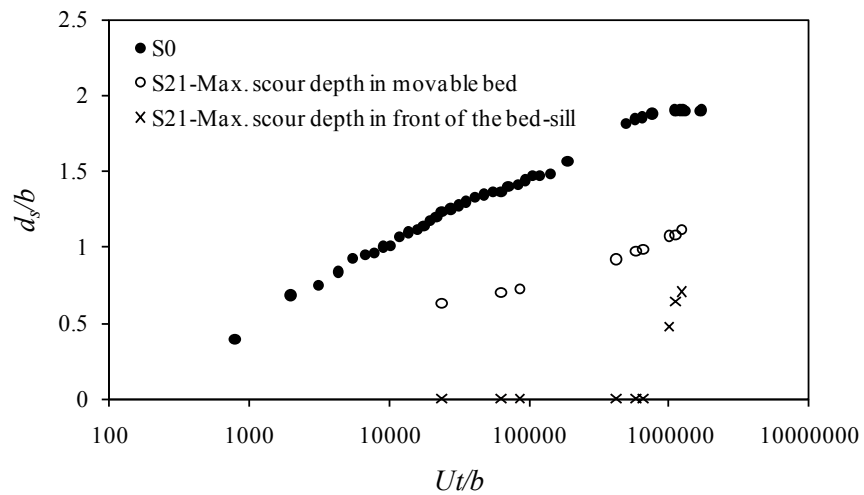


Fig. 155. Temporal evolution of the maximum scour depth in tests S0 and S21

The results of test S21 show that the thickness of  $b$  is not enough for the bed-sill to protect the sediments upstream of it, owing to the fact that the scour progresses laterally with respect to the sill sides towards upstream. In test S22, two 1 cm-thick PVC plates with length  $l_{sw}=b$  and flush with the bed were added orthogonally to both edges of the bed-sill, in order to prevent scour intruding to its front side (Figs. 156a and 157). The bed-sill dimensions in test S22 are the same as in test S21. Also the scour initiation and development are similar to the previous ones; however, the scour could not reach the upstream part of the bed-sill. In test S22, the maximum scour depth in the movable bed was monitored and compared with that around the unprotected pier of test S0 (Fig. 158). At equilibrium condition, the scour reached the upstream edge of the side-walls. The maximum scour around the border was about 2.7 cm and the scour intruded under it ( $t_{cb}=2$  cm). Figures 156b,c and 157 show bed materials around the pier and contour lines of equilibrium scour hole at the end of test, respectively. In this test, the collar could not be detached from the bed-sill and the bed level beneath the collar was not acquired by laser scanner. However, direct observation of the scour hole from inside the pier clarified that the scour did not reach the pier. Based on maximum scour depth under the collar and border, an efficiency of 64.5% was obtained using this combined countermeasure.

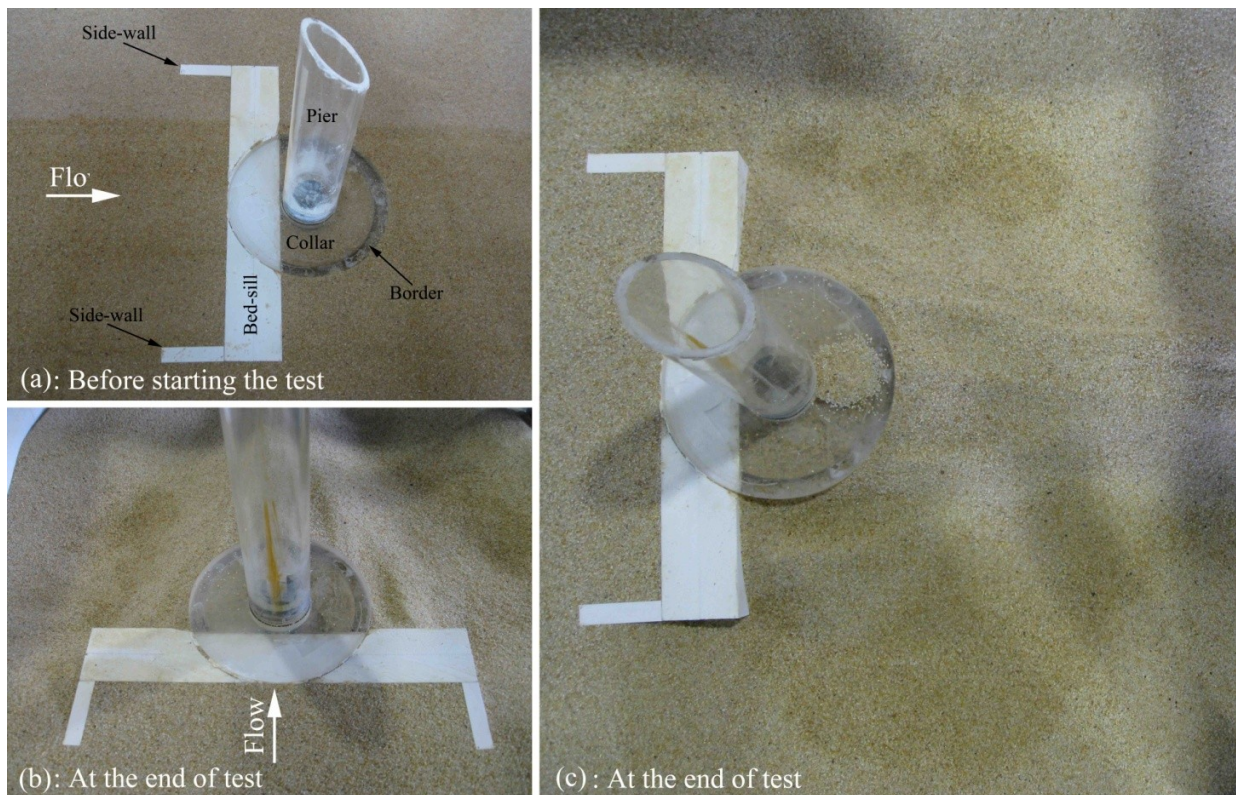


Fig. 156. Movable bed in test S22: (a) initial configuration; (b, c) at the end of the test

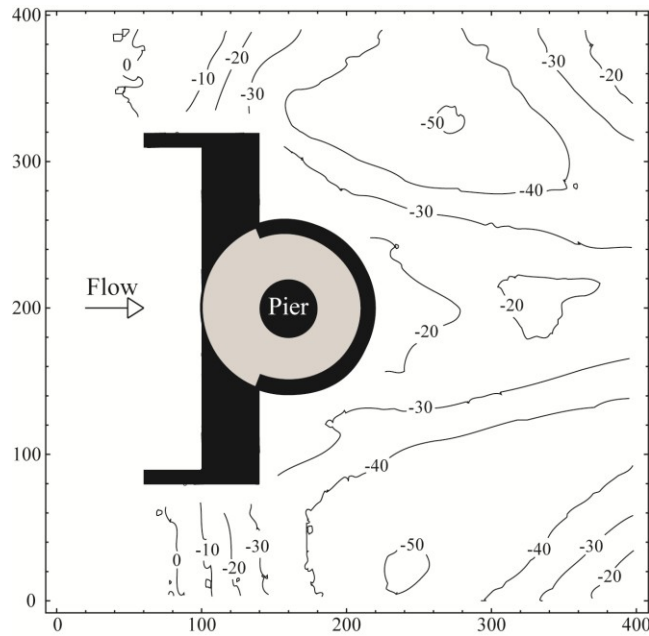


Fig. 157. Contour lines of equilibrium scour hole in test S22 (units: mm)

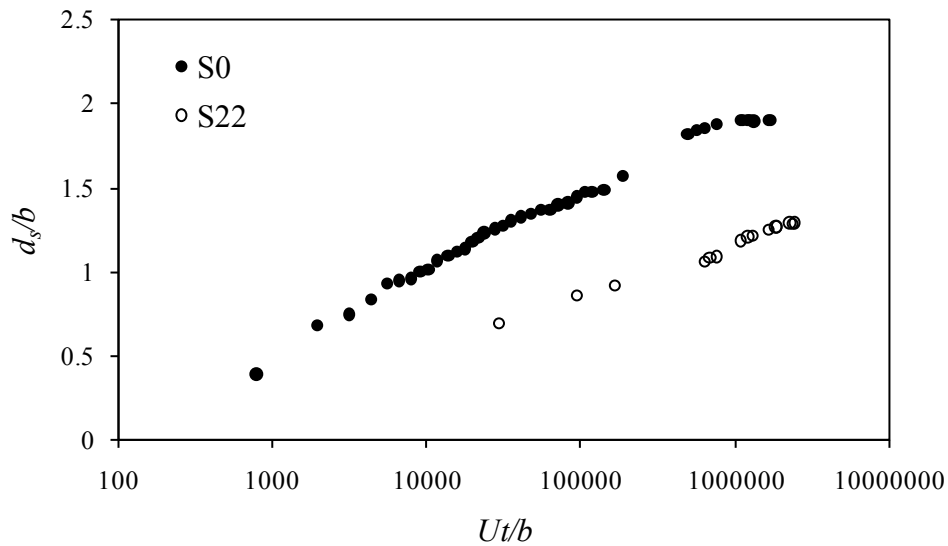


Fig. 158. Temporal evolution of the maximum scour depth in the movable bed in tests S0 and S22

### 5.2.9.3. Recommended configuration for design

Based on the results of this study, a combination of a collar and a single bed-sill as wide as  $9b$  cannot protect the scour intrusion from downstream to upstream of the bed-sill and, although a combination of a bordered-collar and a bed-sill (with the bed-sill upstream and adjacent to the pier) can protect bed sediments around the pier, a deep scour in front of the bed-sill may threaten

its stability and consequently pier safety. Therefore, in a correct design the preference should be given to the bed-sill as wide as the watercourse. As mentioned before,  $t_{bs}$  should be at least equal to the pier width ( $t_{bs}=b$ ), in order to avoid the probable passage of scour from downstream to upstream of the bed-sill. The maximum scour depth beneath the collar in test S15 was about 18 mm which is slightly less than  $b/2$ . Therefore, for a safer design the thickness of the bordered-collar,  $t_{cb}$ , is recommended to be at least equal to  $b$  (Fig. 159).

Therefore, the proposed countermeasure can be shown in Fig. 160. The dimensions of this countermeasure are presented in Tab. 29, which is also related to the lower priority configuration discussed in the remaining part of the present section. In fact, the combination of a  $b$ -thick bed-sill adjacent to a pier protected with a collar is equivalent to a bed-sill and a cut-collar, since the upper part of the collar can be a part of the bed-sill (compare Figs. 160 and 153). In this configuration, bed-sill thickness equal to  $b$  is respected for the whole channel width. However, a smaller thickness probably is adequate near the channel walls, since the influence of the pier reduces as the distance from it increases (Fig. 161). More experiments are necessary to find the exact dimensions of such a bed-sill.

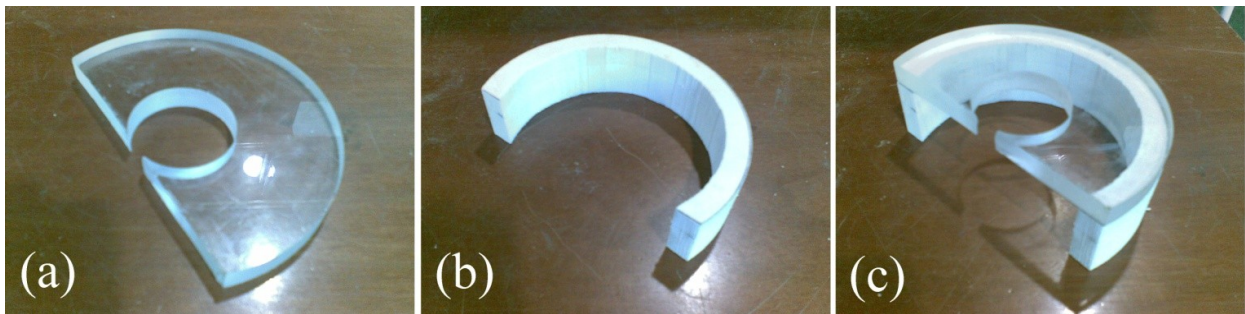


Fig. 159. (a) A cut-collar; (b) border; (c) a bordered cut-collar ( $t_{cb}=b$ )

Tab. 29. Definitions and recommended values for the best configuration

Parameter	Definition	Minimum recommended value	
		Configuration with higher priority (Fig. 160)	Configuration with lower priority (Fig. 166)
$l_{sw}$	Length of side-wall	-	$4b$
$t_{bs}$	Thickness of bed-sill	$b$	$b$
$w_{bs}$	Width of bed-sill	$B$	$8b$
$w_c$	Width of cut-collar	$3b$	$3b$
$t_{cb}$	Thickness of bordered cut-collar	$b$	$1.2b$

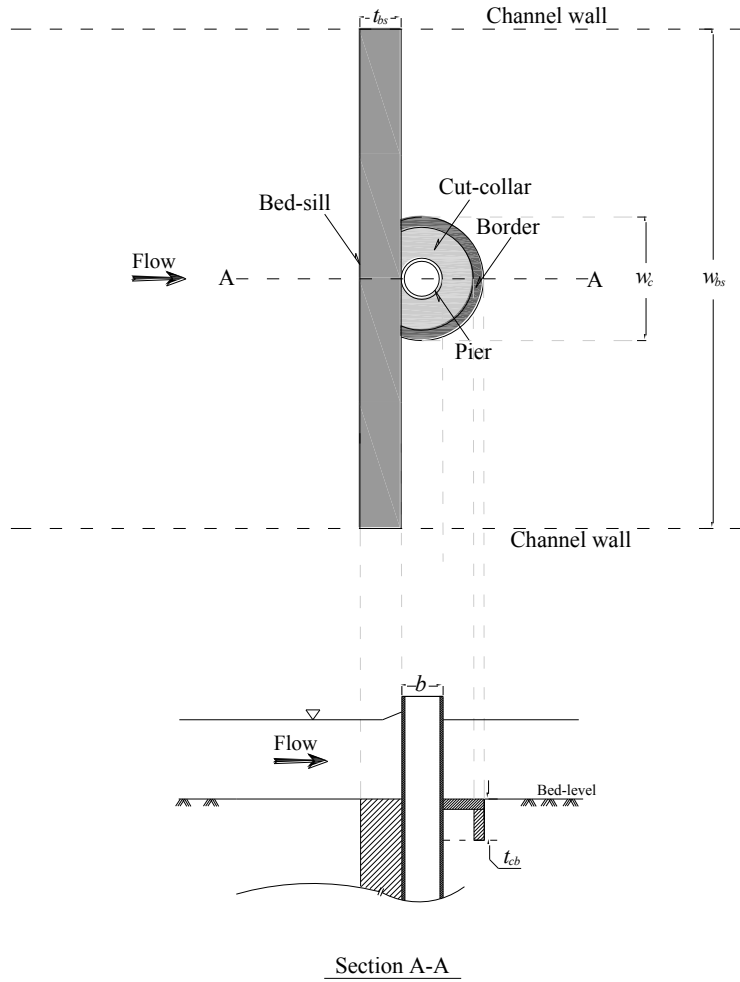


Fig. 160. Proposed configuration for pier protection with higher priority

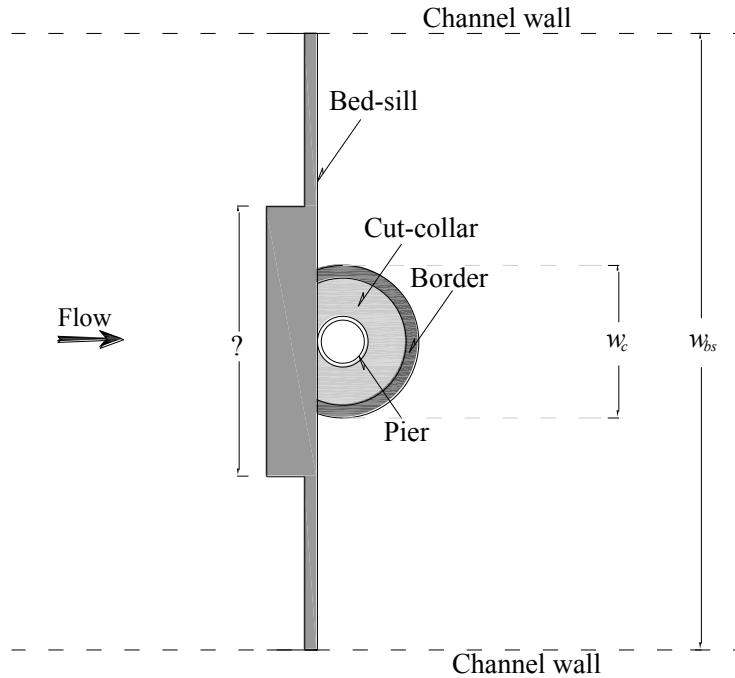


Fig. 161. Sketch showing possible optimum shape of the bed-sill

Test S23 was performed based on the recommended dimensions for the best configuration with higher priority. Figures 162 to 164 show the temporal evolution of the maximum scour depth in the movable bed, the contour lines of equilibrium scour hole and the movable bed at the end of the test, respectively.

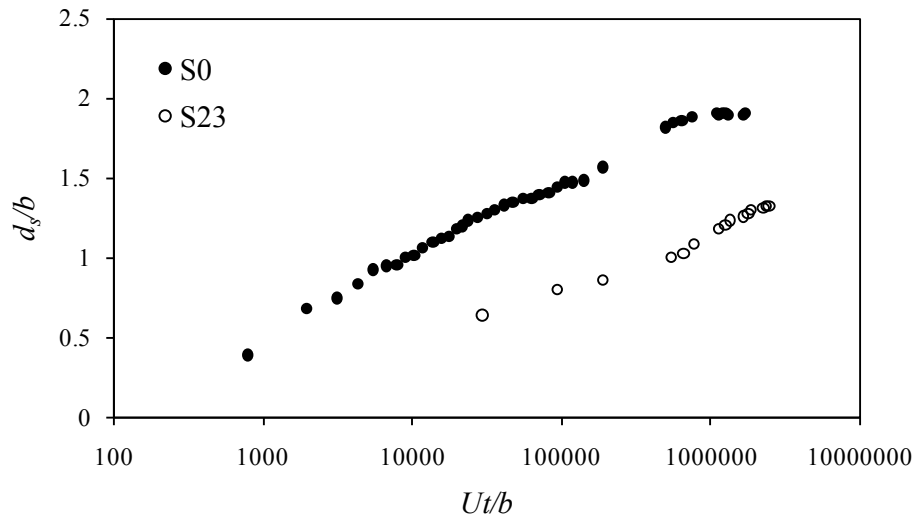


Fig. 162. Temporal evolution of the maximum scour depth in the movable bed in test S23



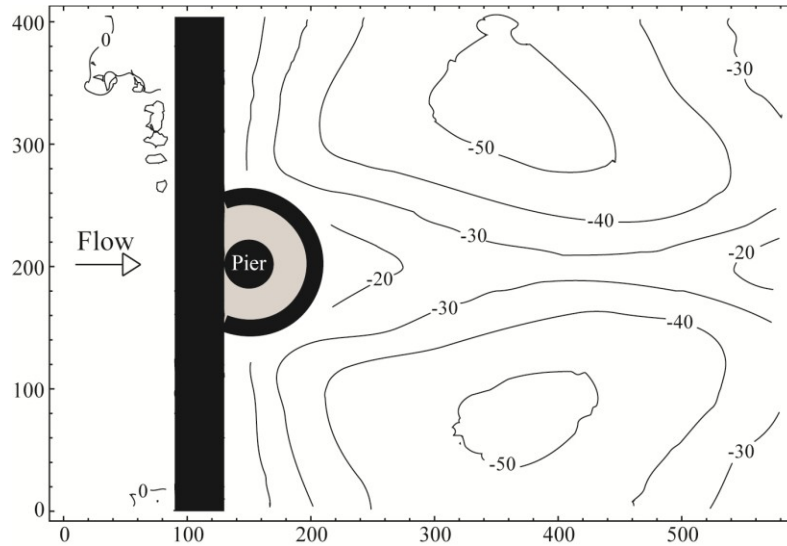


Fig. 163. Contour lines of equilibrium scour hole in test S23

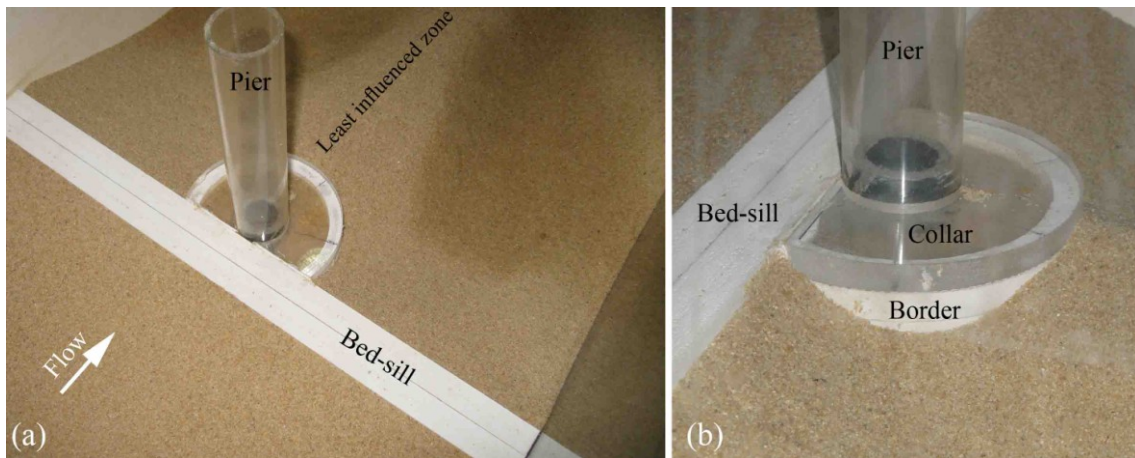


Fig. 164. (a) Movable bed at the end of test S23; (b) exposure of the border

As indicated before, although a bed-sill as wide as the channel is more reliable to prevent the scour intrusion to upstream of it, this configuration may be not applicable to all practical conditions. Therefore, a lower priority configuration is proposed on the basis of the results of test S22. In that test, the scour intruded near the edge of the sill side-walls and 7 mm under the 2cm-deep bordered-collar ( $d_{sec}=2.7$  cm). These conditions could be more critical if a deeper scour was observed in the movable bed. Figure 157 showed that the scour holes near the side-walls are the upstream portions of the two main scour holes downstream of the bed-sill. As the scour depth in these two main holes increases, the scour will intrude more towards the upstream lateral zones. In order to have a preliminary estimation about the maximum scour intrusion, referring to test S22 two arcs with radius  $r_1$  were drawn (centred in the locations of maximum scour depth downstream of the bed-sill; Fig. 165),  $r_1$  being the distance between each centre and the upstream uneroded bed. It is the intention to assess the maximum scour intrusion as the distance  $r_2$  in Fig.

165, computed as follows. The ratio  $d_{se0}/b=1.9$  in test S0 indicates that the maximum scour depth in front of the unprotected pier in the present study is about 20% less than the maximum possible scour depth ( $d_{se0}=2.4b$ ; see §2.8), i.e. the maximum possible scour depth can be assessed as  $1.2d_{se0}$ . If this condition is assumed to be valid also for test S22 and, further, if the average bed slopes along the directions of the right and left radii are considered to be constant (and equal to 1:3.5 and 1:4.6, respectively; see Fig. 165), then the maximum scour intrusion can be estimated as  $r_2=1.2r_1$ . This preliminary assessment shows that the scour border may intrude up to the edges of side-walls having  $l_{sw}=3b$ , as shown in Fig.165. Therefore, for a safe design  $l_{sw}=4b$  is recommended.

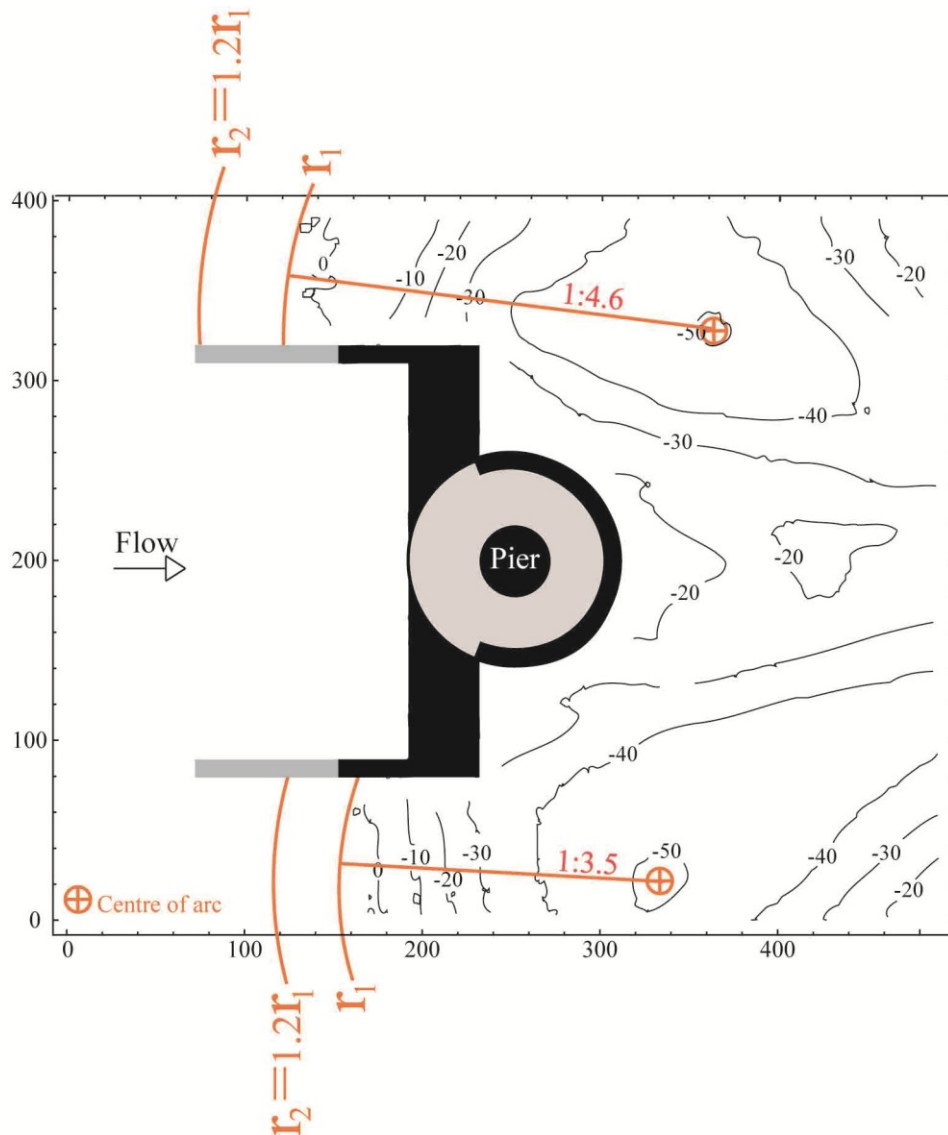


Fig. 165. Preliminary estimation of maximum scour intrusion to upstream of the bed-sill (units: mm)

In addition, in the case of scour intrusion inside the region between the side-walls, they probably will be able to reduce the erosion of bed sediments upstream of the bed-sill, since in the tests without side-walls the bed materials in this region were transported from the edges of the bed-sill towards downstream.

In test S22, the maximum scour around the collar border (having thickness  $t_{cb}=2$  cm) was about 2.7 cm and the scour intruded under it. If the maximum possible scour depth is assessed as  $1.2 \cdot 2.7$  cm=3.24 cm, then the thickness of the bordered collar should be designed as  $t_{cb} > 3$  cm  $\approx 0.8b$ ; therefore, for a safe design, a value of at least  $t_{cb}=1.2b$  is recommended.

Tests S17 and S18 show that the scour near collar and pier reduces as the bed-sill length increases. Therefore, for a better protection, it is recommended that bed-sill width increases up to  $w_{bs}=8b$ . All the recommended dimensions are presented in Tab. 29. Figure 166 illustrates a sketch of the proposed combined countermeasure with lower priority, based on the recommended values.

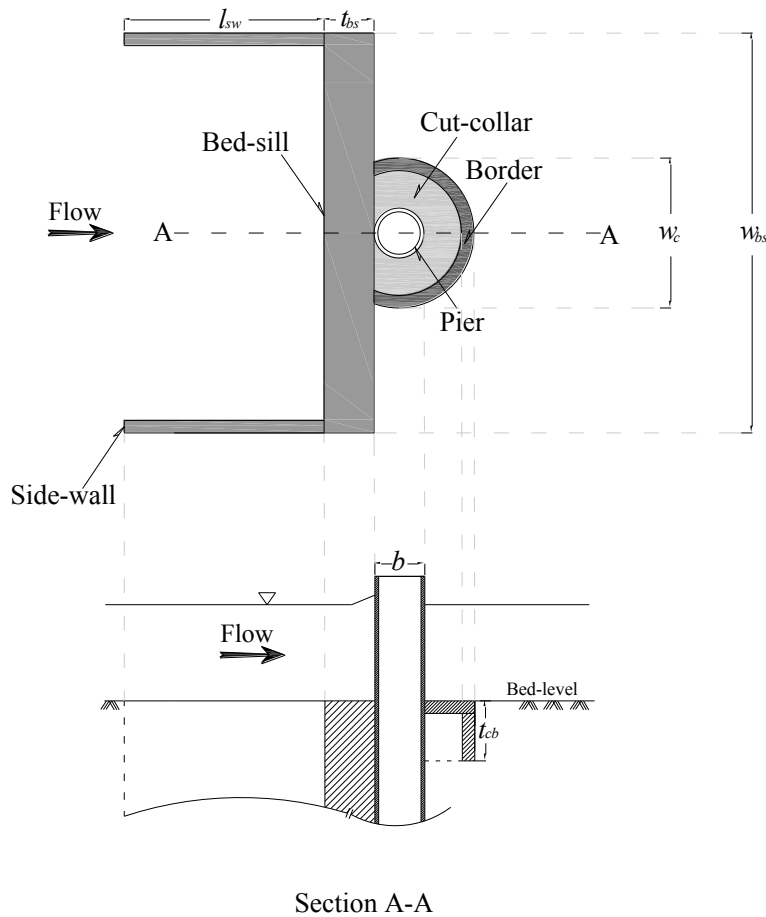


Fig. 166. Configuration of the proposed combined countermeasure with lower priority

### 5.3. Unsteady flow tests

In this section, the proposed combined countermeasure having lower priority, but wider applicability (wall-sided bed-sill and bordered cut-collar; Fig. 167), is applied for several pier configurations (Tab. 30) in unsteady flow conditions, in order to evaluate the adequacy of the countermeasure during floods.

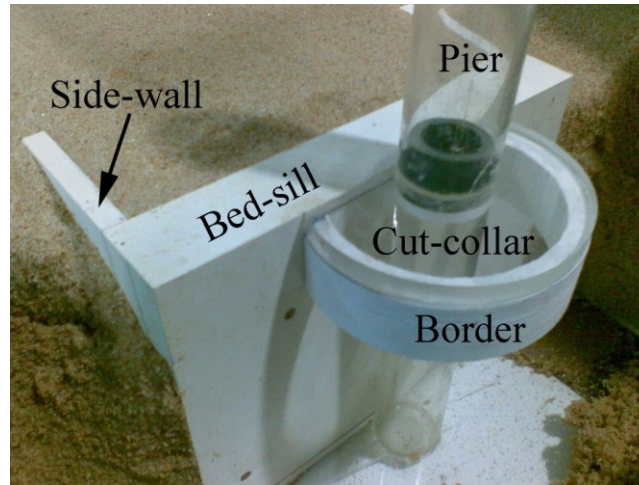


Fig. 167. Proposed combined countermeasure for unsteady flow tests

Tab. 30. Configurations of unsteady flow tests

Test	Pier shape and configuration	Pier dimensions	Clear-water/live-bed	$U/U_c$ (at flow peak)
U00	unprotected circular pier	$b=4$ cm	clear-water	0.92
U0	unprotected circular pier	$b=4$ cm	live-bed	1.1
U1	protected circular pier	$b=4$ cm	live-bed	1.1
U2	unprotected round nose and tail rectangular pier	$b=4$ cm $L=6b=24$ cm	live-bed	1.1
U3	protected round nose and tail rectangular pier	$b=4$ cm $L=6b=24$ cm	live-bed	1.1
U4	two in-line unprotected circular piers	$b=4$ cm	live-bed	1.1
U5	two in-line protected circular piers	$b=4$ cm	live-bed	1.1
U6	two in-line unprotected round nose and tail rectangular piers	$b=4$ cm $L=6b=24$ cm	live-bed	1.1
U7	two in-line protected round nose and tail rectangular piers with separate countermeasures	$b=4$ cm $L=6b=24$ cm	live-bed	1.1
U8	two in-line protected round nose and tail rectangular piers with continuous countermeasure	$b=4$ cm $L=6b=24$ cm	live-bed	1.1

As discussed in Chapter 4, clear-water steady tests were performed near the threshold condition of sediment movement. Now, the flow intensity at the discharge peak in live-bed unsteady flow tests is slightly beyond the threshold ( $U/U_c=1.1$ , Tab. 30). Therefore, the combined countermeasure for unsteady flow tests was designed on the basis of the test with the same combined countermeasure in steady flow condition (test S22), with the difference that longer side-walls and thicker bordered cut-collar were employed for the sake of safety ( $w_{bs}=6b$ ,  $l_{sw}=2b$  and  $t_{cb}=b$ ; Fig. 167). Results will show that the selected configuration is adequate in order not to permit the intrusion of scour upstream of the bed-sill and under the collar.

### 5.3.1. Test U00

Test U00 was conducted in clear-water unsteady flow conditions, in order to constitute a reference case for the next live-bed unsteady flow test U0 with similar configuration of unprotected circular pier. As mentioned before, the peak flow of test U00 was equal to the constant discharge of the corresponding clear-water steady flow test, S22. Since the maximum scour depth occurs in front of the circular pier, a point gauge was used to measure its temporal development, with time steps of 10 min (Fig. 168).

During the first 10 min, the scour in front of the pier was negligible. The reason is that the discharge and consequently the flow intensity during the first 10 min period of the test was low and, in addition, the scour phenomenon started at both sides of the pier, at an angle of  $70\div 75^\circ$  with respect to the streamwise channel axis (Fig. 9), and later extended to the upstream face of the pier. Afterwards, the scour increased rapidly in the first hour, during the raising limb of the hydrograph (Fig. 168). Then, the scour depth also increased, but with a lower rate. Finally, at about 110 min the scour depth development stopped.

Figure 169 shows the scour at the pier at the end of the test. The maximum scour depth  $d_{s,0}\approx 5$  cm was measured in front of the pier.

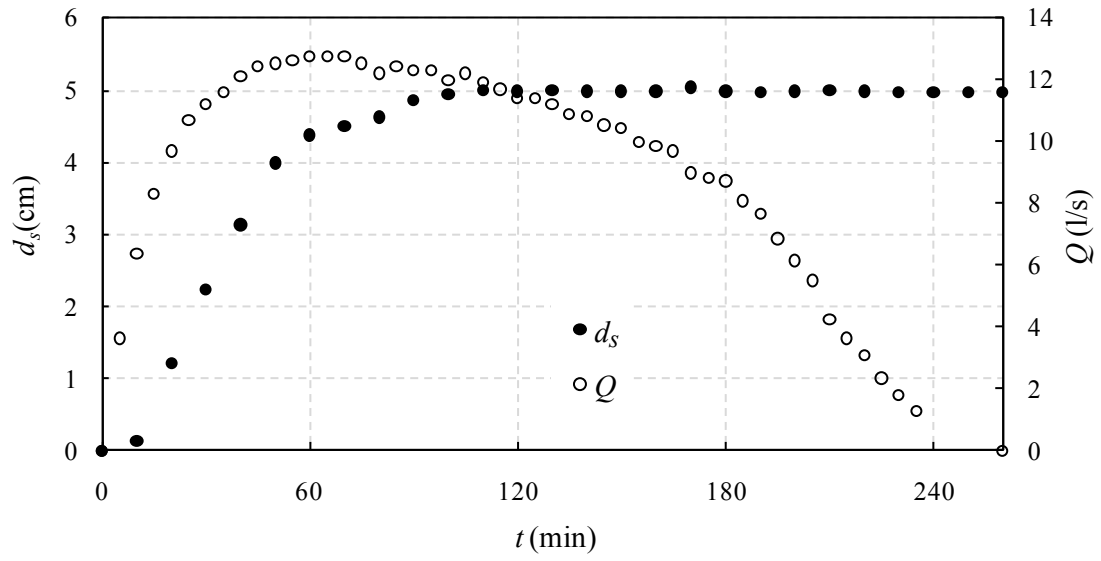


Fig. 168. Hydrograph and temporal evolution of scour depth in front of the pier in test U00

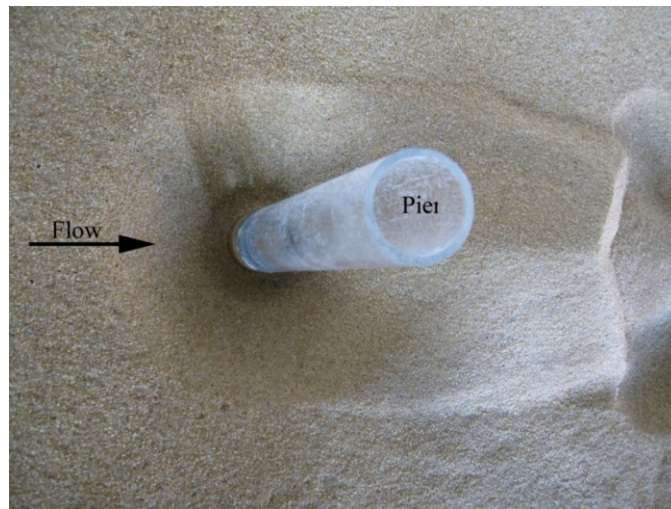


Fig. 169. Scour pattern at the end of test U00

### 5.3.2. Test U0

In test U0, an unprotected circular pier was subjected to a hydrograph with the peak in live-bed conditions. During the first 8 min of this test the scour migrated from the lateral sides of the pier to its front. After this period and until 80 min, the scour in front of the pier increased rapidly as the discharge increased (Fig. 170). Then the scour hole almost stopped its development, with some oscillations around the final value. The maximum scour depth during the test was  $d_{s0}=7.12$  cm, with which the efficiency was computed.

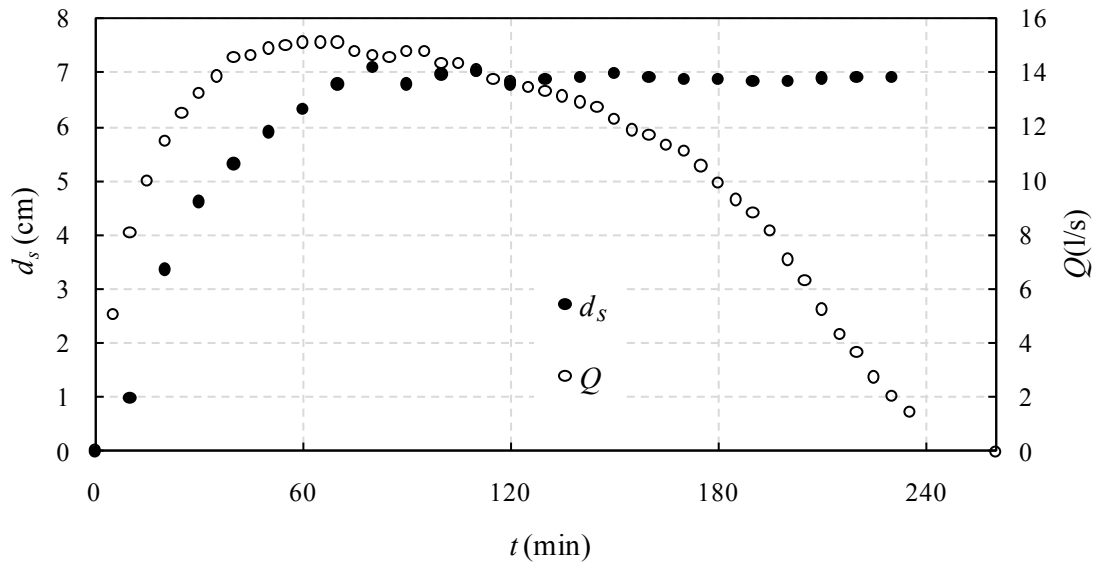


Fig. 170. Hydrograph and temporal evolution of scour depth in front of the pier in test U0

Figures 171 and 172 show the longitudinal profile of the scour hole in the plan of symmetry and the scour pattern at the end of the test, respectively.

Test U0 can be compared with both test S0 in clear-water steady flow conditions and test U00 in clear-water unsteady flow conditions. As to the first comparison, the maximum scour depth in test U0 is close to that measured at the end of test S0 in equilibrium conditions ( $d_{se0}=7.62$  cm; see Tab. 11). Since in test S0 the maximum scour depth was obtained near the threshold condition of sediment movement ( $U/U_c=0.92$ ), the obtained value  $d_{se0}=7.62$  cm is near the maximum possible scour depth for the selected pier size, sediment size, flow depth, etc. In test U0, the flow intensity is in live-bed condition ( $U/U_c=1.1$ ) (Fig. 173a). In fact, the maximum scour depth in test S0 was obtained slowly after several hours, whereas in the live-bed test U0 it was obtained quickly. Figure 173b shows that in live-bed conditions the maximum scour depth may be greater than the maximum scour depth in clear-water conditions; however, the equilibrium scour depth (defined as average scour depth during the passage of bed forms) is less than the maximum clear-water scour depth at equilibrium. In this study, owing to the fact that the flow intensity in live-bed condition is only slightly greater than 1, the fluctuations of the scour

depth were not clearly observed and maximum, minimum and average scour depths are almost identical and slightly less than the clear-water scour depths at equilibrium.

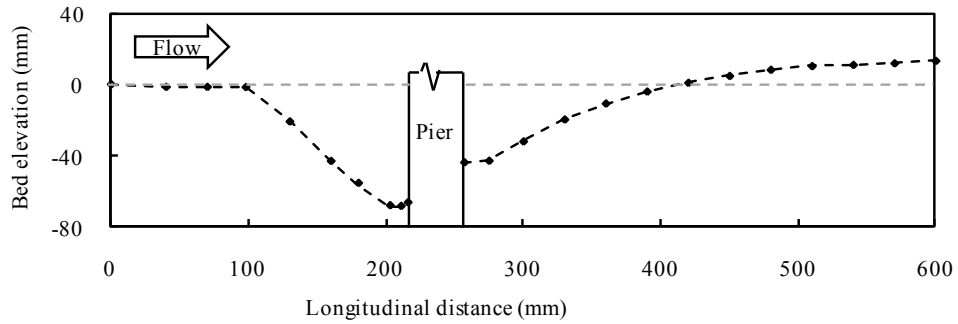


Fig. 171. Longitudinal profile of the scour hole in the plane of symmetry at the end of test U0

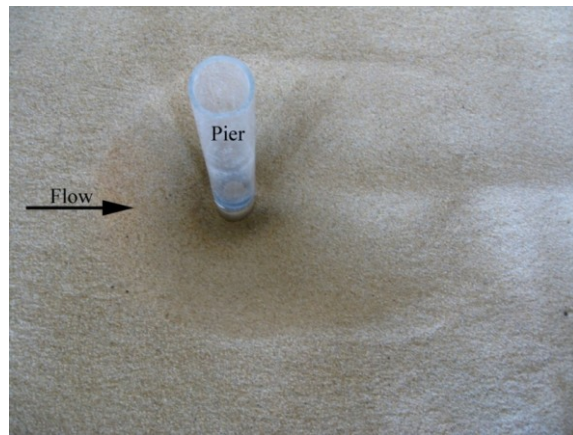
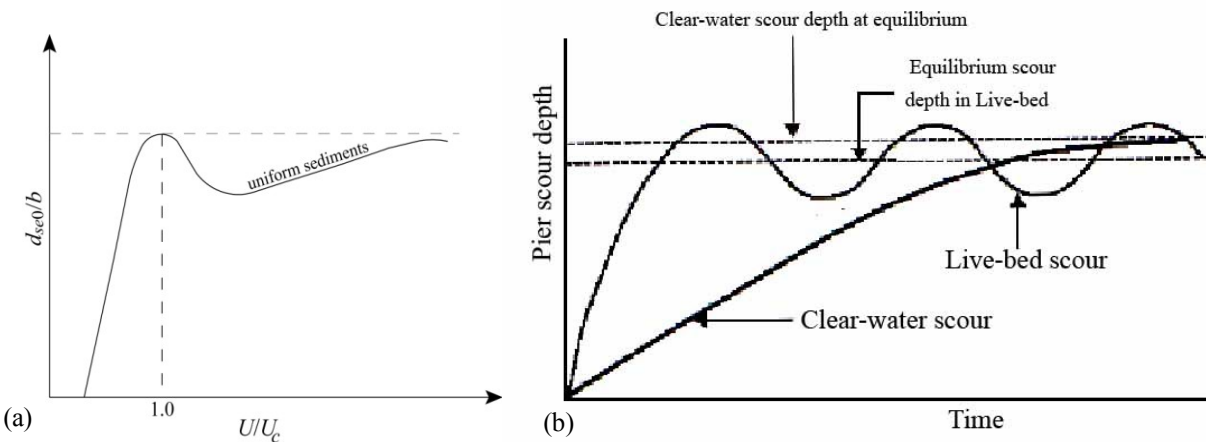


Fig. 172. Scour pattern at the end of test U0





**Fig. 173. (a) Variation of local scour depth with flow intensity (modified from Melville and Coleman, 2000); (b) temporal evolution of scour depth in clear-water and live-bed conditions**

Figure 174 shows the comparison of tests U00, U0 and S0. During the first 60 min of test S0, the scour depth reached 5 cm. This value was also obtained in test U00 during longer period of 110 min, after that the scour stopped increasing, owing to the decreasing flow intensity. On the other hand, in test S0 the scour rate also decreased after 60 min. Therefore, the scour depth in test S0 and U00 in period from 90 to 120 min were not notably different; however, scour depth in test S0 increased continuously to obtain a value of 7.62 cm at equilibrium (not shown in Fig. 174). Figure 174 clarifies that flow intensity values during the hydrograph propagation in test U00 were not enough for proper comparisons with the results of next tests, since the maximum scour depth in test U00 was much less than the maximum scour depth at equilibrium in test S0; however, the maximum scour depth in test U0 reached a value near the maximum scour depth in clear-water conditions (test S0) and, therefore, it can be used as a reference to evaluate the efficiency of the proposed combined countermeasure in unsteady flow conditions.

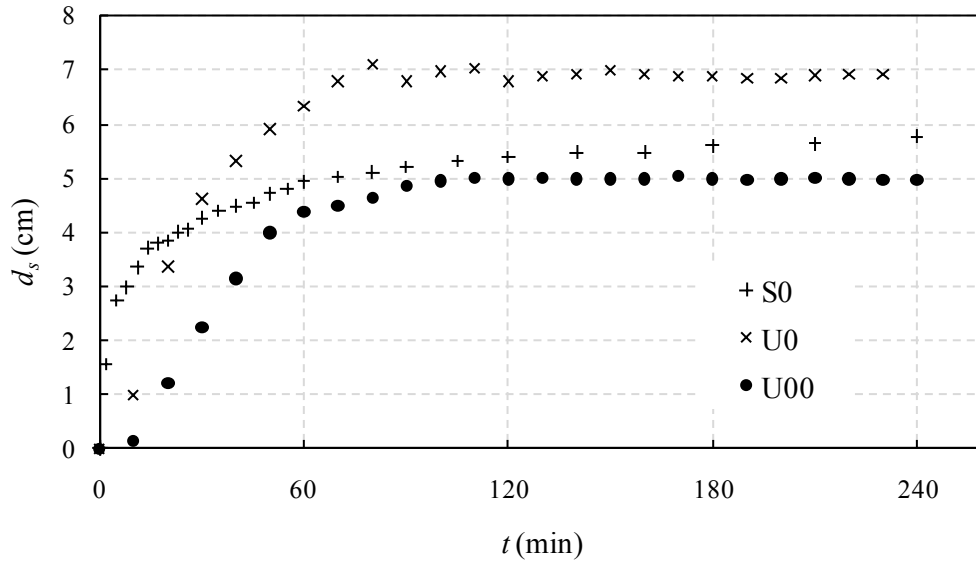


Fig. 174. Temporal evolution of the scour depth in front of the pier in tests S0, U0 and U00

### 5.3.3. Test U1

In test U1, the proposed combined countermeasure was applied to a single circular pier in live-bed conditions (Fig. 175). The temporal evolution of the maximum scour in the movable bed is presented in Fig. 176. As this figure shows, up to about 10 min the scour could not develop in any part of the movable bed. After this period, the scour developed downstream of the collar, as in the previous steady flow tests (S3 and S13 to S23) and grew rapidly in such a way that after a period of less than 30 min the scour extended to the bed-sill. At the end of the test, the maximum scour depth was adjacent to the bordered cut-collar and equal to  $d_{scb}=2.6$  cm. Figure 177 shows the scour hole at the end of test U1. The efficiency of the proposed combined countermeasure is equal to 63.5% (E.17).

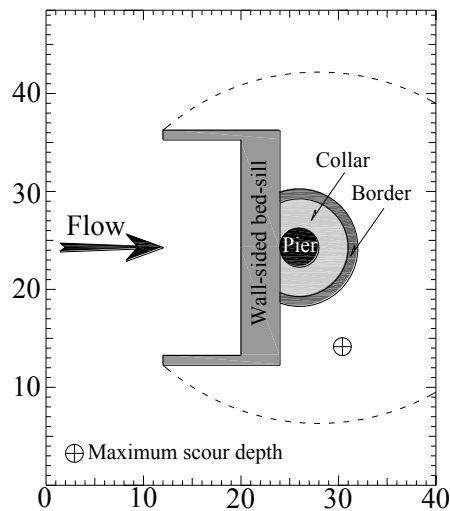


Fig. 175. Configuration and location of maximum scour depth at the end of test U1 (units: cm)

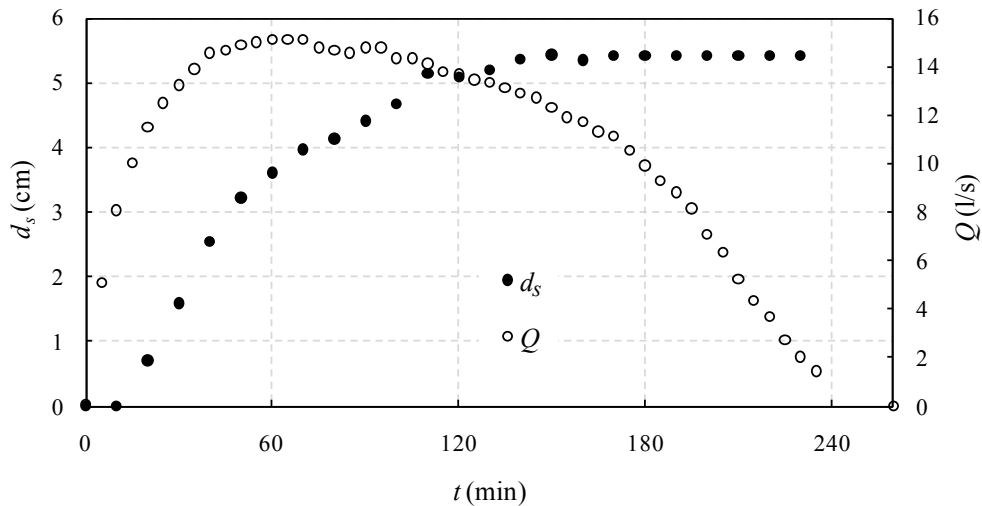
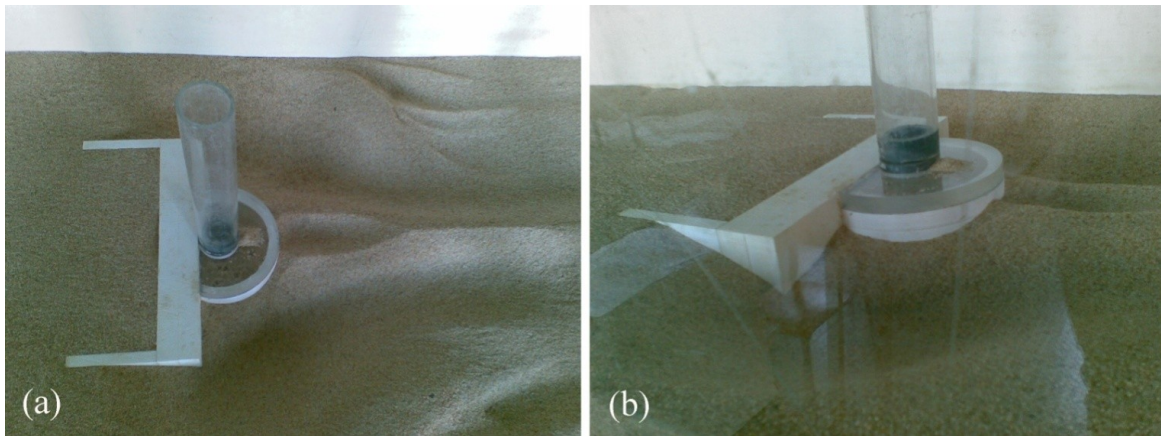


Fig. 176. Hydrograph and temporal evolution of the maximum scour depth in the movable bed in test U1



**Fig. 177. (a) General scour pattern of scour at the end of test U1; (b) close up of the scour hole near the border of the cut-collar at the end of the test**

### 5.3.4. Test U2

In order to evaluate the efficiency of the proposed combined countermeasure for a different pier shape, first an unprotected round nose and tail rectangular pier, which is very commonly used in the Calabria region, Italy (Cardoso *et al.*, 2010), was subjected to a live-bed hydrograph in test U2 (Fig. 178a), which constitutes the reference case for the next test U3 (protected pier, see Tab. 30).

Cardoso *et al.* (2010), on the basis of an extensive survey of 98 bridges in Calabria, found the average value  $L=5.8b$  for the pier length; therefore,  $L=6b$  was selected in the present study and the pier dimensions were  $b=4$  cm and  $L=6b=24$  cm (Tab. 30).

The initiation stage of this test is similar to that of an unprotected circular pier (test U0). During the first 8 min, two grooves developed at both the lateral sides of the pier and then extended to the upstream pier face. Figure 178b shows the scour hole in front of the pier at  $t=12$  min, once the two grooves joined together. Afterwards, the scour hole deepened in front of the pier and also extended laterally at both the pier sides in the streamwise direction. Excavated sediments formed two mounds at both the pier sides (Fig. 178c). As the flow rate increased, the mounds moved downstream with higher velocity and reached the rear of the pier, where they could accumulate (Fig. 178d). The scour extended continuously; however, after about 70 min, once the discharge started decreasing, the scouring rate also decreased, and after about 150 min the scour stopped increasing (Figs. 178e,f and 179). Figures 178e,f and 180 show the scour pattern and the profile of the scour hole in the plane of symmetry at the end of the test. The maximum observed scour depth was  $d_{s0}=6.25$  cm at  $t=120$  min. After this time, the maximum scour depth slightly reduced and the end of test it was equal to equal to 6.11 cm.

With respect to test U0 with an unprotected circular pier, in test U2 a 12% reduction in  $d_{s0}$  was observed. Although for an appropriate comparison long test duration is necessary, it seems that scour depth in longer piers may be reduced (Fig. 87). For round nose piers aligned with the flow direction, Richardson and Davis (2001) recommended the value of 1 for the pier shape factor,  $K_s$ , in the case of round nose pier, which seemingly may not be correct. In fact, Gao *et al.* (1993) recommended  $K_s=0.8$  for round nose piers. A long duration test is then needed in order to find a more accurate value for this parameter.

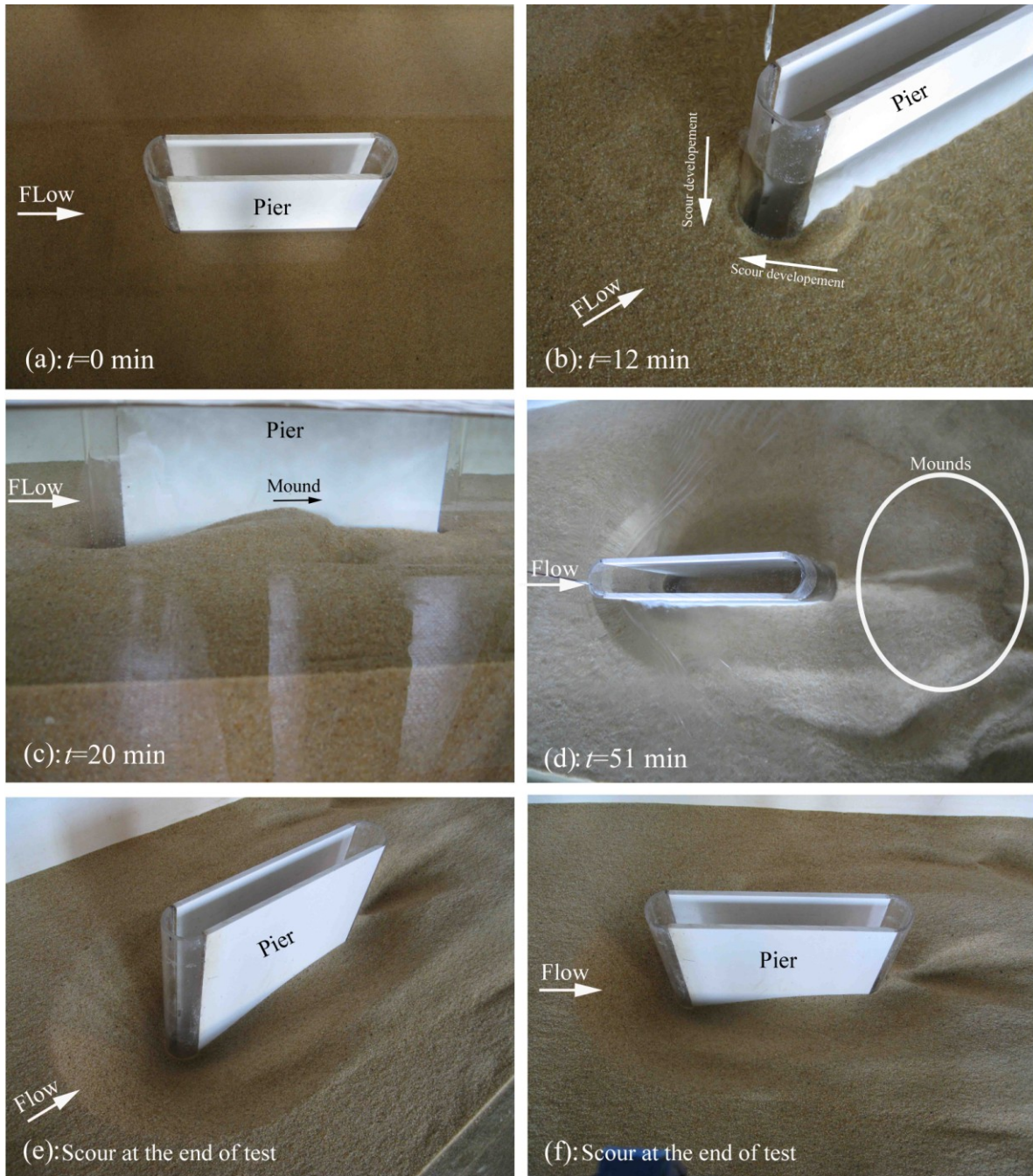


Fig. 178. Scour hole at different time instants in test U2

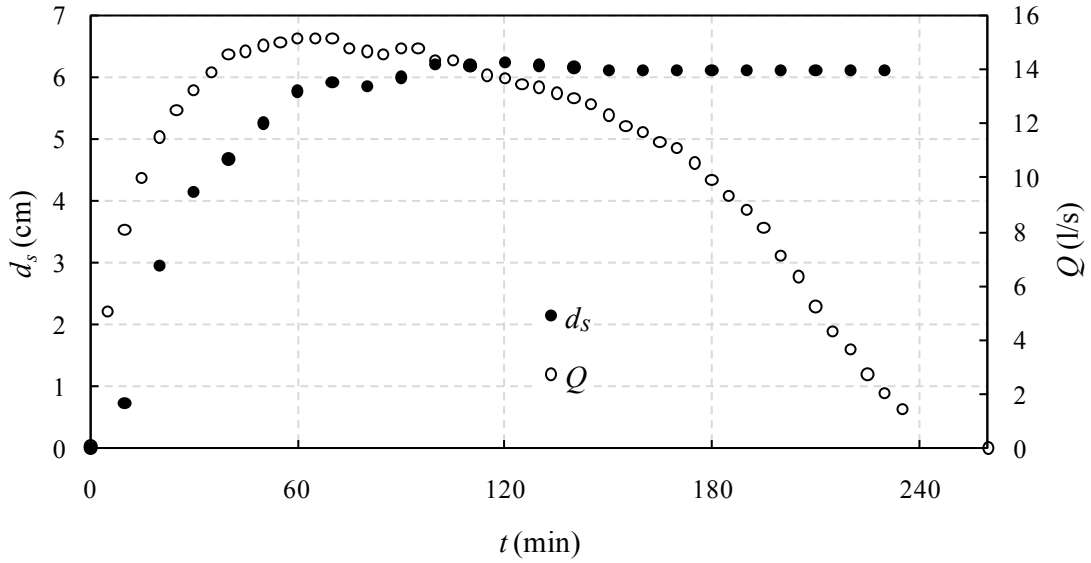


Fig. 179. Hydrograph and temporal evolution of scour depth in front of the pier in test U2

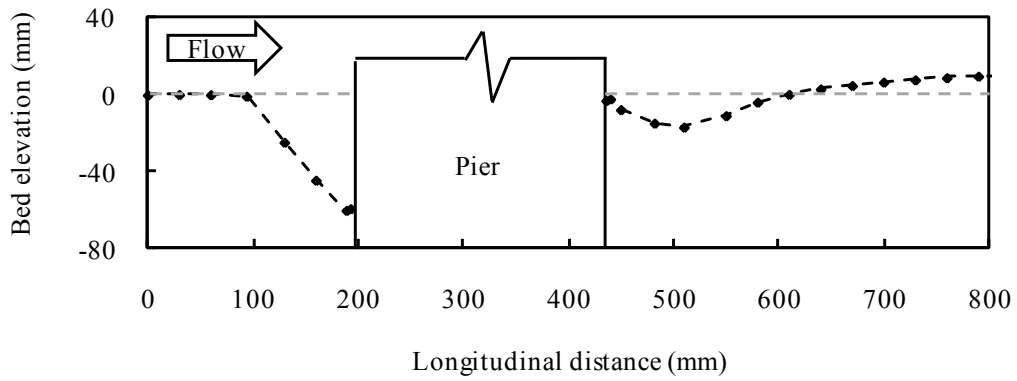


Fig. 180. Longitudinal profile of the scour hole in the plane of symmetry at the end of test U2

### 5.3.5. Test U3

In test U3, the same round nose and tail rectangular pier used in test U2 was protected with the proposed combined countermeasure (wall-sided bed-sill and bordered cut-collar; Fig. 181). During the first 20 min, scour did not occur in any part of the movable bed. After this period, it was observed along the rear side of the pier (Fig. 182, zone B). According to Zarrati *et al.* (2004) this type of scour is due to sucking effect of wake vortices.

In the case of circular pier protected with a collar in steady flow conditions (test S3), two grooves developed downstream of the collar and then extended to upstream part of collar and pier. The grooves at the rectangular pier of test U3 were much smaller than in test S3 and developed slowly. Two other scour holes occurred at the pier sides after 30 min (Fig. 182, zone A). Figures 183 and 184 show that these scour holes have less depth with respect to the downstream scour hole of zone B.

This test shows that, applying the proposed combined countermeasure, the scour depth around the round nose and tail rectangular pier is much less than that around the circular pier with similar protection. Therefore, the countermeasure is more effective when applied to round nose and tail rectangular piers and its stability is greater. The maximum scour depth,  $d_{sm}=1.52$  cm, was measured during the test in zone B of the movable bed (Fig. 182), with efficiency  $r_{ds}=78.7\%$ ; therefore, the efficiency with respect to the pier and countermeasure safety was greater than that. However, a long steady state test achieving the equilibrium conditions is necessary to evaluate the adequacy of this configuration.

Zarrati *et al.* (2004) showed that a  $3b$ -wide collar is more effective when it is used at a round nose and tail rectangular pier with  $L/b=5$  ( $r_{de}=74\%$ ) rather than at a circular pier (Mashahir *et al.*, 2004 obtained  $r_{de}=26.6\%$ ). Probably, round nose and tail rectangular piers interact with the wake vortex system in a positive manner with respect to circular pier, resulting in higher efficiencies.

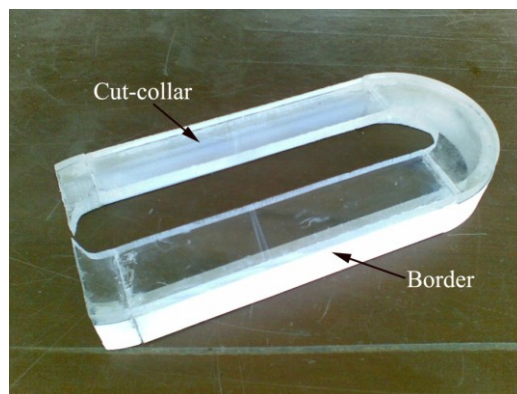


Fig. 181. Bordered cut-collar adapted to a round nose and tail rectangular pier ( $t_{cb}=b$ )



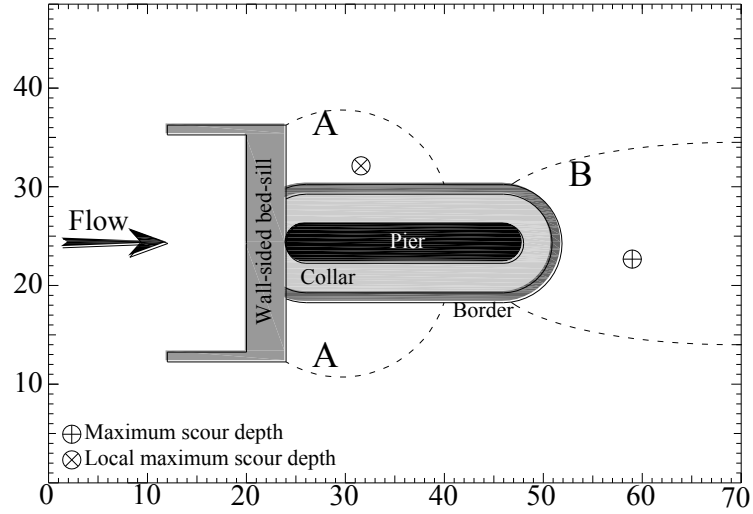


Fig. 182. Configuration and location of the maximum scour depths at the end of test U3 (units: cm)

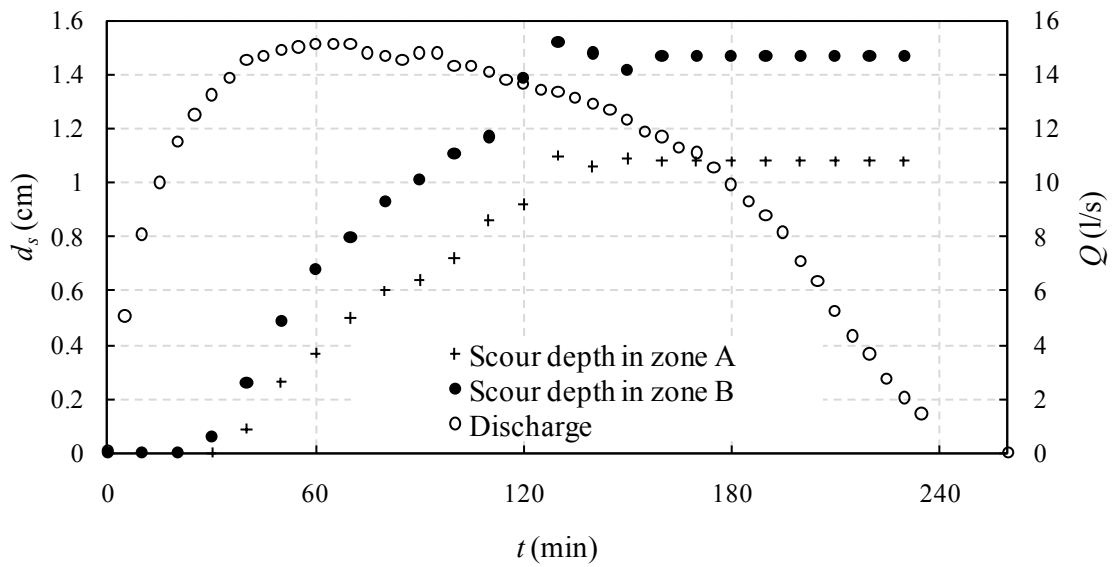
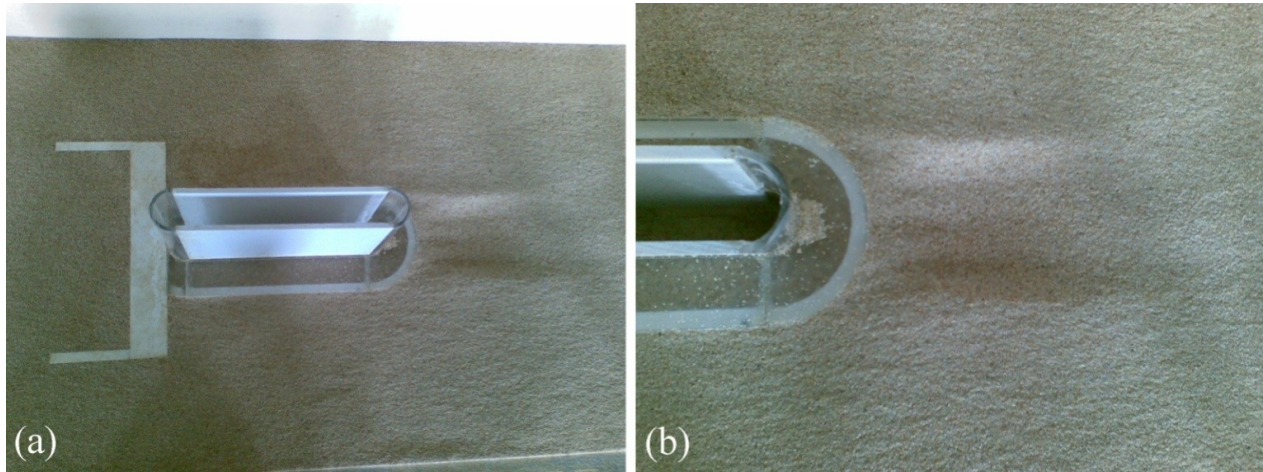


Fig. 183. Hydrograph and temporal evolution of the maximum scour depth in zones A and B in test U3



**Fig. 184. (a) Scour pattern at the end of test U3; (b) close up of scour hole downstream of the bordered cut-collar**

### 5.3.6. Test U4

In order to evaluate the performance of the proposed countermeasure for two in-line piers, configuration which is commonly found in Calabria (Cardoso *et al.*, 2010), tests U4 (two in-line unprotected circular piers) and U5 (two in-line protected circular piers) were conducted. The distance between the two piers in both tests was constantly equal to  $s=5b$  as found by Cardoso *et al.* (2010) (see Figs. 185 and 186a). In test U4, similarly to the previous unprotected pier tests, the scour started from the lateral sides of each pier and then extended to each pier front after about 8 min.

As the scouring started, a greater scour hole as well as a greater mound were found at the front pier (Fig. 186b). After about 20 min the mound tail of the front pier reached the rear pier and after it started to fill in the scour of the rear pier (Fig. 186c). This process caused a depression in the mound of the front pier; however, the mound of the rear pier rose up continuously (Fig. 186d). In fact, the shallower scour depth in front of the rear pier with respect to that in front of the front pier can be justified by the bed sediments coming from the front pier to the rear pier (Fig. 187).

An observation after about 40 min clarifies that the mound of the front pier was almost removed; however, the mound of the rear pier was significantly increased (Fig. 186e). During the test, the region between the two piers was eroded and its elevation was less than the initial bed level; a small mound still remained downstream of the rear pier at the end of the test (Fig. 188). The final scour hole is presented in Fig. 186f. The maximum scour depth in front of the front and rear piers are  $d_{s,0}=7.14$  cm and 6.12 cm, respectively. In fact, the maximum scour depth in front of the front pier is almost the same as for the unprotected single pier (test U0); however, this value for the rear pier is less than that for the single pier or for the front pier in the case of two in-line piers.

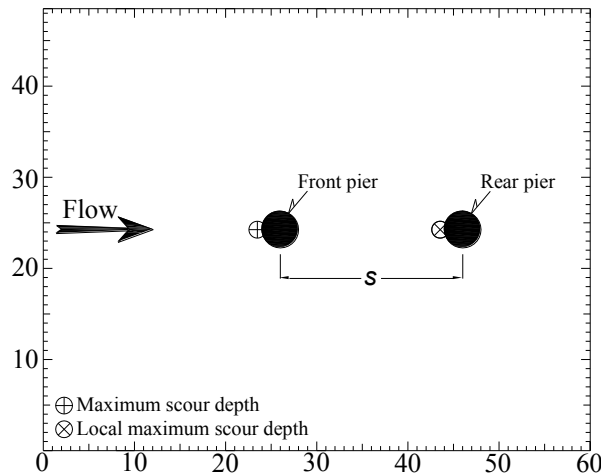


Fig. 185. Configuration of test U4 and location of the maximum scour depths at the end of the test (units: cm)

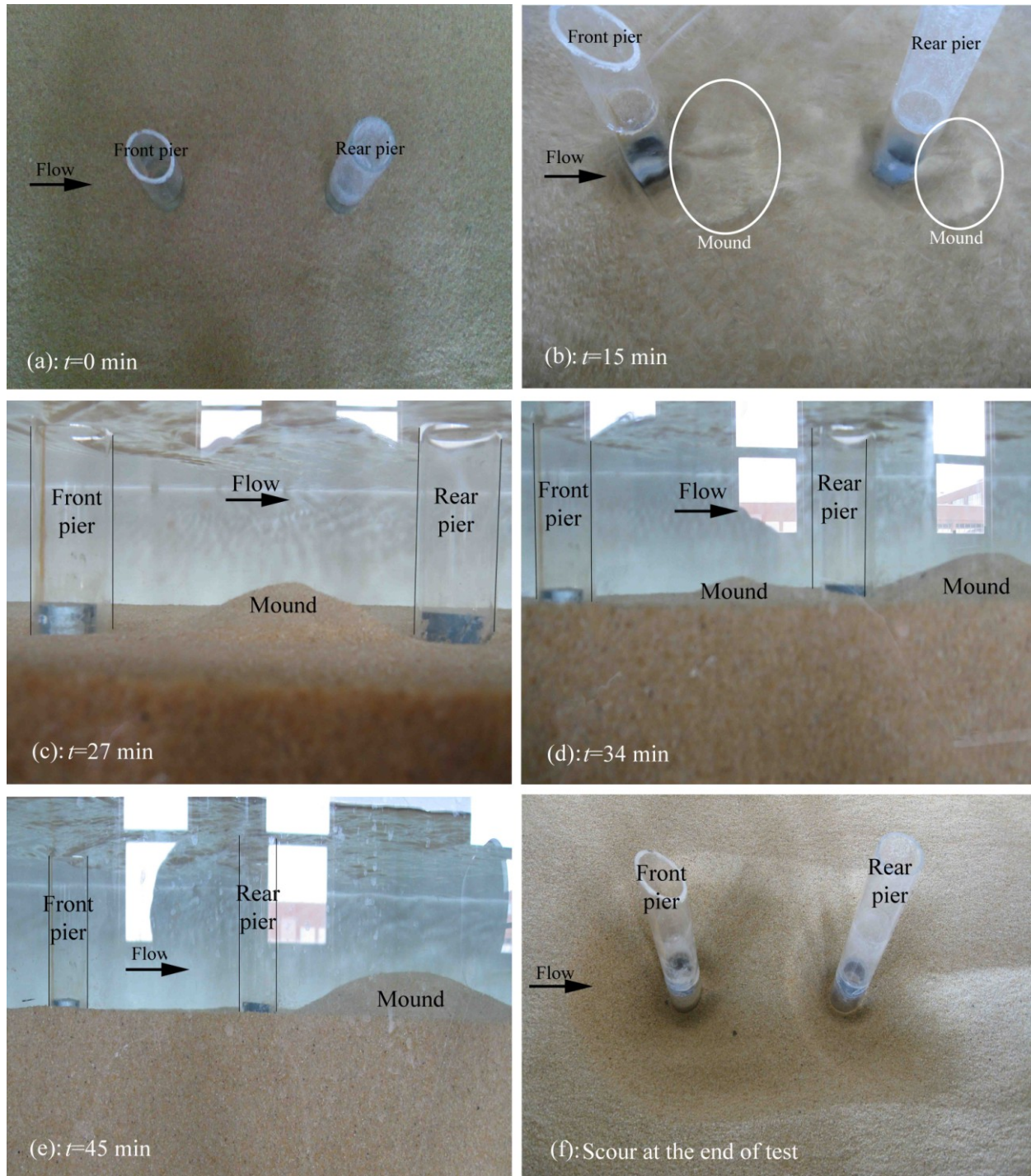


Fig. 186. Scour development in test U4

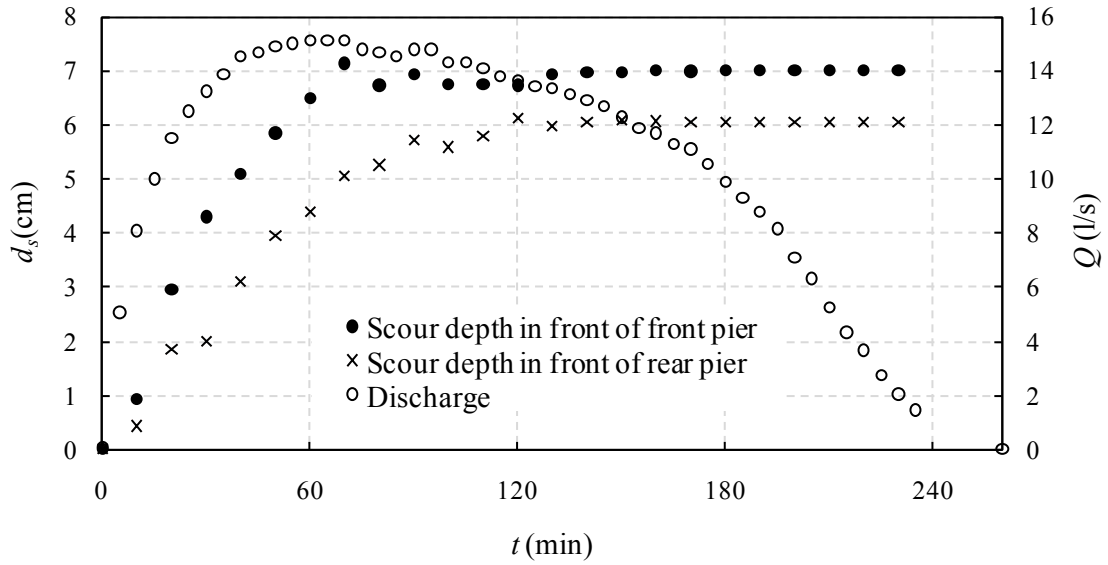


Fig. 187. Hydrograph and temporal evolution of scour depth in front of the piers in test U4

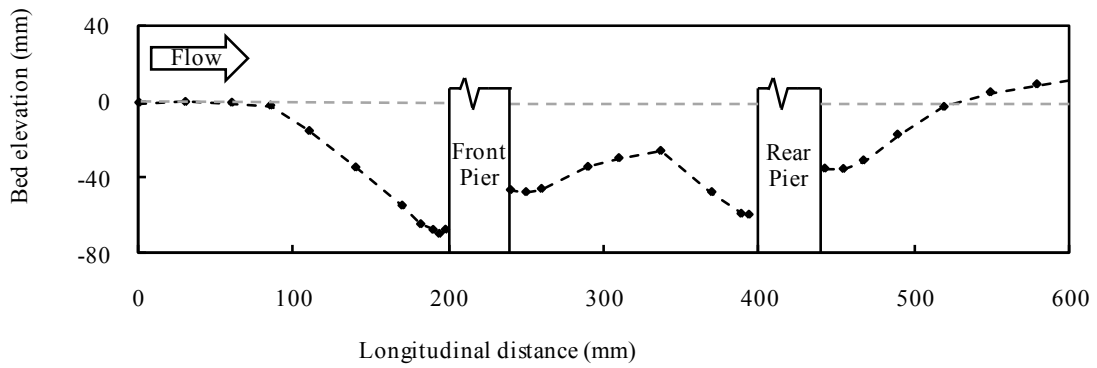


Fig. 188. Longitudinal profile of the scour hole in the plane of symmetry at the end of test U4

### 5.3.7. Test U5

In test U5, the same configuration of test U4 (two in-line circular piers) is protected with the proposed combined countermeasure (Fig. 189). Up to 10 min after starting this test, the scour around the tested configuration was almost negligible (Fig. 190). After this period, two grooves developed and extended continuously downstream of the collar in zone B (Fig. 191a). After 30 min, two grooves also started developing near the front pier (Fig. 189, zone A), probably owing to the turbulent flow around it (Fig. 191b). The sediment scoured in zone A were also transported to the downstream grooves, preventing them from being deeper in the period from 50 to 90 min (see Fig. 190). After about 80 min, the scour rate in the upstream scour hole decreased, and the downstream scour slowly started deepening again. At the end of the test, the maximum scour depths in the upstream and downstream scour holes were almost equal each other, and the maximum exposure of the bordered cut-collar was 1.7 cm (1 cm of the collar thickness plus 0.7 cm of the border thickness) (Fig. 191c). The upstream scour was also blocked by the bed-sill and therefore could not extend upstream of the front pier nor threaten the stability of the collar. Test U5 also shows that the proposed combined countermeasure is more effective with two in-line circular piers rather than a single one, since the maximum scour depth in the movable bed was less than that in the single pier case (test U1). Figure 191d shows the scour pattern at the end of test U5.

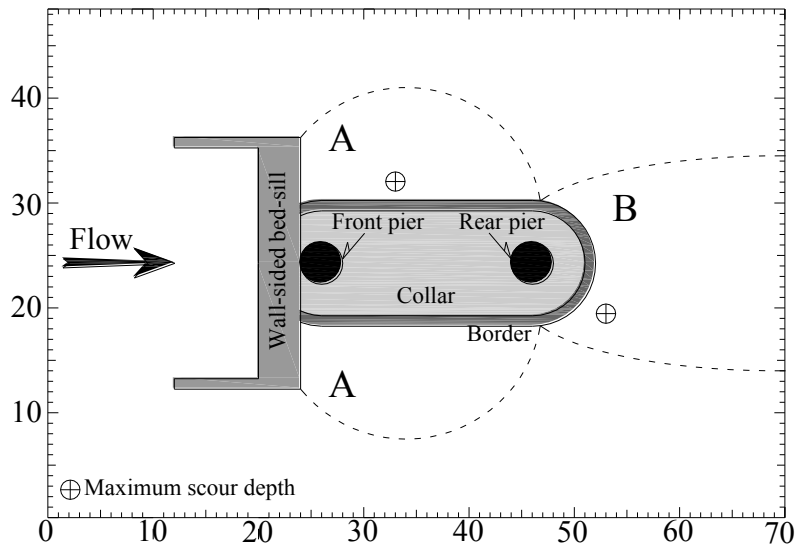


Fig. 189. Configuration and location of the maximum scour depths at the end of test U5 (units: cm)

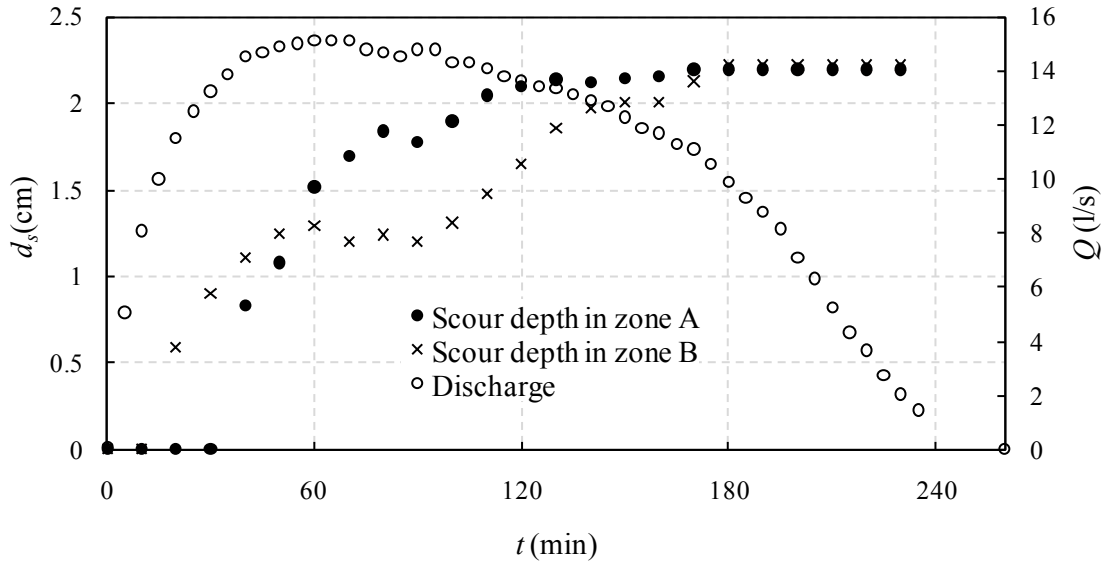


Fig. 190. Hydrograph and temporal evolution of the maximum scour depth in zones A and B in test U5

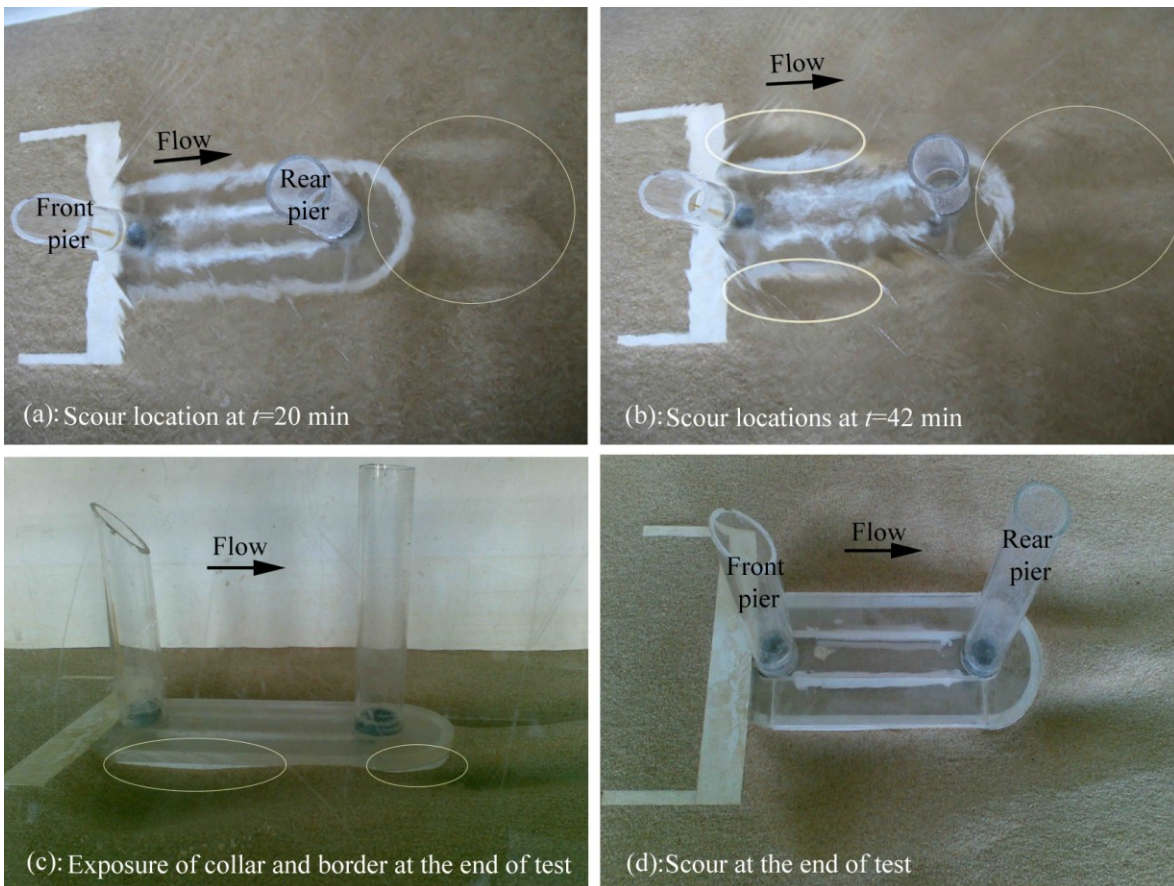


Fig. 191. Scour pattern at different times in test U5

### 5.3.8. Test U6

In test U6, two in-line round nose and tail rectangular piers with a distance of  $s=5b$  were considered (Fig. 192). During the first 8 min, two scour holes developed at the lateral sides of each pier and then moved towards the upstream face of each pier, until the end of the test. The temporal evolution of the scour depth in front of each pier is shown in Fig. 193.

The maximum scour depth in front of the front and rear piers were  $d_{s0}=6.2$  and 5.52 cm, respectively. These values are slightly less than what obtained in the case of two in-line circular piers (test U4). The transportation of eroded sands from the front pier to the rear one justifies that a smaller scour depth was found at the front of the rear pier with respect to the other. Longitudinal profile of the scour holes in the plane of symmetry and the scour holes at the end of the test are shown in Figs. 194 and 195, respectively.

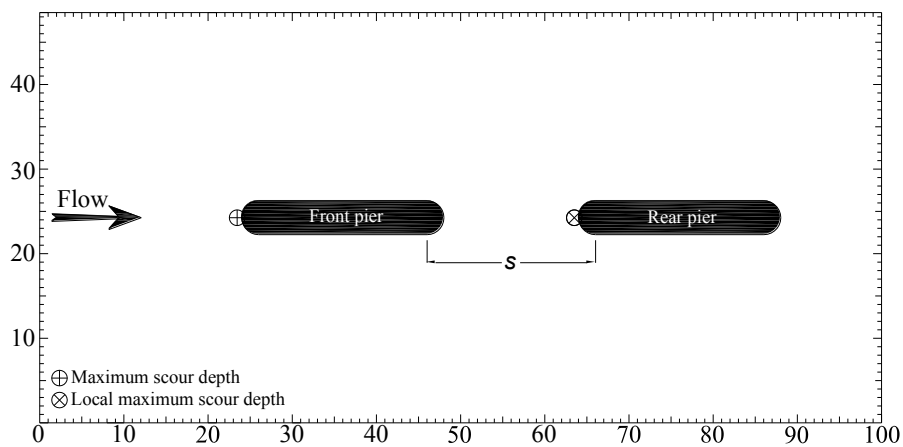


Fig. 192. Configuration and location of the maximum scour depths at the end of test U6 (units: cm)

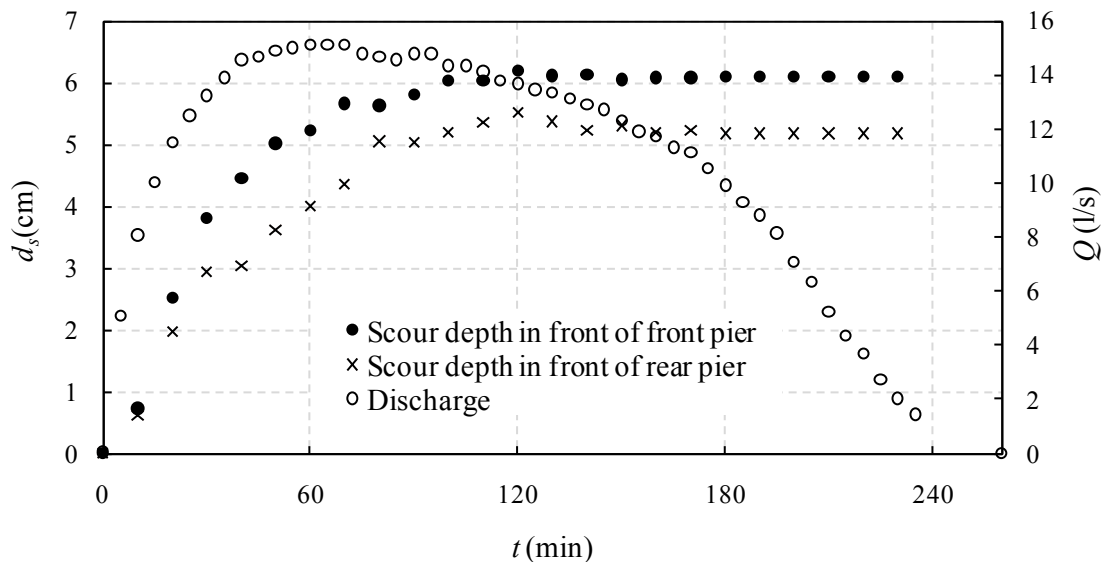


Fig. 193. Hydrograph and temporal evolution of scour depth in front of each pier in test U6



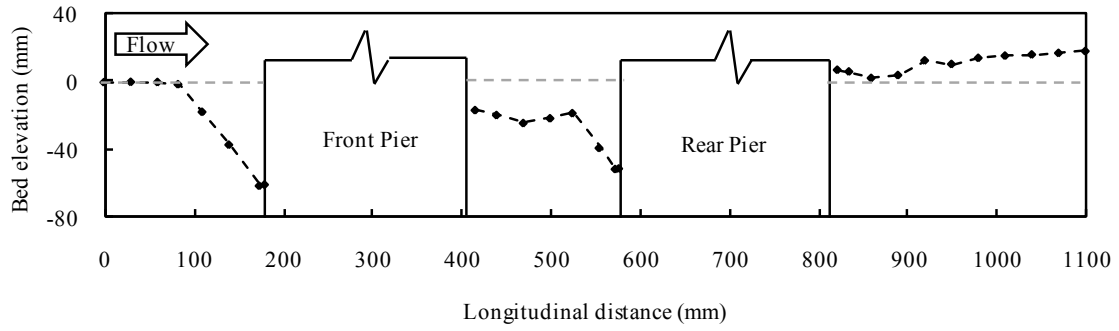


Fig. 194. Longitudinal profile of the scour holes in the plane of symmetry at the end of test U6



Fig. 195. Scour pattern at the end of test U6

### 5.3.9. Test U7

The two in-line round nose and tail rectangular piers used in test U6 were protected separately with the proposed combined countermeasure in test U7 (Fig. 196). This test has a special importance, since it permitted the observation of the following phenomenon: the scour downstream of the front pier generated vortices at the upstream face of the bed-sill of the rear pier. Such a phenomenon may threaten the stability of the rear bed-sill in field applications.

During the first 10 min, the scour did not occur in any part of the movable bed. After this period, three major scour holes were observed, specifically: downstream of the front pier (Fig. 196, zone B) and laterally and downstream of the rear pier (Fig. 196, zones C and D, respectively). The scour hole at lateral part of the front pier (zone A) was found after about 40 min (Fig. 197). At the end of test, the maximum scour depth downstream of the front pier was found adjacent to the bed-sill of the rear pier (Fig. 196, zone B).

Although the maximum scour depth in this zone (2.66 cm) is not significant with respect to the dimensions of the bed-sill, a better configuration will be considered in next test U8. In this test, maximum scour depth in zone B which occurred in front of the bed-sill was used to calculate the efficiency of this countermeasure.

The maximum exposure of the collar and borders at the front and rear piers in test U7 were 1.5 cm and 1.2 cm, respectively. The scour depths at the lateral (A and C) and downstream zones (B and D) of each pier are greater than that measured for the single protected round nose and tail rectangular pier (test U3); however, in both tests, the scour holes are far away from the pier foundation and significantly less deep than those in the unprotected reference tests U2 and U6. Figure 198 shows the scour pattern at the end of test U7.

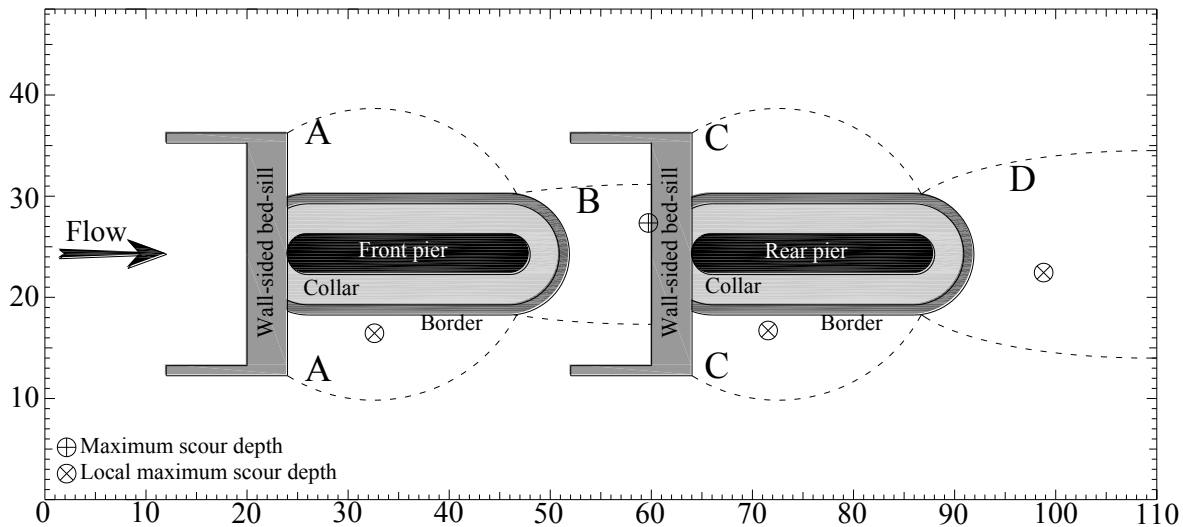


Fig. 196. Configuration and location of the maximum scour depths at the end of test U7 (units: cm)

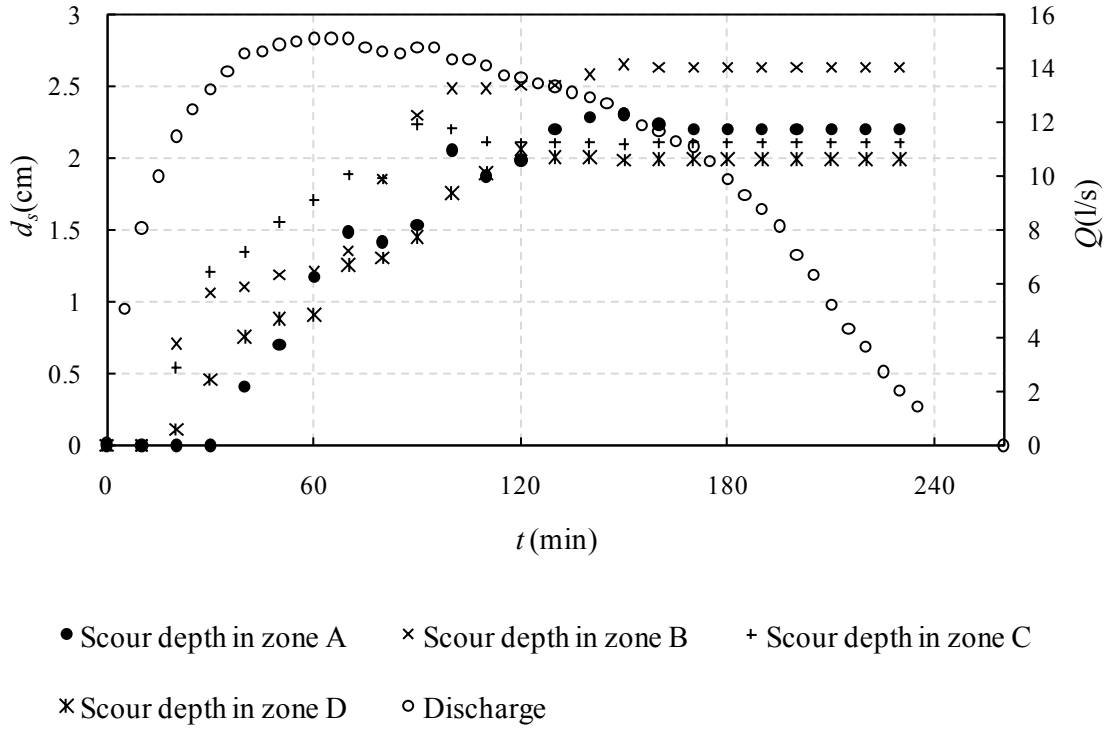


Fig. 197. Hydrograph and temporal evolution of the maximum scour depth in zones A to D in test U7

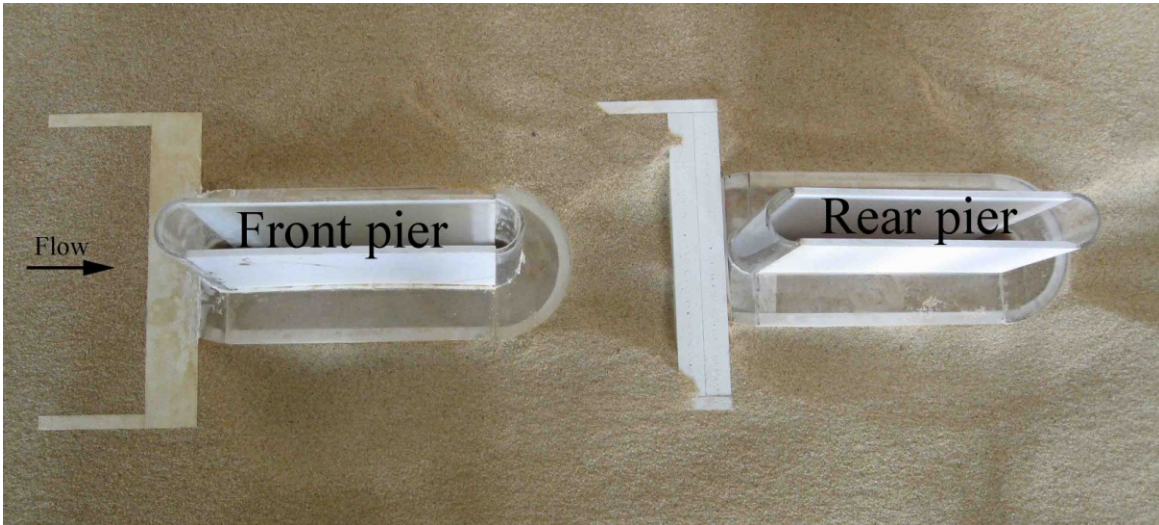


Fig. 198. Scour pattern at the end of test U7

### 5.3.10. Test U8

Test U8 (Fig. 199) was performed by adopting a wall-sided bed-sill at the front pier with a continuous bordered cut-collar around both front and rear piers, in order to prevent scouring between the two in-line round nose and tail rectangular piers (zone B in test U7).

The first scour hole was found downstream of the continuous collar at 20 min. After this period the scour at the lateral side of the collar near the rear pier (Fig. 199, zone B) started developing with a higher rate with respect to the scour hole in zone C. On the other hand, the development of the scour hole near the collar in the vicinity of the front pier had a delay of about 30 min. In this test, owing to the fact that the bed-sill of the rear pier was eliminated, the scour in zone B extended upstream with respect to previous test U7.

At the end of the test, the maximum exposure of the bordered cut-collar in zone A was about 1.3 mm, whereas in zones B it was 1.6 cm and in zone C was negligible. In fact, in test U8 the maximum scour depth in the movable bed was obtained in zone B (Figs. 199 and 200). The scour hole in this zone is more extended than that of previous test U7; however, the continuous bordered cut-collar prevents the scour in the region between the two in-line piers to develop (Fig. 201). In general, the continuous collar has higher priority with respect to the two separate protection systems, since it can prevent the development of scouring near the bed-sill of rear pier; nevertheless, the construction and maintenance of a long collar may cause some difficulties in field applications.

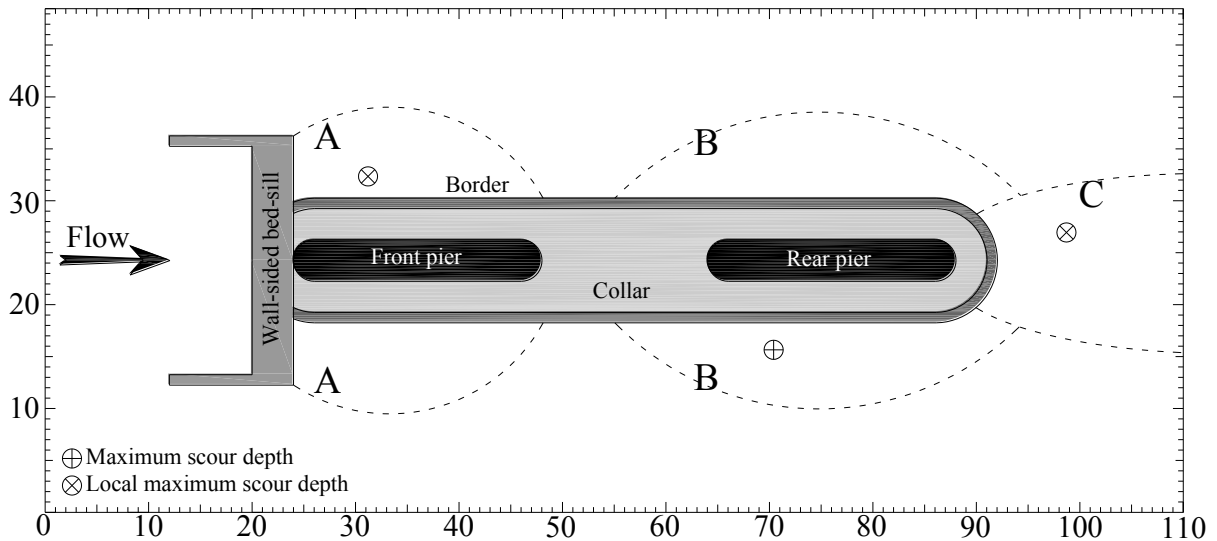


Fig. 199. Configuration and location of the maximum scour depths at the end of test U8 (units: cm)

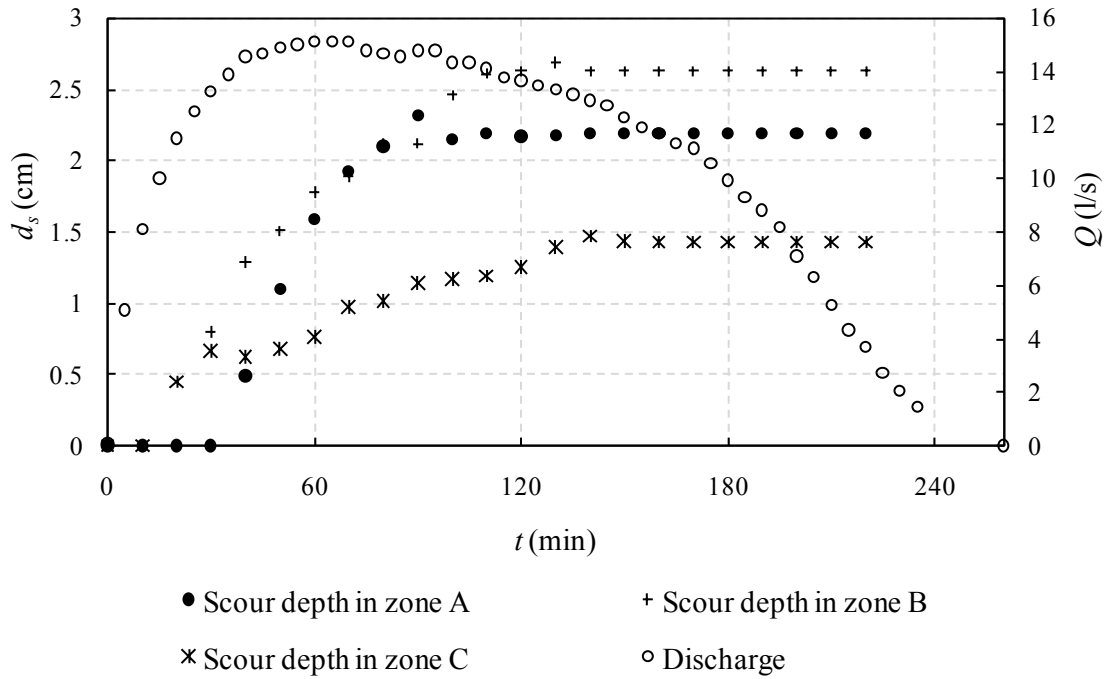


Fig. 200. Hydrograph and temporal evolution of the maximum scour depths in zones A to C in test U8



Fig. 201. Scour pattern at the end of test U8

Tab. 31 shows the efficiencies obtained in unsteady flow tests. When  $d_{scb}$  is “not available” (“N. A.”) because it was not measured for technical problems, the efficiency was calculated with  $d_{sm} > d_{scb}$ , where  $d_{sm}$  is the maximum scour depth in the whole movable bed measured during the test.

**Tab. 31. Efficiency of the proposed combined countermeasures in unsteady flow tests**

Test	Pier configuration	$U/U_c$ (at flow peak)	$d_{s0}$ (cm)	$d_{scb}$ (cm)	$d_{sm}$ (cm)	$r_{ds}$ (%)
U00	unprotected circular pier	0.92	5.04	-	-	-
U0	unprotected circular pier	1.1	7.12	-	-	-
U1	protected circular pier	1.1	-	<u>2.6</u>	5.4	63.5
U2	unprotected round nose and tail rectangular pier	1.1	6.25	-	-	-
U3	protected round nose and tail rectangular pier	1.1	-	N. A.	<u>1.52</u>	>78.7
U4	unprotected two in-line circular piers	1.1	7.14 (front) 6.12 (rear)	-	-	-
U5	protected two in-line circular piers	1.1	-	<u>1.7</u>	2.22	76.1
U6	unprotected two in-line round nose and tail rectangular piers	1.1	6.2 (front) 5.52 (rear)	-	-	-
U7	protected two in-line round nose and tail rectangular piers (separate countermeasures)	1.1	-	1.5	<u>2.66</u>	62.6
U8	protected two in-line round nose and tail rectangular piers (continuous countermeasure)	1.1	-	<u>1.6</u>	2.69	77.5

N. A.: not available (not measured at the end of test owing to technical problems)

## 5.4. Possible problems in application

### 5.4.1. Required space

The proposed combined countermeasures need a relatively large space, which may not be always available or may conflict with other river structures or navigation canals. Furthermore, construction of a bed-sill or collar adjacent to the pier may threaten the stability of the pier, specifically for already existing piers.

### 5.4.2. Application in live-bed conditions

Since the performance of the proposed combined countermeasure was evaluated in short-term tests with the peak flow intensity slightly greater than the threshold one, longer tests with higher flow intensity values are required to evaluate the adequacy of this countermeasure.

The bed-sill was employed in order to prevent scour extending from downstream of the collar to upstream of it (Fig. 202). On the other hand, scouring downstream of the bed-sill is expected in live-bed conditions also in the case without pier or other countermeasures (see, e.g., Gaudio *et al.*, 2000; Gaudio and Marion, 2003). Figure 203 shows the temporal evolution of scour downstream of a bed-sill for  $U > U_c$  without a sediment feeding system. This figure shows that the region downstream of and adjacent to the bed-sill, where the pier is positioned, is less affected by scouring and maximum scour depth may be found beyond the bed-sill location, at 30÷40% of the scour hole length. Furthermore, in live-bed conditions, the scour depth may reduce owing to the deposition of sediments eroded from upstream of the bed-sill.

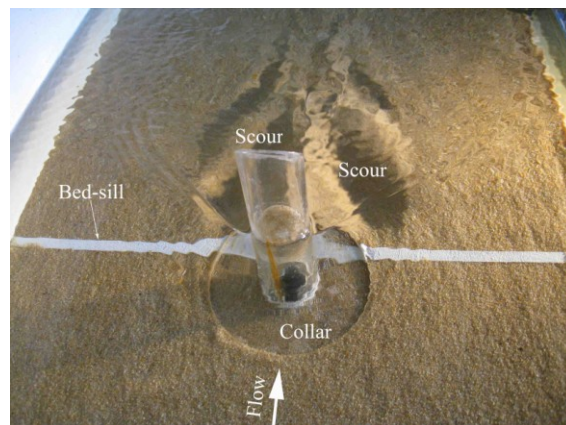


Fig. 202. Scour downstream of a collar in a test with a combined countermeasure of collar and bed-sill

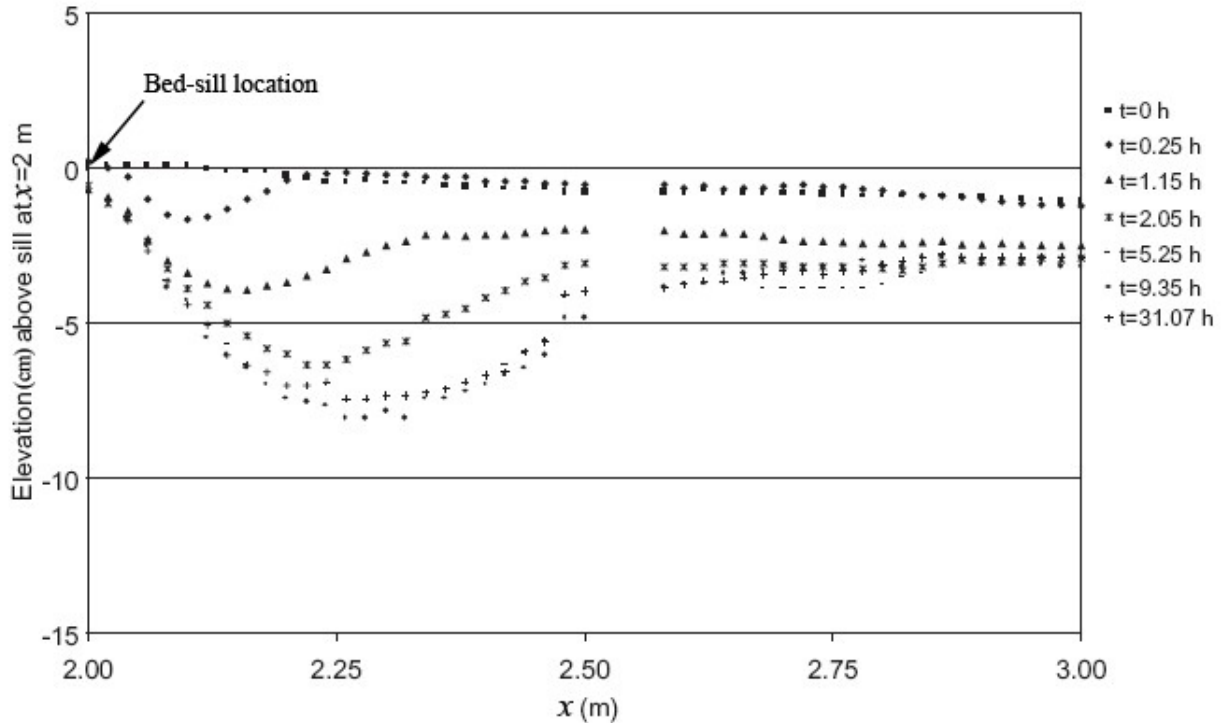


Fig. 203. Temporal evolution of the maximum scour depth downstream of bed-sill (modified from Gaudio and Marion, 2003)

The result of experiments by Chiew and Lim (2003) shows that a sacrificial sill as wide as the pier and located upstream of it at a distance of  $4.3b$  is not notably effective in a live-bed scour test. In fact, in the pier location probably the scour depth is higher than in the cross-section adjacent to the bed-sill. Furthermore, the bed-sill used by the Authors was protruding above the initial bed level with a height equal to the pier width ( $h_{bs}=b$  and  $w_{bs}=b$ , see Fig. 35). This configuration is equivalent to submerged transverse sacrificial piles with  $b_r=1$ . The experiment S2 with 5 transverse piles ( $b_r=1$ ) showed strong wake vortices downstream of the piles eroding the bed sediments in the region between piles and pier and resulted in a deep scour at the pier.

Therefore, although the configuration of the experiment in the present study is different from those performed by Chiew and Lim (2003), new tests in live-bed condition are necessary to investigate the possible field performances of the proposed combined countermeasure.



## Chapter 6

### CONCLUSIONS AND RECOMMENDATIONS

In this study, the results of 34 experiments on the evaluation of flow-altering countermeasures against local scour at bridge piers together with details of scour process, *pros* and *cons*, efficiency and best configuration of each countermeasure were presented.

One of the most important results of the present study is that the efficiency of the flow-altering countermeasures depends significantly on the experimental conditions. In fact, an high and unreliable efficiency in the performance of a countermeasure may be obtained in improper experimental conditions. In particular, in low flow intensity or short duration tests, the obtained efficiencies are not realistic. Some of the most important results of the present study can be summarised as follows.

Three piles with a blockage ratio of 60% represent the best tested configuration, with a scour depth reduction of about 33%. By increasing the pile numbers, the efficiency of this countermeasure may reduce.

In the application of a collar, the test duration should be long, since this countermeasure may slow down the scour process. No criterion has been suggested yet for the time required for this countermeasure to start being scoured nor to reach equilibrium. In this case, long duration test, in the order of months, are required. In contrast, few hour tests cannot show a reliable performance of this countermeasure. The efficiency of a collar in low flow depths, when a bow wave and the horseshoe vortex interact each other, is unknown. Furthermore, in live-bed conditions, during the propagation of bed-forms the performance of a collar is not clear. For both of these conditions, more investigation is required. The result of the present study and previously

performed tests by other researchers show that the efficiency of a  $3b$ -wide collar flush with the bed may be in the range 20÷30%; however, longer tests are needed to verify such values.

Threading is not a proper countermeasure, since it shows efficiency less than 10%.

Slot length and location for the optimum configuration cannot be suggested on the basis of the approach flow depth only. The optimum slot configuration is that in which the slot height is equal to  $h/2$  above the initial bed and the maximum scour depth under the bed level ( $l_s=h/2+d_{se}$  and  $z_s=d_{se}$ ). In this case, an efficiency of 30÷35% may be expected.

This study confirms that the combination of a slot with a collar may prevent the scour reaching the pier, since the flow towards the outside of the slot may affect the strength of the wake vortices system, which is an important scouring agent.

The combination of sacrificial piles and collar/slot is not much more efficient than the individual countermeasures and therefore it is not recommended.

A combination of collar and bed-sill may prevent the scour intrusion to the upstream part of the collar. As the bed-sill moves from downstream to upstream of the collar, the intrusion of the scour beneath the collar at the rear of the bed-sill increases; however, the risk of scour intrusion towards the front of the bed-sill reduces. The best location of a bed-sill in combination with a collar is upstream of and adjacent to the pier. When the bed-sill is not as wide as the channel, the scour may intrude upstream of the bed-sill. In this case a deep scour may be found in front of the bed-sill. By increasing the bed-sill width, the scour in front of it increases; however, lesser scour may be found at the rear of the bed-sill and near the pier.

Although the best configuration is obtained when the bed-sill is as wide as the channel, an alternative with lower priority was also presented when the application of a bed-sill as wide as the channel width is not feasible. The combination of a bed-sill and a collar may result in 68.5% and 64.5% scour depth reduction for higher and lower priority configurations, respectively.

The proposed configuration was also effective in unsteady flow conditions. In particular, the preliminary tests show that the proposed countermeasure is probably more effective for round nose and tail rectangular piers than circular ones.

Since the performance of the proposed combined countermeasure was evaluated in unsteady flow with peak flow intensity slightly greater than the threshold value for the inception of the sediment motion, longer tests with higher flow intensities are necessary to evaluate better the performances of this countermeasure. In fact, in live-bed conditions local scouring is also expected downstream of the bed-sill itself. The interaction of the scour hole downstream of the bed-sill with the scour hole developed owing to turbulent flow around the pier is still unclear.

## REFERENCES

- Abd El-Razek, M., Abd El-Motaleb, M., and Bayoumy, M. (2003). "Scour reduction around bridge piers using internal openings through the pier." *Proc., XXX IAHR Congress*, Thessaloniki, Greece, C2, 285-292.
- Ahmed, F., and Rajaratnam N. (1998). "Flow around bridge piers." *Journal of Hydraulic Engineering*, 124(3), 288-300.
- Alabi, P. D. (2006). *Time development of local scour at a bridge pier fitted with a collar*, Master's degree thesis, University of Saskatchewan, Saskatoon, Saskatchewan, Canada.
- Baker C. J. (1979). "Laminar horseshoe vortex." *The Journal of Fluid Mechanics*, 95(2), 347-367.
- Baker C. J. (1980). "The turbulent horseshoe vortex." *Journal of Wind Engineering and Industrial Aerodynamics*, 6(1-2), 9-23.
- Baker C. J. (1985). "The position of points of maximum and minimum shear-stress upstream of cylinders mounted normal to flat plates." *Journal of Wind Engineering and Industrial Aerodynamics*, 18(3), 263-274.
- Breusers, H. N. C., Nicollet, G., and Shen, H. W. (1977). "Local scour around cylindrical pier." *Journal of Hydraulic Research*, 15(3), 211-252.
- Breusers, H. N. C., and Raudkivi, A. J. (1991). *Scouring. Hydraulic Structures Design Manual*, IAHR, A. A. Balkema, Rotterdam, Netherlands.
- Calomino, F., Fallico, C., Piro, P. (1988). "Sul coefficiente d'efflusso di uno stramazzo Thomson a contrazione incompleta." *Giornale del Genio civile*, 10-11-12, 207-220 (in Italian).
- Cardoso, A. H., and Bettess, R. (1999). "Effects of time and channel geometry on scour at bridge abutments." *Journal of Hydraulic Engineering*, 125(4), 388-399.
- Cardoso, A. H., Calomino, F., Gaudio, R., Bettess, R., Roca Collell, M. (2010). "Relazione finale per il Lotto N. 9 *Rischio idraulico ed erosivo in corrispondenza di punti singolari del POR Calabria 2000-2006*, Asse 1, Misura 1.4, Azione 1.4.c, *Studio e sperimentazione di*

## References

---

- metodologie e tecniche per la mitigazione del rischio idrogeologico.*” Università della Calabria, Dipartimento di Difesa del Suolo “V. Marone”, Rende (CS), Italy, (in Italian).
- Chabert, J., and Engeldinger, P. (1956). “Etude des afouillements autour des piles des ponts.” *Report*, Laboratoire National d’Hydraulique, Chatou, France (in French).
- Chang, F.F.M., Karim, M. (1972). “An experimental study of reducing scour around bridge piers using piles.” *Report*, South Dakota Department of Highways, South Dakota.
- Chee, R. K. W. (1982). “Live-Bed scour at bridge piers.” *Report No. 290*, School of Engineering, University of Auckland, New Zealand.
- Chiew, Y. M. (1984). “Local scour at bridge piers.” *Report No. 355*, School of Engineering, University of Auckland, New Zealand.
- Chiew, Y. M. (1992). “Scour protection at bridge piers.” *Journal of Hydraulic Engineering*, 118(9), 1260-1269.
- Chiew, Y. M. (1995). “Mechanics of riprap failure at bridge piers.” *Journal of Hydraulic Engineering*, 121(9), 635-643.
- Chiew, Y. M., and Lim, F. H. (2000). “Failure behavior of riprap layer at bridge piers under live-bed conditions.” *Journal of Hydraulic Engineering*, 126(1), 43-55.
- Chiew, Y. M., and Lim, S. Y. (2003). “Protection of bridge piers using a sacrificial sill.” *Proc., Institution of Civil Engineering, Water and Maritime Engineering*, 156(1), 53-62.
- Chiew, Y. M., and Lu, Y. (2005). “Suction effects on riprap protection around bridge piers.” *Proc., XXXI IAHR Congress*, Seoul, Korea, September 11-16, 1614-1620.
- Chiew, Y. M., and Melville, B. W. (1987). “Local scour around bridge piers.” *Journal of Hydraulic Research*, 25(1), 15-26.
- Dade, W. B., and Friend, P. F. (1998). “Grain-Size, Sediment-Transport Regime, and Channel Slope in Alluvial Rivers” *The journal of Geology*, 106, 661-675.
- Daido, A., and Yano, S. (1995). “Local scour around bridge piers and its protection with guide wall and slanting plate and piers surface.” *Proc., 6th International Symposium on River Sedimentation*, New Delhi, India, 1181-1187.
- Dargahi, B. (1987). “Flow field and local scouring around a cylinder.” *Bulletin No.137*, R. Inst. Tech. Hydr. Lab., Stockholm, Sweden.
- Dargahi, B. (1989). “The turbulent flow field around a circular cylinder”, *Experiments in Fluids*, 8, 1-12.
- Dargahi, B. (1990). “Controlling mechanism of local scouring.” *Journal of Hydraulic Engineering*, 116(10), 1197-1214.
- Defanti, E., Di Pasquale, G., and Poggi, D. (2010). “An experimental studies of scour at bridge piers: collars as a countermeasure.” *Proc., 1<sup>st</sup> IAHR European Congress*, May 2010, Edinburgh, UK, 6 pp.
- Dey, S., Bose, S. K., and Sastry, G. L. N. (1995). “Clear water scours at circular piers: A model.” *Journal of Hydraulic Engineering*, 121(12), 869-876.
- Dey, S., and Raikar, R. V. (2007). “Characteristics of horseshoe vortex in developing scour holes at piers.” *Journal of Hydraulic Engineering*, 133(4), 399-413.
- Dey, S., Sumer, B. M., and Fredsøe, J. (2006). “Control of scour at vertical circular piles under

- waves and current.” *Journal of Hydraulic Engineering*, 132(3), 270-279.
- Dietz, J. W. (1972). “Construction of long piers at oblique currents illustrated by the BAB-Main Bridge Eddersheim.” and “Systematic model tests on scour formation at piers.” *Mitteilungsblatt der Bundesanstalt for Wasserbau*, No. 31, Karlsruhe, Germany.
- Eckerle W. A., and Langston L. S. (1987). “Horseshoe vortex formation around a cylinder.” *Journal of Turbomachinery*, 109(1), 278-285.
- Ettema, R. (1980). “Scour at bridge piers.” *Report No. 216*, School of Engineering, University of Auckland, Auckland, New Zealand.
- Ettema, R., Kirkil, G., and Muste, M. (2006). “Similitude of Large-Scale Turbulence in Experiments on Local Scour at Cylinders.” *Journal of Hydraulic Engineering*, 132(1), 33-40.
- Ettema, R., Melville, B. W., and Barkdoll, B. (1998a). “Scale effect in pier-scour experiments.” *Journal of Hydraulic Engineering*, 124(6), 639-642.
- Ettema, R., Mostafa, E. A., Melville, B. W., and Yassin, A. A. (1998b). “Local scour at skewed piers.” *Journal of Hydraulic Engineering*, 124(7), 756-759.
- Florida Department of Transportation (2005). *Bridge Scour Manual*, State of Florida, <http://www.dot.state.fl.us>.
- Fotherby, L. M. (1992). *Footings, Mats, Grout bags, and Tetrapods protection methods against local scour at bridge piers*, Master’s thesis, Colorado State University, Colorado.
- Franzetti, S., and Ballio, F. (1998). “Effetti delle correnti fluviali sulle strutture: erosione localizzata alle pile dei ponti” *Proc., Corso di aggiornamento “Moderni criteri di sistemazione degli alvei fluviali – l’ingegneria naturalistica nella sistemazione dei corsi d’acqua”*, U. Maione and A. Brath (eds.), Politecnico di Milano, 5-9 October, Milan, Italy, Editoriale Bios, Cosenza.
- Franzetti, S., Malavasi, S., and Piccinin, C. (1994). “Sull’erosione alla base delle pile di ponte in acque chiare.”, *Proc., XXIV Convegno di Idraulica e Costruzioni Idrauliche*, Naples, Italy, vol. II, T4 13-24 (in Italian).
- Froehlich, D. C. (1988). “Analysis of onsite measurements of scour at piers.” *American Society of Civil Engineers National Conference on Hydraulic Engineering*, Colorado Springs, CO, USA, 534-539.
- Gao, D., Pasada, L., and Nordin, C.F. (1993). Pier scour equations used in the People’s Republic of China - Review and summary. *Rep. No. FHWA-SA-93-076*, Federal Hwy. Administration (FHWA), Washington, DC.
- Garde, R. J. (1970). “Initiation of motion on a hydrodynamically rough surface. Critical velocity approach.” *Irrigation and Power Journal*, 27(3), 271-282.
- Garde, R. J., Rangaraju, K. G., and Kothyari, U. C. (1989). *Research Report on Effect of Unsteadiness of Stratification on Local Scour*, Civil Engineering Department, University of Roorkee, Roorkee, India.

## References

---

- Garg, V., Setia, B., and Verma, D. V. S. (2008). "Prevention of scour by combination of scour protection devices around bridge piers." *Proc., River flow 2008*, İzmir, Turkey, September 3-5, 1637-1643.
- Gaudio, R., Grimaldi, C., Tafarajnoruz, A., and Calomino, F. (2010). "Comparison of formulae for the prediction of scour depth at piers." *Proc., First IAHR European Division Congress*, Edinburgh (UK), 4-6 May, 2010, 6 pp.
- Gaudio, R., Marion, A. (2000). "Morphological Effects of Bed Sills in Degrading Rivers." *Journal of Hydraulic Research*, 38(2), 89-96.
- Gaudio, R., Marion, A. (2003). "Time evolution of scouring downstream of bed sills." *Journal of Hydraulic Research*, 41(3), 271-284.
- Ghorbani, B., and Kells, J. A. (2008). "Effect of submerged vanes on the scour occurring at a cylindrical pier." *Journal of Hydraulic Research*, 46(5), 610-619.
- Goncharov, V. N. (1964). *Dynamics of channel flow*, Israel Programme for Scientific Translation, Moscow, 185.
- Graf, W. H., and Altinakar, M. S. (1998). *Fluvial Hydraulics*, J. Wiley and Sons Ltd, Chichester, England.
- Graf, W. H., and Istiarto, I. (2002). "Flow pattern in the scour hole around a cylinder." *Journal of Hydraulic Research*, 40(1), 13-20.
- Graf, W. H., and Yulistiyanto, B. (1998). "Experiments on flow around a cylinder: The velocity and vorticity fields." *Journal of Hydraulic Research*, 36(4), 637-653.
- Grimaldi, C. (2005). *Non-conventional countermeasures against local scouring at bridge piers*, Dissertazione per il conseguimento del titolo di Dottore di Ricerca in Ingegneria Idraulica per l'Ambiente e il Territorio, Università della Calabria, Dipartimento di Difesa del Suolo "V. Marone", Rende (CS), Italy.
- Grimaldi, C., Gaudio, R., Calomino, F., and Cardoso, A. H. (2009a). "Control of scour at bridge piers by a downstream bed-sill." *Journal of Hydraulic Engineering*, 135(1), 13-21.
- Grimaldi, C., Gaudio, R., Calomino, F., and Cardoso, A. H. (2009b). "Countermeasures against Local Scouring at Bridge Piers: Slot and Combined System of Slot and Bed-sill." *Journal of Hydraulic Engineering*, 135(5), 425-431.
- Grimaldi, C., Gaudio, R., Cardoso, A. H., and Calomino, F. (2006). "Local scouring at bridge piers and abutments: time evolution and equilibrium." R. M. L. Ferreira, E. C. T. L. Alves, J. G. A. B. Leal, A. H. Cardoso (eds.), *River Flow 2006, Proc., International Conference on Fluvial Hydraulics*, Lisbon, Portugal, 6-8 September 2006, Taylor & Francis Group plc, London, UK, 2006, Vol. 2, pp. 1657-1664.
- Gupta, A. K. (1987). "Hydrodynamic modification of the horseshoe vortex at a vertical pier junction with ground." *Physics of fluids*, 30, 1213-1215.
- Gupta, A. K., and Gangadharaiah, T. (1992). "Local scour reduction by a delta-Wing like passive device" *Proc., 8th Congress of the Asia and Pacific Division of IAHR*, Pune, India, B471-B481.
- Haque, M. A., Rahman, Md. M., Islam, G. M. T., Hussain, M. A. (2007). "Scour mitigation at

- bridge piers using sacrificial piles.” *International Journal of Sediment Research*, 22(1), 49-59.
- Heidarpour, M. (2002). “Control and reduction of local scour at bridge piers by using slot.” *Proc., River Flow 2002*, Balkema, The Netherlands, Vol. 2, 1069-1072.
- Heidarpour, M., and Afzalimehr, H. (2005). “Local scour protection at bridge piers groups using collar.” *Proc., XXXI IAHR Congress*, Seoul, Korea, September 11-16, 5463-5470.
- Heidarpour, M., Khodarahmi, Z., and Mousavi, S. F. (2003). “Control and reduction of local scour at bridge pier groups using slot.” *Proc., XXX IAHR Congress*, Thessaloniki, Greece, August 24-29, 301-307.
- Herbertson, J. G., and Ibrahim, A. A. (1992). “Interaction between Bridge Piers and Scour Protection Devices.” *Proc., International Conference on Protection and Development of the Nile and other Major Rivers*, Cairo, Egypt.
- Hjorth, P. (1975). “Studies on the nature of local scour.” *Swedish Bulletin*, Lund Institute of Technology, Series A, No. 46, Lund, Sweden.
- Huang, C. K., Tang, C. J., and Kuo, T. Y. (2005). “Use of surface guide panels as pier scour countermeasures.” *International Journal of Sediment Research*, 20(2), 119-130.
- Huang, W., Yang, Q., and Xiao, H. (2009). “CFD modeling of scale effects on turbulence flow and scour around bridge piers.” *Computers & Fluids*, 38, 1050-1058.
- Jain, S. C. (1981). “Maximum clear water scour around circular piers”, *Journal of the Hydraulics Division*, 107(5), 611-626.
- Jain, S. C., and Fischer, E. E. (1979). “Scour Around Circular Piers at High Froude Numbers.”, *Report No. FHWA-RD-79-104*, U.S. Department of Transportation, Federal Highway Administration, Washington, DC, USA.
- Johnson, K. R., and Ting, F. C. K. (2003). “Measurements of water surface profile and velocity field at a circular pier.” *Journal of Engineering Mechanics*, 129(5), 502-513.
- Johnson, P. A. (1995). “Comparison of Pier-Scour Equations Using Field Data.” *Journal of Hydraulic Engineering*, 121(8), 626-629.
- Jones, J. S., Kilgore, R. T., and Mistichelli, M. P. (1992). “Effects of footing location on bridge pier scour.” *Journal of Hydraulic Engineering*, 118(2), 280-290.
- Kayatürk, Ş. Y., Kökpınar, M. A., and Göğüş, M. (2005). “Application of collars and sacrificial piles to control scouring around the piers.” *Proc., XXXI IAHR Congress*, Seoul, Korea, September 11-16, 2991-2999.
- Kim, U. Y., Kim, J. S., Ahn, S. J., Hahm, C. H. (2005). “Scour countermeasure using additional facility in front of bridge pier.” *Proc., XXXI IAHR Congress*, Seoul, Korea, 5823-5829.
- Kirkil, G., Constantinescu, G., and Ettema, R. (2009). “Detached eddy simulation investigation of turbulence at a circular pier with scour hole.” *Journal of Hydraulic Engineering*, 135(11), 888-901.
- Kirkil, G., Constantinescu, S. G., and Ettema, R. (2008). “Coherent structures in the flow field around a circular cylinder with scour hole.” *Journal of Hydraulic Engineering*, 134(5), 572-587.
- Kothiyari, U. C., Garde, R. J., and Ranga Raju, K. G. (1992). “Temporal variation of scour around

## References

---

- circular bridge piers.” *Journal of Hydraulic Engineering*, 118(8), 1091-1106.
- Kramer, H. (1935). “Sand mixtures and sand movement in fluvial levels.” *Transactions of the American Society of Civil Engineers*, 100, 798-838.
- Kumar, V., Ranga Raju, K. G., and Vittal, N. (1999). “Reduction of local scour around bridge piers using slots and collars.” *Journal of Hydraulic Engineering*, 125(12), 1302-1305.
- Lança, R., Fael, C., and Cardoso, A. (2010). “Assessing equilibrium clear water scour around single cylindrical piers.” *Proc., River Flow 2010 congress*, Braunschweig, Germany.
- Landers, M. N., and Mueller, D. S. (1996). “Evaluation of selected pier-scour equations using field data.” *Journal of the Transportation Research Board*, 1523, 186-195.
- Lauchlan, C. S. (1999). *Pier Scour Countermeasures*, PhD. Thesis, University of Auckland, Auckland, NZ.
- Lauchlan, C. S., and Melville, B. W. (2001). “Riprap protection at bridge piers.” *Journal of Hydraulic Engineering*, 127(5), 412-418.
- Laursen, E. M., and Toch, A. (1956). “Scour around bridge piers and abutments.” Iowa Highway Research Board, *Bulletin No. 4*, Bureau of Public Roads, Iowa.
- Lee, S. O., and Sturm T. W. (2009). “Effect of Sediment Size Scaling on Physical Modeling of Bridge Pier Scour.” *Journal of Hydraulic Engineering*, 135(10), 793-802.
- Levi, E., and Luna, H. (1961). “Dispositifs pour reduire l’Affouillement au pied des piles de pont.” *Proc., 9th International Association of Hydraulic Research Congress*, Dubrovnik, Yugoslavia, 1061-1069.
- Mansueto, A. (2009). *Studio sperimentale su una contromisura combinata contro l’escavazione localizzata a una pila di ponte*, Tesi di Laurea Specialistica in Ingegneria Civile (Idraulica), Università della Calabria, Dipartimento di Difesa del Suolo “V. Marone”, Rende (CS), Italy (in Italian).
- Mashahir, M. B., and Zarrati, A. R. (2002). “Effect of Collar on Time Development of Scouring around Rectangular Bridge Piers.” *Proc., 5th International Conference on Hydro science and Engineering*, Warsaw, Poland.
- Mashahir, M. B., Zarrati, A. R., and Mokallaf, E. (2007). “Effect of bed shear stress on development of scouring around bridge piers protected by a collar.” *Proc., 32nd IAHR Congress*, Venice, Italy, pp. 8.
- Mashahir, M. B., Zarrati, A. R., and Mokallaf, E. (2010). Application of riprap and collar to prevent scouring around rectangular bridge piers. *Journal of Hydraulic Engineering*, 136(3), 183-187.
- Mashahir, M. B., Zarrati, A. R., and Rezayi, M. J. (2004). “Time development of scouring around a bridge pier protected by collar.” *Proc., Second Int. Conf. on scouring and Erosion*, Nanyang, Singapore.
- Masjedi, A., Shafaei Bejestan, M., and Esfandi, A. (2010). “Experimental study on local scour around single oblong pier fitted with a collar in a 180 degree flume bend.” *International Journal of Sediment Research*, 25, 304-312.
- Maza, J. A. (1967). “Scour in Natural Channels.” *Report no. 114*, Department of Civil Engineering, University of Auckland, Auckland, New Zealand.



- Melville, B. W. (1975). "Local scour at bridge sites." *Report no. 117*, University of Auckland, Auckland, New Zealand.
- Melville, B. W. (1992). "Local scour at bridge abutments." *Journal of Hydraulic Engineering*, 118(4), 615-630.
- Melville, B. W. (1997). "Pier and abutment scour: integrated approach." *Journal of Hydraulic Engineering*, 123(2), 125-136.
- Melville B. W., and Chiew, Y. M. (1999). "Time Scale for local scour at bridge piers." *Journal of Hydraulic Engineering*, 125(1), 59-65.
- Melville, B. W., and Coleman, S. E. (2000). *Bridge Scour*, Water Resources Publications, LLC Highlands Ranch, Colorado, USA.
- Melville, B. W., and Hadfield, A. C. (1999). "Use of sacrificial piles as pier scour countermeasures", *Journal of Hydraulic Engineering*, 125(11), 1221-1224.
- Melville, B. W., and Raudkivi, A. J. (1977). "Flow characteristics in local scour at bridge piers." *Journal of Hydraulic Research*, 15(4), 373-380.
- Melville, B. W., and Raudkivi, A. J. (1996). "Effect of foundation geometry on bridge pier scour." *Journal of Hydraulic Engineering*, 122(4), 203-209.
- Melville, B. W., and Sutherland, A. J. (1988). "Design method for local scour at bridge piers." *Journal of Hydraulic Engineering*, 114(10), 1210-1226.
- Mohamed, T. A., Pillai, S., Noor, M. J. M. M., Ghazali, A. H., Huat, B. K., and Yusuf, B. (2006). "Validation of some bridge pier scour formulae and models using field data." *Journal of King Saud University*, 19, *Eng. Sci.* (1), 31-41.
- Moncada-M, A. T., Aguirre-PE, J., Bolívar, J. C., and Flores, E. J. (2009). "Scour protection of circular bridge piers with collars and slots." *Journal of Hydraulic Research*, 47(1), 119-126.
- Monti, R. (1994). *Indagine sperimentale delle caratteristiche fluidodinamiche del campo di moto intorno a una pila circolare*, Tesi di Laurea, Politecnico di Milano, Milan, Italy (in Italian).
- Mueller, D. S., and Wagner, C. R. (2005). "Field observations and evaluations of streambed scour at bridges." *Report no. FHWA-RD-03-052*, U.S. Department of Transportation, Federal Highway Administration, Washington, DC.
- Murillo (1987). "The scourge of scour." *Civil Engineering*, 57(7), 66-69.
- Muzzammil, M., Gangadhariah, T. (2003). "The mean characteristics of horseshoe vortex at a cylindrical pier." *Journal of Hydraulic Research*, 41(3), 285-297.
- Neill, C. R., ed. (1973). *Guide to bridge hydraulics*, Toronto, Canada, University of Toronto Press, 191 p.
- Odgaard, A. J., and Wang, Y. (1987). "Scour Prevention at Bridge Piers." *Proc., National Conference of Hydraulic Engineering*, Williamsburg, Virginia, 523-527.
- Odgaard, A. J., and Wang, Y. (1991a). "Sediment management with submerged vanes. I: Theory." *Journal of Hydraulic Engineering*, 117(3), 267-283.
- Odgaard, A. J., and Wang, Y. (1991b). "Sediment management with submerged vanes. II: Applications." *Journal of Hydraulic Engineering*, 117(3), 284-302.

## References

---

- Oliveto, G., and Hager, W. H. (2002). "Temporal evolution of clear-water pier and abutment scour." *Journal of Hydraulic Engineering*, 128(9), 811-820.
- Olsen, N. R. B., and Kjellesvig, H. M. (1998). "Three-dimensional numerical flow modeling for estimation of maximum local scour depth." *Journal of Hydraulic Research*, 36(4), 579-590.
- Olsen, N. R. B., and Melaaen, M. C. (1993). "Three-dimensional calculation of scour around cylinders." *Journal of Hydraulic Engineering*, 119(9), 1048-1054.
- Paice, C., Hey, R. (1993) "The Controlling and Monitoring of Local Scour at Bridge Piers." *Proc., Hydraulic Engineering Conference*, San Francisco, California, 1061-1066.
- Parker, G., Toro-Escobar, C., and Voigt, R. L. Jr. (1998). "Countermeasures to Protect Bridge Piers from Scour", *User's Guide* (revised 1999) and *Final Report*, NCHRP Project 24-7, prepared for transportation Research Board by St. Anthony Falls Laboratory, University of Minnesota, MN, USA.
- Parola, A. C., Mahavadi, S. K., Brown, B. M., and El-Khoury, A. (1996). "Effects of rectangular foundation geometry on local pier scour." *Journal of Hydraulic Engineering*, 122(1), 35-40.
- Pogozelski, E. M., Katz, J., and Huang, T. T. (1997). "The flow structure around a surface piercing strut." *Physics of Fluids*, 9(5), 1387-1399.
- Qadar, A. (1981). "The Vortex Scour Mechanism at Bridge Piers." *Proc., the Institution of Civil Engineers*, Part 2, 71, 739-757.
- Radice, A., Franzetti, S., Balio, F. 2002. "Local scour at bridge abutments." *Proc. River Flow 2002*, Bousmar & Zech (eds.), Balkema Publishers, The Netherlands, 1059-1068.
- Raudkivi, A. J., and Ettema, R. (1983). "Clear-water scour at cylindrical piers." *Journal of Hydraulic Engineering*, 109(3), 338-350.
- Richardson, E. V., and Davis, S. R. (2001). "Evaluating scour at bridges." Hydraulic Engineering Circular No. 18 (HEC-18), *Report no. FHWA NHI 01-001*, U.S. Department of Transportation, Federal Highway Administration, Washington, DC, USA.
- Richardson, J. E., and Panchang, V. G. (1998). "Three-dimensional simulation of scour-inducing flow at bridge piers." *Journal of Hydraulic Engineering*, 124(5), 530-540.
- Richardson, J. R., and York, K. (1999). "Hydrodynamic Countermeasures for Local Pier Scour", *Journal of the Transportation Research Board*, volume 1690/1999, paper no. 99-1375, 186-192.
- Robison, R. (1995). "Schoharie Creek Bridge collapse." in N. Schlager., 1995. *Breakdown*. Visible Ink Press, Detroit, 234-240.
- Rooney, D. M., and Machemehl, J. L. (1977). "Using suction to minimize sand-bed scour." *Journal of the Hydraulics Division*, 103(HY4), 443-449.
- Roulund, A., Sumer, M., Fredsøe, J., and Michelsen, J. (2005). "Numerical and experimental investigation of flow and scour around a circular pile." *The Journal of Fluid Mechanics*, 534, 351-401.
- Salaheldin, T. M., Imran, J., and Chaudhry, M. H. (2004). "Numerical modeling of three-dimensional flow field around circular piers." *Journal of Hydraulic Engineering*, 130(2), 91-100.

- Sani Khani, H., Hosseinzadeh Dalir, A., and Farsadizadeh, D. (2008). "Performance of quadrangular collars in scour reduction around bridge piers." *Proc., 4th National Congress on Civil Engineering*, (4NCCE) University of Tehran, Tehran, Iran, (in Persian).
- Sarker, M. A. (1998). "Flow measurement around scoured bridge piers using Acoustic-Doppler Velocimeter (ADV)." *Flow Measurement and Instrumentation*, 9(4), 217-227.
- Schneible, D. E., (1951). *An investigation on the effect of bridge pier shape on the relative depth of scour*, Master's thesis, State University of Iowa, USA.
- Shen, H. W., Schneider, V. R. & Karaki, S. S. (1966a). "Mechanics of local scour." *Report No. CER66HWS22*, U.S. Dept. of Commerce, National Bureau of Standards, Institute for Applied Technology.
- Shen, H. W., Schneider, V. R., Karaki, S. S., (1966b). "Mechanics of Local Scour, and supplement Methods of Reducing scour." *Report No. CER66HWS36*, U.S. Dept. of Commerce, National Bureau of Standards, Institute for Applied Technology.
- Sheppard, D. M., Odeh, M. & Glasser, T. (2004). "Large scale clear-water local pier scour experiments." *Journal of Hydraulic Engineering*, 130(10), 957-963.
- Simarro, G., Teixeira, L., and Cardoso, A. H. (2007). "Flow Intensity Parameter in Pier Scour Experiments." *Journal of Hydraulic Engineering*, 133(11), 1261-1264.
- Singh, C. P., Setia, B., and Verma, D.V.S. (2001). "Collar-sleeve combination as a scour protection device around a circular pier." *Proc., XXIX IAHR Congress*, Beijing, China, September 16-21, 202-209.
- Singh, K. K., Verma, D. V. S., and Tiwari, N. K. (1995). "Scour protection at circular bridge piers." *Proc., Sixth International Symposium on River Sedimentation*, New Delhi, India, 1057-1068.
- Tafarjnoruz, A., Gaudio, R., and Dey, S. (2010a). "Flow-altering countermeasures against scour at bridge piers: A review." *Journal of Hydraulic Research*, 48(4), 441-452.
- Tafarjnoruz, A., Gaudio, R., Grimaldi, C., Calomino, F. (2010b). "Required conditions to achieve the maximum local scour depth at a circular pier." *Proc., XXXII Convegno Nazionale di Idraulica e Costruzioni Idrauliche*, Palermo, Italy, 14-17 settembre 2010, Farina, Palermo, Italy, 6 pp.
- Tanaka, S., and Yano, M., (1967). "Local scour around circular cylinder." *Proc., XII IAHR Congress*, Fort Collins, CO., Vol. 3, 125-134.
- Tang, H. W., Ding, B., Chiew, Y. M., and Fang, S. L. (2009). "Protection of bridge piers against scouring with tetrahedral frames." *International Journal of Sediment Research*, 24, 385-399.
- Tison, L. J. (1940). "Erosion autour des piles de ponts en riviere." *Annales des Travaux Publics de Belgique*, 41(6), 813-817 (in French).
- Thomas, Z. "An interesting hydraulic effect occurring at local scour." *Proc., XII IAHR Congress*, Fort Collins, Colorado, Vol. 3, 193-201.
- Unger J., and Hager W. H. (2005). "Discussion to the mean characteristics of horseshoe vortex at a bridge pier." *Journal of Hydraulic Research*, 43(5), 585-588.

## References

---

- Unger, J., and Hager, W. H. (2006). "Riprap failure at circular bridge piers." *Journal of Hydraulic Engineering*, 132(4), 354-362.
- Unger, J., and Hager, W. H. (2007). "Down-flow and horseshoe vortex characteristics of sediment embedded bridge piers." *Experiments in Fluids*, 42, 1-19.
- U.S. Dept. of Transportation (2001). "Evaluating scour at bridges" *Hydraulic Engineering Circular No. 18 (HEC-18)*, Rep. No. FHWA NHI 01-001.
- Van Rijn, L. C. (1987). *Mathematical modeling of morphological processes in the case of suspended sediment transport*, PhD Thesis, Delft University of Technology.
- Venkatadri, C. (1965). "Scour around bridge piers and abutments." *Irrigation Power*, 35-42.
- Vittal, N., Kothyari, U. C., and Haghightat, M. (1994). "Clear-water scour around bridge pier group." *Journal of Hydraulic Engineering*, 120(11), 1309-1318.
- Vysotsky, I. S. (2001). "Research of active hydrodynamical method of bridge piers local erosion's reduction." *Proc., XXIX IAHR Congress*, Beijing, China.
- Vysotsky, I. S. (2005). "Experimental investigation of active hydrodynamical method reduction scour bridge piers" *Proc., XXXI IAHR Congress*, Seoul, Korea, 5172-5182.
- Wang, T. W. (1994). "A study of pier scouring and scour reduction." *Proc., 9th Congress of the APD of the IAHR*, Singapore, Vol. 2, 18-28.
- Zarrati, A. R., Chamani, M. R., Shafaie, A., and Latifi, M. (2010). "Scour countermeasures for cylindrical piers using riprap and combination of collar and riprap." *International Journal of Sediment Research*, 25, 313-322.
- Zarrati, A. R., Gholami, H., and Mashahir, M. B. (2004). "Application of collar to control scouring around rectangular bridge piers." *Journal of Hydraulic Research*, 42(1), 97-103.
- Zarrati, A. R., Nazariha, M., and Mashahir, M. B. (2006). "Reduction of local scour in the vicinity of bridge pier groups using collars and riprap", *Journal of Hydraulic Engineering*, 132(2), 154-162.

## Appendix A

### DISCHARGE MEASUREMENT

In the present study, the discharge was measured using a 90° triangular weir. This type of weir, which is also called the Thomson weir, is commonly used to measure flow rates, both in laboratory and practical works related to hydraulics engineering. Several experiments have already been carried out in application of this weir type, starting with those performed by Thomson, from which the 90° triangular weir is named. The Thomson weir available at the *Laboratorio di Grandi Modelli Idraulici* that was employed in this study is installed on a caisson; it was calibrated by Calomino *et al.* (1988). The dimensions of the weir plate are shown in Fig. A1.

The caisson and the weir dimensions were reproduced according to the drawings used at the *Laboratorio di Idraulica del Politecnico di Milano*. The caisson is stocky and rectangular in shape with dimensions of 1.7 m-long, 1.2 m-wide and 1 m-deep. The weir is installed on the downstream wall of the caisson. As depicted in Fig. A2, two grids with different mesh sizes are interposed inside the caisson in order to provide a permanent undisturbed flow approaching to the weir.

In order to measure the water head, a piezometer was connected to the caisson and a point gauge was used to measure the level inside it, as illustrated in Fig. A3a. A curved point gauge was installed on a sliding small carriage on the top of the caisson and it was used to assess the zero level (Fig. A3b).

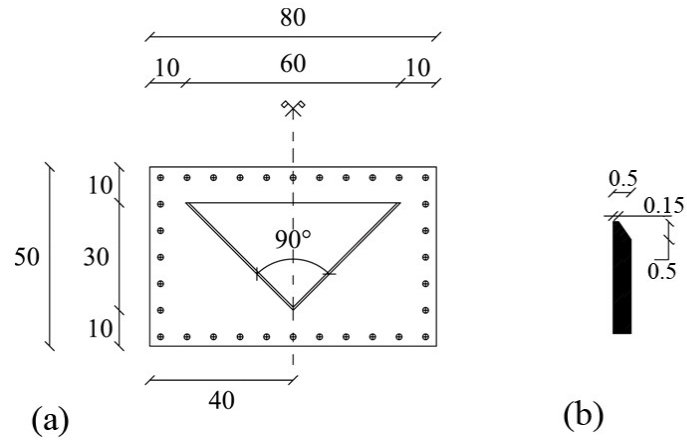


Fig. A1. Geometrical properties of the Thomson weir used to measure flow; (a) front view of the weir; (b) detail of the weir edge (units: cm)

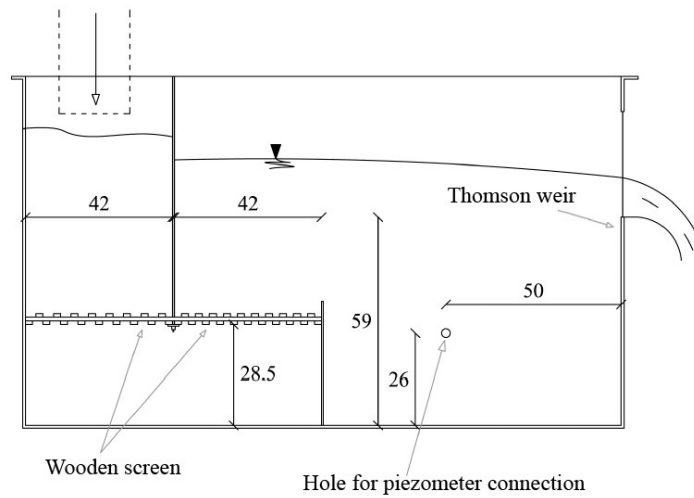


Fig. A2. Longitudinal section of the caisson holding the weir (units: cm)

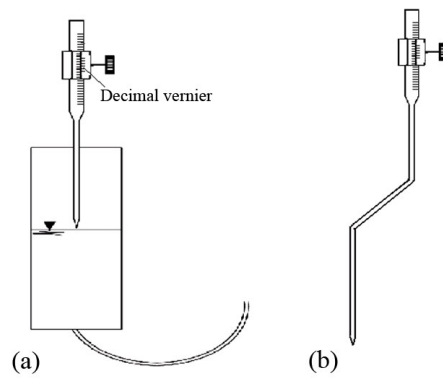


Fig. A3. Schema of point gauge fitted with a decimal vernier; (a) placed in the piezometer; (b) installed above the caisson

For determination of overflow rate in a partially contracted weir, dimensional analysis is applied. Using the Buckingham II theorem, and choosing  $h_T$ ,  $g$  and  $\rho$  as basic variables, the following relationship may be obtained:

$$\frac{Q}{h_T^{5/2} \cdot \sqrt{2 \cdot g}} = \Phi \left( \frac{B}{h_T}, \frac{p_w}{h_T}, \frac{t_w}{h_T}, \frac{\nu}{h_T^{3/2} \cdot \sqrt{g}}, \frac{\sigma}{\rho \cdot g \cdot h_T^2} \right) \quad (\text{E.A1})$$

- $Q$ =discharge;
- $h_T$ =water head with respect to the vertex of the Thomson weir;
- $B$ =channel width (for a weir installed on a caisson wall, it is equal to the caisson width);
- $p_w$ =weir height;
- $t_w$ =weir thickness;
- $g$ =gravity acceleration;
- $\rho$ =density of water;
- $\nu$ =kinematic viscosity of water;
- $\sigma$ =surface tension.

Dimensional analysis shows the influence of some geometric and fluid dynamic variables on overflow phenomenon. For low flow values, the thickness of the weir is also an effective parameter. In addition, for triangular weirs, channel width,  $B$ , and the weir height,  $p_w$ , affect the discharge. Equation (E.A1) can be rewritten as follows:

$$Q = h_T^{5/2} \cdot \sqrt{2 \cdot g} \cdot \Phi \left( \frac{B}{h_T}, \frac{p_w}{h_T}, \frac{t_w}{h_T}, \frac{\nu}{h_T^{3/2} \cdot \sqrt{g}}, \frac{\sigma}{\rho \cdot g \cdot h_T^2} \right) = \mu \cdot \sqrt{2 \cdot g} \cdot h_T^{5/2} \quad (\text{E.A2})$$

The discharge coefficient in equation (E.A2),  $\mu$ , can also be presented as follows:

$$\mu = \Phi \left( \frac{B}{h_T}, \frac{p_w}{h_T}, \frac{t_w}{h_T}, \frac{\nu}{h_T^{3/2} \cdot \sqrt{g}}, \frac{\sigma}{\rho \cdot g \cdot h_T^2} \right) \quad (\text{E.A3})$$

In the literature, there are several empirical formulae obtained by applying dimensional analysis and validated for weirs. Some Authors such as Thomson provided the formulae for fully contracted weirs, while some others (e.g., Hégly) gave formulae applicable to both fully and partially contracted weirs.

Calomino *et al.* (1988) conducted two test series in order to find an empirical formula for estimation of the discharge coefficient of the Thomson weir. They found that the shape of the rectangular caisson and the presence of the grids make the flow highly centralised with “dead” zones, resulting in the reduction of the effective weir height ( $p_w=24$  cm).

They proposed a Hégly type formula to estimate the discharge coefficient,  $\mu$ :

$$\mu = \left( \mu_0 + \frac{\alpha_T}{h_T} \right) \cdot \left[ 1 + \frac{h_T^4}{r_A \cdot B^2 \cdot (h_T + p_w)^2} \right] \quad (\text{E.A4})$$

where  $r_A$  is a factor related to liquid area reduction in the caisson (equal to 0.17) and  $\mu_0$  and  $\alpha_T$  are constant coefficients, slightly different from Hégly's ones, as indicated follows

$$\mu_0 = 0.296 \quad (0.310 \text{ according to Hégly})$$

$$\alpha_T = 0.0022 \quad (0.002 \text{ according to Hégly})$$

Finally, the discharge may be determined by the following equation:

$$Q_T = \mu \cdot \sqrt{2 \cdot g} \cdot h_T^{5/2} \quad (\text{E.A5})$$

The water level measurements, obtained by the point gauge inside the piezometer, must be referred to the horizontal plane passing through the lowest point of weir vertex. To determine the reference value which is defined as “zero<sub>T</sub>”, the following preliminary procedure should be performed:

As shown in Fig. A4, a hydrostatic condition in which the water level in the caisson is approximately the same as the level of the weir vertex should be obtained.

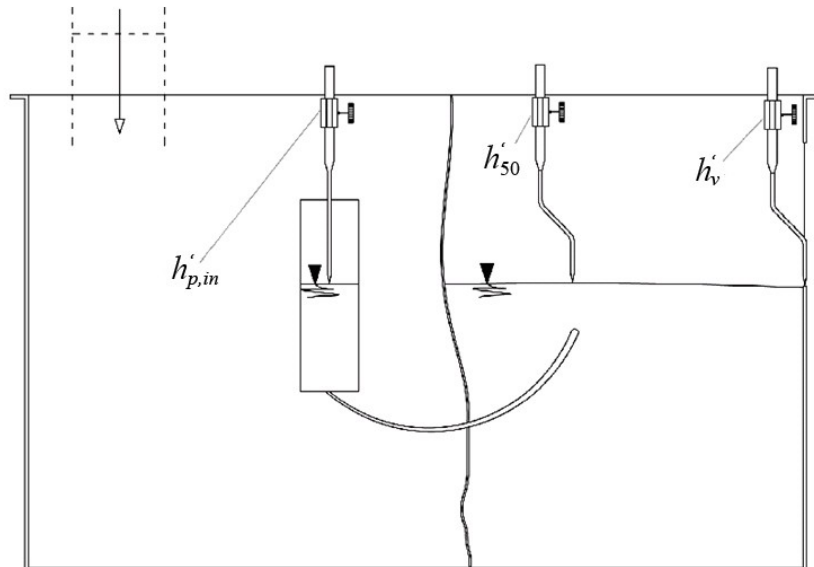


Fig. A4. Identification of measurement sections, inside the caisson to determine zero<sub>T</sub>

Using point gauges inside the caisson the reference value of the weir vertex is obtained by measurement of three points:



- the first one,  $h'_v$ , is performed on weir vertex;
- the second one,  $h'_{50}$ , on the water surface in the caisson, 50 cm upstream to the weir vertex;
- the third one,  $h'_{p,in}$ , inside the piezometer, with the point gauge (the subscript “in” indicates “initial”).

The reference value of the weir vertex is obtained as follows:

$$zero_T = h'_{p,in} + h'_v - h'_{50} \quad (E.A6)$$

To determine the water head above the vertex,  $h_T$ , it is only necessary to measure the final level of the free surface in the piezometer connected to the caisson indicated as  $h'_{p,fin}$ :

$$h_T = h'_{p,fin} - zero_T \quad (E.A7)$$

By inserting this value in (E.A5) and calculation of  $\mu$  using (E.A4) the discharge value is estimated.

In unsteady flow tests, the discharge was measured at 5 min intervals. In these tests, the value of  $h'_{p,fin} - h'_{p,in}$  was measured with a pressure transducer *Druck*. The accuracy of the pressure transducer was checked by a piezometer that stores more than 90 cm-high water column (Fig. A5a). To do this, the pressure transducer was connected to a LED display panel of *DPI 280 Series* (Fig. A5b). The control test showed that the error in measuring the difference between two water columns with 90 cm different levels was only 0.5 mm. This value was appropriate for measuring the water head in the piezometer, since it was less than 90 cm. Otherwise, it is necessary to calibrate the instrument by measuring atmospheric pressure and a certain water head.

On the other hand, the dynamic property of flow and small waves on water surface in the caisson during the tests increase the error value with respect to static condition. In fact, owing to fluctuation of water surface in the caisson, the LED panel displays various values also during steady flow conditions. In order to reduce this error, the pressure transducer was connected to a PC through a channel board (Fig. A5c) and through the software *DPLUS*, the output voltage of pressure transducer was obtained. In this study, averages of measured voltage during intervals of 30 seconds were used to reduce the error due to fluctuation of water surface inside the caisson. A relation between the average measured voltage and the water level in the piezometer is presented in Fig. A6a. During the experiments the location of the piezometer was changed slightly. Then, this relation was calculated again (Fig. A6b).

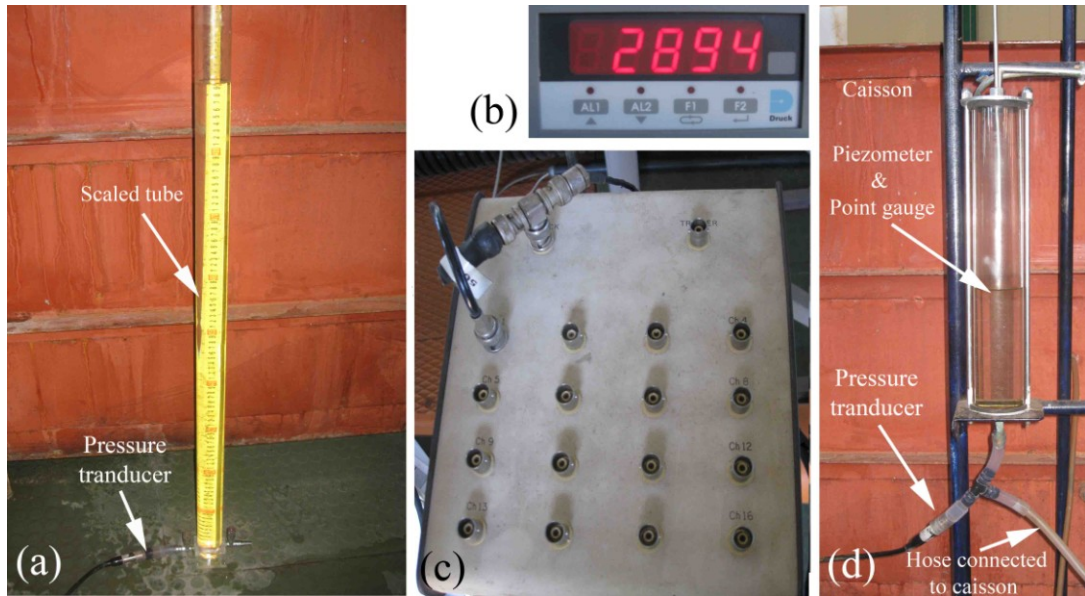


Fig. A5. (a) Verification of the pressure transducer *Druck*; (b) LED display panel of *DPI 280 Series*; (c) channel board; (d) pressure transducer connected to the piezometer

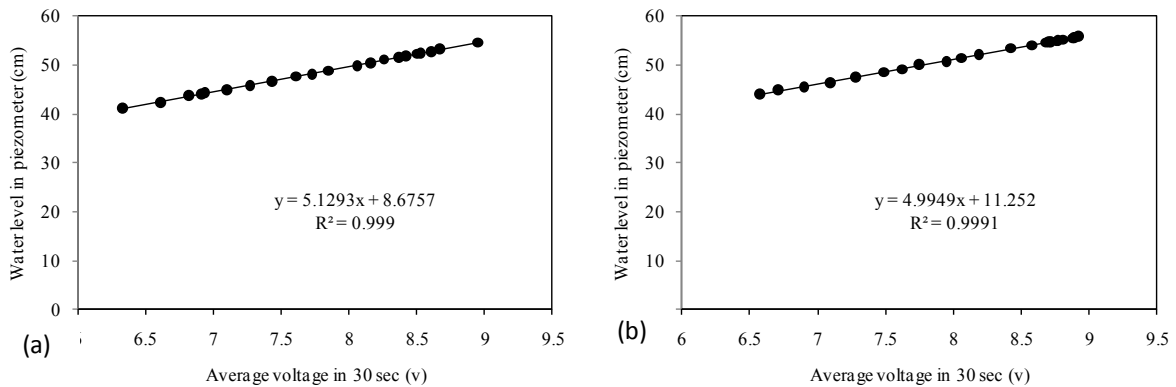


Fig. A6. Relations of average voltage in 30 seconds and water level inside the piezometer

## Appendix B

### BED-SURFACE ACQUISITION

At the end of most steady flow tests, the topography of eroded surface was digitised using a 3D laser scanner (model Vivid 300/VI-300, produced by Minolta, Fig. B1a). The laser scanner adopts the principle of similar triangles to identify the location of points on the surface. This technique is one of the most commonly used methods by 3D scanners, since the laser can digitize data with high accuracy during acquisition time. A dimension diagram and the main components of the instrument are shown in Figs. B1b and B2.

To illuminate the object surface, just a beam of light that is emitted by a laser diode and propagates to the direction of object is adequate (Fig. B3). The light beam that is reflected from the object is projected by a lens system and then acquired by a device sensitive to light which is called the receiver element, or position sensitive photo-detector (PSD). Two amplifiers convert the two photocurrents generated by the PSD voltage signals. Afterwards, these signals are processed from analogue signals into digital signals through the A/D converters and processed by a processor.

The displacement of the stripe of light along a predetermined direction of relevance is carried out through the use of a Galvano mirror. The device consists of a mirror able to rotate around a horizontal axis. Therefore, changing inclination angle of the mirror, results in the movement of the light beam reflected from the same location (Fig. B4). As Fig. B4 shows, all the surface can be acquired by the beam of light emitted from inside the scanner.

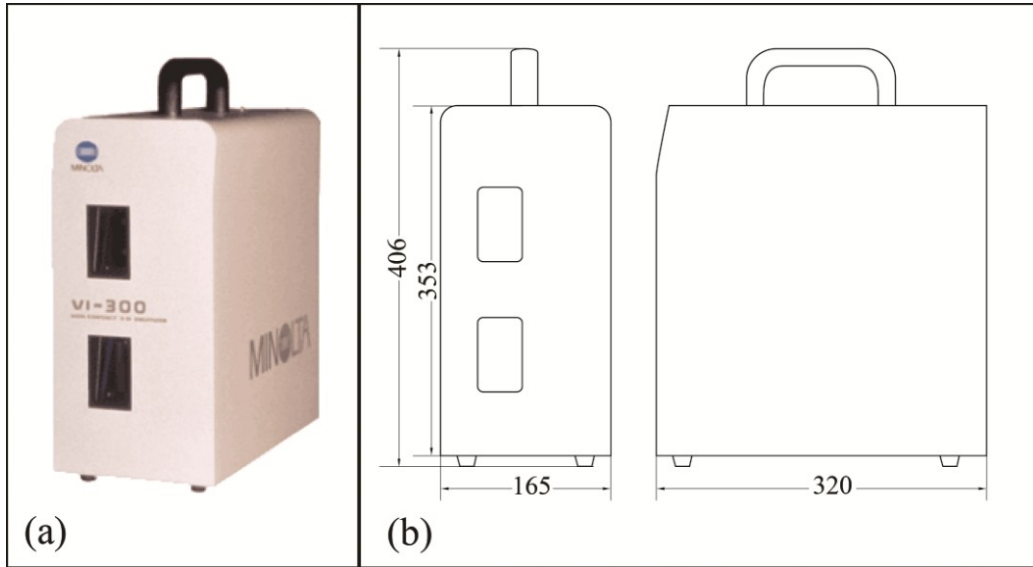


Fig. B1. (a) 3D laser scanner (model Vivid 300/VI-300 produced by Minolta); (b) sketch (units: mm)

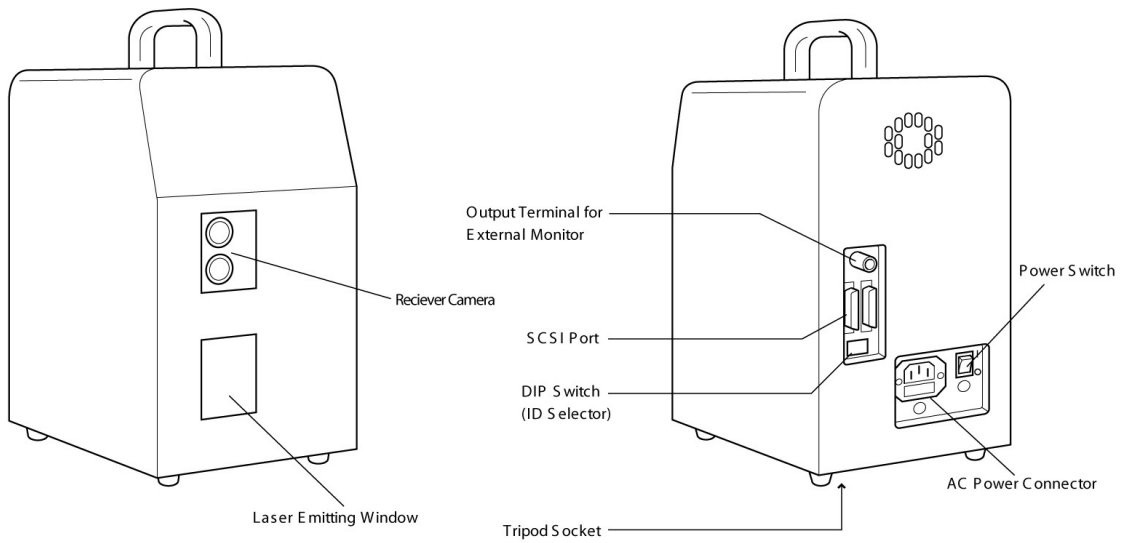


Fig. B2. Main elements of the 3D laser scanner

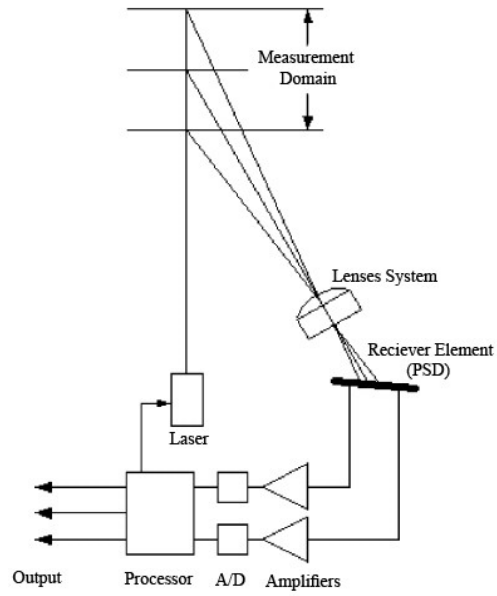


Fig. B3. Schema of a sensor that operates on the basis of the principle of similar triangles

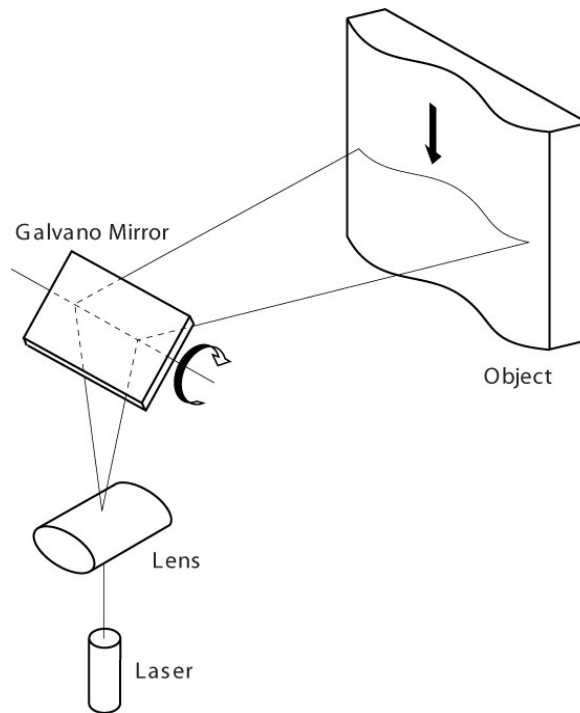
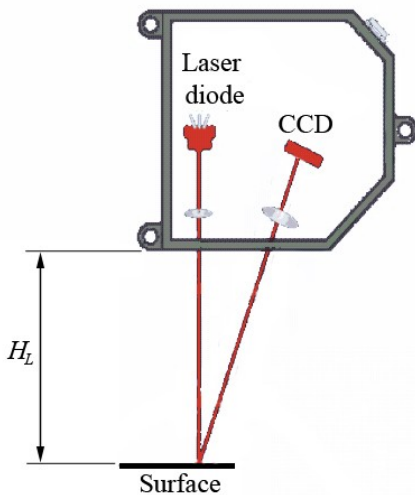


Fig. B4. Operation of the Galvano mirror for emission of laser on predetermined area

### Accuracy and installation of 3D laser scanner

By using the 3D laser scanner Minolta Vivid 300/VI-300, the objects can be captured from a distance of  $H_L = 0.55$  m to a maximum distance of 1.2 m from the instrument (Fig. B5). The acquisition range consists of a square area with sides equal to 185 mm in the position of minimum distance (0.55m) to 395 mm in position of maximum distance of  $H_L$  (1.2m).

The accuracy of the instrument in detection of points inside the acquisition area is dependent on  $H_L$ . The accuracy in parallel direction respect to acquired bed varies from 0.95 mm when  $H_L$  is minimal, to 1.91 mm for maximum  $H_L$ , while in the vertical direction, it ranges from 0.45 mm to 1 mm for minimum and maximum distances. Operation in an optimal condition is dependent on surface area and the distance to the instrument. In fact, lower distance of the instrument to the surface results in higher resolution and accuracy in acquisition of the data. In contrast, lower distance may need more images and an error is expected during merging the images, since similar points of two images are not always superimposed exactly. Figure B6 shows two images before and after merging by the post processing software of the instrument that is called *Polygon Editing Tool* (PET).



**Fig. B5. Distance between 3D laser scanner and object surface ( $H_L$ )**

In this study, in order to measure the eroded surface, the laser scanner was placed on a suitable support-box and carriage in a form that the laser emission window and entrance of the camera were parallel to the fixed bottom of the channel and the baseline of the instrument being in the same direction of the longitudinal axis of the channel (Fig. B7). The support-box was installed on a carriage free to move longitudinally along the rails above the walls of the channel and transversally across the channel, so that the bed surface could be acquired in most areas of the same part of channel, as well as in most parts of the channel. To perform the acquisition and subsequent processing of the data the 3D laser scanner was connected through an SCSI port to a computer with a 2.2 GHz processor and 512 MB RAM.

In this study, for only one test, the Laser scanner was located at a distance of  $H_L \approx 70$  cm

from the bed-surface. In this test, accuracy values in parallel and vertical directions with respect to the bed-surface are equal to 1.2 and 0.6 mm, respectively. This accuracy was calculated assuming that the accuracy in maximum and minimum distance of laser scanner to bed-surface varies linearly. The acquired area for each image was a rectangular area (about 22.5 cm×24.5 cm) and in this test, 12 images were taken to cover the required surface. In the following tests, the laser scanner was placed at higher elevation, i.e.  $H_L \approx 95$  cm. In this test, the errors of measurement in parallel and vertical directions are 1.5 and 0.8 mm; however the number of required images is reduced to 4 images, since the laser scanner acquires a larger area for each image (about 28.2 cm×32 cm). In fact, the accuracy of measurement in these two locations is not significantly different, even though reduction in the number of required images significantly reduces the error due to merging the images.

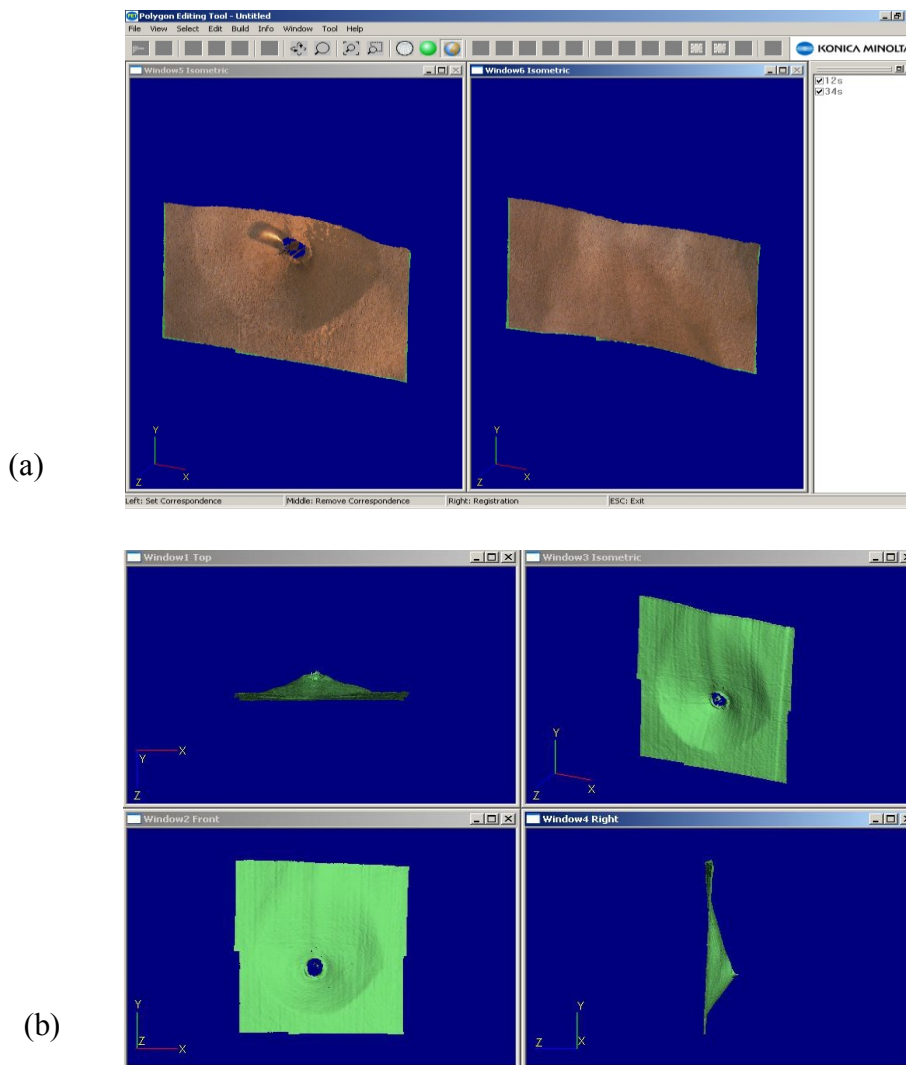


Fig. B6. Two separate images (a) before and (b) after merging

## Appendix B. Bed-surface acquisition

Since the holding carriage box was not fully parallel to the flume bed, the resulted acquired data showed a distortion with respect to the horizontal plane. This distortion was easily rectified by measuring the elevation of several points inside the acquired area using a point gauge and by imposing of an opposite slope to the data. Furthermore, areas related to pier and non erodible parts were filtered or corrected in the output file. This process of operating with 3D laser scanner is summarised in Fig. B8.

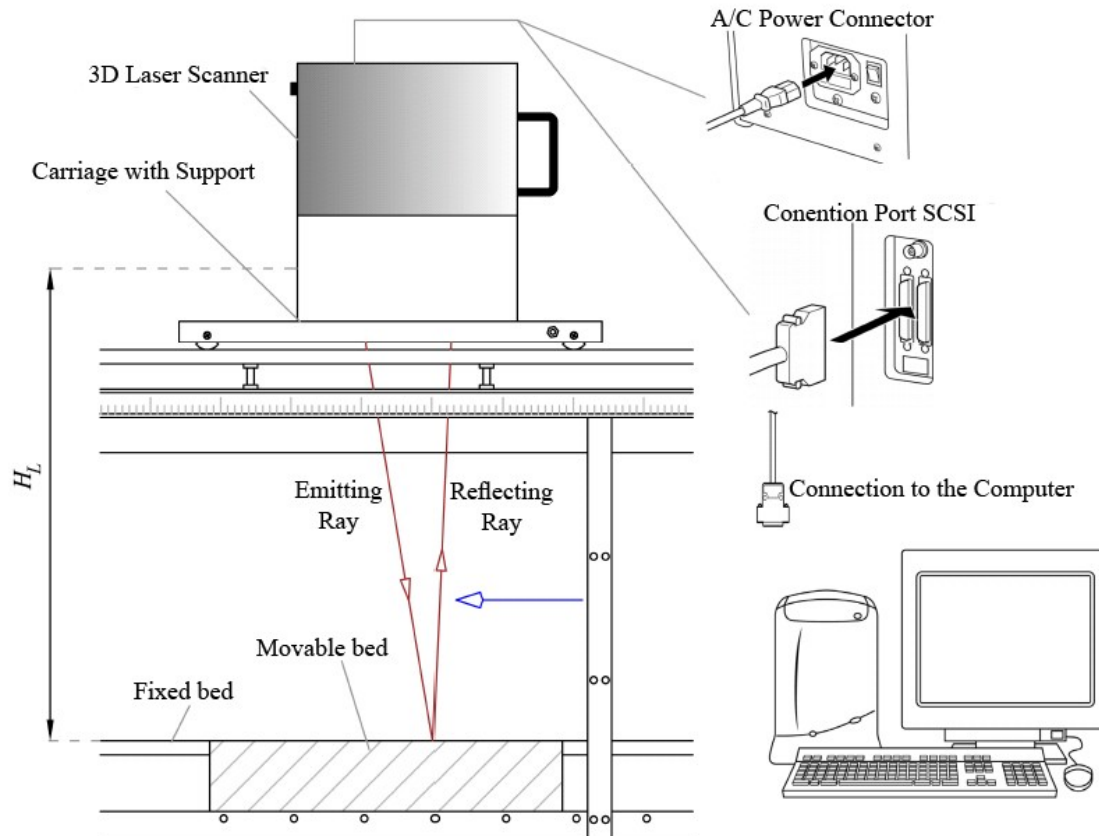


Fig. B7. Details of the installation used to acquire the eroded surface



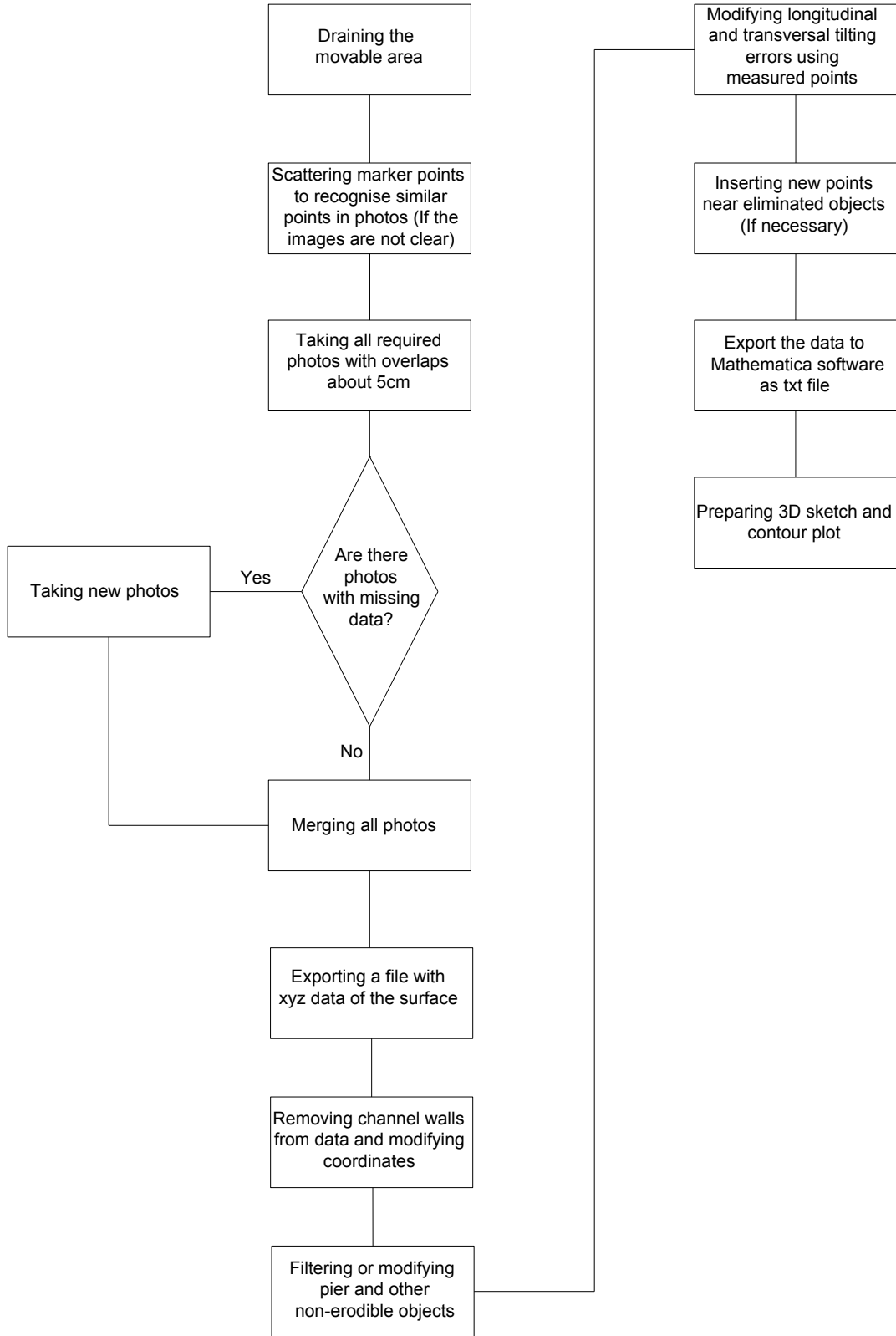


Fig. B8. Flowchart of preparing 3D pattern and contour lines of bed surface using 3D laser scanner